

# For Reference

NOT TO BE TAKEN FROM THIS ROOM

Ex libris  
UNIVERSITATIS  
ALBERTAENSIS



BRUCE PEEL SPECIAL COLLECTIONS LIBRARY  
UNIVERSITY OF ALBERTA LIBRARY

REQUEST FOR DUPLICATION

I wish a photocopy of the thesis by

Vernon - Chamberlain, VE (author)

entitled The Geochemist Geochemistry of the Malton  
Gress Complex, B.C.

The copy is for the sole purpose of private scholarly or scientific study and research. I will not reproduce, sell or distribute the copy I request, and I will not copy any substantial part of it in my own work without permission of the copyright owner. I understand that the Library performs the service of copying at my request, and I assume all copyright responsibility for the item requested.

---





THE UNIVERSITY OF ALBERTA

RELEASE FORM

NAME OF AUTHOR Valerie Elaine Vernon-Chamberlain  
TITLE OF THESIS "The Geochemistry and Geochronology of the Malton Gneiss  
Complex, British Columbia"  
DEGREE FOR WHICH THESIS WAS PRESENTED Doctor of Philosophy  
YEAR THIS DEGREE GRANTED Spring, 1983

Permission is hereby granted to THE UNIVERSITY OF ALBERTA LIBRARY to reproduce single copies of this thesis and to lend or sell such copies for private, scholarly or scientific research purposes only.

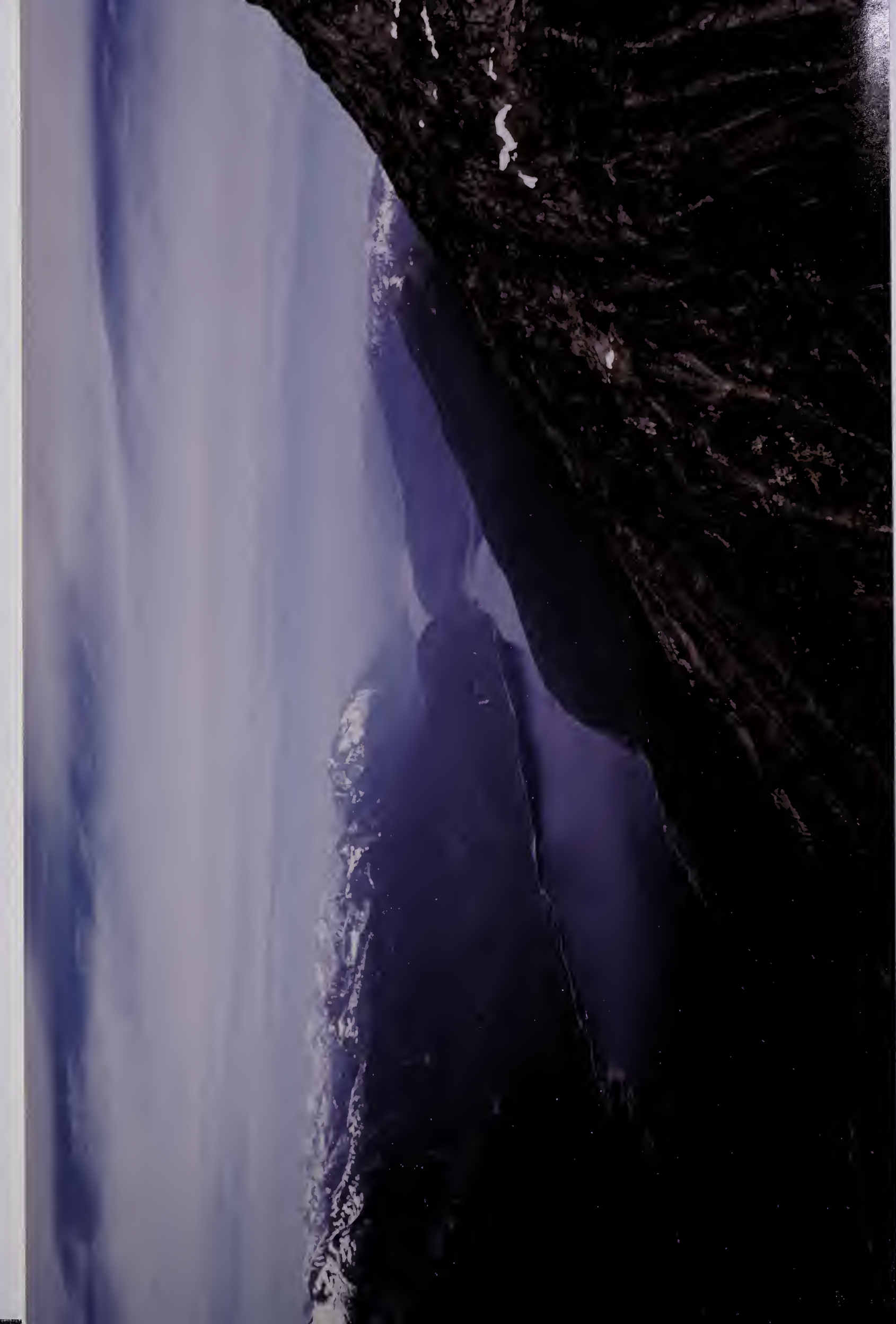
The author reserves other publication rights, and neither the thesis nor extensive extracts from it may be printed or otherwise reproduced without the author's written permission.



Digitized by the Internet Archive  
in 2019 with funding from  
University of Alberta Libraries

<https://archive.org/details/Vernon-Chamberlain1983>





Frontispiece View along the Rocky Mountain Trench, looking north west, with the Malton Block to the west and Mount Blackman in the foreground. Miette Group metasediments and Bulldog Creek Gneiss form promontories into Canoe Reach, having been down faulted by late Tertiary normal faults.

THE UNIVERSITY OF ALBERTA

"The Geochemistry and Geochronology of the Malton Gneiss Complex, British Columbia".

by



Valerie Elaine Vernon-Chamberlain

A THESIS

SUBMITTED TO THE FACULTY OF GRADUATE STUDIES AND RESEARCH

IN PARTIAL FULFILMENT OF THE REQUIREMENTS FOR THE DEGREE

OF Doctor of Philosophy

Department of Geology

EDMONTON, ALBERTA

Spring, 1983





THE UNIVERSITY OF ALBERTA  
FACULTY OF GRADUATE STUDIES AND RESEARCH

The undersigned certify that they have read, and recommend to the Faculty of Graduate Studies and Research, for acceptance, a thesis entitled "The Geochemistry and Geochronology of the Malton Gneiss Complex, British Columbia" submitted by Valerie Elaine Vernon-Chamberlain in partial fulfilment of the requirements for the degree of Doctor of Philosophy.



Dedication

To Melinda and Felicity



## Abstract

The Malton Gneiss Complex consists of approximately 1000 square kilometers of middle amphibolite facies gneissic rock outcropping in discrete blocks east and west of the Rocky Mountain Trench, south of Valemount, British Columbia.

The gneisses west of the Trench, in the Malton Block, consist of a bimodal suite of Archean orthogneisses intruded by post-Archean peralkaline leucocratic orthogneisses and amphibolites. The Archean felsic orthogneiss, termed the Grey Gneiss, probably originated as a calc-alkaline tonalite derived directly from the mantle at  $3093 \pm 46$  Ma with an initial strontium 87/86 ratio of  $0.7001 \pm 6$ .  $\delta^{18}\text{O}$  SMOW values range from 5.7 ‰ to 9.7 ‰, which appears to be typical for Archean felsic orthogneisses. The Archean mafic orthogneiss is probably of alkali basaltic parentage, the protolith having formed probably as a cumulate, possibly by clinopyroxene plus labradorite fractionation, at about 2950 Ma.  $\delta^{18}\text{O}$  SMOW values are very low even for Archean mafic orthogneisses, ranging from 4.8 ‰ to 5.3 ‰. The post-Archean peralkaline leucocratic orthogneisses consist of Augen Gneiss and Leucocratic Gneiss. The former possibly originated by the partial melting of the local Archean mafic rocks, at  $1767 \pm 20$  Ma, with an initial strontium 87/86 ratio of  $0.7105 \pm 2$ .  $\delta^{18}\text{O}$  SMOW values are 7.1 ‰ and 7.8 ‰. The Leucocratic Gneiss may have been intruded in two separate episodes. The first probably occurred at or before 840 Ma, as recorded by the Pb 207/206 age of zircon separates. A second intrusion of Leucocratic Gneiss possibly occurred at about 550 Ma, as suggested by the rubidium – strontium data. The initial strontium 87/86 ratio of  $0.7107 \pm 2$  is consistent with formation by the remobilization and mixing of the Augen Gneiss and the 840 Ma Leucocratic Gneiss. A possible cause of this melting may have been a further influx of alkaline mafic magma at  $528 \pm 29$  Ma, with an initial strontium 87/86 ratio of  $0.7069 \pm 1$ . These Leucocratic Gneisses yield  $\delta^{18}\text{O}$  SMOW values ranging from 6.2 ‰ to 7.9 ‰, which are consistent with their post-Archean meta-igneous character.

The gneisses east of the Rocky Mountain Trench consist of the Mount Blackman Gneiss, the Bulldog Creek Gneiss and the Hugh Allan Creek Gneiss. The Mount Blackman





Gneiss consists of felsic paragneisses intruded by mafic orthogneisses, the felsic paragneisses apparently having formed from immature granitic sediments. A Pb 207/206 age on zircons of 1950 Ma may be a minimum age for their source rock. The rubidium – strontium evidence is difficult to interpret but may mean that the paragneisses experienced metamorphism at about 1990 Ma and at about 900 Ma. Their  $\delta^{18}\text{O}$  SMOW values of 9.4 ‰ to 10.1 ‰ appear to confirm their paragneissic nature. The mafic gneisses in the Mount Blackman area appear to be of tholeiitic basaltic parentage intruding as sills into the felsic paragneisses. Their  $\delta^{18}\text{O}$  SMOW values of 7.3 ‰ to 8.2 ‰ are consistent with their post-Archean orthogneissic character. The Bulldog Creek Gneiss appears to have originated as a suite of calc-alkaline mafic and felsic igneous rocks, produced by normal plagioclase fractionation. The rubidium – strontium data on these rocks is inconclusive, suggesting only that they probably formed between 300 and 1100 Ma. The Hugh Allan Creek Gneiss appears to have been an S-type granite, intruded at  $806 \pm 13$  Ma with an initial ratio of  $0.7222 \pm 15$ .

Uranium – lead isotopic analyses on zircons from the felsic suites suggest multi-stage models, with the gneisses suffering episodic lead loss at times consistent with those suggested by the rubidium – strontium data.

The metasedimentary rocks surrounding the Malton Gneiss Complex consist of the Kaza Group to the southwest, the Miette Group to the northeast and the Monashee Horsethief Creek Group to the south. Geochemical and petrological studies on the metasediments adjacent to the Complex suggest that the Kaza Group here formed as mature sediments, the Monashee Horsethief Creek Group as greywackes and the Miette Group in this locality as immature arkoses and lithic arenites. A literature survey shows that the three Groups differ in lithology, structure and metamorphic history. Geochronological studies suggest that the Monashee Horsethief Creek Group suffered its major metamorphism at about 1250 Ma, the Kaza Group possibly at about 250 Ma and the Miette Group possibly at about 900 Ma and during the Cretaceous.

The geological history suggested for the area is that of accretion of a minimum of three and a maximum of five originally separated plates, mini-plates or parts of plates. The terranes west of the Rocky Mountain Trench appear to have accreted to each other prior to their collision with the North American plate, the latter possibly occurring during



the Cretaceous by westward dipping subduction. A Cretaceous collision may have been followed by dextral transcurrent movement along the Rocky Mountain Trench fault zone, by further easterly thrusting and finally by late Tertiary extension.



## Acknowledgements

My sincere thanks go to the very many people who between them contributed considerable time and effort towards the successful completion of this thesis.

Dr. Richard Lambert, my supervisor and advisor, enjoined in any number of helpful discussions, besides giving help, encouragement and advice. Dr. Halfdan Baadsgaard and Dr. George Cumming gave much helpful advice in their capacity as thesis committee members. Dr. Baadsgaard also helped with the chemical separations and the zircon analyses. Dr. Cumming wrote the mass spectrometer programs as well as building many of the mass spectrometers and keeping them all in working order. In this he was ably assisted by Dragan Kristic and Hugh McCullough, who also frequently came to my aid and deserve my special thanks.

My grateful thanks also go to Dr. Grenville Holland, who, assisted by George Randall, ran the X.R.F. analyses; Dr. Karlis Muehlenbachs, who, assisted by Erzsebeth Toth, helped with the oxygen isotope work; Des Wynne, who wrote the computer programs for the diagrams; Carolyn Lambert, Tony Lambert, Tim Lambert, Arthur Whitney and Doug Ragan, all of whom gave valuable help in the field; Gary Foreman, who piloted us safely to many mountain top destinations; and Richard Miller, Paul Wagner and Rosemary Basaraba, who typed the manuscript.

Support for field work was provided by a grant from the Department of Mines Energy and Resources, and financial assistance by a Teaching Assistantship from the Department of Geology at the University of Alberta, both of which are gratefully acknowledged.





## Table of Contents

Chapter	Page
1. INTRODUCTION .....	1
1.1 Location and Structure of the Malton Gneiss Complex .....	1
1.2 Geophysical Significance of the Rocky Mountain Trench .....	4
1.3 Metamorphic Core Complexes .....	6
1.4 Metasediments adjacent to the Malton Gneiss Complex .....	10
1.5 Statement of the Problem .....	13
1.5.1 Age and Petrogenesis of the Gneisses .....	13
1.5.2 Age and Metamorphic History of the Metasediments .....	14
1.5.3 Nature of the Rocky Mountain Trench .....	14
1.5.4 Relationship between the Gneisses and the Metasediments .....	14
2. PETROGRAPHY .....	16
2.1 Introduction .....	16
2.2 Mafic Gneisses .....	16
2.2.1 Introduction .....	16
2.2.2 Mafic Gneiss West of the Rocky Mountain Trench .....	16
2.2.3 Mafic Gneiss East of the Rocky Mountain Trench .....	18
2.3 Felsic Gneisses .....	21
2.3.1 Introduction .....	21
2.3.2 Grey Gneiss .....	21
2.3.3 Leucocratic Gneiss .....	24
2.3.4 Augen Gneiss .....	24
2.3.5 Felsic Gneiss from the Bulldog Creek Area .....	28
2.3.6 Felsic Gneiss from the Mount Blackman Area .....	28
2.3.7 Felsic Gneisses from the Hugh Allan Creek Area .....	28
2.4 Metasediments .....	30
2.4.1 Introduction .....	30
2.4.2 Metasediments from the Kaza Group .....	30
2.4.3 Metasediments from the Robina Creek Area .....	30
2.4.4 Metasediments from the Miette Group .....	32
2.4.5 Metasediments from the Monashee Horsethief Creek Group .....	32



3. GEOCHEMISTRY OF THE GNEISSES .....	37
3.1 Introduction .....	37
3.1.1 Sample Collection and Analysis .....	38
3.2 Geochemistry of the Different Sub-Units of the Malton Gneiss .....	40
3.3 Mafic Gneisses .....	40
3.4 Felsic Gneisses .....	51
3.4.1 Introduction .....	51
3.4.2 Felsic Gneisses West of the Rocky Mountain Trench .....	51
3.4.3 Grey Gneiss .....	51
3.4.4 Leucocratic Gneiss and Augen Gneiss .....	56
3.4.5 Felsic Gneiss East of the Rocky Mountain Trench .....	62
3.5 Factor Analysis .....	63
3.6 Conclusions .....	67
4. STRATIGRAPHY AND GEOCHEMISTRY OF THE METASEDIMENTS SURROUNDING THE MALTON GNEISS COMPLEX .....	69
4.1 Introduction and Review .....	69
4.2 Correlations across the Rocky Mountain Trench north of the Malton Gneiss Complex .....	69
4.3 Correlation of the Horsethief Creek Group .....	73
4.4 Correlations across the Rocky Mountain Trench and the North Thompson Fault south of the Malton Gneiss Complex .....	75
4.5 Sample Collection and Analysis .....	77
4.6 Geochemistry .....	78
5. GEOCHRONOLOGY .....	92
5.1 Introduction .....	92
5.2 Analyses .....	94
5.3 Results and Discussion .....	95
5.3.1 Grey Gneiss .....	95
5.3.2 Mafic Gneiss .....	99
5.3.3 Augen Gneiss .....	99
5.3.4 Leucocratic Gneiss .....	102
5.3.5 Kaza Group Metasediments .....	104
5.3.6 Monashee Horsethief Creek Group Metasediments .....	106



5.3.7	Hugh Allan Creek Gneiss .....	108
5.3.8	Mount Blackman Gneiss .....	108
5.3.9	Bulldog Creek Gneiss .....	108
5.3.10	Miette Group Metasediments .....	113
5.4	Comparison with other areas .....	113
6.	OXYGEN ISOTOPE STUDIES .....	120
6.1	Introduction .....	120
6.2	Analytical Procedure .....	120
6.2.1	Oxygen extraction .....	120
6.2.2	Mass spectrometry .....	121
6.3	Results .....	121
6.4	Discussion .....	125
6.4.1	Intoduction .....	125
6.4.2	Archean mafic gneiss .....	128
6.4.3	Archean Grey Gneiss .....	130
6.4.4	Post-Archean Leucocratic and Augen Gneisses .....	130
6.4.5	Gneisses East of the Rocky Mountain Trench .....	131
6.5	Strontium Isotopic Evidence .....	132
7.	CONCLUSIONS AND SPECULATION .....	134
7.1	The nature of the Rocky Mountain Trench .....	134
7.2	Geological History of the Area .....	135
8.	REFERENCES CITED .....	141
9.	APPENDICES .....	152
9.1	Appendix A (X.R.F. Analyses of Gneissic Rocks) .....	153
9.2	Appendix B (X.R.F. Analyses of Metasedimentary Rocks) .....	182
9.3	Appendix C (Isotope Data) .....	200





## List of Tables

Table	Page
3.1 Mean analyses of mafic gneisses of the Malton Gneiss Complex compared with those of igneous rocks .....	42
3.2 Major element analyses of the Grey Gneisses of the Malton Gneiss Complex compared with those of igneous rocks .....	52
3.3 Major and trace element analyses of the Leucocratic Gneisses of the Malton Gneiss Complex .....	53
3.4 Mean analyses of felsic gneisses of the Malton Gneiss Complex .....	54
3.5 Principal Factor loadings in the Promax Oblique Primary Pattern Matrix .....	66
6.1 Oxygen isotopic measurements on whole rock and feldspar samples from the Malton Gneiss Complex .....	122



## List of Figures

Figure	Page
1.1 Geological Map of the southeastern Canadian Cordillera, after Campbell (1972), Okulitch <i>et al.</i> (1975), Oke and Simony (1981), Read and Brown (1981), Tipper <i>et al.</i> (1981) and Brown and Murphy (1982) .....	map pocket
1.2 The Malton Gneiss Complex, after Campbell (1968), Ghent <i>et al.</i> (1977), Morrison (1979) and Oke and Simony (1981) .....	2
1.3 The Canadian Cordillera, showing geophysical variations and the five belts of Wheeler and Gabrielse (1972), after Monger and Price (1979) .....	5
1.4 Metamorphic core complexes of the North American Cordillera, after Coney (1980) .....	7
1.5 Structure and characteristics of a 'typical' metamorphic core complex of the North American Cordillera.(Coney, 1980) .....	9
1.6 The 'suspect terranes' of the North American Cordillera. (Coney <i>et al.</i> , 1980) .....	11
3.1 The Malton Gneiss Complex, after Campbell (1968), Ghent <i>et al.</i> (1977), Morrison (1979) and Oke and Simony (1981) .....	39
3.2 SiO <sub>2</sub> histograms for the gneissic rocks of the Malton Gneiss Complex .....	41
3.3 A–F–M triangular diagram for the mafic gneisses of the Malton Gneiss Complex ....	44
3.4 Nb/Y histograms for the mafic gneisses of the Malton Gneiss Complex .....	45
3.5 Zr–Ti/100–3Y triangular diagram for the mafic gneisses of the Malton Gneiss Complex .....	47
3.6 Ti v Zr plot for the mafic gneisses of the Malton Gneiss Complex .....	48
3.7 CaO v Y plot for the mafic gneisses of the Malton Gneiss Complex .....	50
3.8 Ab–An–Or triangular diagram for the Grey Gneiss of the Malton Gneiss Complex .....	55
3.9 A–F–M tringular diagram for the Grey Gneiss of the Malton Gneiss Complex .....	57
3.10 CaO v Y plot for the Grey Gneiss and the mafic gneisses of the Malton Block .....	58



3.11 Ab–An–Or triangular diagram for the felsic gneisses of the Malton Gneiss Complex .....	59
3.12 A–F–M triangular diagram for the Leucocratic Gneiss and the Augen Gneiss of the Malton Gneiss Complex .....	60
3.13 CaO v Y plot for the Leucocratic Gneiss, the Augen Gneiss and the mafic gneisses of the Malton Block .....	61
3.14 A–F–M triangular diagram for the felsic gneisses east of the Rocky Mountain Trench in the Malton Gneiss Complex .....	64
3.15 CaO v Y plot for the mafic and felsic gneisses east of the Rocky Mountain Trench in the Malton Gneiss Complex .....	65
3.16 Factor analysis plot for the gneisses of the Malton Gneiss Complex .....	68
4.1 Correlation table for formations east and west of the Rocky Mountain Trench (Young, 1979) .....	71
4.2 Classification of the pelitic rocks from the Kaza, Miette and Monashee Horsethief Creek Groups in the Valemount area .....	79
4.3 Classification of the psammitic rocks from the Kaza, Miette and Monashee Horsethief Creek Groups in the Valemount area .....	80
4.4 SiO <sub>2</sub> v CaO plot for metasediments from the Kaza, Miette and Monashee Horsethief Creek Groups in the Valemount area .....	81
4.5 CaO v Y plot for metasediments from the Kaza, Miette and Monashee Horsethief Creek Groups in the Valemount area .....	82
4.6 Sr/Y v SiO <sub>2</sub> plot for pelites and psammities from the Kaza, Miette and Monashee Horsethief Creek Groups in the Valemount area .....	83
4.7 Rb v Sr plot for metasediments from the Kaza, Miette and Monashee Horsethief Creek Groups in the Valemount area .....	84
4.8 SiO <sub>2</sub> v Al <sub>2</sub> O <sub>3</sub> plot for metasediments from the Kaza, Miette and Monashee Horsethief Creek Groups in the Valemount area .....	85
4.9 Al <sub>2</sub> O <sub>3</sub> v Fe <sub>2</sub> O <sub>3</sub> plot for metasediments from the Kaza, Miette and Monashee Horsethief Creek Groups in the Valemount area .....	86
4.10 Al <sub>2</sub> O <sub>3</sub> v Na <sub>2</sub> O plot for metasediments from the Kaza, Miette and Monashee Horsethief Creek Groups in the Valemount area .....	87





4.11 $\text{SiO}_2$ v Ba plot for metasediments from the Kaza, Miette and Monashee Horsethief Creek Groups in the Valemount area .....	88
4.12 $\text{SiO}_2$ v K/Rb plot for psammites and pelites from the Kaza, Miette and Monashee Horsethief Creek Groups in the Valemount area .....	89
5.1 Rb–Sr isochron diagram for the Grey Gneiss of the Malton Gneiss Complex .....	96
5.2 Strontium evolution diagram for rocks west of the Rocky Mountain Trench in the Valemount area .....	97
5.3 Concordia plot of zircons from the Grey Gneiss, the Leucocratic Gneiss and the Mount Blackman Gneiss of the Malton Gneiss Complex .....	98
5.4 Rb–Sr isochron diagram for the mafic gneisses west of the Rocky Mountain Trench in the Malton Gneiss Complex .....	100
5.5 Rb–Sr isochron diagram for the Augen Gneiss of the Malton Gneiss Complex .....	101
5.6 Rb–Sr isochron diagram for the Leucocratic Gneiss of the Malton Gneiss Complex .....	103
5.7 Rb–Sr isochron diagram for metasediments from the Kaza Group in the Valemount area .....	105
5.8 Rb–Sr isochron diagram for metasediments from the Monashee Horsethief Creek Group in the Valemount area .....	107
5.9 Rb–Sr isochron diagram for the Hugh Allan Creek Gneiss of the Malton Gneiss Complex .....	109
5.10 Strontium evolution diagram for rocks east of the Rocky Mountain Trench in the Valemount area .....	110
5.11 Rb–Sr isochron diagram for the Mount Blackman Gneiss of the Malton Gneiss Complex .....	111
5.12 Rb–Sr isochron diagram for the Bulldog Creek Gneiss of the Malton Gneiss Complex .....	112
5.13 Rb–Sr isochron diagram for metasediments from the Miette Group in the Valemount area .....	114
5.14 Age determinations west of the Rocky Mountain Trench .....	115
5.15 Age determinations east of the Rocky Mountain Trench .....	117





6.1 Oxygen isotopic compositions of whole rocks from the Malton Gneiss Complex compared with those from other Archean complexes and with those from the Berridale Batholith .....	124
6.2 Oxygen isotopic composition versus silica content for certain gneisses from the Malton Gneiss Complex .....	129
6.3 $\delta^{18}\text{O}$ v $\text{Sr } 87/86$ initial ratio plot for the rocks of the Malton Gneiss Complex ..	133
7.1 Tabulation of the geological history of the Malton Gneiss Complex area .....	136
7.2 Relative movements of the North American, Farallon and Kula plates during the last 100 Ma (Riddihough, 1982) .....	138



## List of Photographic Plates

Plate	Page
Frontispiece View along the Rocky Mountain Trench, looking north west, with the Malton Block to the west and Mount Blackman in the foreground. Miette Group metasediments and Bulldog Creek Gneiss form promontories into Canoe Reach, having been down faulted by late Tertiary normal faults.	
1.1 Malton Gneiss exposed in the floor of a corrie west of Dominion Mountain, the topographical surface approximating the main foliation. The polydeformational history of the gneiss is evidenced by the extreme complexity of the structure. ....	3
2.1 Photomicrograph in plane polarized light of mafic gneiss (sample number AC8) from the C.N. Track, in the Malton Range, showing part of a biotite laminar along a shear zone, traversing a primary amphibole-plagioclase texture. ....	17
2.2 A composite amphibolite dyke, with a garnet amphibolite centre, intruding Leucocratic Gneiss, north of Mount Albreda. ....	17
2.3 A garnet amphibolite dyke intruding Grey Gneiss, north of Mount Albreda. Note the reaction rims around the garnets. ....	19
2.4 Photomicrograph, under crossed nicols, of mafic gneiss (sample number 5833) from the Bulldog Creek area, east of the Rocky Mountain Trench. Kaolinized plagioclases and chloritized biotites attest to the retrogressive metamorphism of this rock to Greenschist facies. ....	20
2.5 Discordant amphibolite sheet intruding felsic gneisses in the Mount Blackman area, east of the Rocky Mountain Trench ....	20
2.6 100m high cliff of Grey Gneiss on the north side of Moonbeam Creek in the Monashee Mountains. ....	22
2.7 Photomicrograph in plane polarized light of Grey Gneiss (sample number 5498), from the type locality on the C.N. Track, showing a spongy garnet porphyroblast with an epidote core. ....	23
2.8 Photomicrograph in plane polarized light of Leucocratic Gneiss (sample number 6152F), from a corrie north of Mount Albreda showing the very dark green pleochroic colour of the amphiboles. ....	23
2.9 Sheets of Leucocratic Gneiss intruding hornblende gneisses, near Mount Thompson in the Malton Range. ....	25
2.10 Sheet of Leucocratic Gneiss intruding Augen Gneiss, near the head of Clemina Creek in the Monashee Mountains. ....	25



2.11 Early Leucocratic Gneiss intruded by later Leucocratic Gneiss, and then by a mafic dyke, north of Mount Albreda. ....	26
2.12 Photomicrograph under crossed nicols of Augen Gneiss (sample number 5901N), showing evidence of two metamorphisms: Microperthite and plagioclase form overgrowths on an original metamorphic texture. ....	26
2.13 Augen Gneiss showing lineated augen, evidence of the polymetamorphic character of this rock. ....	27
2.14 Photomicrograph in plane polarized light of Bulldog Creek Gneiss (sample number 5831C), showing epidote replacement of allanite. ....	29
2.15 Photomicrograph under crossed nicols of Mount Blackman paragneiss (sample number 5890B), showing deformed muscovite and the gritty texture typical of a metasediment. ....	29
2.16 Robina Creek metasediments thrust over Malton Gneiss, at the head of Robina Creek. The contact is near the head of the hammer. ....	31
2.17 The slide zone between the Malton Gneiss and the Robina Creek metasediments exposed on the south wall of Robina Creek. ....	33
2.18 Photomicrograph under crossed nicols of Miette Group metasediment (sample number AC20), showing pebbles of feldspar. ....	33
2.19 Windfall Creek Thrust, showing the rusty weathered metasediments of the Monashee Horsethief Creek Group thrust over the Malton Gneiss on the south wall of Moonbeam Creek. ....	34
2.20 Infold of Malton Gneiss into the Monashee Horsethief Creek Group metasediments, above the Windfall Creek Thrust on the south wall of Moonbeam Creek. ....	35
2.21 Rusty weathering kyanite grade metasediments of the Monashee Horsethief Creek Group in the foreground, with an infold of Malton Gneiss forming the peak of Dominion Mountain in the background. ....	36
2.22 Metaturbidites of the Monashee Horsethief Creek Group exposed on Highway 5, eight km south of the Malton Block. The strong isoclinal folding on southward dipping axial planes is clearly visible. The sequence is intruded by an amphibolite dyke. ....	36





## 1. INTRODUCTION

### 1.1 Location and Structure of the Malton Gneiss Complex

The Malton Gneiss Complex lies within the Omineca Crystalline Belt of Wheeler and Gabrielse (1972) and sits astride the Southern Rocky Mountain Trench, southeast of Valemont, British Columbia (figure 1.1)[In back pocket]. It was first mapped by Campbell in 1968 on the Canoe River map sheet of the Geological Survey of Canada, and is centered at approximately  $52^{\circ} 30' \text{ N}$  and  $119^{\circ} \text{ W}$ . The complex consists of about 1000 square kilometres of amphibolite facies gneisses outcropping as several discrete masses of gneissic rock. The largest of these, termed the Malton Block, lies to the west of the Rocky Mountain Trench fault zone, which forms its eastern boundary. Three smaller blocks of gneiss, the Bulldog Creek Gneiss, the Mount Blackman Gneiss and the Hugh Allan Creek Gneiss, lie to the east of the Rocky Mountain Trench (figure 1.2). The Malton gneiss is bounded to the west by the North Thompson Fault, to the south by the Windfall Creek Fault and to the north possibly by a Tertiary normal fault (Morrison, 1979).

The structure of the Malton Block has been described by Morrison (1979). The dominant foliation ( $S_{1-2}$ ) is folded into a large upright antiform-synform pair, with ESE plunging axes ( $F_4$ ). The dips on the limbs of these folds are around  $30^{\circ}$ , which gives a maximum gneissic thickness of about 8 km (including about 1.5 km of topography). The  $S_{1-2}$  foliation appears to be due to an isoclinal folding ( $F_2$ ) which also involves and infolds the metasedimentary cover rocks of the Monashee Horsethief Creek Group, outcropping to the south of the Malton Block.  $F_2$  is folding at least one pre-existing foliation,  $S_{1-2}$ , which again also involves the Monashee Horsethief Creek Group.  $F_3$  is a series of large, tight folds overturned to the northeast and plunging to the southeast.  $F_5$  consists of doming. There are also at least two periods of thrust faulting and one of normal faulting. The first thrusting is post  $F_2$  and pre  $F_3$  and involves the Monashee Horsethief Creek Group. The second thrusting is co-eval with  $F_3$ . The normal faulting is the final phase of deformation and has fault planes dipping steeply to the northwest. Thus the structure of the Malton Block is highly complex as can be seen in plate 1.1, where the structural surface of the Grey Gneiss of the Malton Block is exposed by erosion on the floor of a cirque west of Dominion Mountain. The peak of metamorphism occurred after the  $F_2$











Plate 1.1 Malton Gneiss exposed in the floor of a corrie west of Dominion Mountain, the topographical surface approximating the main foliation. The polydeformational history of the gneiss is evidenced by the extreme complexity of the structure.





folding (Ghent *et al.*, 1977; Morrison, 1979).

The structure of the Mount Blackman and Hugh Allan Creek Gneisses, east of the Rocky Mountain Trench, has been described by Oke and Simony (1981). The folding in the Mount Blackman Gneiss is complex, with axial plane orientations varying, suggesting ductile deformation during at least one of the two or more folding phases. This gneiss forms the core of a large overturned antiform, plunging to the southeast at about 20°. The antiform is also faulted with the Mount Blackman Gneiss being thrust over the overturned northeast limb of Miette cover, north of Mount Blackman. On the west of the Mount Blackman Block, striated fault surfaces indicate post metamorphic movement. The Hugh Allan Creek Gneiss is bounded to the north and east by a thrust fault (possibly a continuation of the Purcell Thrust), to the west by a normal fault and to the southeast by a near-vertical normal fault on which there has also been substantial transcurrent movement.

## 1.2 Geophysical Significance of the Rocky Mountain Trench

The Southern Rocky Mountain Trench is a major lineament in the earth's continental crust. It occurs as a narrow linear depression approximately 1000 km long, extending from 120° 30' W and 53° 30' N in southern British Columbia to 144° W and 47° 30' N in Montana, where it is cut off by St. Mary's transcurrent fault. The Northern Rocky Mountain Trench and the Tintina Fault extend to its northwest, for about another 1500 km, in approximately the same line. Stratigraphic evidence suggests that the line of the Southern Rocky Mountain Trench marked the approximate edge of the North American Craton in Cambrian times and it appears to have been a long existing line of weakness in the earth's crust. It is probably best described as a complex fault zone, its present surface expression being that of normal and thrust faults for most of its length (figure 1.1). Comparable lineaments in the earth's crust are all major transcurrent faults; e.g. the San Andreas Fault in California, the Great Glen Fault in Scotland and the Anatolian Fault in Turkey. The nature and number of geophysical changes occurring across the Rocky Mountain Trench (figure 1.3) demonstrates its significance as a geophysical and geological boundary. Seismic studies have shown that as the trench is crossed from east to west, the crust thins from 50 km to 35 km (Wickens, 1977; Mereu *et al.*, 1977;



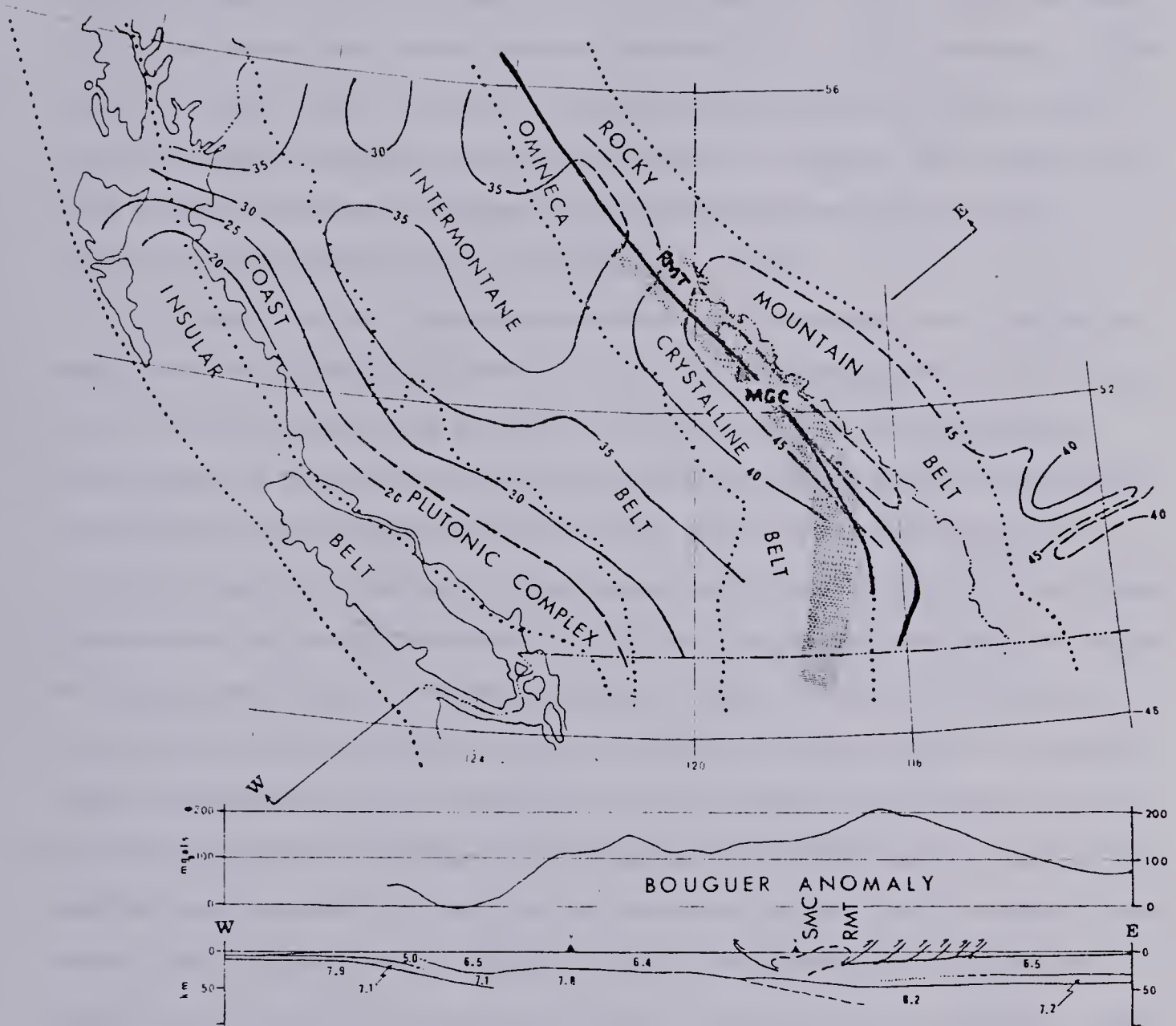


Figure 1.3 The Canadian Cordillera, showing geophysical variations and the five belts of Wheeler and Gabrielse (1972), after Monger and Price (1979). Structure contours at 5 km intervals give the depth to the Moho. Stippled area marks the boundary between highly conductive crust and upper mantle (to the southwest) and less conductive crust and upper mantle (to the northeast). RMT = Rocky Mountain Trench. MGC = Malton Gneiss Complex. Section WE shows P wave velocity in km/sec. SMC = Shuswap Metamorphic Complex. v = Recent and Quaternary volcanics.





Spence *et al.*, 1977), the lithosphere thins to approximately 35 km (Wickens and Pec, 1968; Wickens, 1977), a 7.2 km/sec lower crustal P-wave high velocity zone disappears (Chandra and Cumming, 1972; Berry and Forsyth, 1975) and the upper mantle P-wave velocity decreases from 8.5 km/sec to 7.8 km/sec (Berry and Forsyth, 1975; Wickens, 1977). Other studies have shown a westerly decrease in lithosphere thickness to 20 km (Fulton and Walcott, 1975), a westerly increase in heat flow (Judge, 1977), a westerly increase in electrical conductivity (Caner, 1970; Dragert and Clarke, 1977; Gough *et al.*, 1982), a westerly decrease in Bouguer gravity anomalies and an abrupt change in magnetic anomalies (Haines *et al.*, 1971; Coles *et al.*, 1976).

The seismic activity in the area is moderate, with an average, taken over the last twenty years, of one earthquake every two years with a magnitude greater than, or equal to 3.0 on the Richter Scale (Ellis and Chandra, 1981). Compared with the generally diffuse pattern of seismicity in central British Columbia, there is a definite concentration of earthquake activity in this area (Rogers, 1981). Most of these earthquakes have occurred as swarms of hundreds of small shallow events, but a magnitude 6.0 earthquake occurred south of the Hugh Allan Block in 1918, and a magnitude 4.8 earthquake close to the Bulldog Creek Block in 1978 (Ellis and Chandra, 1981). Rogers *et al.* (1980) have shown that the motion on the latter was a combination of thrust and strike-slip faulting. These earthquakes and a local conductivity high may be related to the Anahim Volcanic Belt and postulated hot spot (Rogers, 1981; Gough *et al.*, 1982). The very high (–200) negative Bouguer anomaly in the area may also be related to this hot spot (Bouguer Gravity Anomaly Map of Canada, 1967). Taking the eastern Intermontane Belt as datum, the magnitude of this anomaly is closely comparable to that which occurs between an island arc and a trench. (150 mgals in 200km).

### 1.3 Metamorphic Core Complexes

Coney (1980) has described over twenty-five isolated metamorphic terranes, which he has termed "Metamorphic Core Complexes", extending in a narrow sinuous belt along the axis of the North American Cordillera from northwest Mexico to Southern Canada (figure 1.4). These metamorphic core complexes are defined by their distinctive structure namely, a metamorphic-plutonic basement terrane separated by a decollement



1, Frenchman's Cap; 2, Thor-Odin; 3, Pinnacles; 4, Valhalla; 5, Okanagan; 6, Kettle; 7, Selkirk; 8, Bitterroot (Idaho batholith); 9, Pioneer; 10, Albion-Raft River-Grouse Creek; 11, Ruby; 12, Snake Range; 13, Whipple; 14, Harcuvar; 15, Harquiball; 16, South Mountains-White Tank; 17, Picacho; 18, Tortolita; 19, Catalina-Rincon; 20, Santa Teresa-Pinaleno; 21, Comobabi-Coyote; 22, Pozo Verde; 23, Magdalena; 24, Madera; 25, Mazatan; 26, Death Valley turtlebacks.

# EXPLANATION

- Metamorphic Core Complex
- Major Batholith
- Early to Middle Tertiary Volcanic Rocks
- Shuswap Metamorphic Rocks
- Laramide Thrust Fault
- Sevier Thrust Fault



Figure 1.4 Metamorphic core complexes of the North American Cordillera, after Coney (1980). M = Malton Gneiss Complex.





zone from an overlying less highly metamorphosed or unmetamorphosed cover, the whole having a domal or anticlinal structure, usually elongated in the direction of the trend of the belt, and often asymmetrical with one flank steeper than the other, (figure 1.5). The basement terrane of these metamorphic core complexes varies greatly in age and lithology, ranging from early Precambrian metasedimentary and plutonic rocks to middle Tertiary plutons (Reynolds and Rehrig, 1980; Banks, 1980). Metamorphic grade is also variable, tending to be higher in older terranes which then have a younger mylonitic fabric superimposed on them nearer the decollement zone, which typically occurs close to the Precambrian–Phanerozoic unconformity. The overlying cover likewise varies greatly in age and lithology, ranging from slices of Precambrian basement to Tertiary sediments (Davis, 1980; Davis *et al.*, 1980; Rehrig and Reynolds, 1980). The cover is often highly eroded, remaining only in isolated klippen, but where sufficient cover remains, extensional listric normal faults are common and the total amount of extension dramatic (Todd, 1980).

The Malton Block appears to possess all the characteristics of a Metamorphic Core Complex. It consists of an early Precambrian metamorphic basement terrane forming an asymmetrical dome, elongated in the direction of the trend of the belt with its eastern flank steeper than its western. This basement terrane is separated by a decollement zone from a less metamorphosed, highly eroded cover, now existing as isolated klippen. It is approximately colinear with four of the recognized Metamorphic Core Complexes of the Omineca Crystalline Belt, namely, the Valhalla Dome, the Pinnacles, the Thor Odin Dome and the Frenchman's Cap Dome of the Shuswap Metamorphic Complex (figure 1.4). The Omineca Crystalline Belt and the Coast Plutonic Complex are the only two of the five northwest–southeast trending belts of the Canadian Cordillera (figure 1.3) which are comprised of highly deformed metamorphic and plutonic complexes, the other three belts being composed largely of lower grade or unmetamorphosed rocks which preserve much of the stratigraphic record of the Cordillera (Monger, 1977; Tipper, 1981).

South of the 49th parallel, these two crystalline belts first tend to merge into the Idaho batholith and then separate again further south, where the eastern belt containing the metamorphic core complexes follows a sinuous path through Idaho, Utah, Nevada and



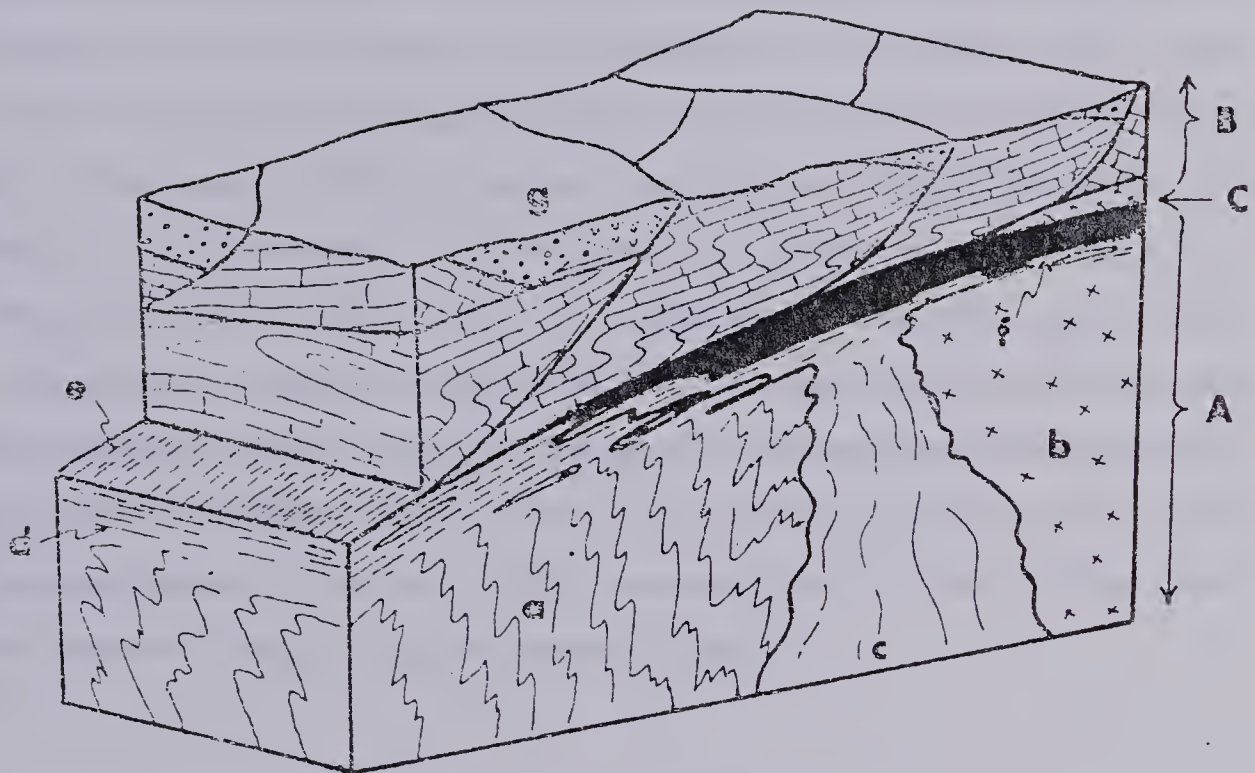


Figure 2. Schematic structural block diagram of typical domains of Cordilleran metamorphic core complexes; A, basement terrane; B, cover terrane; C, decollement zone; a, older metasedimentary rocks; b, older pluton; c, younger pluton (early to middle Tertiary); d, mylonitic foliation; e, mylonitic lineation; f, marble tectonite (black); g, lower to middle Tertiary sedimentary and volcanic rocks.

Figure 1.5 Structure and characteristics of a 'typical' metamorphic core complex of the North American Cordillera. (Coney, 1980).





Arizona into Mexico. This apparent geographical continuity does not necessarily indicate contemporaneity. The ages of metamorphism and decollement in the eastern belt, as well as the age of the batholiths in the western belt tend to get progressively younger to the south.

Geological explanations of these physiographic manifestations have been many and varied. Important contributions include Misch (1960), Armstrong (1968, 1972), Price and Mountjoy (1970), Roberts and Crittenden (1973), Todd (1973) and Coney (1974). In the Canadian Cordillera, attention has focused on an explanation of the five structural belts (Monger *et al.*, 1972; Dickinson, 1976; Eisbacher, 1977; Griffiths, 1977; Muller, 1977). More recently, faunal and paleomagnetic evidence has shown the Cordillera to be a collage of microplates of differing age and origin, the term "collage" being first coined by Helwig in 1974, (Schweikert, 1976; Monger, 1977; Jones *et al.*, 1977; Davis *et al.*, 1978; Monger and Price, 1979; Coney *et al.*, 1980; Monger and Irving, 1980; Tipper, 1981). Monger *et al.*, 1982 have suggested that the Omineca and Coast plutonic belts, or welts, formed as a result of tectonic overlap and compressional thickening during collisions between the North American craton and the various accreted terranes, such as Wrangellia and Stikinia. Coney *et al.* (1980) have described all of the Cordillera west of the North American craton as "suspect terrane" (figure 1.6).

#### **1.4 Metasediments adjacent to the Malton Gneiss Complex**

Precambrian metasediments of the Kaza Group, overlain by the Cariboo Group, are faulted against the western edge of the Malton Block by the North Thompson Fault (figure 1.2). The stratigraphy and structure of these metasediments have been described by Sutherland Brown (1957, 1963), Campbell (1970), Campbell and Charlesworth (1970), Young (1979) and Pell and Simony (1981).

The Miette group metasediments, also of Precambrian age, outcrop to the east of the Rocky Mountain Trench. They have been described by Price and Mountjoy (1966), Slind and Perkins (1966), Price (1967), Giovanella (1967), Campbell and Charlesworth (1970), Pinsent (1971) and Young (1979).

The Monashee Horsethief Creek Group Precambrian metasediments outcrop south of the Malton Block, west of the Rocky Mountain Trench, east of the North





Fig. 1-6 Generalized map of Cordilleran Suspect Terranes. Dashed pattern, North American autochthonous cratonic basement. Barbed line, eastern limit of Cordilleran Mesozoic-Cenozoic deformation. Barbed arrows, direction of major strike-slip movements. Terranes are described below.

#### Alaska

(for further information on the distribution and character of terranes in Alaska, see refs 14, 17-20, 53)

- Sp, Seward Peninsula—structurally complex assemblage of Precambrian metamorphic and sedimentary rocks, and Palaeozoic carbonate rocks.
- Ns, North Slope—Precambrian, Palaeozoic, and Mesozoic clastic and carbonate sequence—part of North America, but may have moved from original position.
- Kv, Kagvik—Thin sequence of radiolarian chert, argillite, shale, and minor volcanics, Mississippian to Triassic in age.
- En, Endicott—metamorphosed Lower to Upper Palaeozoic clastic and carbonate rocks intruded by Palaeozoic granitic rocks.
- R, Ruby—composite terrane comprising at least three separate units, including Precambrian metamorphic rocks, mid to Upper Palaeozoic volcanic and sedimentary rocks, and thick piles of Lower Mesozoic basalt and chert.
- I, Innoko—structurally deformed sequence of Upper Palaeozoic to early Mesozoic chert, argillite, graywacke, and basic to intermediate volcanics.
- NF, Nixon Fork—Precambrian metamorphic rocks overlain by Palaeozoic and Mesozoic carbonate, clastic, and cherty rocks.
- G, Goodness (composite)—includes three terranes: (1) a complex assemblage of deformed Upper Palaeozoic volcanics, chert, and graywacke with blocks of older limestone; (2) Precambrian gneisses and schist, and (3) Mesozoic arc-derived volcanic flows, tuff, and graywacke, with interbedded chert.
- Cl, Chulitna (composite)—includes three terranes: (1) Devonian ophiolite overlain by Palaeozoic chert, volcanic conglomerate, limestone, and flysch, and Mesozoic limestone, redbeds, flysch, and chert; (2) Mesozoic chert, argillite, crystal tuff, and conglomeratic sandstone; (3) Upper Palaeozoic tuff, and chert, volcanic graywacke, with blocks of Lower Palaeozoic limestone.
- PM, Pingston & McKinley (composite)—includes three terranes: (1) Upper Palaeozoic phyllite and Triassic thin-bedded limestone and sooty black shale; (2) Upper Palaeozoic chert, Triassic pillow basalt, and Upper Mesozoic flysch and conglomerate; (3) Lower Palaeozoic limestone; tuff and flysch of unknown ages.
- YT, Yukon-Tanana (composite)—includes regionally metamorphosed schist and gneiss of Precambrian(?) age, Devonian limestone, Upper Palaeozoic silicic metavolcanic rocks, Permian ophiolite, and foliated granitic rocks of unknown age.
- W, Wrangellia—Upper Palaeozoic arc complex composed of flows, breccias, and volcanoclastic rocks overlain by limestone, clastics, and chert, and Mesozoic pillowed and subaerial basalt flows succeeded by limestone, cherty limestone, and clastic rocks.
- P, Peninsular—rare Palaeozoic limestone, Triassic basalt, argillite, and limestone, Lower Jurassic volcanic and volcanoclastic rocks, younger clastics.
- Cg, Chugach (composite)—includes (1) deformed Upper Mesozoic flysch and melange units, and (2) deformed Lower Cenozoic flysch and volcanic rocks.
- Ax, Alexander—complex terrane of Precambrian(?) and Palaeozoic volcanic rocks, clastics, and limestone, and Mesozoic volcanics, limestone, and clastic rocks.
- T, Taku—structurally complex assemblage of Upper Palaeozoic volcanoclastics, limestone, flysch(?), and Lower Mesozoic basalt, limestone, and flysch.
- TA, Tracy Arin—structurally complex assemblage of marble, pelitic gneisses, and schist of unknown ages.

#### Canada

- Ch, Cache Creek terrane—Mississippian to Middle (Upper?) Triassic, highly disrupted radiolarian chert, argillite, basalt, alpine-type ultramafics, large shallow-water carbonates, and local blueschist metamorphism.
- BR, Bridge River terrane—Middle Triassic to Lower Middle Jurassic, highly disrupted radiolarian chert, argillite, basalt, alpine-type ultramafics and minor carbonate.
- St, Stikine terrane—Mississippian and Permian volcanoclastics, basic to acidic volcanics and carbonates, locally deformed and intruded in middle to late Triassic time, overlain by Upper Triassic to Middle Jurassic volcanogenic strata.
- E, Eastern assemblage (composite)—includes possible late Precambrian-early Palaeozoic metamorphic terranes, of possible continental affinity, together with Mississippian to Triassic basalt, ultramafics and chert and volcanoclastics and carbonates, overlain unconformably by Middle Triassic to Lower Jurassic volcanogenic strata.

#### Washington and Oregon

- SJ, San Juan (composite)—includes highly deformed Mesozoic chert, argillite, graywacke, and volcanic rocks, partly in melanges, with blocks of lower Palaeozoic plutonic rocks, Palaeozoic chert, carbonates, and volcanic rocks. Permian limestone blocks contain Tethyan fusulinids (see ref. 54).
- Ca, Northern Cascades (composite)—includes crystalline and pelitic gneisses, and thrust sheets composed of (1) Upper Palaeozoic andesitic volcanics and associated sedimentary rocks; (2) green schist and blue schist; and (3) Jurassic ophiolite (see ref. 55).
- O, Olympic—Lower Cenozoic volcanic rocks and associated deep and shallow water sedimentary rocks. Basement unknown, but presumed to be oceanic (see ref. 56).
- S, Lower Cenozoic volcanic and sedimentary rocks lying west of the Cascade Range. Palaeomagnetic data imply post-Eocene clockwise rotation of 70° (see refs 55, 56).
- BL, Blue Mountains (composite)—includes melange with blocks of Palaeozoic ophiolite, limestone, and chert, and Mesozoic chert and sandstone, structurally overlain by Triassic and Jurassic volcanic sandstone, conglomerate, and argillite (see refs 57, 58).

#### California

- Fh, Foothills—Upper Jurassic andesitic volcanic and volcanoclastic rocks associated with phyllite, slate, and graywacke, and Upper Jurassic ophiolite (see refs 59, 60).
- Trp, Triassic and Palaeozoic of Klamath Mountains (composite)—includes a structurally complex assemblage of Lower Mesozoic ophiolite, chert, basalt, Jurassic andesitic rocks, and associated sedimentary rocks (see refs 61, 62).
- KL, Eastern Klamath Mountains—Middle to Upper Palaeozoic clastic, volcanic, and carbonate rocks, overlain by Triassic and Jurassic volcanics and minor limestone (see refs 63, 64).
- Si, Northern Sierra—Lower Palaeozoic clastic sedimentary rocks, Upper Palaeozoic and Lower Mesozoic volcanic and associated sedimentary rocks (see ref. 65).
- C, Calaveras (composite)—including a western belt of melange with ophiolite and Mesozoic chert, and an eastern belt of quartzose clastic rocks, argillite, and minor Permian limestone (see ref. 66).
- F, Franciscan (composite)—includes Upper Mesozoic Great Valley sequence with ophiolite at base, and structurally underlying disrupted and partially metamorphosed rocks of the Franciscan Complex (see ref. 67).
- Sa, Salinia—includes metamorphosed pelitic rocks, marble, and graywacke of unknown ages, intruded by Cretaceous granite plutons (see ref. 68).
- SG, San Gabriel (composite)—two structurally complex and juxtaposed Precambrian crystalline terranes intruded by Mesozoic plutons (see ref. 69).
- OR, Orocopia—metagraywacke and mudstone and minor chert and basic volcanic rocks, age unknown. No known basement (see ref. 70).
- Mo, Mohave (composite)—juxtaposed and disrupted Palaeozoic sedimentary sequences, Lower Mesozoic sedimentary and volcanic rocks intruded by Mesozoic plutons (see ref. 71).

#### Mexico

- B, Baja—includes scattered localities of Upper Palaeozoic limestone and Lower Mesozoic clastic rocks, overlain by a thick pile of Upper Mesozoic volcanic and volcanoclastic rocks, capped by latest Cretaceous quartzofeldspathic sandstone (see ref. 72).
- V, Vizcaino (composite)—includes Triassic basalt, chert, and limestone, Upper Jurassic arc-derived volcanic and volcanoclastic rocks, Upper Jurassic and Cretaceous clastic rocks, ophiolite, and structurally underlying Upper Mesozoic blue schist and disrupted rocks similar to the Franciscan Complex (see ref. 73).

#### Nevada

- S, Sonoma (composite)—includes Upper Palaeozoic volcanics in the south, and Lower Mesozoic volcanics in the north. Si and KL terranes originally included in Sonoma (see ref. 74).
- GL, Golconda—structurally deformed assemblage of chert, argillite, minor limestone, and volcanics of Mississippian to Permian age (see ref. 75).
- RM, Roberts Mountains—structurally complex assemblage of chert, argillite, sandstone, basalt, and minor limestone of Cambrian to latest Devonian or early Mississippian ages (see ref. 76).



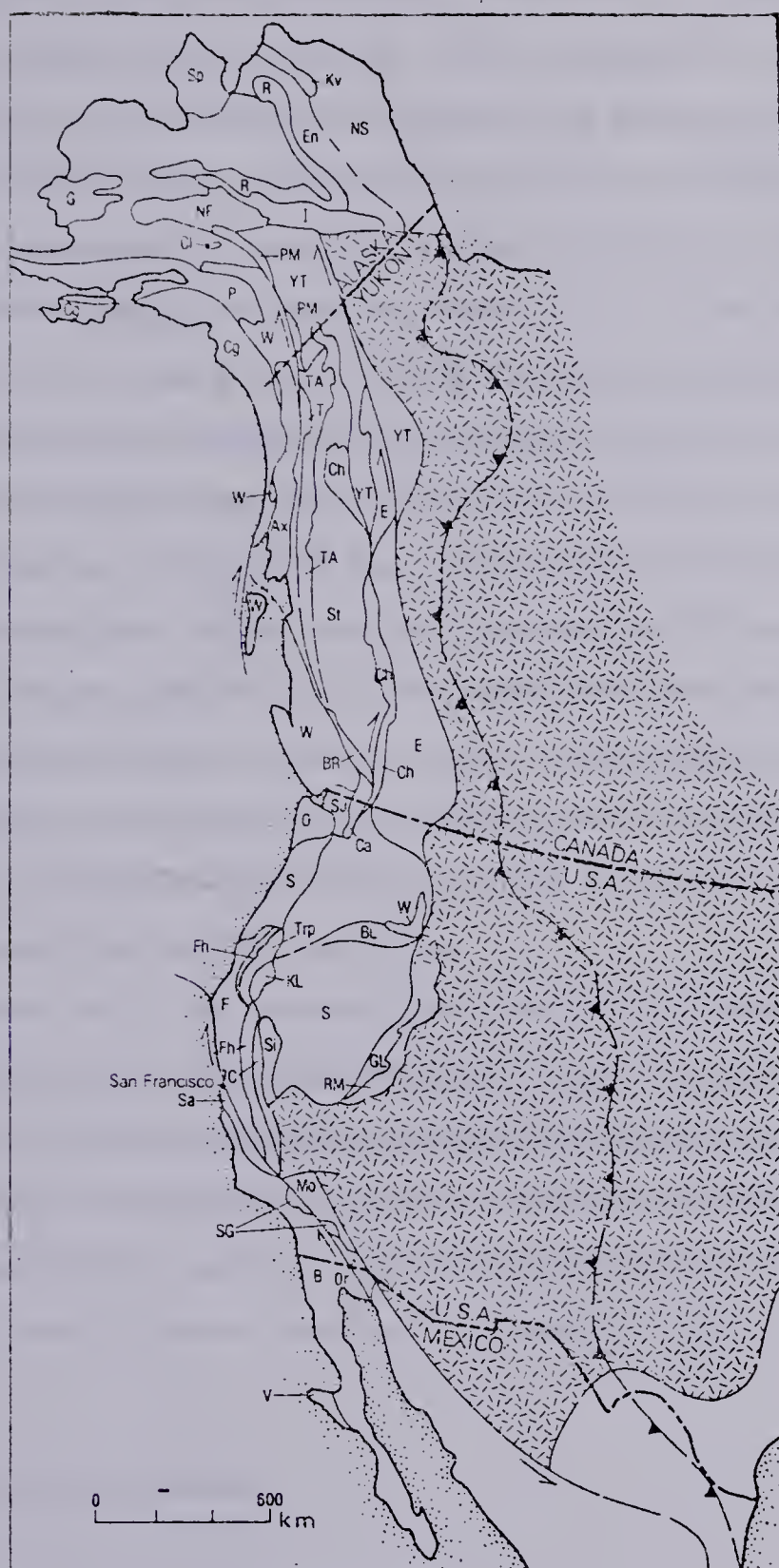


Figure 1.6 The 'suspect terranes' of the North American Cordillera. (Coney et al., 1980)



Thompson Fault and south of the Windfall Creek Fault. Their stratigraphy, structure and metamorphic history have been described by Wheeler *et al.* (1972), Brown *et al.* (1978), Simony *et al.* (1980), Poulton and Simony (1980) and Ghent *et al.* (1980).

The ages of the Precambrian metasedimentary groups are not known with any accuracy. Geological Survey of Canada K–Ar ages prior to 1965 are unreliable because many were not corrected for atmospheric argon. Wanless *et al.* (1967) obtained a K–Ar age of 1535 Ma on detrital mica from the Miette Group. Charlesworth *et al.* (1967) made K–Ar isotopic measurements on whole rock slates containing metamorphic micas, and on detrital muscovite separates from psammities of the Old Fort Point and Wynd formations (Miette Group) near Jasper. These gave a 1700 Ma minimum source rock age and a 75 Ma maximum metamorphic age. Further measurements on slates and schists 80 km west of Jasper gave a 69 Ma whole rock slate age and 93 Ma and 105 Ma on biotite and muscovite (respectively) from a schist. These were interpreted as incompletely reset detrital ages giving maximum metamorphic ages. Price and Mountjoy (1970) quoted an age of 111 Ma on post-kinematic metamorphic biotites from the Miette Group in the Selwyn Range. Campbell (1968) equated the Miette Group with both the Monashee Horsethief Creek group and the Kaza Group.

Cambrian rocks in the area have been described by Campbell and Charlesworth (1970) as outcropping in a northwest trending strip north of the Malton Block, as well as east and south of the Mount Blackman and Hugh Allan Creek Gneisses. Oke and Simony (1981), however, interpreted the quartzite in contact with the Mount Blackman Gneiss as basal Hadrynian (Miette Group) and not as Cambrian Gog Group (figure 1.2). The fossiliferous Mural Formation (top of Lower Cambrian) is absent in this area.

## 1.5 Statement of the Problem

### 1.5.1 Age and Petrogenesis of the Gneisses

The age and origin of the gneisses are unknown. Once these have been determined by geochronological, geochemical and petrographical methods, their relationship to each other can be discussed. It is possible that the gneisses east and west of the Rocky Mountain Trench are unrelated, being fortuitously exposed at the same





latitude (possibly due to uplift on the Mount Robson Anticlinorium). It is possible that dextral transcurrent movement has occurred on the Rocky Mountain Trench (Eisbacher, 1977). Correlation between dated gneisses on opposite sides of the Trench will place limits on the amount and timing of any such movement. Thrusting may also have taken place across the Trench (Ghent *et al.*, 1977; Simony and Wind, 1970). Again correlation or non-correlation of gneissic rocks will aid in timing those movements and in establishing a tectonic history of the area.

### **1.5.2 Age and Metamorphic History of the Metasediments**

Ages determined on metasediments may represent their metamorphic, depositional or source rock ages. It may be feasible to distinguish between these possibilities and to establish preliminary geological histories for the metasediments. Geochemical and petrographical studies in conjunction with the geochronological studies will help to establish correlation or lack of correlation between the three main metasedimentary units, and hence aid in establishing the timing and type of movement on the faults separating them.

### **1.5.3 Nature of the Rocky Mountain Trench**

The geophysical evidence presented above suggests that the Rocky Mountain Trench is a major geological boundary. Correlation or lack of correlation of gneissic and metasedimentary units across the Rocky Mountain Trench will help to establish whether or not this is so, and also, perhaps, to determine what type of boundary it is.

### **1.5.4 Relationship between the Gneisses and the Metasediments**

The boundary between the Malton Block gneisses and the Monashee Horsethief Creek Group metasediments has been described as metamorphic by Price and Mountjoy (1970) and as structural by Ghent *et al.* (1977). Similarly, the boundary between the Mount Blackman Gneiss and surrounding metasediments has been described as metamorphic by Giovanella (1967) and as unconformable by Oke and Simony (1981). Most of the other boundaries are believed to be faults. It may be possible to resolve some of the problems on the controversial boundaries and establish the type of faulting



on the faulted boundaries.



## **2. PETROGRAPHY**

### **2.1 Introduction**

Over 400 samples were collected from the gneisses and metasediments of the Malton Gneiss Complex. Sample localities and geographical areas are shown in figure 1.5. Each sample was examined in hand specimen and in thin section. Petrographical descriptions of the main rock types exposed in the Complex are given here.

### **2.2 Mafic Gneisses**

#### **2.2.1 Introduction**

Mafic gneiss is the most common gneissic rock in the Complex, being exposed at nearly every gneissic locality visited, both east and west of the Rocky Mountain Trench and consisting largely of either hornblende gneiss or amphibolite. Mafic gneiss is rare or absent however, around and to the south east of Mount Albreda, where there is a large outcrop of felsic augen gneiss; and south of Hugh Allan Creek, where most of the exposure is of felsic granitic gneiss.

#### **2.2.2 Mafic Gneiss West of the Rocky Mountain Trench**

The hornblende gneisses west of the Trench are mesocratic to melanocratic sheared biotitized lineated gneisses with biotite often concentrated on the shear surfaces (Plate 2.1). These equigranular gneisses consist of 20%–60% slightly sericitized oligoclase, 20%–50% hornblende, 10%–30% green biotite and 10% quartz, with predominant accessory sphene, less common epidote and rare apatite, oxide and garnet. The garnet is often spongy, containing epidote inclusions. (Plate 2.1). The concentration of biotite on shear planes, the epidotized garnets and the epidote plus sodic plagioclase replacement of plagioclase all suggest at least two stages of metamorphism, the first being of middle amphibolite facies and the second of upper greenschist facies. Some samples from the C.N. track at the northern end of the Malton Range contain pale green clinopyroxene porphyroblasts, suggesting that locally the first metamorphism may have





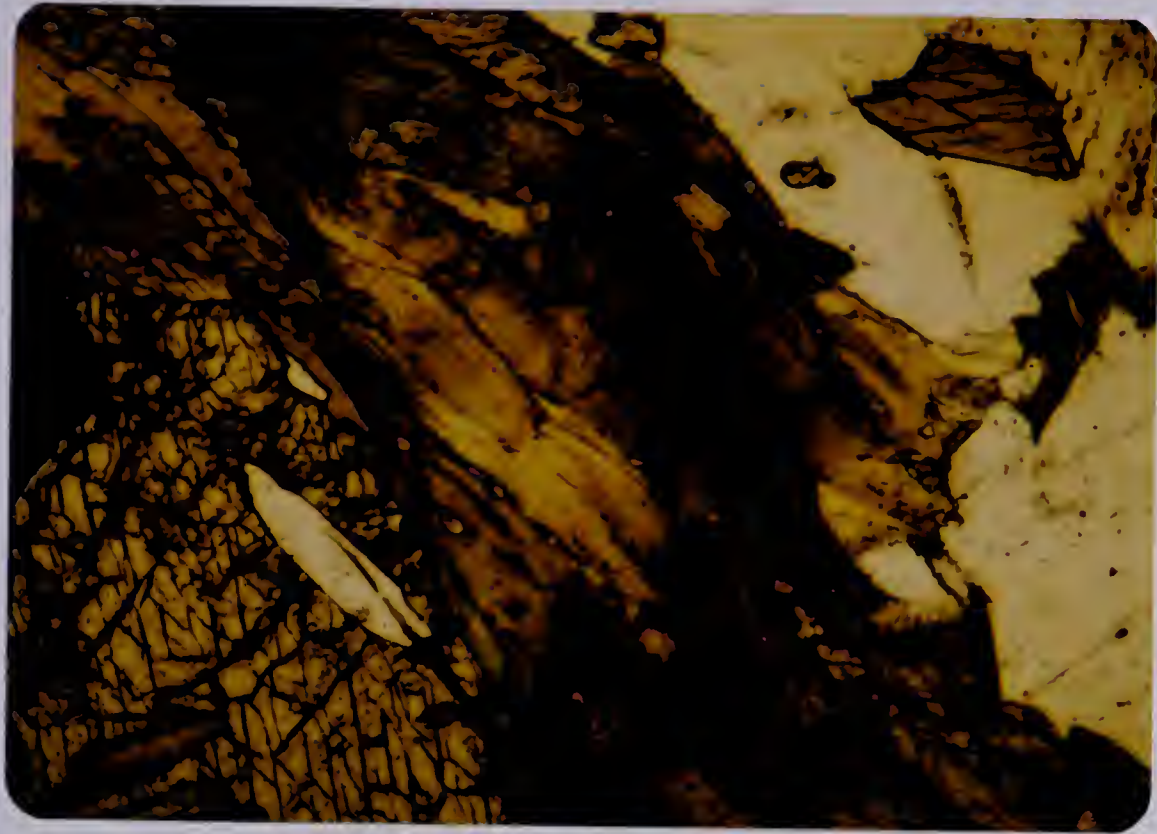


Plate 2.1 Photomicrograph in plane polarized light of mafic gneiss (sample number AC8) from the C.N. Track, in the Malton Range, showing part of a biotite laminar in a shear zone traversing an earlier amphibole - plagioclase texture.



Plate 2.2 A composite amphibolite dyke, with a garnet amphibolite centre, intruding Leucocratic Gneiss, north of Mount Albreda.



reached upper amphibolite facies. The amphibole lineation is associated with the first period of metamorphism, and the shearing, biotitization and epidotization is associated with the second retrogressive metamorphic episode. The foliation is horizontal or dipping at small angles to the south.

The amphibolites west of the Trench contain <80% biotitized pale green hornblende, <40% slightly sericitized oligoclase, <30% red brown biotite and small amounts of quartz, chlorite and sphene. Some amphibolites contain garnets. Plate 2.2 shows a composite dyke with a garnet amphibolite centre and plate 2.3 shows the reaction rims around the garnets. This mineralogy again suggests at least two stages of metamorphism, the amphibolites and garnets crystallizing during the first metamorphic episode, whilst the biotitization, chloritization, epidotization, sericitization and shearing occurred during a later episode or episodes. The field relations show that most of the amphibolites postdate the hornblende gneisses.

### **2.2.3 Mafic Gneiss East of the Rocky Mountain Trench**

The hornblende gneisses in the Bulldog Creek and Mount Blackman areas east of the Trench have a mineralogy similar to those west of the Trench, except that epidote is much more abundant, consisting of up to 15% of the rock. Biotite is less abundant, being 0%–5% of the rock, suggesting less alkaline protoliths for these rocks. In the Mount Blackman Gneiss, quartz is more common (up to 20% of the rock) and oligoclase less common (down to 15%), suggesting a more silicic protolith for these rocks.

Retrogressive greenschist facies metamorphism, following amphibolite facies metamorphism, is evidenced by the kaolinized plagioclases and chloritized biotites. (Plate 2.4).

The amphibolites in the Mount Blackman area are similar to those found to the west of the Trench, but are often garnetiferous and are also more severely epidotized. They again appear to be younger than the hornblende gneisses, the latter being generally concordant with the felsic gneisses whilst the former outcrop as discordant mafic sheets. (Plate 2.5).







Plate 2.3 A garnet amphibolite dyke intruding Grey Gneiss, north of Mount Albreda. Note the reaction rims around the garnets.





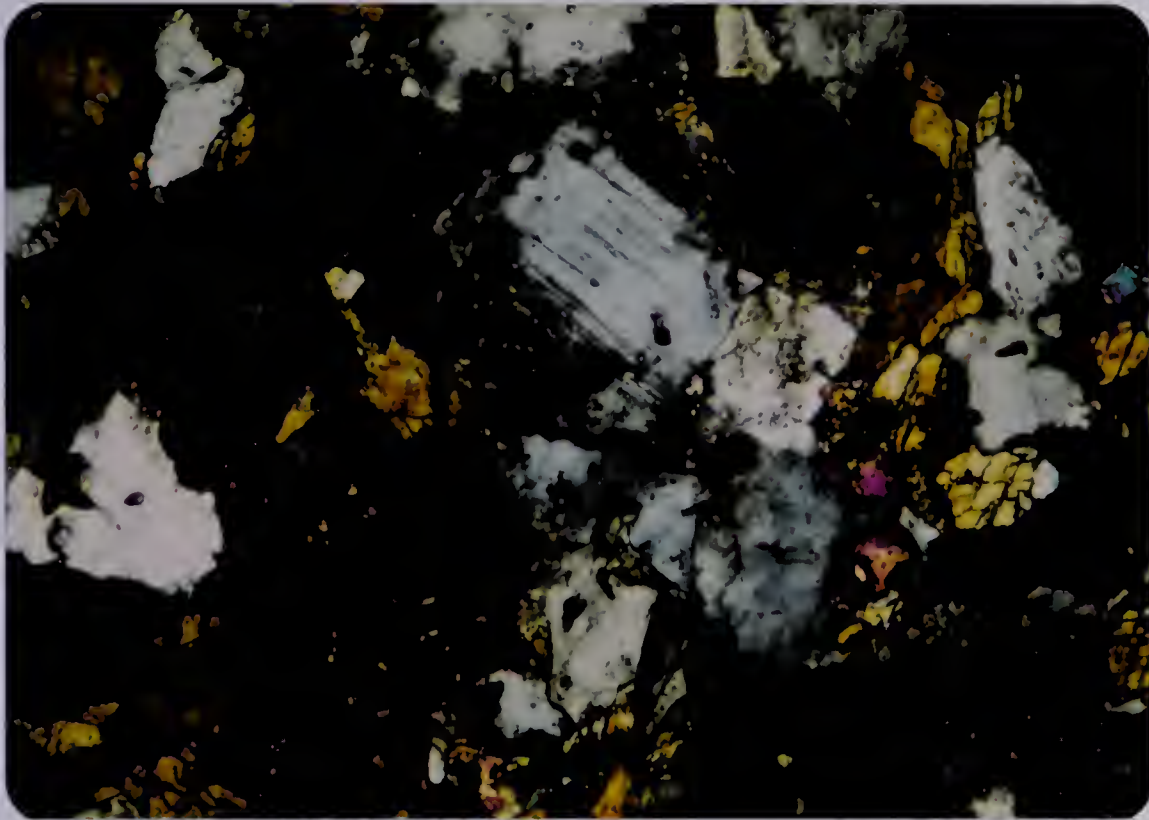


Plate 2.4 Photomicrograph, under crossed nicols, of mafic gneiss (sample number 5833) from the Bulldog Creek area, east of the Rocky Mountain Trench. Kaolinized plagioclases and chloritized biotites attest to the retrogressive metamorphism of this rock to Greenschist facies.



Plate 2.5 Discordant amphibolite sheet intruding felsic gneisses in the Mount Blackman area, east of the Rocky Mountain Trench.





## 2.3 Felsic Gneisses

### 2.3.1 Introduction

There are six main types of felsic gneiss in the Malton Gneiss Complex. Three of them, termed Grey Gneiss, Leucocratic Gneiss and Augen Gneiss, are exposed only in the Malton Block which lies to the west of the Rocky Mountain Trench. Three more types occur in each of the three main gneissic areas to the east of the Trench, namely the Bulldog Creek area, the Mount Blackman area and the Hugh Allan Creek area.

### 2.3.2 Grey Gneiss

The Grey Gneiss was so named because of its geochemical similarity to the Grey Gneiss of the North Atlantic craton (Chamberlain *et al.* 1980a). (Plate 2.6). The gneisses are non-porphyroblastic and lineated or foliated. The width of the banding varies from 1 mm to 20 mm, and the colour varies from light to dark grey according to the proportion of biotite. Many samples contain small subhedral to anhedral garnets, some of which are hollow, spongy or epidotized. (Plate 2.7). This is the only visible sign of retrogressive metamorphism, the rocks in general showing no evidence of an unusual metamorphic history nor of greatly disturbing metasomatism. Their high potassium and low calcium contents may be indicative of slight alkali metasomatism, and their occasional cataclastic texture evidence of late shearing. This shearing is probably related to fault movement, because it is especially evident in those Grey Gneisses outcropping along Highway 5, which follows the line of a major fault, the North Thompson Fault. The gneisses here are frequently cataclastic, containing deformed plagioclases, granulated quartz and bent biotites, as well as much epidote and muscovite. The type locality for the Grey Gneiss of the Malton Gneiss Complex occurs 9 km. up the C.N. Track on Mount Thompson at the northern end of the Malton Range, where the gneisses are generally concordant with the hornblende gneisses outcropping in the same locality, dipping at low angles to the south.

The mineralogy of the Grey Gneiss is albite-oligoclase (20%–50%), microcline (or occasionally orthoclase microperthite) (0%–30%), quartz (10%–30%), biotite (5%–15%), garnet (<15%) and epidote (<5%), together with much sphene, occasional apatite, allanite,







Plate 2.6 100m. high cliff of Grey Gneiss on the north side of Moonbeam Creek in the Monashee Mountains.





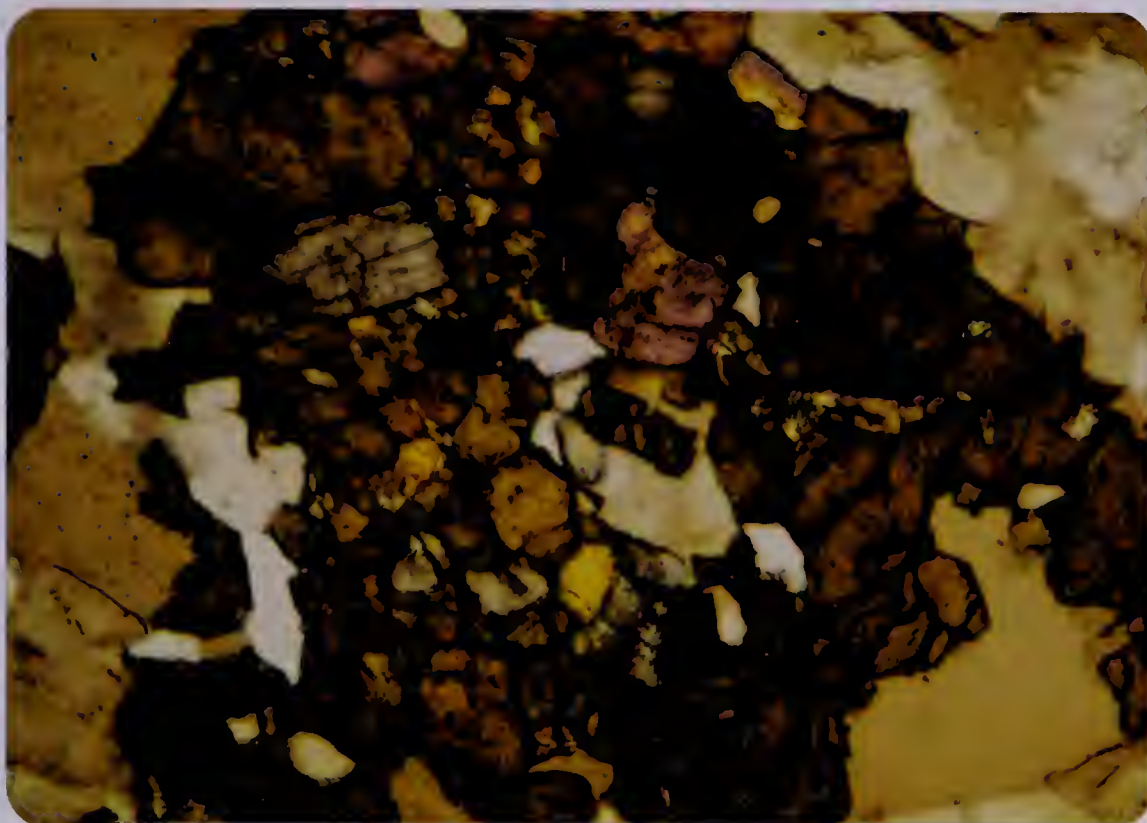


Plate 2.7 Photomicrograph in plane polarized light of Grey Gneiss (sample number 5498), from the type locality on the C.N. Track, showing a spongy garnet porphyroblast with an epidote core.



Plate 2.8 Photomicrograph in plane polarized light of Leucocratic Gneiss (sample number 6152F), from a corrie north of Mount Albreda, showing the very dark green pleochroic colour of the amphiboles.





oxide and zircon, and rare deep green hornblende. Hence, these gneisses are classified as leucocratic to mesocratic tonalitic gneisses.

### 2.3.3 Leucocratic Gneiss

The Leucocratic Gneiss is a lineated to well foliated leucocratic to hololeucocratic gneiss, often sheared or granulated. It outcrops in the Malton Block as granitic sheets or minor intrusives into the mafic gneisses and the Grey Gneiss. Its mineralogy is that of a mildly peralkaline granite gneiss. Quartz, plagioclase and K-feldspar occur in about equal proportions (up to 30% each). The plagioclase is normally oligoclase but is sometimes albite. The K-feldspar is almost always microcline, but occasionally orthoclase. Biotite is <10% and is frequently chloritized. Amphibole, when present, is of a distinctive deep green colour, verging on opaque, (plate 2.8) suggesting that it is riebeckitic and hence that the rock is mildly peralkaline. Epidote is rare, and may be replacing amphibole and allanite in a retrogressive metamorphic episode. Sphene is the most common of the accessories, but apatite, zircon, oxide, rutile, tourmaline and garnet are frequently present and secondary muscovite and calcite occasionally so. Field relationships show that the Leucocratic Gneiss is one of the youngest in the Complex. It cross cuts the Grey Gneiss, the hornblende gneiss (plate 2.9) and the Augen Gneiss (plate 2.10), but is itself cut by younger amphibolites. (Plate 2.11).

### 2.3.4 Augen Gneiss

The Augen Gneiss outcrops around and southeast of Mount Albreda. It has a mineralogy similar to that of the Leucocratic Gneiss, but the texture is more irregular and the K-feldspar tends to occur in augen. Riebeckitic amphibole is absent, and magnetite and garnet are much more common in this rock type than in the Leucocratic Gneiss, being almost ubiquitous. The presence of microperthite may be evidence of the meta-igneous character of this gneiss whilst the secondary feldspar overgrowths (plate 2.12), together with the lineated augen (plate 2.13), provide evidence of its polymetamorphic character. Epidote and chlorite give evidence of later retrogressive metamorphism.





Plate 2.9 Sheets of Leucocratic Gneiss intruding hornblende gneisses, near Mount Thompson in the Malton Range.



Plate 2.10 Sheet of Leucocratic Gneiss intruding Augen Gneiss, near the head of Clemina Creek in the Monashee Mountains.







Plate 2.11 Early Leucocratic Gneiss intruded by later Leucocratic Gneiss, and then by a mafic dyke, north of Mount Albreda.

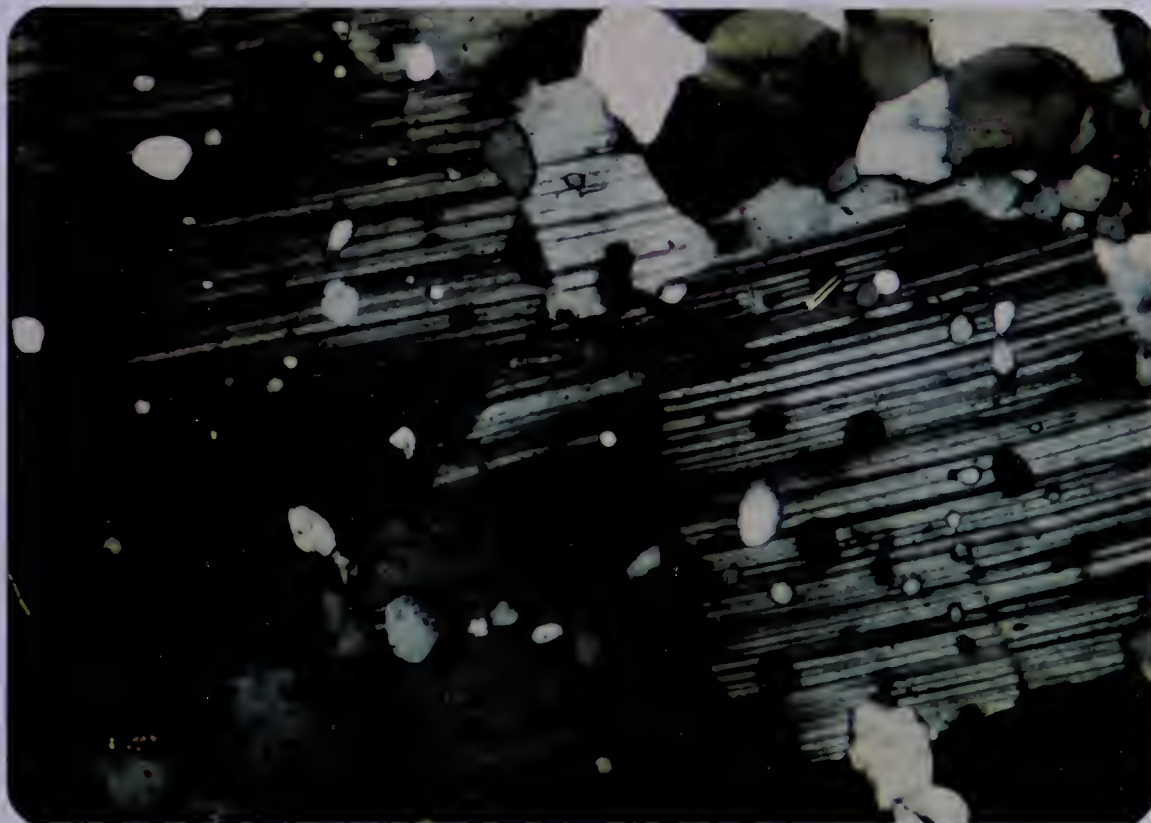


Plate 2.12 Photomicrograph under crossed nicols of Augen Gneiss (sample number 5901N), showing evidence of two metamorphisms: Microperthite and plagioclase form overgrowths on an original metamorphic texture.





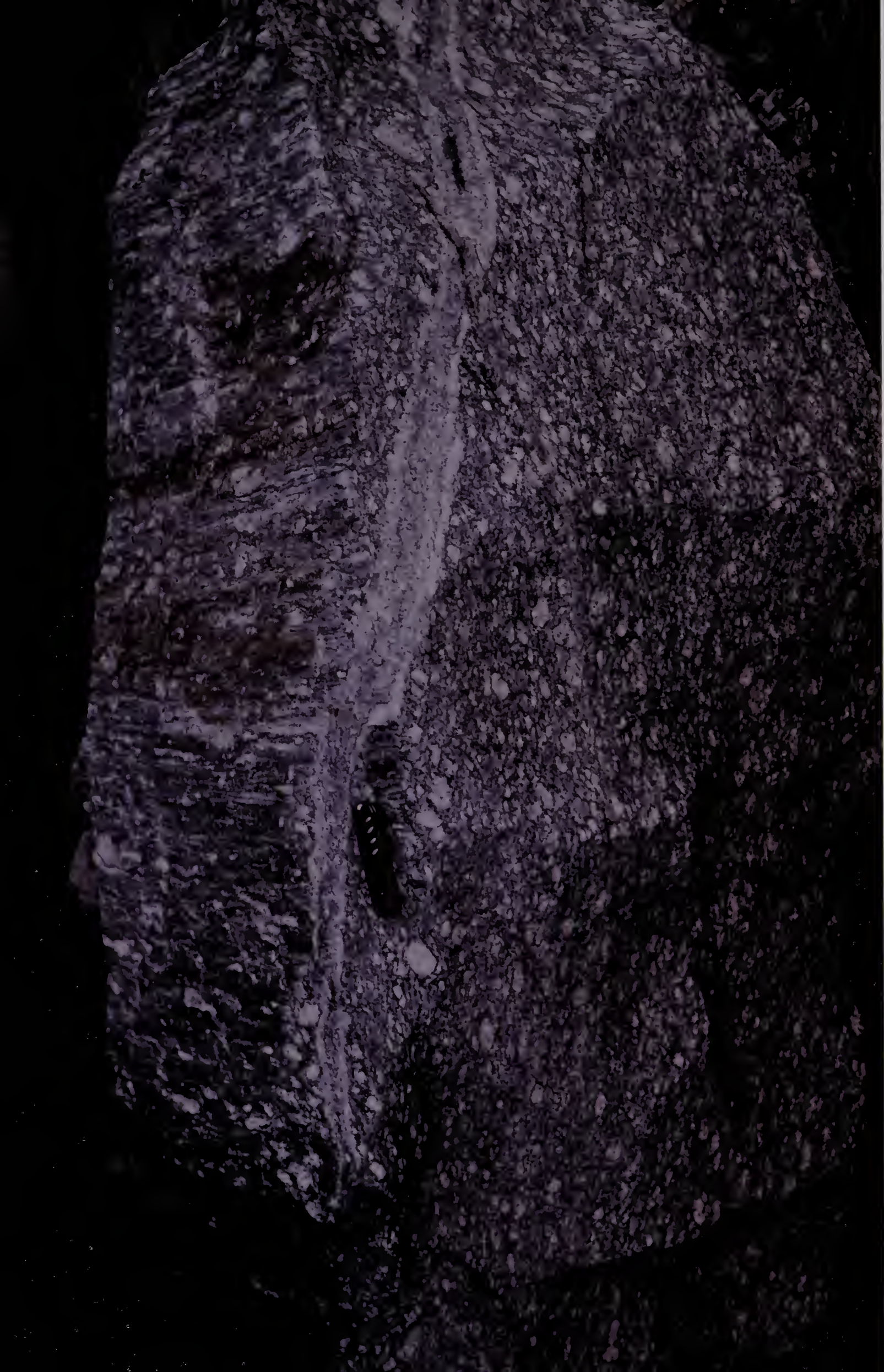


Plate 2.13 Augen Gneiss showing lineated augen, evidence of the polymetamorphic character of this rock.





### 2.3.5 Felsic Gneiss from the Bulldog Creek Area

The felsic gneisses from the Bulldog Creek area are quartz diorites, having modal quartz, oligoclase, biotite, (hornblende) and sphene. The rocks are frequently cataclastic or granulated, indicating post-metamorphic shearing, and the presence of biotite on these shear planes indicates that the shearing took place at relatively high temperatures. Epidote (sometimes replacing allanite (plate 2.14)), clinozoisite, chlorite and muscovite are indicators of a later retrogressive metamorphic event. Oxides and calcite are also occasionally present.

### 2.3.6 Felsic Gneiss from the Mount Blackman Area

The felsic gneisses from Mount Blackman, north of Hugh Allan Creek, are granulated muscovitic quartzites. The texture of the grains, the preponderance of muscovite and the virtual absence of ferromagnesian minerals suggest that they are paragneisses. (Plate 2.15). Both plagioclase and microcline occasionally form porphyroblasts up to about 5 mm long. The K-feldspar is microcline (sometimes microperthitic) and the plagioclase oligoclase (frequently sodic). 5%–10% biotite is sometimes present, but hornblende and garnet are absent. Thus the metamorphic grade of these gneisses appears to be lower amphibolite facies. Apatite is the most common of the accessories, but sphene, oxides and zircon also occur. Epidote, chlorite and calcite are rare, because of the primary petrology of the rocks, but their occasional presence suggests later retrogressive metamorphism in this area.

### 2.3.7 Felsic Gneisses from the Hugh Allan Creek Area

The felsic gneisses from the Hugh Allan Creek Gneiss, south of Hugh Allan Creek, are granitic gneisses, with a high quartz content. Their mode is quartz 40%, microcline (often microperthitic) 20%, sodic oligoclase 20%, biotite 10%, chlorite 5%, sphene 5% with accessory oxides. Garnet is sometimes present and is usually altered to epidote, again suggesting at least two periods of metamorphism.



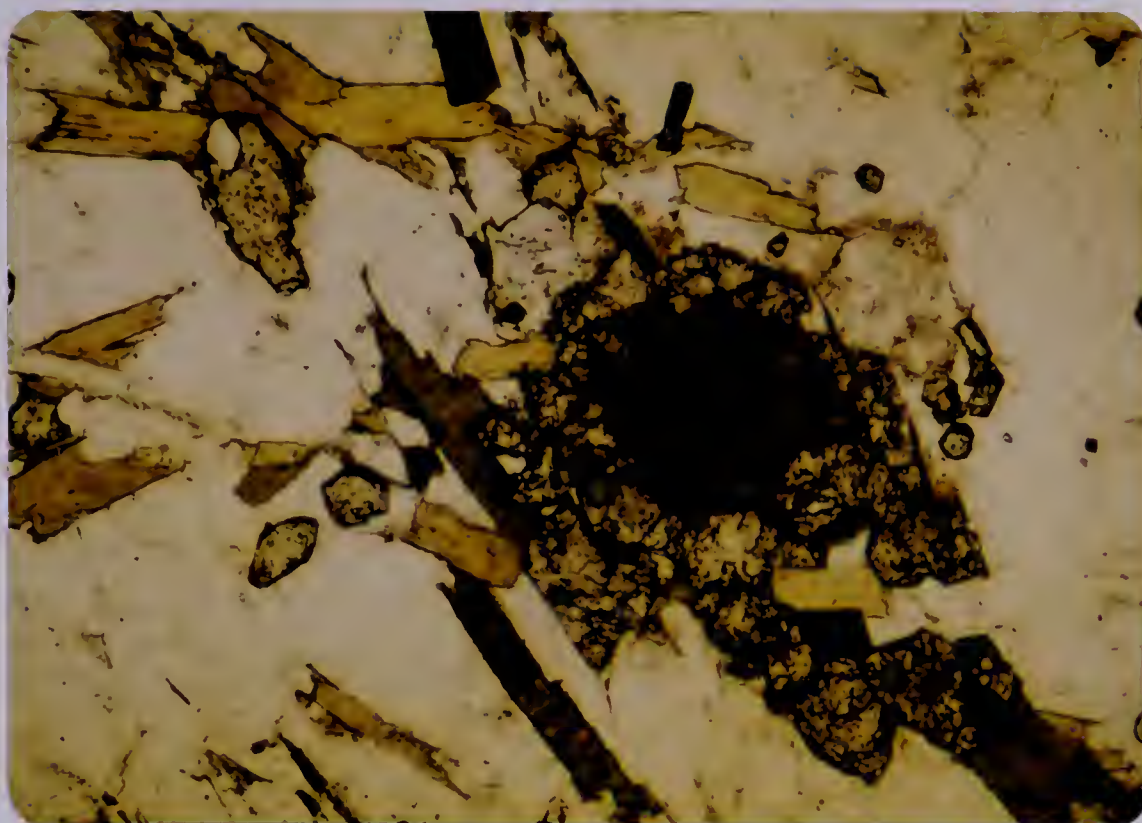


Plate 2.14 Photomicrograph in plane polarized light of Bulldog Creek Gneiss (sample number 5831C), showing epidote replacement of allanite.

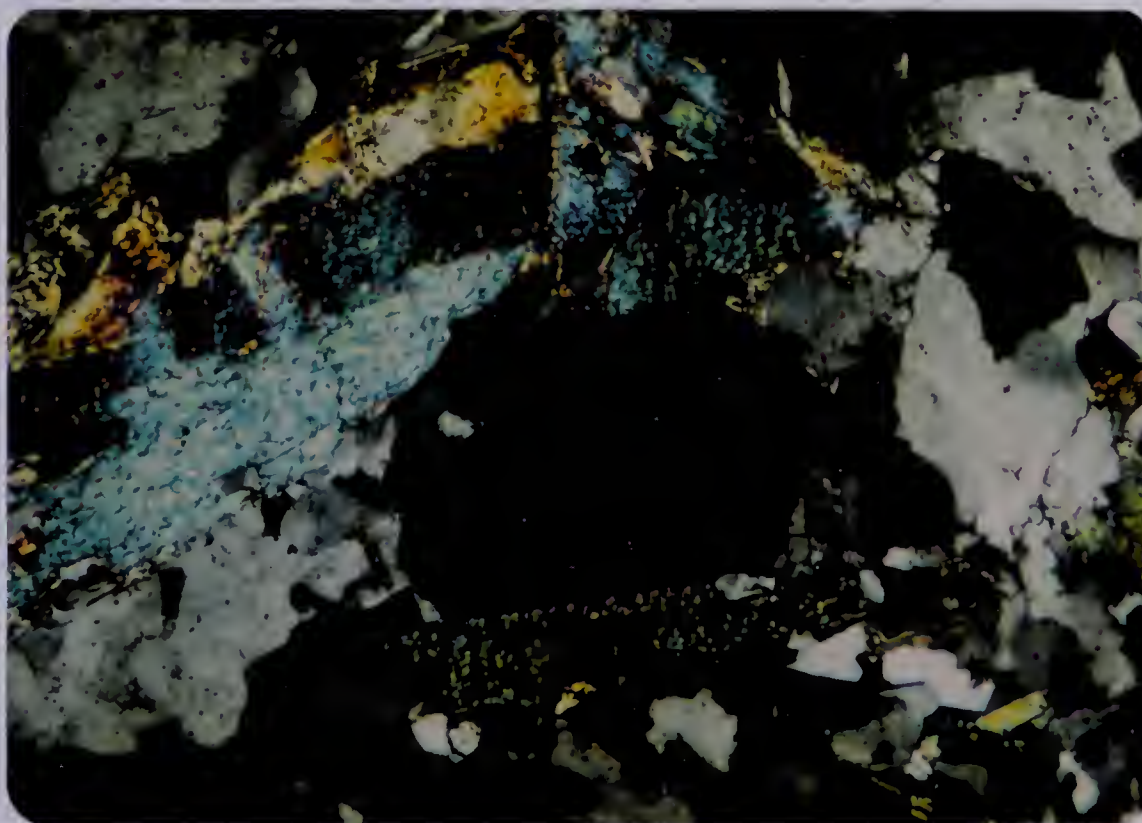


Plate 2.15 Photomicrograph under crossed nicols of Mount Blackman paragneiss (sample number 5890B), showing deformed muscovite and the gritty texture typical of a metasediment.





## 2.4 Metasediments

### 2.4.1 Introduction

Metasedimentary formations surround the gneisses of the Malton Gneiss Complex, the boundaries between gneiss and metasediment being almost always faulted. Kaza Group metasediments lie to the southwest of the gneiss complex, Miette Group metasediments to the northeast, and Monashee Horsethief Creek Group metasediments to the south. Outliers of metasedimentary rock lie on top of the gneisses over the northern part of the Malton Block, for example near Robina Creek, whereas at the southern end of the Malton Block, metasediments are infolded with the gneiss.

### 2.4.2 Metasediments from the Kaza Group

Metasediments from the garnet and the kyanite–staurolite zones of the Kaza Group are faulted against the western margin of the Malton Gneiss Block, and most samples show a granular or cataclastic texture. The most common rock type is a pelite, with a mineralogy of biotite, epidote, quartz, oligoclase, garnet and sphene. The psammitic layers contain >40% quartz, <40% oligoclase, 15% biotite, 5% muscovite, 5% garnet (or kyanite) plus accessory apatite and oxides, the latter sometimes occurring in heavy mineral layers. Deep brown tourmaline is fairly common, but sphene and zircon are rare. The primary mineralogy is typical of middle amphibolite facies, but the rocks have also suffered retrogression. Evidence of later retrograde metamorphism is shown by chloritized biotites, spongy partially chloritized or resorbed garnets and sericitized oligoclase. A band of calc–silicate in the Kaza Group, containing andesine ( $An_{36}$ ) and chlorite pseudomorphs after actinolite, outcrops on Highway 5, 11 km. south of Valemount.

### 2.4.3 Metasediments from the Robina Creek Area

Metasediments in the Robina Creek area overlie the gneisses of the Malton Block (plate 2.16), the contact being a 1 cm thick slide zone of 100% micaceous rock. The thrust plane dips south west at approximately  $20^\circ$ , and the foliation of the underlying Malton Gneiss is about  $30^\circ$  to the south east. The contact can be traced down the south





Plate 2.16 Robina Creek metasediments thrust over Malton Gneiss, at the head of Clemina Creek. The contact is near the head of the hammer.





wall of Robina Creek. (Plate 2.17). Below the slide zone, the gneiss is pulverized and consists of about 100 m of mylonitized quartzite, mylonitized muscovitic quartzite and mylonitized grey biotite gneiss. In places, there are lenses of staurolite schist within the gneiss. The metasediments above the slide zone consist of 20 m of biotite schist containing quartz and gneiss lenses, which may have been a conglomerate, overlain by 10 m of garnetiferous muscovite schist and at least 20 m of staurolite garnet schist.

#### **2.4.4 Metasediments from the Miette Group**

Metasediments from the garnet and the kyanite–staurolite zones of the Middle and Upper Miette Groups are faulted against the east side of the Rocky Mountain Trench. These metasediments are extremely immature, containing pebbles of feldspar. (Plate 2.18). The mineralogy of the psammites is very close to that of a granite, since quartz, K–feldspar and oligoclase are present in about equal amounts, together with about 10% biotite and with minor secondary muscovite, sericite, epidote and chlorite. The pelites and semi–pelites contain much oligoclase, often quite coarse grained, but little or no K–feldspar. Green–brown biotite, muscovite and quartz are also present, together with garnet or kyanite, tourmaline, rutile, zircon, sphene, epidote, calcite and primary and secondary chlorite. Apatite and oxide are rare. Retrogressive metamorphism is again evident from the spongy chloritized garnets. Post–metamorphic shearing and folding has occurred, chloritizing the muscovite flakes and bending them into spectacular isoclinal folds, as well as granulating many of the other minerals.

#### **2.4.5 Metasediments from the Monashee Horsethief Creek Group**

The Monashee Horsethief Creek Group metasediments are thrust over and infolded with the gneisses of the Malton Gneiss Complex along the southern boundary of the Malton Block. (Plates 2.19 and 2.20). These metasediments are extremely rich in iron (pelites average 13%  $\text{Fe}_2\text{O}_3$ ) and typically have a rusty appearance when weathered. (Plate 2.21). The original sediments appear to have been fairly immature sandstones and shales with many turbidite sequences. (Plate 2.22). In the Mount Lempriere area immediately south of the Malton Block, the metasediments have reached kyanite grade, and the polymetamorphic nature of the rocks is shown by their later chloritization.







Plate 2.17 The slide zone between the Malton Gneiss and the Robina Creek metasediments exposed on the south wall of Robina Creek.

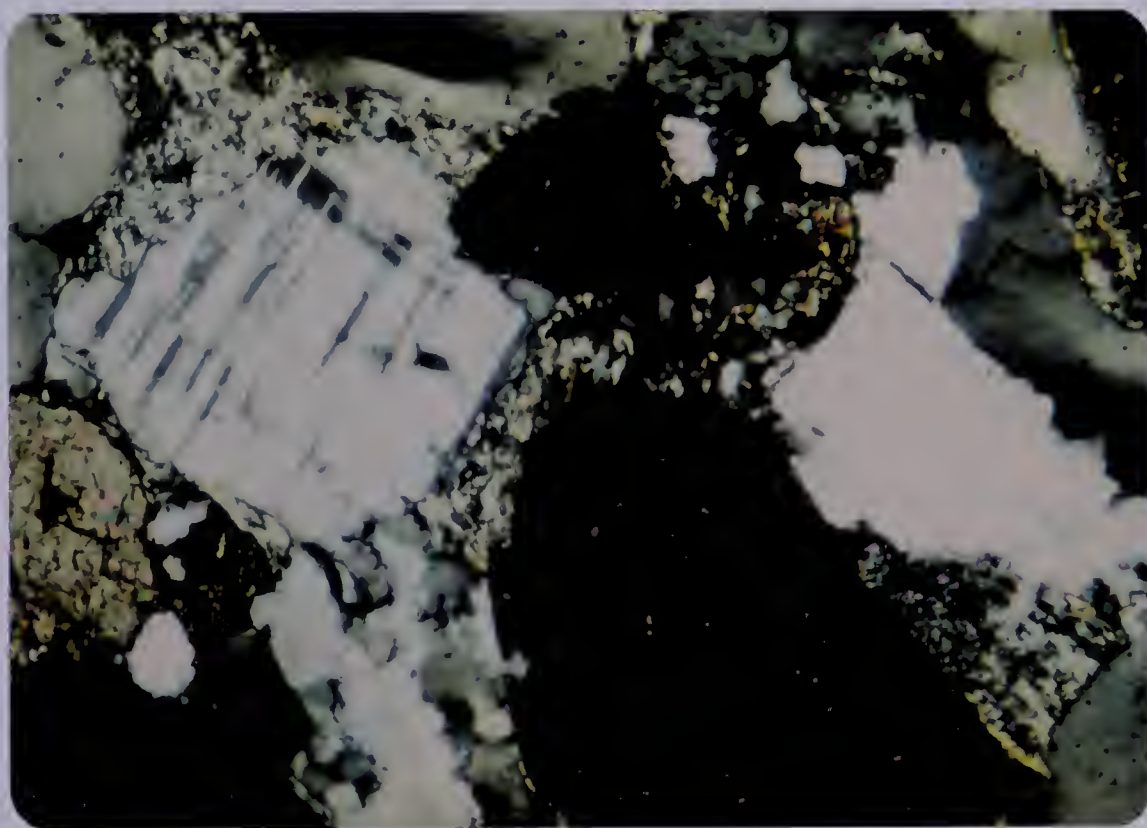


Plate 2.18 Photomicrograph under crossed nicols of Miette Group metasediment (sample number AC20), showing pebbles of feldspar.







Plate 2.19 Windfall Creek Thrust, showing the rusty weathered metasediments of the Monashee Horsethief Creek Group thrust over the Malton Gneiss on the south wall of Moonbeam Creek.





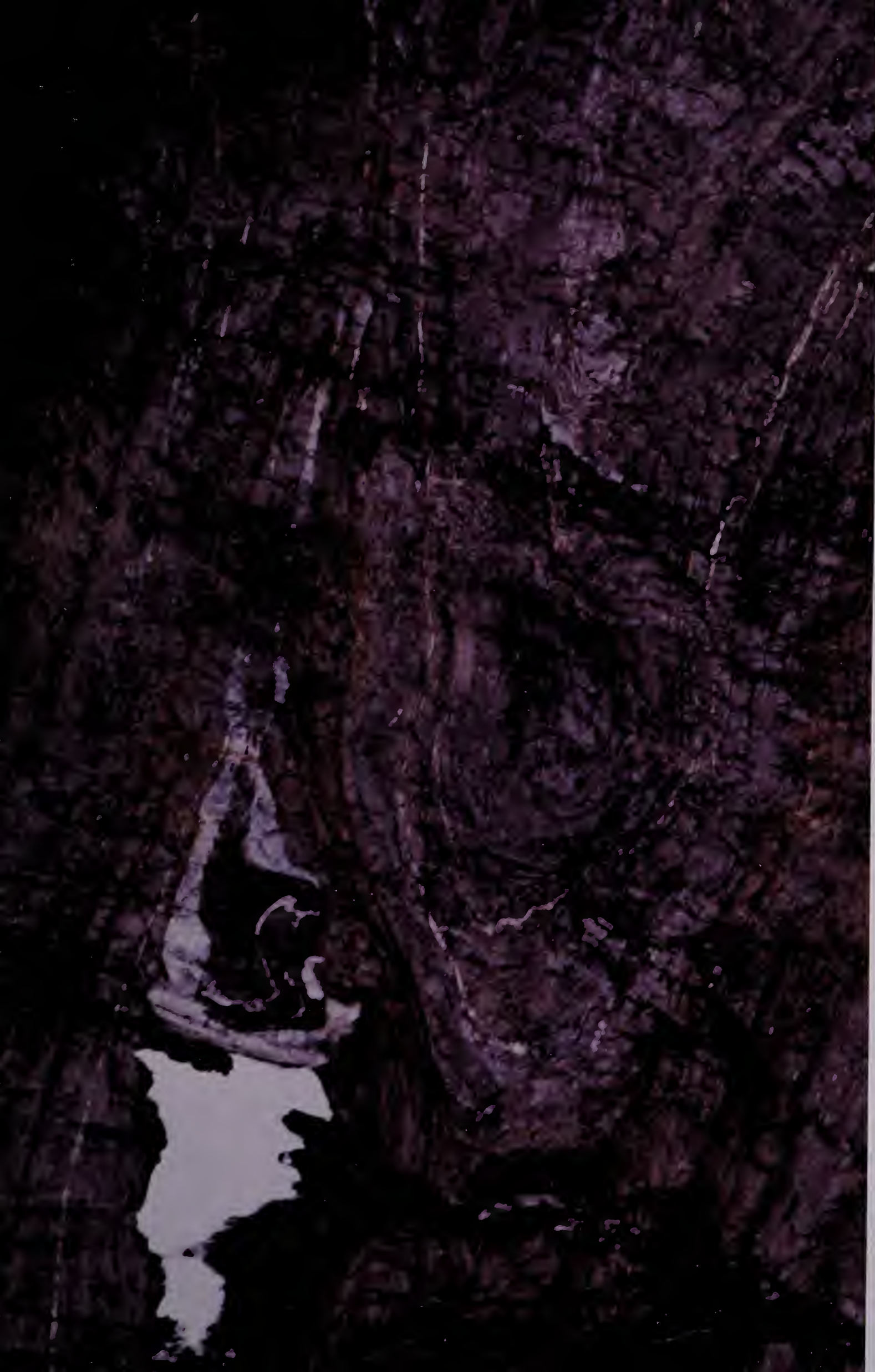


Plate 2.20 Infold of Malton Gneiss into the Monashee Horsethief Creek Group metasediments, above the Windfall Creek Thrust on the south wall of Moonbeam Creek.







Plate 2.22 Metaturbidites of the Monashee Horsethief Creek Group exposed on Highway 5, eight km. south of the Malton Block. The strong isoclinal folding on southward dipping axial planes is clearly visible. The sequence is intruded by an amphibolite dyke.



Plate 2.21 Rusty weathering kyanite grade metasediments of the Monashee Horsethief Creek Group in the foreground, with an infold of Malton Gneiss forming the peak of Dominion Mountain in the background.



### 3. GEOCHEMISTRY OF THE GNEISSES

#### 3.1 Introduction

The purpose of the geochemical study was to divide the gneissic complex into its separate components, and to establish, so far as is possible, the identity and petrogenesis of the precursors of each suite. The fulfillment of these objectives is hampered by the extent to which the rocks concerned have been in open chemical systems and by the lack of certainty concerning the chemical evolution of the crust and mantle and concerning Precambrian pre – plate tectonic igneous rock genesis.

The use of trace elements to elucidate the petrogenesis of rocks ,to estimate the original composition of altered rocks, and also, in several instances, to identify the tectonic settings of altered volcanic rocks (by the comparison of trace element composition of altered rocks with that of unaltered rocks) has been applied successfully by geochemists in recent years to rocks of all ages and from all parts of the world (Hallberg and Williams, 1972; Bloxham and Lewis, 1972; Bickle and Nisbet, 1972; Cosgrove, 1972; Pearce and Cann, 1973; Lambert and Holland, 1974; Winchester and Floyd, 1976; Weaver *et al.*, 1981; Winchester *et al.*, 1981). Pearce and Cann defined the characteristics ideally required in an element (or combination of elements) to be used in identifying magma types. These included insensitivity to secondary processes, ease of measurement and concentration variations which are greater between samples of different magmatic types than between samples of the same magmatic type. The elements found to best fulfill these conditions were Ti, Zr, Y, Nb, Cr and Ni. (Cann 1970, Pearce and Cann 1973, Field and Elliot 1974).

Thus, the problems of open system behaviour in the Malton Gneiss Complex should be largely overcome by studying the supposedly immobile elements Ti, Zr, Nb and Y to identify possible gneissic precursors; by studying the ratios of these immobile elements, for example Nb/Y, to characterize rock suites; and by studying the ratio of specific trace elements to the major elements for which they commonly substitute, Y : Ca for example, to identify fractionation trends. AFM plots are also used to show fractionation trends, SiO<sub>2</sub> histograms to provide basic generalizations about the overall geochemistry, and factor analysis to show the overall variation and to provide labels for







the various divisions.

Geochemical diagrams shown in Chamberlain *et al.* (1980b) are not repeated here, unless they show some especially important feature. Those not repeated include Sr v Rb, K v Rb, Sr v Ba, K v Ba, Y v  $\text{Fe}_2\text{O}_3/(\text{Fe}_2\text{O}_3 + \text{MgO})$  and  $\text{SiO}_2$  v  $(\text{Na}_2\text{O} + \text{K}_2\text{O})$ . Plots which showed nothing of significance include K v Sr, Y v Zr and Q-Ab-Or.

### 3.1.1 Sample Collection and Analysis

The complex was divided into five geographical areas and collections were made from each area to a total of nearly 250 samples. Suitable collection sites were severely limited by the vegetation and topography, since the lower slopes are covered by glacial debris and dense forest, and the upper slopes contain much weathered material and are difficult of access, consisting of sheer vertical cliffs in many places. Creeks tended to be either sheer sided or full of alluvium. The few road cuts in the area provided good samples, but the majority of suitable locations were inaccessible by road, and were sampled by foot, helicopter, boat or ski. At each location, samples were selected as objectively as possible to form a representative suite.

The five geographical areas are the C.N. Track, the Malton Range and the Monashee Mountains areas to the west of the Rocky Mountain Trench; and the Bulldog Creek and Mount Blackman areas to the east of the Rocky Mountain Trench. Sample localities and geographic areas are shown on figure 3.1.

The C.N. Track, at the northern end of the Malton Range, was extensively sampled and a representative suite of about 50 rocks collected. In the Malton Range area, which extends south from Canoe River as far as Clemina, and which includes all parts of the Malton Range except the C.N. Track vicinity, about 40 samples were collected, from 10 different locations. In the Monashee Mountains area, extending south from Clemina to Lempriere, and including only the extreme northern part of the Monashee Mountain Range, about 80 samples were collected from 11 locations. To the east of the Rocky Mountain Trench, a small collection of about 15 rocks was made in the fairly inaccessible Bulldog Creek area, taken mostly from around the mouth of the creek. A collection of about 60 rocks was made in the Mount Blackman area, taken from four locations to the north of Hugh Allan Creek, and one to the south.









The samples were analysed by Dr. J. G. Holland, at Durham University, England, using a PW 1212 X-ray spectrometer. Eleven major elements and between nine and fourteen trace elements (Ba, Nb, Zr, Y, Sr, Rb, Zn, Cu and Ni  $\pm$  Ce, La, Co, Cr, V, Sc and Li) were determined using both international (Flanagan 1973), and a set of specially cast glass (Brown *et al.*, 1970), standards. Analyses are given in Appendix A.

### 3.2 Geochemistry of the Different Sub-Units of the Malton Gneiss

In Chamberlain *et al.* (1980a) and (1980b), it was shown that the gneissic rocks of the Malton Gneiss Complex are largely meta-igneous. Those to the west of the Rocky Mountain Trench were subdivided into four types, characterised by their petrology and Y/Nb ratios. Further study on more samples has shown that these rocks appear to be a composite of several units with different tectonomagmatic histories. The overall petrogenesis is that of a bimodal suite or suites, cut by later intrusives. In detail it appears that the bimodal suites may well be composed of two unrelated parts, locally intruded by unrelated later melts.

Figure 3.2 shows silica histograms for the rocks analysed from each area. Each histogram, except that for the Bulldog Creek area, shows a Daly gap at approximately 53% – 58% silica (Daly 1925). Yoder (1973) suggested that such bimodal suites are formed by fractional melting. The later granitic intrusions in the C.N. Track, Malton Range and Monashee Mountains areas show up on these histograms at the 70% – 80% silica content level.

The discussion which follows is divided by rock type, so that the petrogenetic and geographic distinctions can be considered simultaneously.

### 3.3 Mafic Gneisses

The average analyses of mafic gneisses from each of the five geographical areas are shown in table 3.1, together with an average DSDP 37 tholeiite, Nockolds' (1954) average tholeiitic basalt and Goodwin and Smith's (1980) averages for Abitibi tholeiite and calc-alkaline andesite. The igneous precursors of the mafic gneisses of the Malton Gneiss Complex appear, by their silica content and by  $20\% > \text{CaO} + \text{MgO} > 12\%$  (Pearce





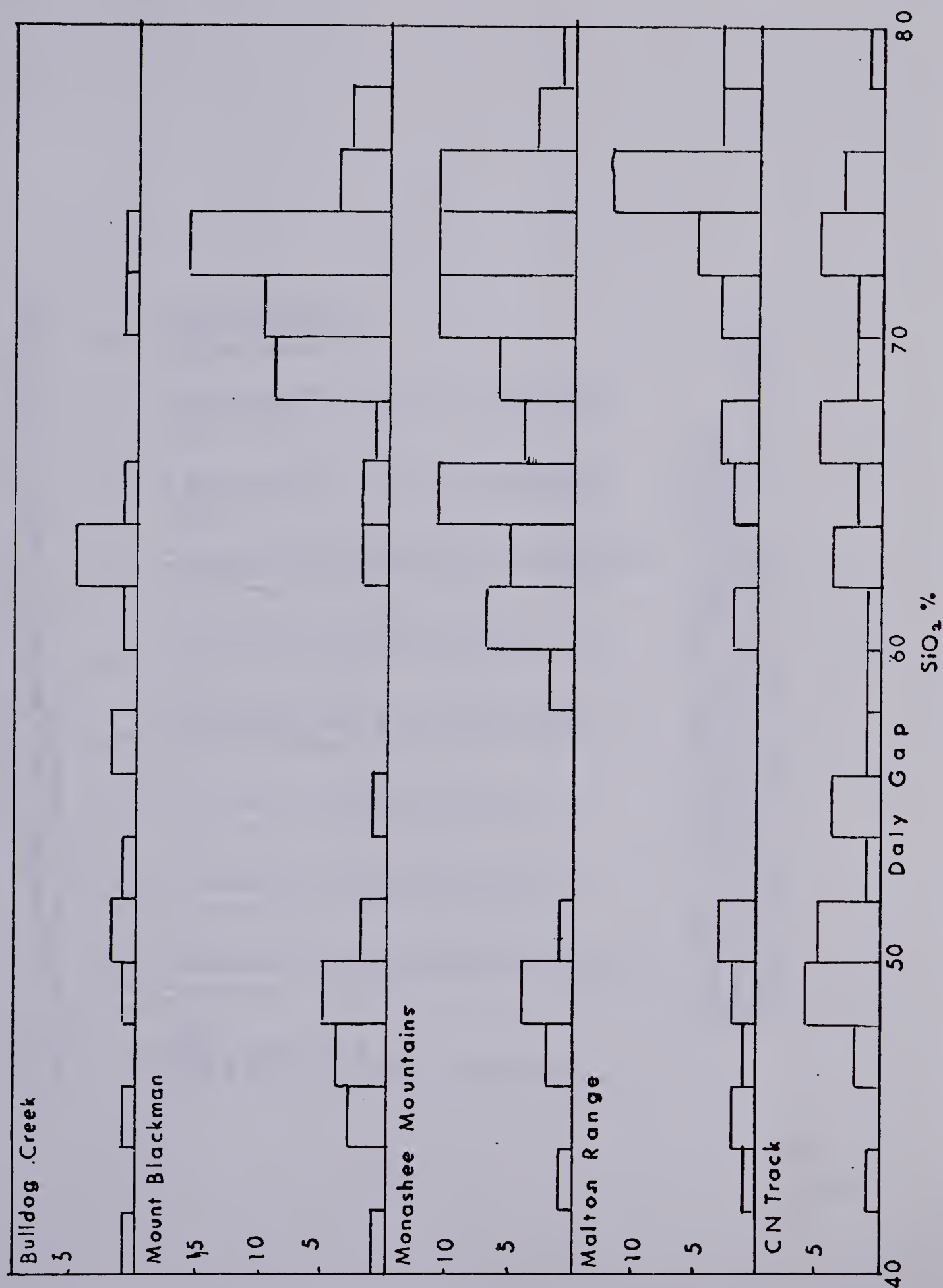


Figure 3.2  $\text{SiO}_2$  histograms for the gneissic rocks of the Malton Gneiss Complex



Table 3.1 Mean analyses of mafic gneisses of the Malton Gneiss Complex compared with those of igneous rocks

n	1	2	3	4	5	6	7	8	9
	21	9	8	8	13				
SiO <sub>2</sub>	51.19	47.82	47.88	49.28	48.29	49.61	48.00	56.90	50.83
Al <sub>2</sub> O <sub>3</sub>	13.94	14.17	14.41	14.57	13.71	15.62	13.90	16.10	14.07
Fe <sub>2</sub> O <sub>3</sub>	12.32	13.33	15.21	13.88	15.00	9.99	13.20	7.57	12.87
MgO	6.31	8.50	5.81	6.59	8.17	7.75	7.30	4.20	6.34
CaO	8.38	9.22	8.33	7.39	8.76	12.64	8.80	5.70	10.42
Na <sub>2</sub> O	2.97	2.75	2.89	2.29	1.97	2.12	2.69	3.65	2.23
K <sub>2</sub> O	2.18	1.92	3.16	3.34	1.90	0.24	0.20	0.95	0.82
TiO <sub>2</sub>	1.44	1.54	2.14	2.00	1.87	0.99	1.30	0.82	2.03
MnO	0.20	0.21	0.24	0.18	0.20	0.16	0.21	0.21	0.18
S	0.01	0.01	0.08	0.47	0.04	0.15			
P <sub>2</sub> O <sub>5</sub>	0.55	0.39	0.72	0.47	0.27	0.07	0.13	0.13	0.23
Ba	856	439	824	856	445	66	110	218	
Nb	36	32	51	31	11	9			
Zr	196	139	236	238	93	57	82	84	
Y	33	32	41	41	18	24			
Sr	383	284	343	452	67	108	124	173	
Rb	59	78	102	102	119	5			
Zn	163	148	150	133	35	70	77	64	
Cu	25	21	31	64	130	75	99	62	
Ni	68	100	43	38	47	124	232	67	
Co	88			103		46	39	26	
Cr	159	137	46	82	100	288	292	89	
V	214					229	406	198	
Li	9					10			
Sc	19					42			

KEY 1=C.N. track 2=Malton Range 3=Monashee Mountains  
 4=Bulldog Ck 5=Mount Blackman 6=Mean DSDP37 basalt  
 7=Mean Abitibi tholeiite (Goodwin and Smith, 1980)  
 8=Mean Abitibi calc-alkaline andesite (Goodwin and Smith, 1980)  
 9=Normal tholeiitic basalt (Nockolds, 1954)





and Cann, 1973), to have been basalts.

The mafic gneisses to the west of the Rocky Mountain Trench, in the C.N. Track, Malton Range and Monashee Mountains areas, have most major elements similar to Goodwin and Smith's (1980) average Abitibi tholeiite, but  $K_2O$ ,  $P_2O_5$ , and many trace elements, including Ba, Zr and Sr are distinctly high, suggesting that the igneous precursors of these rocks were formed from alkali olivine basalt magmas, formed by olivine and/or pyroxene fractionation (Cu, Ni and Cr low). However, the individual analyses of these mafic gneisses show considerable scatter about the mean (tables 1, 5 and 9 in appendix A), suggesting that more than one mafic suite is present; or that a redistribution of the elements has occurred; or that the rocks originated as cumulates. The more mobile elements,  $K_2O$ , Ba and Sr, may have moved into these rocks since their formation, but there is no evidence in the rocks themselves to suggest that they have suffered partial melting or large scale mafic intrusion, which might mobilize Ti and Zr.

The mafic gneisses to the east of the Trench, especially in the Mount Blackman area, show greater similarity to the average Abitibi tholeiite,  $K_2O$ ,  $P_2O_5$ , Ba, Zr and Sr all being lower than in those gneisses to the west of the Trench, suggesting that the igneous precursors to the Mount Blackman mafic gneisses may have been tholeiitic basalts. However,  $K_2O$  is high, and CaO low compared with Nockolds' normal tholeiitic basalt and with the average DSDP 37 tholeiite, indicating that there may have been some exchange of potassium and calcium, perhaps during the biotitization of the amphiboles.

In figure 3.3, the mafic gneisses from each of the five geographical areas are plotted on an AFM diagram (after Irvine and Baragar, 1971): Most of the samples from the east of the Trench (Bulldog Creek and Mount Blackman) appear to be more tholeiitic than those to the west, but the diagram lacks sensitivity due to the considerable scatter, probably caused by mobility of the alkalis.

The petrogenesis of the mafic suites can be more accurately determined using the immobile trace elements. Winchester and Floyd (1976) have shown that Nb : Y ratios can be used to distinguish altered and metamorphosed alkaline rocks from tholeiitic rocks, provided that  $SiO_2 < 60\%$ , the alkaline rocks having  $Nb/Y > 0.66$ , and the tholeiitic rocks having  $Nb/Y < 0.66$ . Figure 3.4 shows that the majority of the mafic gneisses west of the Trench have Nb : Y ratios characteristic of alkaline rocks, whereas most of those to



- CN Track
- △ Malton Range
- Monashee Mountains
- + Bulldog Creek
- λ Mount Blackman

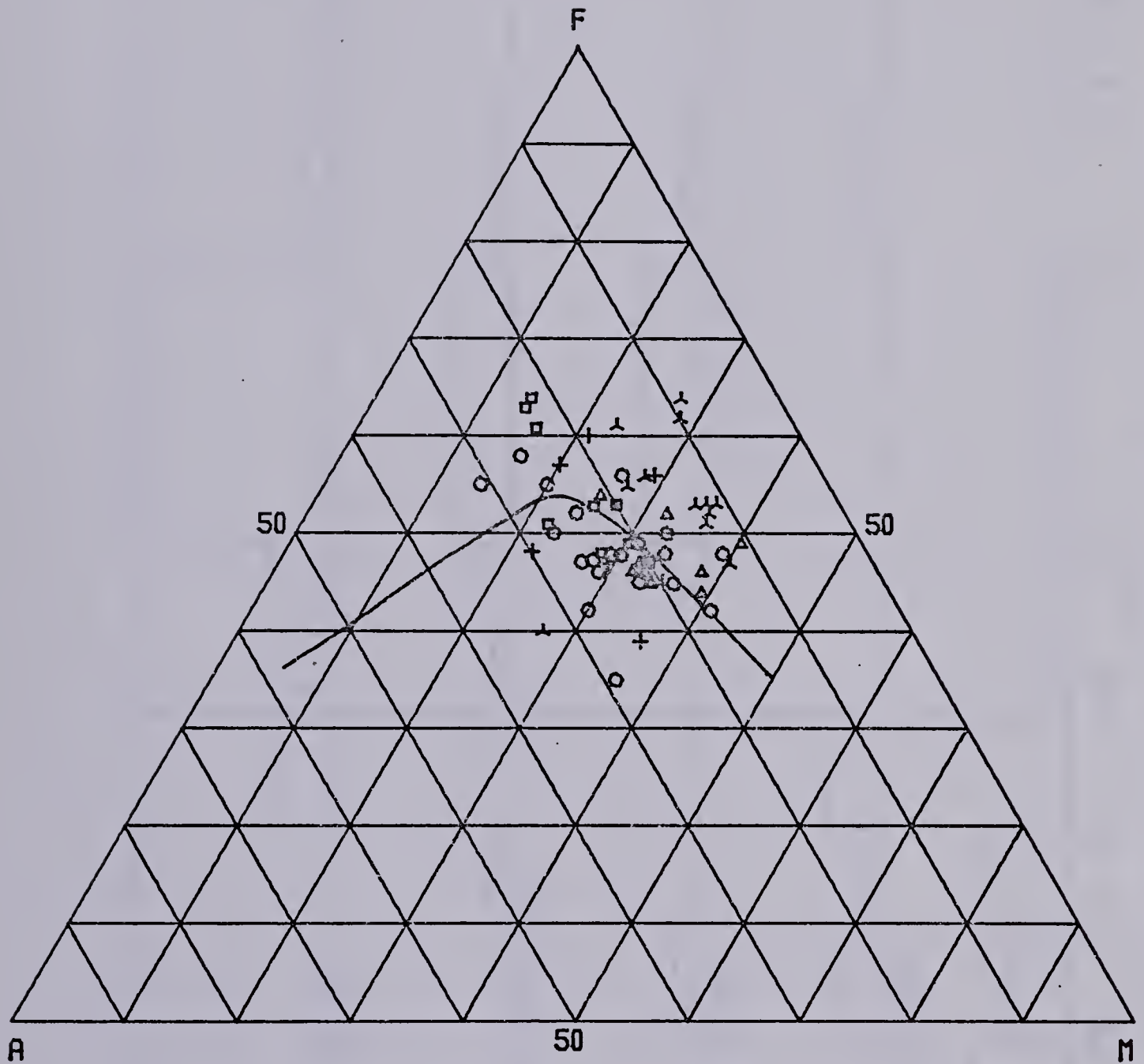


Figure 3.3 A-F-M triangular diagram for the mafic gneisses of the Malton Gneiss Complex



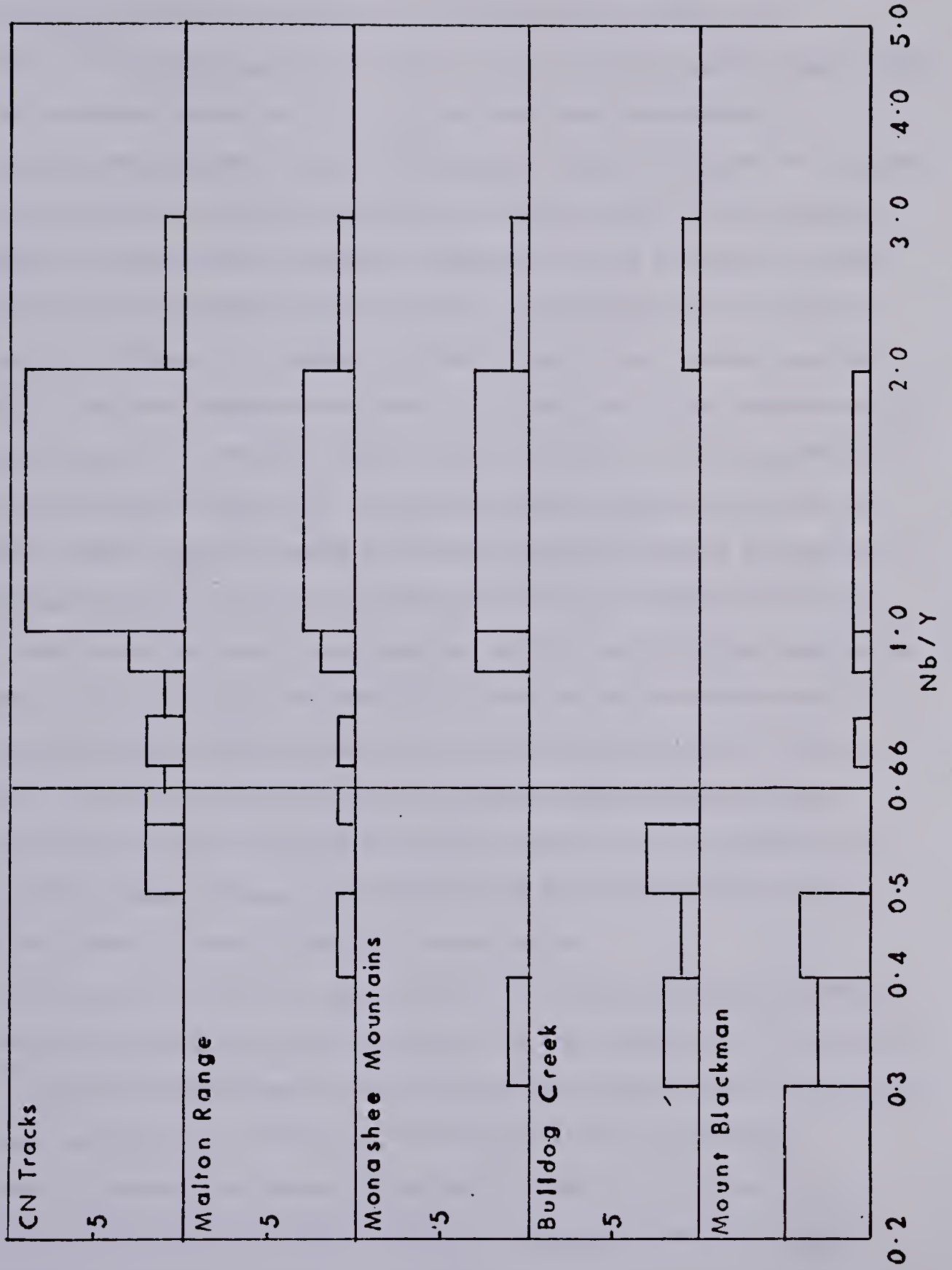


Figure 3.4 Nb/Y histograms for the mafic gneisses of the Malton Gneiss Complex





the east of the Trench have Nb : Y ratios characteristic of tholeiitic rocks.

Pearce and Cann (1973) have used  $Zr - Ti/100 - 3Y$  and  $Ti \text{ v } Zr$  plots for altered samples to discriminate between basalts from different tectonic settings, the  $Zr - Ti/100 - 3Y$  plot being used first, to identify the "within plate" basalts (oceanic island basalts and continental basalts), and the  $Ti \text{ v } Zr$  plot being used subsequently to discriminate between calc-alkali basalts, low potassium tholeiites and ocean floor basalts. Figures 3.5 and 3.6 show the mafic gneisses of the Malton Gneiss Complex plotted on these diagrams, but the plots are somewhat inconclusive. Figure 3.5 seems to indicate that most of the mafic gneisses west of the Trench were derived from calc-alkaline basalts, but most of these same gneisses plot well outside the calc-alkaline basalt field on figure 3.6. The mafic gneisses to the east of the Trench plot in calc-alkaline basalt or ocean floor basalt or low K tholeiite fields in figure 3.5 and both within and without the ocean floor basalt field on figure 3.6. Hence these diagrams appear not to work for these rocks. Little is known for certain about magma genesis during the Archean, but it is possible that plate tectonics was not established at the time that these rocks were formed. Alkali basalts are rare in the Archean, but not unknown: the Abitibi Greenstones have a small volume of trachyte, the Pittsburgh gneisses include some alkali basalts and the lowermost member of each sequence in the Talga Talga Supergroup of Pilbara are alkali basalts. Alternatively, these mafic rocks may be cumulates of alkaline gabbro affinity, the scatter of points on figure 3.6 being consistent with this suggestion: the Ti and Zr contents of lavas are usually more uniform, and since Ti and Zr are extremely immobile, the scatter is unlikely to be due to remobilization.

Fractionation trends also may be deduced from figure 3.6, which shows that the mafic gneisses to the west of the Trench are very rich in Zr, and have low Ti : Zr ratios, possibly indicating original formation involving subordinate magnetite and/or hornblende fractionation (Lambert *et al.*, 1974; Drury, 1983, figure 6) although hornblende fractionation is considered an unlikely petrogenesis for mafic rocks (Weaver *et al.*, 1981). These gneisses also have high Ti contents, which, coupled with their high Zr contents may be an indication of garnet fractionation, with high temperature, high  $PH_2O$  conditions of formation (Lambert *et al.*, 1974). However, Y contents are high, 20–60 ppm in all these mafic suites, compared with 20–25 ppm Y in standard modern



- CN Track
- △ Malton Range
- Monashee Mountains
- + Bulldog Creek
- ^ Mount Blackman

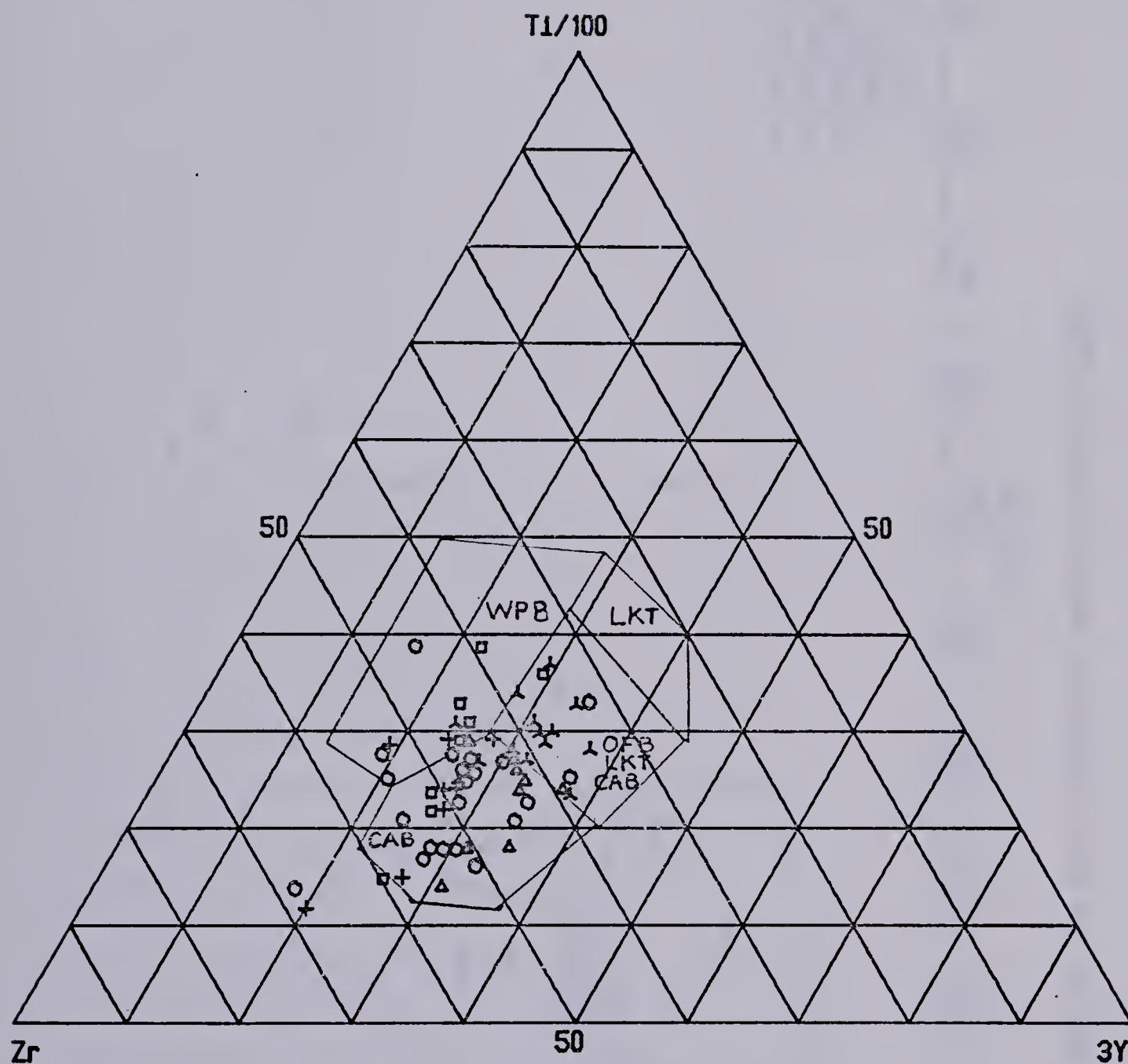


Figure 3.5 Zr-Ti/100-3Y triangular diagram for the mafic gneisses of the Malton Gneiss Complex. (CAB = calc-alkali basalts; LKT = low potassium tholeiites; OFB = ocean floor basalts; WPB = within-plate basalts.)





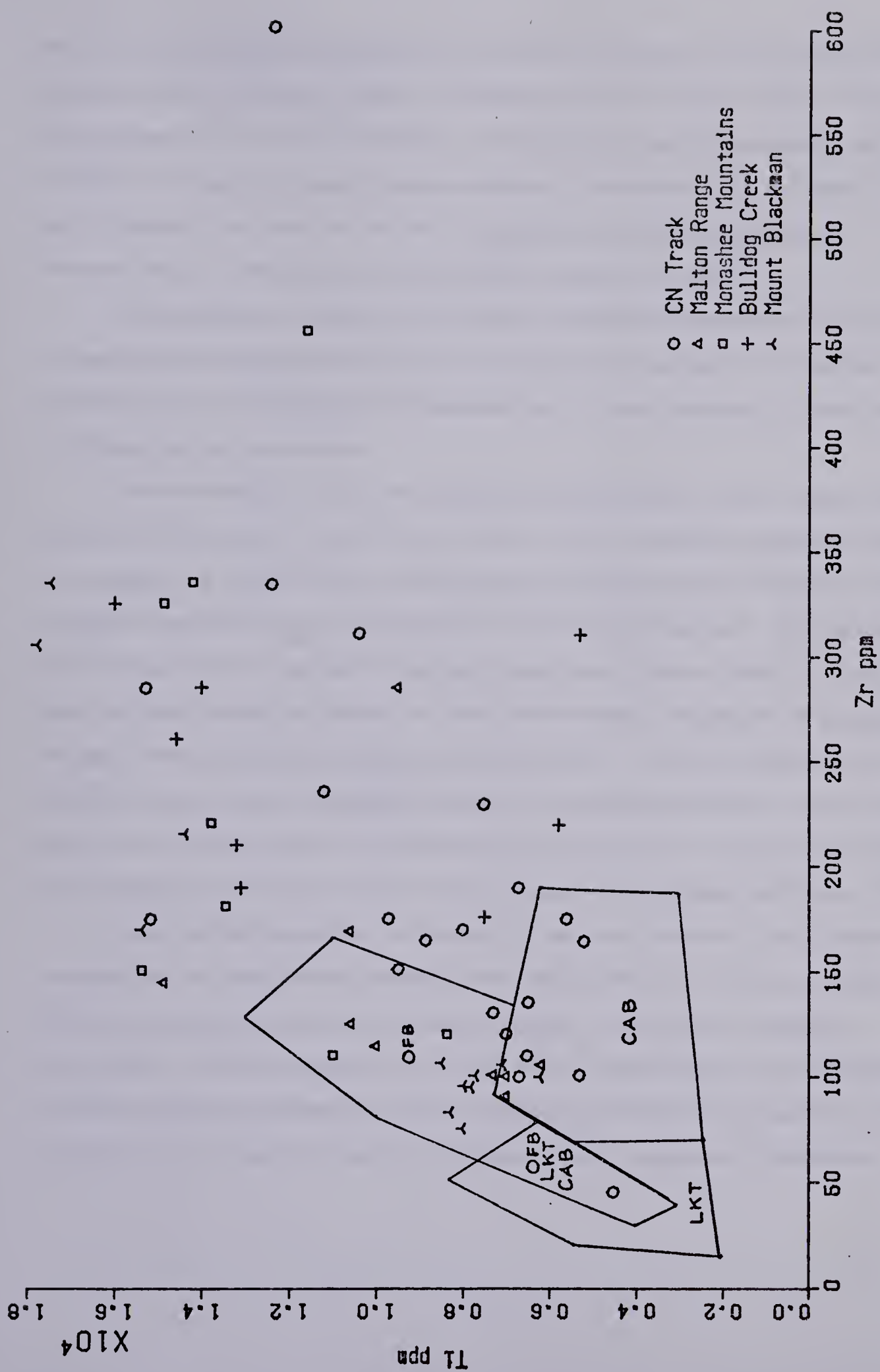


Figure 3.6 T1 v Zr plot for the mafic gneisses of the Malton Gneiss Complex



calc-alkali rocks (Lambert and Holland, 1974) and in pyroxenes from modern volcanic suites (pyroxene Y contents = basalt Y contents) (Ewart and Taylor, 1969). These high Y values appear to rule out any possibility of hornblende or garnet fractionation during formation. In figure 3.6, there is some indication of a positive Ti : Zr correlation in these mafic gneisses to the west of the Trench, suggesting original petrogenesis by clinopyroxene or orthopyroxene fractionation (Weaver *et al.*, 1981).

Of the gneisses to the east of the Trench, the Mount Blackman mafic suite (and to a lesser extent the Bulldog Creek mafic suite) show a pronounced Ti : Zr positive correlation, typical of tholeiites, and characteristic of rocks produced by clinopyroxene or orthopyroxene fractionation.

Further evidence on the petrogenesis and fractionation trends of these rocks can be gained from figure 3.7, which shows a CaO v Y plot of the mafic gneisses, together with Lambert and Holland's (1974) standard calc-alkali trend and the directions of liquid movement resulting from the crystallization of the minerals indicated. Mafic gneisses from all areas west of the Rocky Mountain Trench tend to define a high Y, L-type trend, which normally indicates an alkaline or peralkaline character, resulting from labradorite + clinopyroxene fractionation (Lambert and Holland, 1974). The Mount Blackman mafic gneisses have a somewhat scattered distribution, one sample plotting on the calc-alkali trend, and two plotting near the Monashee Mountains extreme L-type rocks, but the majority appear to show an olivine or orthopyroxene + plagioclase fractionation trend.

Hence the mafic gneisses to the west of the Rocky Mountain Trench appear to be orthogneisses of alkali basaltic parentage, the igneous precursors having formed by clinopyroxene plus labradorite fractionation together with subsidiary magnetite fractionation. The mafic gneisses to the east of the Trench appear to be orthogneisses of tholeiitic basaltic parentage, the Mount Blackman suite having trace element contents consistent with formation by olivine or orthopyroxene + plagioclase fractionation.



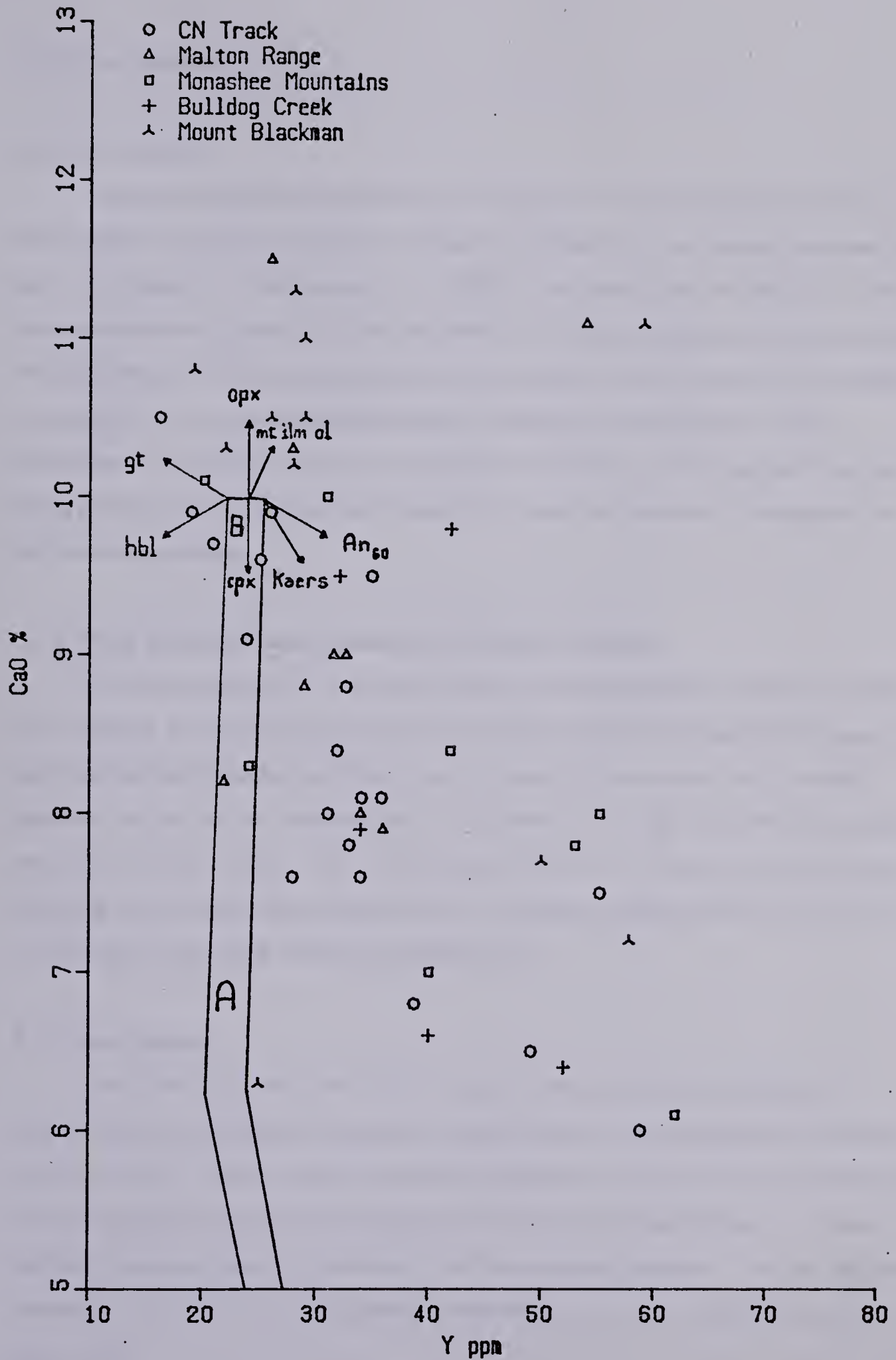


Figure 3.7 CaO v Y plot for the mafic gneisses of the Malton Gneiss Complex. BA shows Lambert and Holland's (1974) standard calc-alkaline trend. Arrows show the direction of liquid movement resulting from the crystallization of the minerals indicated





### 3.4 Felsic Gneisses

#### 3.4.1 Introduction

Average analyses of major and trace elements of the felsic gneisses of the Malton Gneiss Complex are shown in tables 3.2, 3.3 and 3.4, the individual analyses being given in Appendix A. Chamberlain *et al.* (1980b) have shown that the majority of these gneisses are meta-igneous, and this has been confirmed by applying discriminant analysis. The discriminant function used was that found by Shaw (1972) to be the most suitable for gneisses of a this average geochemical composition and petrology. These discriminant functions are shown in the tables in Appendix A, a value greater than zero being characteristic of igneous parentage and a value less than zero characteristic of sedimentary parentage.

#### 3.4.2 Felsic Gneisses West of the Rocky Mountain Trench

The felsic gneisses of the Malton Block can be subdivided on the basis of their field relations, petrography, geochemistry and Y/Nb ratios into three distinct types: a low silica tonalitic Grey Gneiss, which is broadly structurally concordant with the mafic gneisses, and which has a characteristic Y : Nb ratio of 2; a high silica, mildly peralkaline granitic Leucocratic Gneiss, with Y : Nb ratios of 0.3 to 1.5, which occurs as intrusive sheets; and an intrusive Augen Gneiss, with Y : Nb ratios ranging from 0.3 to 3.9, which forms major outcrops in the Mount Albreda area.

#### 3.4.3 Grey Gneiss

The Grey Gneisses of the Malton Gneiss Complex have been shown by Chamberlain *et al.* (1980a) to be geochemically similar to the Grey Gneiss of the North Atlantic Craton. Table 3.2 shows that their composition is close to that of a tonalite, but that they appear to have suffered slight calcium loss and potassium gain. In figure 3.8, the Grey Gneisses appear to be more K rich than standard tonalites. This may be due to changes in Na : K or Ca : K ratios during metasomatism, or to the high biotite content of these rocks.



Table 3.2 Major element analyses of the Grey Gneisses of the Malton Gneiss Complex compared with those of igneous rocks.

	1	2	3	4	5	6
n	9	10	14	33		
SiO <sub>2</sub>	68.65	70.55	67.03	68.54	66.15	69.15
Al <sub>2</sub> O <sub>3</sub>	14.57	14.38	14.09	14.31	15.56	14.63
Fe <sub>2</sub> O <sub>3</sub>	4.77	3.35	5.10	4.48	5.16	3.74
MgO	1.20	1.34	2.05	1.60	1.94	0.99
CaO	2.77	2.55	3.12	2.85	4.65	2.45
Na <sub>2</sub> O	3.72	3.62	3.54	3.61	3.90	3.35
K <sub>2</sub> O	4.31	3.60	4.20	4.05	1.42	4.58
TiO <sub>2</sub>	0.58	0.43	0.61	0.55	0.62	0.54
MnO	0.07	0.05	0.09	0.07	0.08	0.06
S	0.02	0.01	0.03			
P <sub>2</sub> O <sub>5</sub>	0.15	0.12	0.19		0.21	0.20

KEY 1=C.N. track 2=Malton Range 3=Monashee Mts  
 4=Mean Grey Gneiss (Malton Block)  
 5=Average tonalite (Nockolds, 1954)  
 6=Average adamellite (Nockolds, 1954)





Table 3.3 Major and trace element analyses of the Leucocratic Gneisses of the Malton Gneiss Complex

n	High Niobium Type			Low Niobium Type			Leucocratic Gneisses of the Malton Gneiss Complex						
	1	2	3	4	5	6	7	8	9	10	11	12	13
SiO <sub>2</sub>	68.11	74.26	68.70	70.21	73.74	70.08	69.55	71.30	73.91	71.40	72.08	73.86	71.08
Al <sub>2</sub> O <sub>3</sub>	15.71	13.48	14.57	13.58	13.11	13.99	14.58	13.62	12.79	12.93	13.86	13.75	11.26
Fe <sub>2</sub> O <sub>3</sub>	3.60	2.40	4.93	4.60	2.96	4.43	4.27	3.99	2.97	4.47	2.71	2.03	6.71
MgO	0.73	0.32	0.59	0.58	0.54	1.15	0.57	0.83	0.25	0.35	0.52	0.26	0.25
CaO	1.39	0.77	1.66	2.04	1.35	1.59	1.46	1.61	1.00	1.31	1.33	0.72	0.84
Na <sub>2</sub> O	4.67	4.66	5.04	3.72	3.83	4.12	4.90	3.94	4.00	4.13	3.08	3.51	4.92
K <sub>2</sub> O	5.00	3.94	4.40	4.63	4.19	3.88	0.42	4.14	3.54	4.49	5.46	5.13	4.21
TiO <sub>2</sub>	0.54	0.19	0.50	0.45	0.27	0.48	0.45	0.41	0.20	0.42	0.37	0.20	0.40
MnO	0.09	0.04	0.15	0.08	0.06	0.07	0.12	0.07	0.05	0.25	0.06	0.05	0.11
S	0.01	0.01	0.03	0.02	0.02	0.03	0.02	0.02	0.02	0.11	0.18	0.14	0.07
P <sub>2</sub> O <sub>5</sub>	0.14	0.01	0.11	0.13	0.07	0.12	0.10	0.11	0.02	0.11	0.18	0.14	0.07
Ba	1273	289	580	1054	327	687	649	647	647				
Nb	69	130	134	51	85	89	122	80	71				
Zr	223	528	524	470	293	491	473	422	451				
Y	29	56	65	50	95	77	57	77	140				
Sr	162	97	117	173	115	162	121	149	82				
Rb	106	93	76	148	159	115	84	136	90				
Zn	56	25	121	87	54	103	94	84	150				
Cu	13	7	38	12	11	20	28	15	0				
Ni	5	11	11	11	15	14	10	14	0				
Co	62(n=5)	52(n=3)			46(n=2)		58(n=8)	46(n=2)					
Cr	80(n=3)	4(n=2)	8		20(n=12)	20	15(n=32)	20(n=32)					

KEY 1=C.N.track 2=Malton Range 3=Monashee Mountains 4=C.N.track 5=Malton Range  
 6=Monashee Mountains 7=Mean High Nb Type 8=Mean Low Nb Type  
 9= Representative East Icelandic Rhyolites (Wood, 1978) 10=Skye Epigranites (Thompson, 1969)  
 11= Average calc-alkali granite (Nockolds, 1954) 12=Average alkali granite (Nockolds, 1954)  
 13=Average peralkaline granite (Nockolds, 1954)



Table 3.4 Mean analyses of felsic gneisses of The Malton Gneiss Complex.

	1	2	3	4	5	6	7
n	33	41	43	9	8	40	3
SiO <sub>2</sub>	68.54	69.55	71.30	70.90	63.88	71.39	72.40
Al <sub>2</sub> O <sub>3</sub>	14.31	14.58	13.62	13.91	15.58	14.76	13.96
Fe <sub>2</sub> O <sub>3</sub>	4.48	4.27	3.99	4.19	6.50	2.53	3.71
MgO	1.60	0.57	0.83	0.71	2.83	1.06	0.07
CaO	2.85	1.46	1.61	1.44	3.41	1.82	1.01
Na <sub>2</sub> O	3.61	4.90	3.94	3.71	3.65	4.21	3.58
K <sub>2</sub> O	4.05	4.42	4.14	4.55	3.02	3.89	5.16
TiO <sub>2</sub>	0.55	0.45	0.41	0.49	0.79	0.33	0.28
MnO	0.07	0.12	0.07	0.08	0.08	0.06	0.07
S	0.02	0.02	0.02	0.02	0.07	0.04	0.01
P <sub>2</sub> O <sub>5</sub>	0.16	0.10	0.11	0.10	0.14	0.05	0.00
Ce			166 (n=9)	262	63 (n=2)	96 (n=15)	332
La			89 (n=9)	140	30 (n=2)	55 (n=15)	182
Ba	1140	649	647	647	1307	993	66
Nb	17	122	80	66	23	10	108
Zr	209	473	422	386	270	180	691
Y	37	57	77	66	26	12	99
Sr	309	121	149	134	493	273	24
Rb	123	84	136	130	96	123	132
Zn	61	94	84	52	67	36	80
Cu	11	28	15	8	30	9	6
Ni	16	10	14	11	20	11	2
Co		58 (n=8)	46 (n=2)				
Cr	40	15 (n=32)	20 (n=32)	11	29 (n=4)	28	7

KEY 1=Mean Grey Gneiss 2=Mean High Nb Leucocratic Gneiss  
 3=Mean Low Nb Leucocratic Gneiss 4=Mean Augen Gneiss  
 5=Mean Bulldog Creek felsic gneiss  
 6=Mean Mount Blackman felsic gneiss  
 7=Hugh Allan Creek felsic gneiss



- CN Track
- △ Malton Range
- Monashee Mountains

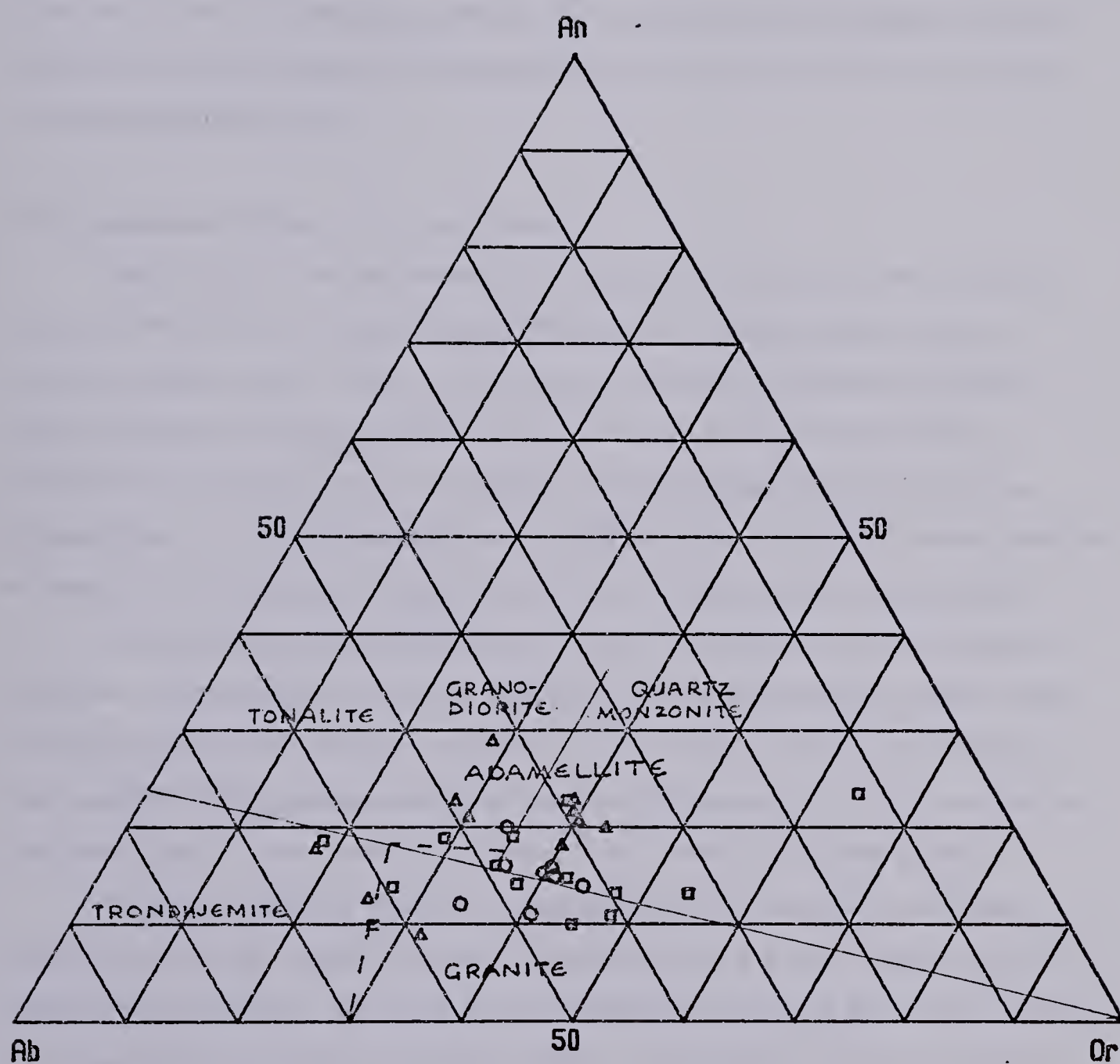


Figure 3.8 Ab-An-Or triangular diagram for the Grey Gneiss of the Malton Gneiss Complex

- O'Connor (1965)
- - - - - Barker (1979)





On an AFM plot (figure 3.9), these gneisses appear to show a calc-alkaline trend, but this may simply be an apparent trend due to the remobilization of alkalis. On a CaO v Y plot (figure 3.10), an approximately equal number of points lie on each side of the standard calc-alkaline trend of Lambert and Holland (1974), but none appear to lie on the trend of the mafic gneisses. Thus despite the association and broad structural conformity of the mafic and Grey gneisses west of the Trench, they appear not to be cogenetic; the former possibly having alkali igneous precursors, and the latter having calc-alkaline igneous parents.

#### 3.4.4 Leucocratic Gneiss and Augen Gneiss

Table 3.3 gives average analyses for the Leucocratic Gneisses, which outcrop only west of the Rocky Mountain Trench, together with average analyses of East Icelandic rhyolites (Wood, 1978), Skye epigranites (Thompson, 1969) and Nockolds' (1954) calc-alkali, alkali and peralkali granites. The Leucocratic Gneisses can be subdivided, on the basis of their Y : Nb ratios, into high niobium ( $Y/Nb = 0.5$ ) and low niobium ( $Y/Nb = 1$ ) types (Chamberlain *et al.*, 1980b), but there appears to be no essential difference between these two types, other than their niobium and yttrium contents.

The Augen Gneiss average analysis is given in table 3.4 and individual analyses in Appendix A. From table 3.4, it can be seen that the Augen Gneiss is very similar to the low niobium Leucocratic Gneiss, and figures 3.11, 3.12 and 3.13 show its similarity to the Leucocratic Gneisses in general. As far as can be determined from the geochemical data, they appear to be members of the same suite of mildly peralkaline granites.

The mildly peralkaline character is suggested for the Leucocratic and Augen Gneisses by their high sodium and iron contents (tables 3.3 and 3.4), together with their trace element contents, Y, Nb and Zr being comparatively high while Ba, Sr, Ni, Co and Cr are comparatively low (Noble and Haffty, 1969). This peralkaline character is further demonstrated by their comparatively high Ab values on an Ab-An-Or plot (figure 3.11), and by the presence of reibeckitic amphibole in the Leucocratic Gneiss. (Chapter 2).

On an AFM diagram (figure 3.12), these gneisses show an alkaline (or possibly a tholeiitic) trend (Irvine and Baragar, 1971); and on a CaO v Y plot (figure 3.13), the Y rich samples, including many of the felsic gneisses of the Malton Range, demonstrate a



- CN Track
- △ Malton Range
- Monashee Mountains

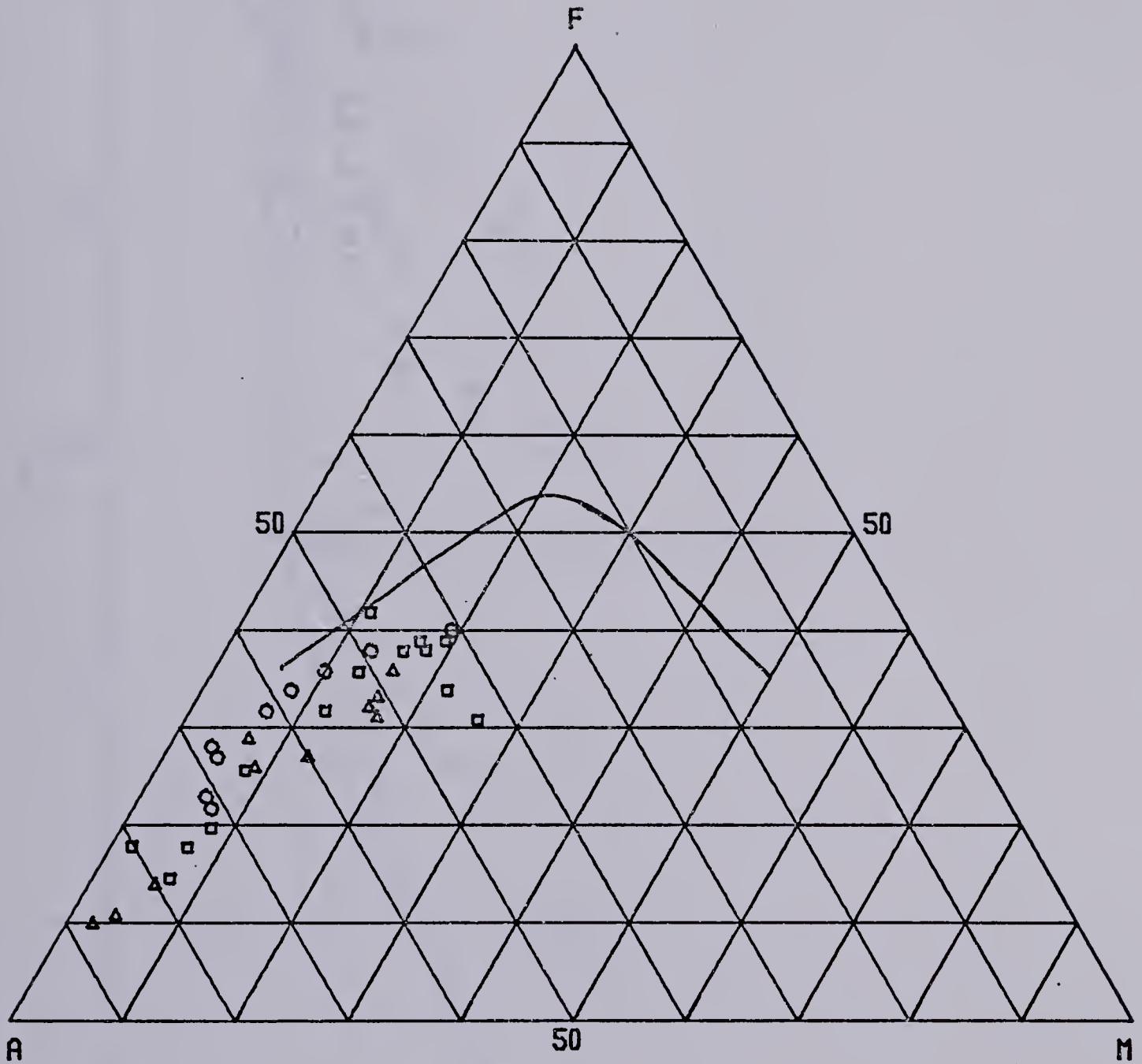


Figure 3.9 A-F-M triangular diagram for the Grey Gneiss of the Malton Gneiss Complex





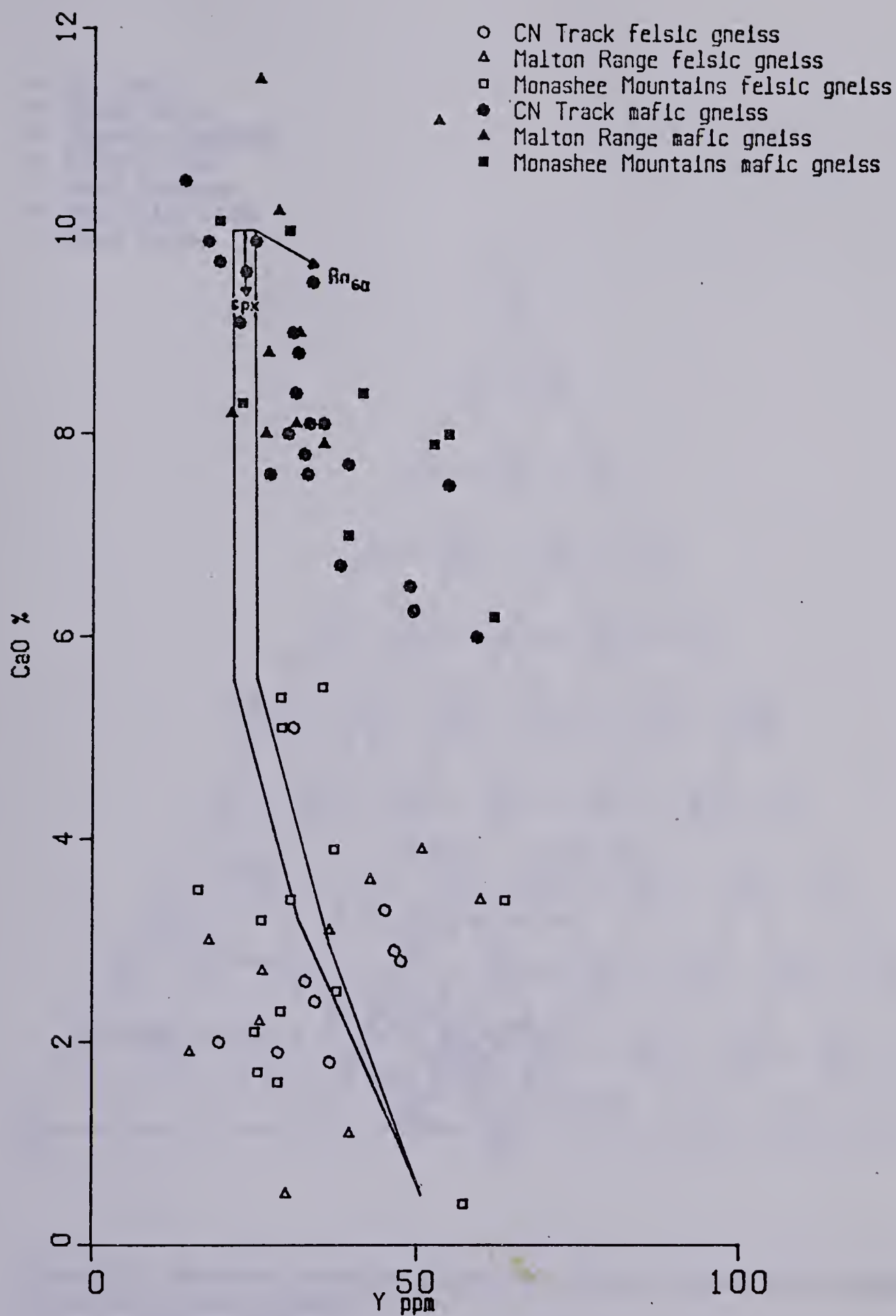


Figure 3.10 CaO v Y plot for the Grey Gneiss and the mafic gneisses of the Malton Block, showing Lambert and Holland's (1974) standard calc-alkaline trend.



- CN Track
- △ Malton Range
- Monashee Mountains
- + Bulldog Creek
- λ Mount Blackman
- × Hugh Allen Creek
- ◇ Augen Gneiss

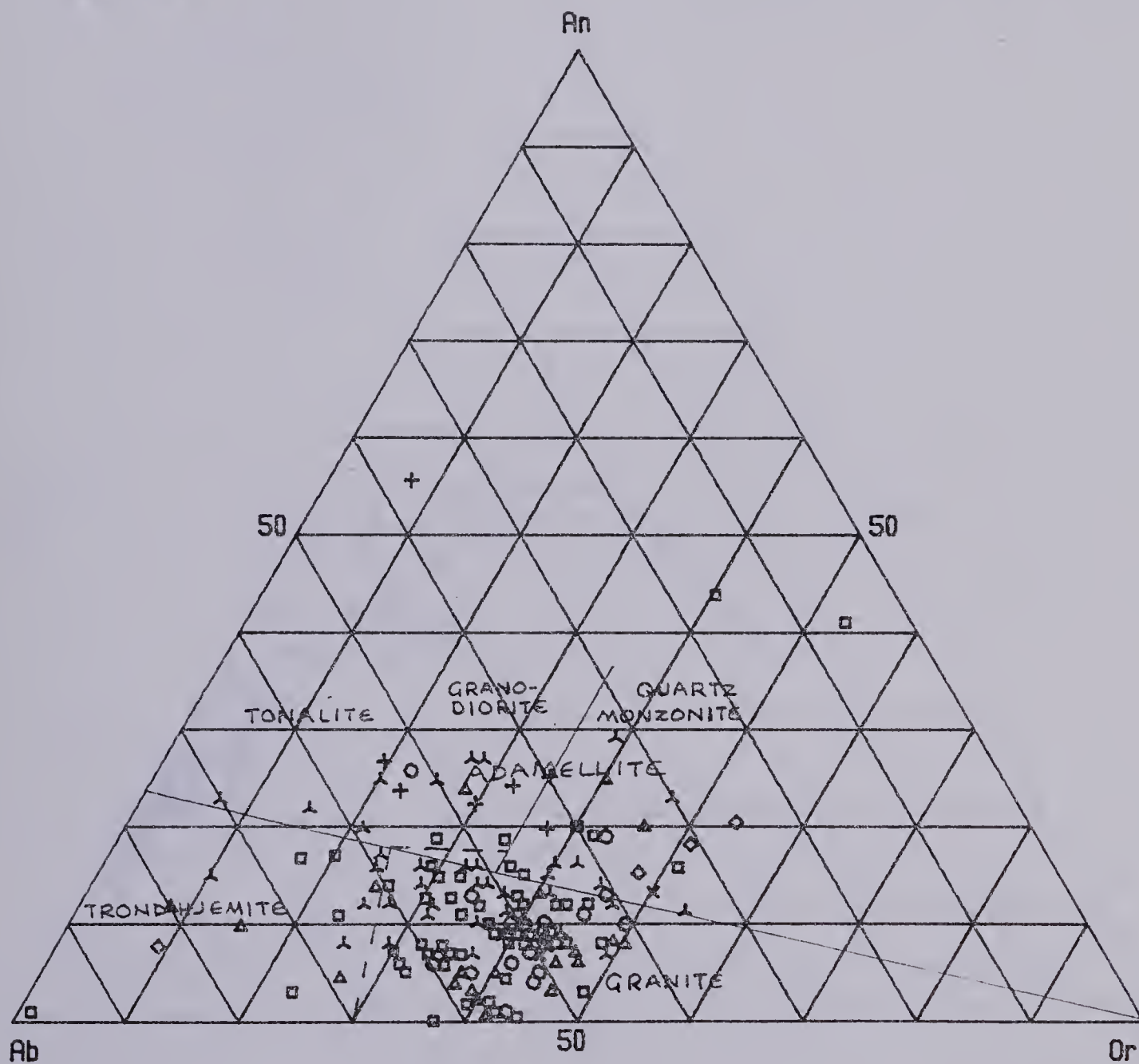


Figure 3.11 Ab-An-Or triangular diagram for the post Archean felsic gneisses of the Malton Gneiss Complex

———— O'Connor (1965)  
 - - - - - Barker (1979)



- CN Track
- △ Malton Range
- Monashee Mountains
- ◇ Augen Gneiss

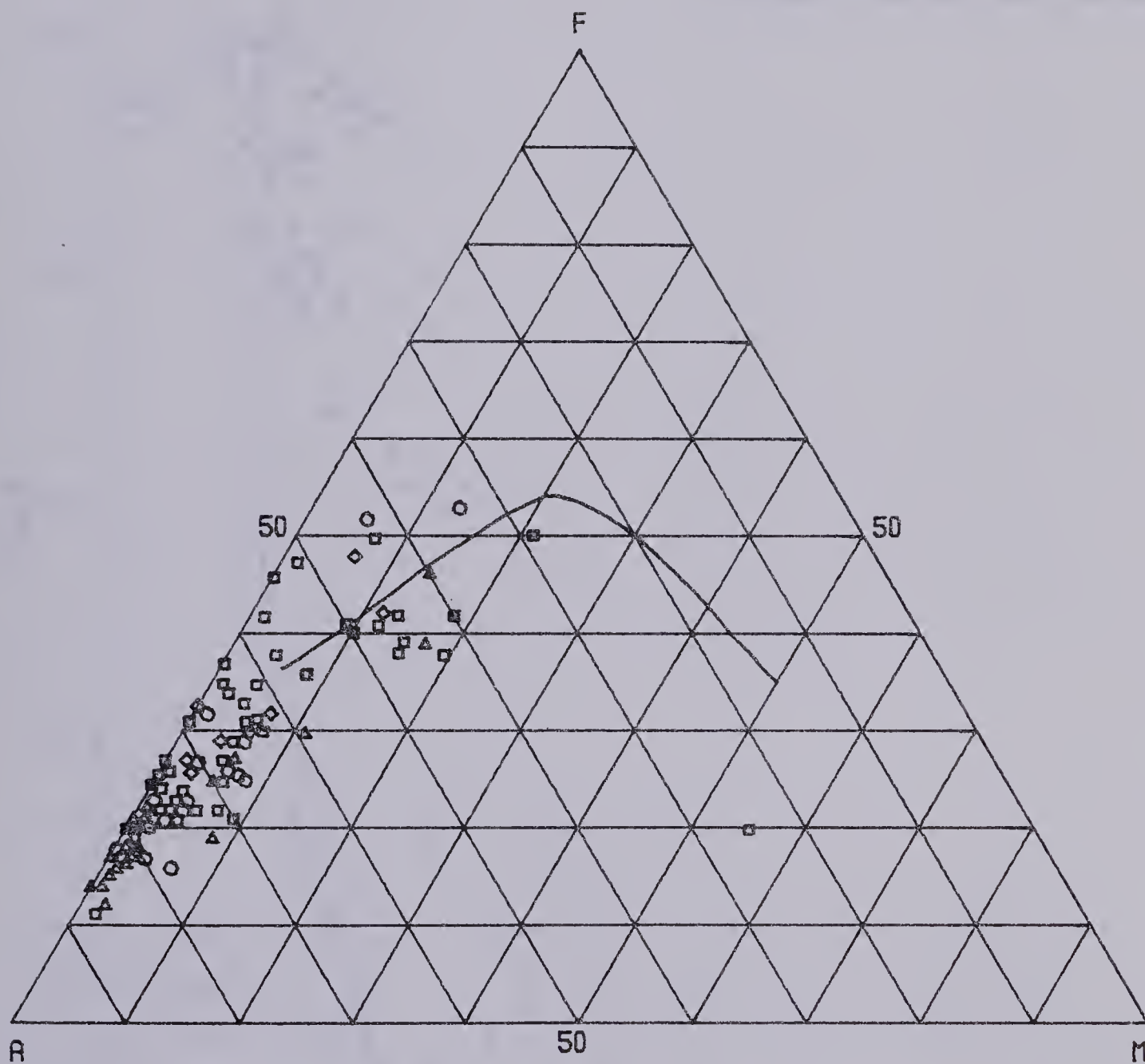


Figure 3.12 A-F-M triangular diagram for the Leucocratic Gneiss and the Augen Gneiss of the Malton Gneiss Complex





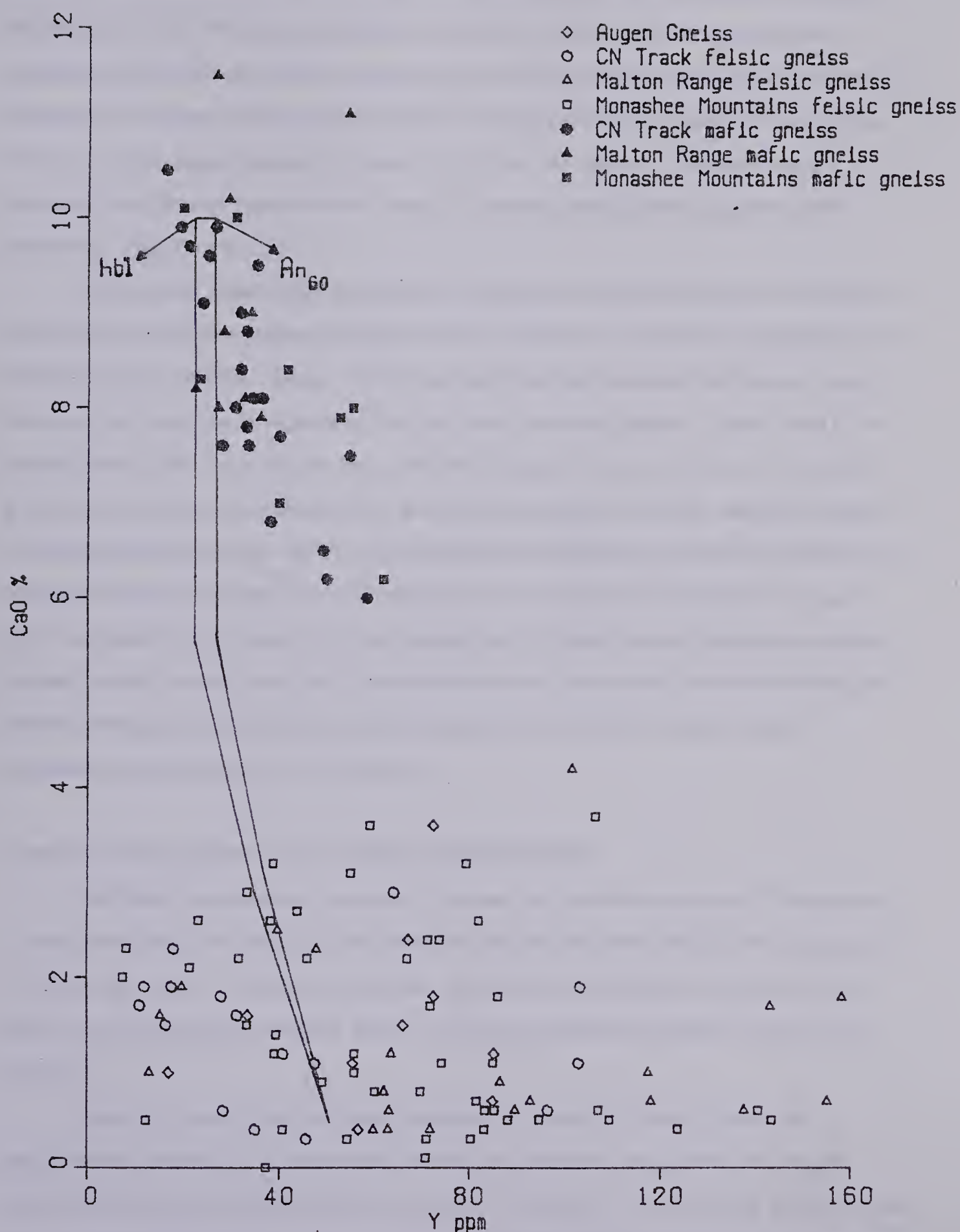


Figure 3.13 CaO v Y plot for the Leucocratic Gneiss, the Augen Gneiss and the mafic gneisses of the Malton Block, showing the standard calc-alkaline trend of Lambert and Holland (1974) and the direction of liquid movement resulting from hornblende or plagioclase fractionation.



marked L-type alkaline trend, whereas others show a calc-alkaline character (Lambert and Holland, 1974). The large spread on the CaO v Y plot may be an indication of secondary effects or of a suite formed by the mixing of alkaline and calc-alkaline melts. The alkaline members could be partial melts of the alkaline mafic gneisses west of the Trench, which are also plotted on figure 3.13. The calc-alkaline members may be remelted Grey Gneiss, the strontium isotope evidence lending some support to this possibility. (See Chapter 5).

On the other hand, these Leucocratic Gneisses are geochemically very similar to the Tertiary rhyolites of eastern Iceland (Wood, 1978) and to the Tertiary epigranites of Skye (Thompson, 1969). Wood (1978) has described the Icelandic rhyolites as being produced by fractional crystallization of light R.E.E. enriched basalts. Dickin (1981), by studying Pb, Sr and Nd isotopes, has provided evidence for the formation of the Skye granites by fractional crystallization of an original tholeiite, with minor selective addition of fusible crustal material. Hence, it is possible that these mildly peralkaline granites of the Malton Gneiss Complex were produced by the fractional crystallization of a light R.E.E. enriched tholeiitic basalt, with some addition of fusible crustal material, especially potash, possibly during a period of continental rifting. In this case, the AFM plot could be interpreted as a tholeiitic trend, and the spread in the CaO v Y plot as due to hornblende plus plagioclase fractionation.

### 3.4.5 Felsic Gneiss East of the Rocky Mountain Trench

The felsic gneisses outcropping to the east of the Rocky Mountain Trench occur in three main areas, the Bulldog Creek area, the Mount Blackman area and the area south of Hugh Allan Creek. The Mount Blackman area was well sampled, but the other two areas were incompletely sampled, due to difficult terrain and access as well as poor exposure.

Table 3.4 shows that the felsic gneisses from each of these 3 areas are geochemically distinct from each other as well as from the Grey Gneiss, the Augen gneiss and the Leucocratic Gneiss to the west of the Trench. The average Bulldog Creek felsic gneiss does show some similarity to the average Grey Gneiss, but the former has higher iron and magnesium and lower silica contents. Figure 3.11 shows that the Bulldog





Creek felsic gneisses are mainly of granodioritic composition, and are generally richer in plagioclase than the Grey Gneiss west of the Trench (figure 3.8). The same diagram shows that the Mount Blackman and Hugh Allan Creek felsic gneisses are generally of granitic composition, and that the felsic gneisses east of the Trench tend to be more anorthite rich than the average Leucocratic Gneiss.

Figure 3.14 shows that the Bulldog Creek and Mount Blackman felsic gneisses have a calc-alkaline trend on an AFM diagram, whereas the Hugh Allan Creek felsic gneisses appear to be tholeiitic or alkaline. On a CaO v Y plot (figure 3.15), the Bulldog Creek felsic gneisses show a normal calc-alkaline trend, the Mount Blackman felsic gneisses a J-type trend, and the Hugh Allan Creek felsic gneisses an L-type or alkaline trend. As a whole, the gneisses east of the Trench have clearly had a simpler geochemical history than those west of the Trench.

No firm conclusions can be drawn about the Hugh Allan Creek gneiss from the three available samples, but they do appear to be distinctly different from the other felsic gneisses east of the Rocky Mountain Trench.

The Bulldog Creek felsic gneisses appear to have formed from igneous calc-alkaline felsic rocks, produced by normal plagioclase controlled fractionation. They are probably genetically related to the mafic igneous calc-alkaline rocks (now mafic gneisses) in the same area.

The Mount Blackman felsic gneisses are paragneisses, as shown in chapter 2. They appear, however, to be derived from very immature sediments, approximating to granite in chemical composition. They are probably not genetically related to the mafic gneisses in the area, some of which appear to be former tholeiitic sills.

### 3.5 Factor Analysis

R-mode factor analysis was performed on all the data, and the significant factor loadings of the promax oblique primary pattern matrix ( $K_{min} = z$ ) are shown in table 3.5 (Hendrickson and White, 1964). 97% of the total variance in the data has been resolved into 5 factors, again suggesting that the majority of these rocks are not metasedimentary. (Lambert *et al.*, 1982). Factor 1 represents 5.4% of the variance and is interpreted as mica; factor 2 (9.9%) as plagioclase; factor 3 (16.8%) as Ba and Sr opposing Y; factor 4



- + Bulldog Creek
- ^ Mount Blackman
- x Hugh Allen Creek

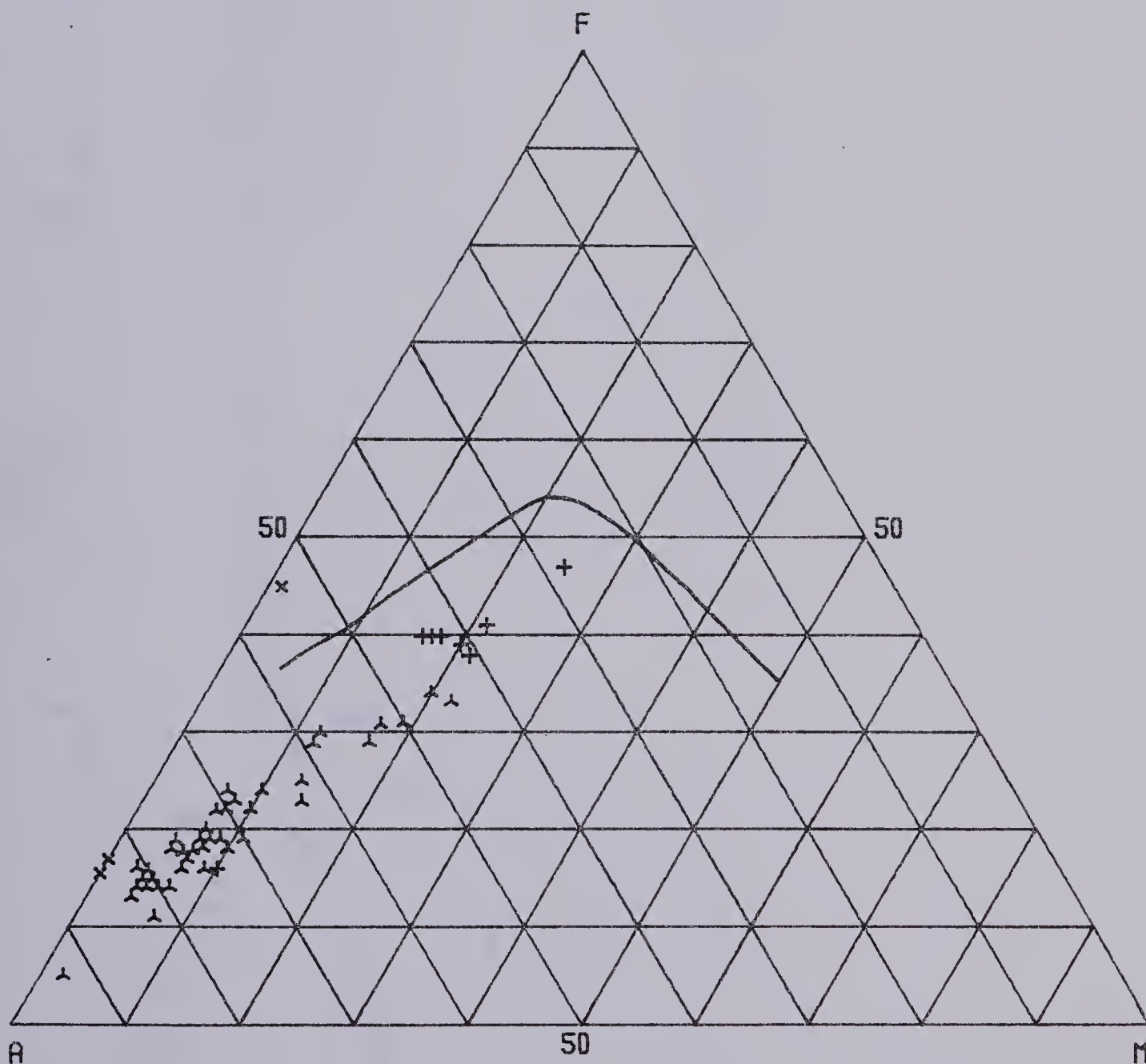


Figure 3.14 A-F-M triangular diagram for the felsic gneisses east of the Rocky Mountain Trench in the Malton Gneiss Complex



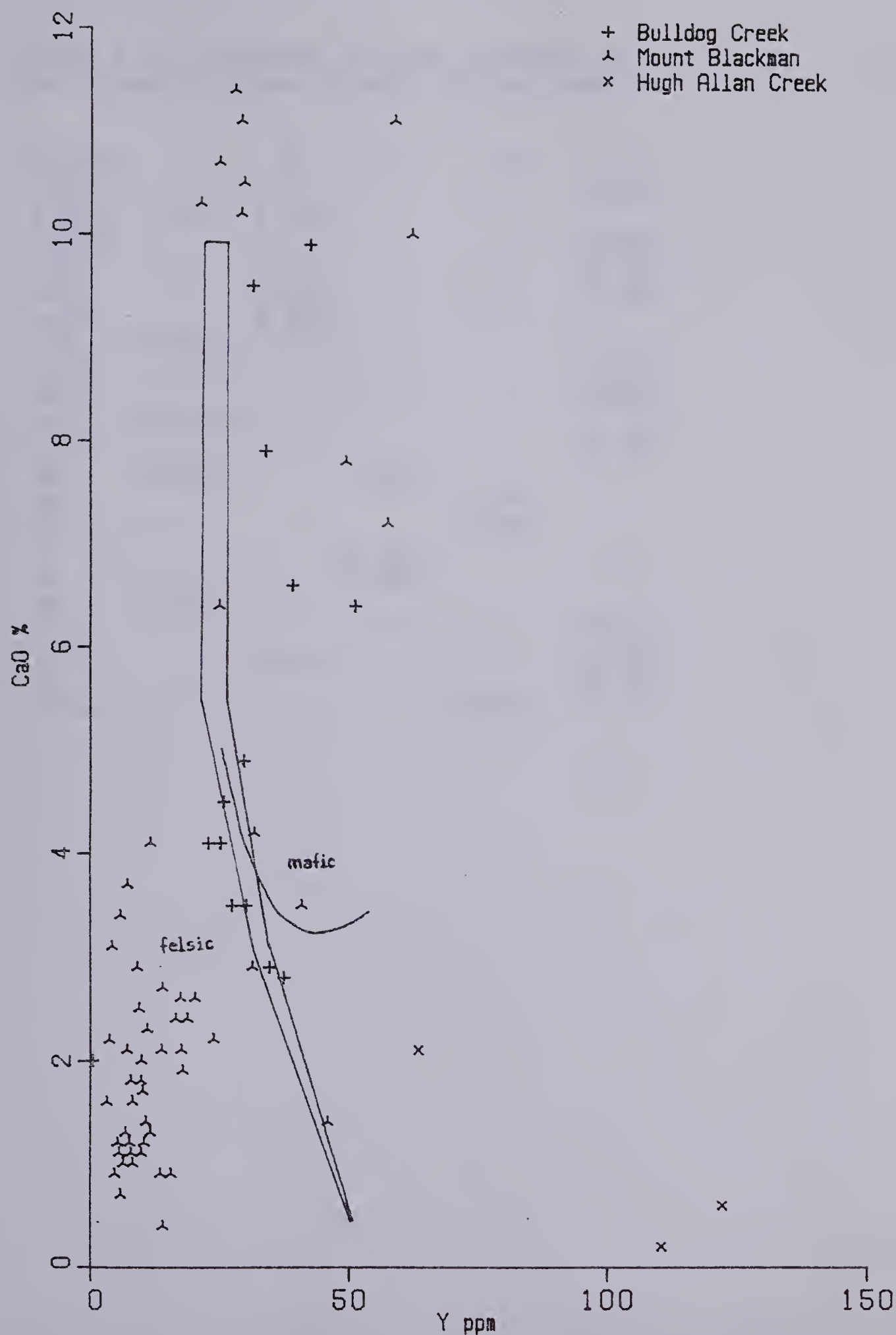


Figure 3.15 CaO v Y plot for the mafic and felsic gneisses east of the Rocky Mountain Trench in the Malton Gneiss Complex, showing the standard calc-alkaline trend of Lambert and Holland (1974).





Table 3.5 Principal factor loadings in the Promax Oblique Primary Pattern Matrix

Factor	1	2	3	4	5
SiO <sub>2</sub>					0.879
Al <sub>2</sub> O <sub>3</sub>	-0.438	0.618			
Fe <sub>2</sub> O <sub>3</sub>					-0.997
MgO					-0.602
CaO		0.493			-0.452
Na <sub>2</sub> O		0.879			
K <sub>2</sub> O	-0.896				
TiO <sub>2</sub>					-0.928
MnO					-0.857
S	-0.138				
P <sub>2</sub> O <sub>5</sub>					-0.453
Ba	-0.569		0.642		
Nb				0.794	
Zr				0.703	
Y			-0.627		
Sr			0.639		
Rb	-0.891				
Zn					-0.611
Cu					-0.306
Ni					-0.375
Y/Nb				-0.531	



(20.4%) as accessory minerals; and factor 5 (44.5%) as quartz opposing ferromagnesian.

Figure 3.16, in which factor 2 (plagioclase) is plotted against factor 5 (differentiation index), shows clearly the different gneissic groupings in the Complex. There were insufficient data from the Bulldog Creek area to consider the mafic and felsic gneisses separately, but the mean Bulldog Creek analysis is significantly different from both the Mount Blackman gneiss and the gneisses to the west of the Rocky Mountain Trench. The mafic gneisses west of the Trench plot separately from those in the Mount Blackman area, and both the Grey Gneiss and the Leucocratic Gneiss west of the Trench appear as groupings separate from the felsic gneiss in the Mount Blackman area.

### 3.6 Conclusions

The results show that the Complex consists of at least two unrelated bimodal suites with unrelated individual members. The bimodal suite to the west of the Rocky Mountain Trench consists of felsic orthogneisses of tonalitic calc-alkali parentage and mafic orthogneisses of possible alkali basaltic parentage. (The events which have occurred since the formation of the latter have tended to obscure its exact petrogenesis). This bimodal suite is intruded by later, possibly related, mildly peralkaline granitic magma as well as by further basaltic magma.

To the east of the Rocky Mountain Trench, the largest gneissic outcrop is in the Mount Blackman area and consists of felsic paragneisses, intruded by mafic tholeiitic orthogneisses. Orthogneisses of probable calc-alkaline affinity outcrop in the Bulldog Creek area; and orthogneisses of possible granitic parentage in the Hugh Allan Creek area.





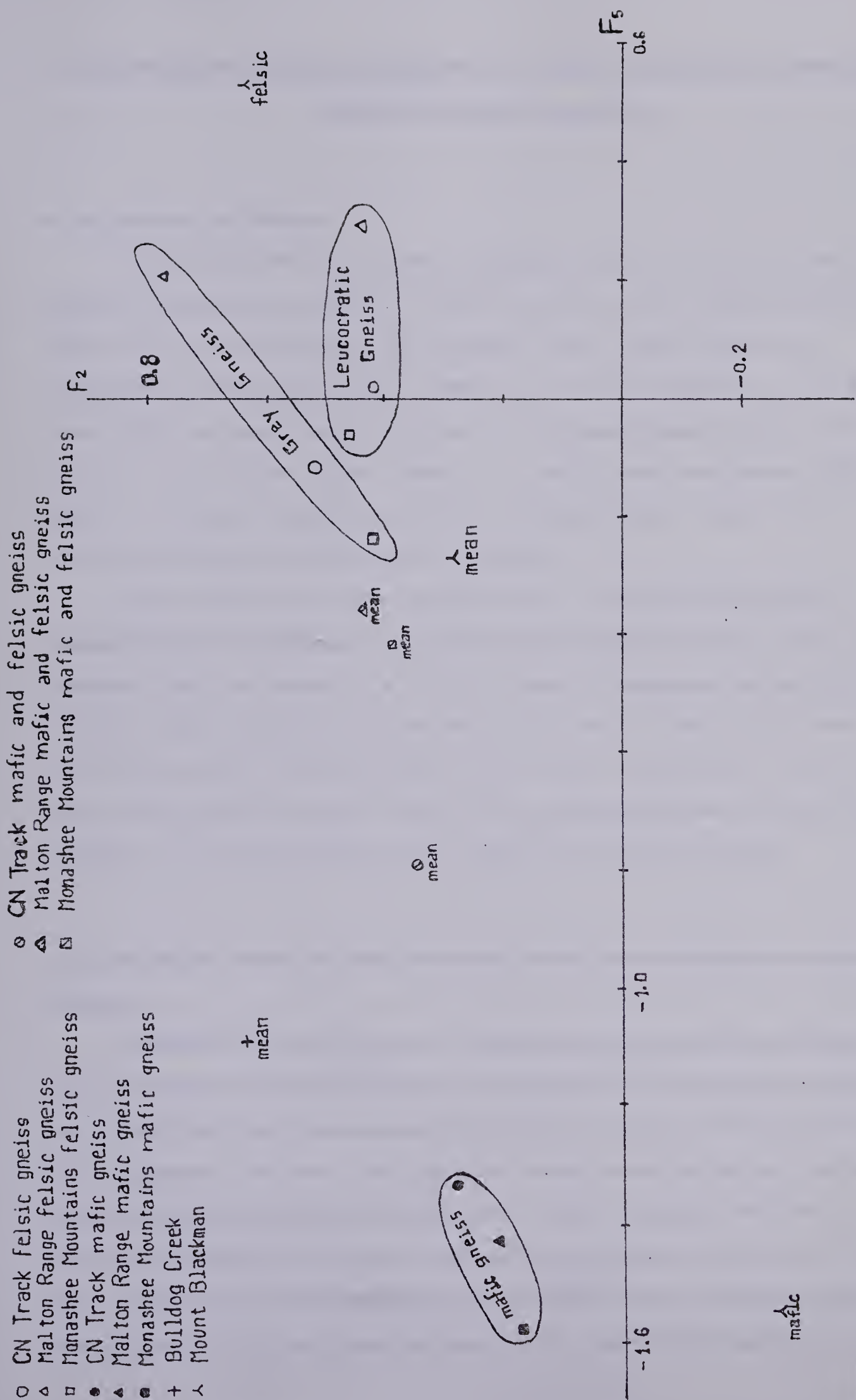


Figure 3 16 Factor analysis plot for the gneisses of the Malton Gneiss Complex



## 4. STRATIGRAPHY AND GEOCHEMISTRY OF THE METASEDIMENTS SURROUNDING THE MALTON GNEISS COMPLEX

### 4.1 Introduction and Review

The metasediments in the vicinity of the Malton Gneiss Complex have been studied by Sutherland Brown (1957, 1963), Price and Mountjoy (1966), Slind and Perkins (1966), Price (1967), Giovanella (1967), Campbell (1967, 1968), Campbell and Charlesworth (1970), Pihsent (1971), Wheeler *et al.* (1972), Campbell *et al.* (1973) and Young (1979), working primarily to the north of the Malton Gneiss Complex, and by Brown *et al.* (1978), Craw (1978), Simony *et al.* (1980), Poulton and Simony (1980), Ghent *et al.* (1980), Oke and Simony (1981) and Pell and Simony (1981), working primarily to the south of the Malton Gneiss Complex.

Most of these workers have described most of the boundaries between metasediments and the gneisses of the Malton Gneiss Complex as faults. Price (1967), Giovanella (1967) and Wheeler *et al.* (1972), however, all suggested that the gneiss schist boundary on Mount Blackman was metamorphic, but Oke and Simony (1981) have recently shown that it is almost certainly unconformable, complicated by later thrusting. These faulted contacts contrast strongly with the generally accepted sillimanite isograd boundary of the Shuswap Metamorphic Complex 20 km to the southwest.

### 4.2 Correlations across the Rocky Mountain Trench north of the Malton Gneiss Complex

Campbell (1967) was the first to correlate strata across the Rocky Mountain Trench. He discovered an archeocyathid-rich carbonate unit in the Cariboo Group to the west of the Trench, which he equated with the Mural formation in the Gog Group of the Rocky Mountains to the east. Both limestones contain archeocyathids and trilobites of the *Faillotaspis* zone of the early Cambrian (Fritz, 1975). Campbell (1967) then tentatively correlated the units below the Mural formation east of the Trench with those below the newly discovered carbonate unit west of the Trench, equating the Middle Miette Group with the Kaza Group, the Upper Miette Group with the Isaac and



Cunningham formations, and the McNaughton formation with the Yankee Bell, Yanks Peak and Midas formations. These correlations were modified slightly by Campbell *et al.* (1973) and Young (1979). The correlation chart of Young is shown in figure 4.1.

The correlations are described by Campbell *et al.* (1973) as being based on fossil zonations in the Cambrian, but on homotaxial (lithology and thickness) relationships below the Mural formation. Accurate thickness measurements, however, are impossible to obtain, and because of lack of exposure and complex deformation (Pinsent, 1971; Campbell *et al.*, 1973). Only minimal similarities in the lithologies of the correlated strata are revealed by the detailed descriptions of Sutherland Brown (1957, 1963), in the Antler Creek and Cariboo River areas, of Campbell *et al.* (1973) and Young (1979) in the McBride area, of Pinsent (1971) in the Mount Robson area, and of Poulton and Simony (1980) in the Selkirk, Purcell and western Rocky Mountains.

For example, Young (1979) correlates the Lower Miette Group, outcropping in one place only on the east flank of the Mount Robson synclinalorium, with the lower part of the Kaza Group (figure 4.1). The Lower Miette Group, however, consists of 600 m to 1200 m of folded and cleaved black shale, argillite and micritic limestone, and there is no known part of the Kaza with similar lithology (Campbell *et al.*, 1973).

The Middle Miette Group and the Kaza Group do appear to possess a superficial similarity, both consisting largely of greenish and brownish grey argillite, phyllite and schist alternating with units of poorly sorted immature feldspathic sandstones (Campbell *et al.*, 1973; Pinsent, 1971); and the Middle Miette Group is about 2700 m thick whereas the Kaza is 3600 m thick (Campbell *et al.*, 1973). However, the Middle Miette Group is described as chloritic, rich in tourmaline and zircon and containing many coarsening upward cycles and turbidite sedimentary structures, suggesting deposition by rapid slumping in an offshore marine environment from an igneous or high grade metamorphic provenance lying to the north east (Pinsent, 1971). None of these features are mentioned in published accounts of the Kaza Group.

The Upper Miette Group is correlated by different authors with different formations in the Cariboo Group: with the Isaac Formation only by Pinsent (1971), with the Isaac, Cunningham and the lower part of the Yankee Bell Formation by Campbell *et al.* (1973) and Young (1979), and with the Isaac, Cunningham and the whole of the Yankee





CARIBOO MOUNTAINS			ROCKY MOUNTAINS			
UPPER AND LOWER CAMBRIAN	CARIBOO GROUP	DOME CREEK FORMATION (0-200 m)	MIDDLE CAMBRIAN	TATE-CHELANG FORMATION (60-360 m)	Banded slaty shale, argillaceous limestone, micritic limestone maroon to grey brown shale, shaly lacies on Bearpaw Ridge?	
LOWER CAMBRIAN		Gradational contact	PALEOZOIC	GOG GROUP	Conformable contact	
		MURAL FM (150-600+ m)			MAHTO FM (245-300 m)	Grey to pink quartzite, minor siltstone and shale
		Gradational contact			Gradational contact	
		MIDAS FM (90-300+ m)			MURAL FM (215-380 m)	Limestone, dolostone, green to grey shale, sandstone, minor siltstone
		Conformable contact			Conformable contact	
? LOWER CAMBRIAN		YANKS PEAK FM (0-580 m)	? LOWER CAMBRIAN	McNAUGHTON FORMATION (600-2300 m)	Quartzite, feldspathic and pebbly at base, interbedded shale and fine grained quartzite (Holmes River Member)	
		Gradational contact	PROTEROZOIC	Locally disconformable contact		
		YANKEE BELLE FM (270-900 m)		Undivided quartz sandstone, olive to brown mudstone, trails (0-550 m)		
		Gradational to disconformable contact (?)		Conformable contact		
	CUNNINGHAM FORMATION (? 60-550 m)	BYNG FM (0-300 m)		Dolostone, pale grey and yellow in part sandy		
Gradational contact	HADRYNIAN	Unnamed grey mudstone, siltstone, and minor sandstone, in part calcareous at top (210-550 m)				
ISAAC FM (? 900-1500 m)		MILTFE GROUP (WINDLERMEHF SUPERGROUP)	Conformable contact			
Gradational contact		MIDDLE MIE TTF (2100-2700+ m)	Coarse, arkosic, partly pebbly sandstone (qrit), grey phyllitic shale			
HADRYNIAN	KAZA GROUP (includes SNOWSHOE FM) (3600+ m)	PROTEROZOIC	HADRYNIAN	Lower MIE TTF (600-1200+ m)	Black slaty shale	
				Base not exposed	Base not exposed	

Figure 4.1 Correlation table for formations east and west of the Rocky Mountain Trench (Young, 1979)



Bell by Wheeler *et al.* (1972). Pinsent (1971) equates the Cunningham limestone with the Mural Formation (Gog Group). Young (1979) equates the Cunningham with the Byng Formation (0–300 m of dolostone in the Upper Miette Group) and Campbell *et al.* (1973) state that the Cunningham is younger than the Byng.

The Upper Miette Group does bear some resemblance to the Isaac Formation, both being similar thicknesses (approximately 1500 m) of cleaved and folded grey or black argillite. The Upper Miette, however, weathers to an orange, brownish or greenish grey colour and is interbedded with coarsening-upward argillaceous siltstones and with a few lenses of coarse-grained immature sandstone and conglomerate in the west. It contains the trace fossils *Planolites* type burrows and *Didymaulichnus* sp. trails, but no skeletal fossils (Campbell *et al.*, 1973). In contrast, the Isaac Formation weathers typically to a peculiar steel blue colour and is interbedded with calcareous siltstone, micritic limestone, very fine-grained sandstone and lenses of massive limestone conglomerates up to 30 m thick and 300 m long. The only fossils found have been "worm" trails (Campbell *et al.*, 1973).

The Cunningham and Yankee Bell Formations consist of alluvial to shallow marine deposits of limestone, dolostone, shale, siltstone and sandstone, thickening westwards away from the Trench and from an evident north-easterly source. The Bahamian type limestones, laterally continuous into a sandy littoral facies, the lack of any turbidite sole markings and the rhythmic shale, siltstone, limestone facies suggest deposition in a broad relatively shallow shelf adjacent to a littoral zone. The basal Yankee Bell unit is locally disconformable upon the Cunningham and contains evidence of subaerial exposure (mud-cracks and hematite staining) (Campbell *et al.*, 1973). Campbell *et al.* (1973) do describe one section, 190 m thick, near Holy Cross Mountain where the upper part of the Upper Miette Group lithologically resembles the Cunningham and Yankee Bell Formations; but in general the Cariboo Group formations are neither lithologically similar to nor a deep water facies of the Upper Miette Group.

Furthermore, Young (1979) gives evidence of tectonic instability in the Uppermost Miette of the Rocky Mountains east of McBride (diamictites and coarse-grained proximal turbidite flows), whereas the Cariboo area to the west of the Trench was comparatively stable during Yankee Bell times (numerous marine clastic and carbonate cycles).





Another problem with the Upper Miette and Lower Cariboo Group correlation is that of stratigraphy and structure. The Upper Miette is described as conformable throughout (Young 1979) whereas Campbell *et al.* (1973) describe an abrupt boundary between the Isaac and Cunningham Formations. Wheeler *et al.* (1972) state that the rocks above the Isaac Formation are essentially unmetamorphosed in contrast with those below. Campbell (1970) describes the structure in the Cariboo Mountains as being a series of northwestward plunging anticlinoria and synclinoria composed of structurally and metamorphically distinct units. He relates the degree of metamorphism and the different structural styles between the infrastructure and the superstructure to the geothermal gradient, but his description of an infrastructure characterised by staurolite kyanite grade metamorphism and polyphase folding (isoclines, coaxial with bedding being arched across an antiform); and a superstructure of essentially unmetamorphosed rocks folded in large similar, composite or concentric folds (with axial planes arranged in a broad fan more or less normal to the antiformal surface and to the axial planes of the isoclines), or tilted and broken in fault blocks; suggests to the author a major unconformity or fault between the rocks of the infrastructure (Kaza Group and Isaac Formation) and those of the superstructure (Cunningham Formation and younger). Moreover, his description of a transition zone consisting of a simple anticline with foliation parallel to bedding suggests that the superstructure has been thrust over the infrastructure (possibly during a period of northeast–southwest compression).

#### 4.3 Correlation of the Horsethief Creek Group

To the south of the Malton Gneiss Complex, the Precambrian strata have been correlated by Poulton and Simony (1980). The correlation is complicated by frequent thrusting and, as Poulton and Simony (1980) state, "successions and assemblages are complex and are different in detail from one outcrop area to another". Poulton and Simony (1980) describe the Hadrynian strata from the northern Purcell Mountains, approximately 300 km southeast of the Malton Gneiss Complex, and correlate it with strata from the intervening Selkirk and Monashee Mountains, as well as with strata from the western Rocky Mountains. In the Dogtooth Range of the northern Purcell Mountains, they describe the Horsethief Creek Group of the Windermere Supergroup as consisting



of approximately 3000 m of Hadrynian strata, divided into the four divisions of Grit (up to 1500 m), Slate (approximately 900 m), Carbonate (approximately 200 m) and Upper Clastics (approximately 500 m). This fourfold division, as well as the general lithology appears to correlate well with Hadrynian strata in the western Rocky Mountains, for example at Wood Arm (Poulton and Simony, 1980) and at Mount Blackman (Oke and Simony, 1981).

Correlation of the Horsethief Creek Group with Precambrian strata of the Selkirk and Monashee Ranges of the Columbia Mountains, however, is neither so easy nor so convincing. The Precambrian strata in this region are, in general, thicker and more complex than in the Horsethief Creek Group. Specifically, the Slate division is thicker and more argillaceous, having fewer grit bands in its lower part, and including a new semipelite amphibolite unit in its upper part. The Carbonate division is thinner, thinning to 10 m in places. The Upper Clastic division is thicker and finer grained, but includes coarse conglomeratic lenses. Poulton and Simony (1980) and Simony *et al.* (1980) describe these variations as facies changes, explaining that the strata in the Columbia Mountains, to the north and west of the Horsethief Creek Group type area, may have been deposited in a depocentre, which was subject to mafic activity and situated further away from the coarse clastic source area. The two facies may have moved closer together during later crustal shortening.

The possibility exists, however, that the Precambrian strata of the Columbia Mountains differ lithologically from those of the Rocky and Purcell Mountains, simply because they were deposited in a different place and possibly at a different time. This possibility is strengthened by the fact that both the metamorphic grade and the structural complexity of the strata are greater in the Columbia Mountains. The boundary appears to follow the Rocky Mountain Trench (here occupied by the Columbia River) and then the Beaver River, with the possibility of some thrusting over this boundary, for example in the western Dogtooths.

Because of this lack of confidence concerning the correlation of the Precambrian strata of the Monashee Mountains with the Precambrian strata in the Horsethief Creek Group type area, the Precambrian strata of the Monashee Mountains will, in this thesis, be referred to as the Monashee Horsethief Creek Group





#### 4.4 Correlations across the Rocky Mountain Trench and the North Thompson Fault south of the Malton Gneiss Complex

Poulton and Simony (1980) have correlated the Precambrian strata south of the Malton Gneiss Complex across both the Rocky Mountain Trench and the North Thompson Fault, equating the Middle Miette Group of the Rocky Mountains with the Monashee Horsethief Creek Group of the Columbia Mountains and with both the Cariboo Group and the Kaza Group of the Cariboo Mountains. These correlations have also been accepted by other workers, for example, at Wood Arm by Poulton and Simony (1980) and at Mount Blackman by Oke and Simony (1981).

Brown *et al.* (1978) correlated the upper part of the Monashee Horsethief Creek Group with the Cariboo Group, despite great differences in thickness and lithology. Poulton and Simony (1980) supported this correlation pointing out the similarities between the slate division of the Monashee Horsethief Creek Group and the Isaac Formation of the Cariboo Group (steel blue colour, high muscovite content, pyrite and siderite porphyroblasts); and between the upper clastic division of the Monashee Horsethief Creek Group and the Yankee Bell Formation of the Cariboo Mountains (predominance of green tinted rocks, abundance of ferruginous sandstones and the occurrence of ferruginous sandy carbonates). The same authors also correlated the Monashee Horsethief Creek Group with the Kaza Group of Campbell (1968, 1972) in the Canoe River map area (west side). Poulton and Simony (1980) state that the Kaza Group "is continuous with rocks considered by us to comprise the entire Horsethief Creek Group and to closely resemble the Cariboo Group in succession and lithologies".

Thus the Kaza Group and the Miette Group (or parts thereof) are correlated by virtually all previous workers in the region. Most have also correlated these two groups with the Monashee Horsethief Creek Group, and some also with the Cariboo Group (Brown *et al.*, 1978; Poulton and Simony, 1980). Many of these correlations seem to rely on the fact that the overlying Lower Hadrynian to Lower Cambrian strata have been correlated. Aitken (1969), however, showed that there is a profound regional unconformity at the base of the Cambrian in the Rocky Mountains east of Revelstoke, and Poulton and Simony (1980) have suggested that the same may be true in the Dogtooth Range.





Poulton and Simony (1980) refrain from confident correlation between the Horsethief Creek Group and the Cariboo Group, because of "structural and stratigraphical complications", pointing out the fact that "more than one recurrent succession of similar lithologies" may occur. This fact has become apparent in the Cariboo Mountains, where the Hadrynian strata in the Blue River area, described by Campbell (1968) as Kaza Group and as underlying the Cariboo Group, were identified by Pell and Simony (1981) as upper Horsethief Creek Group (semipelite–amphibolite unit to upper clastic division). Pell and Simony (1981) report a preliminary opinion in resolution of this problem, expressed by Campbell, Brown and Simony after a joint helicopter reconnaissance traverse of the area in 1980; namely that the Horsethief Creek Group underlies both the Kaza Group and the Cariboo Group. If this is confirmed, and if underlying also means stratigraphically older, then the Miette Group, if confirmed as being the equivalent of the Horsethief Creek Group, cannot also be the equivalent of the Kaza Group.

Furthermore, the structural and metamorphic evidence appears to refute the suggestion of correlation between the Miette, the Monashee Horsethief Creek, and the Kaza Groups. Ghent *et al.* (1980) and Simony *et al.* (1980) have described three sets of major fold structures in the Monashee Horsethief Creek Group of the Columbia Mountains, with migmatization and the strongest metamorphism (to sillimanite grade) occurring after, or during the later stages of, the second folding episode. In the adjacent Middle Miette Group of the Rocky Mountains, lying to the west of the Rocky Mountain Trench, only one major set of buckle folds and thrust faults is evident. This is preceded by mesoscopic isoclinal folding synchronous with a low pressure sillimanite grade metamorphism (which drops to lower greenschist facies in the Dogtooth Range of the northern Purcell Mountains) and here there is no evidence of migmatization. The disappearance of staurolite within the kyanite zone in the Columbia Mountains, but its persistence in the Rocky Mountains, together with geobarometric studies led Simony *et al.* (1980) to suggest that metamorphic pressures were some 2 kb higher in the Columbia Mountains than in the Rocky Mountains, indicating a vertical displacement of about 7 km. Pell and Simony (1981) used similar reasoning and the appearance or non-appearance of staurolite to show that the Precambrian strata in the Cariboo Mountains, west of the North Thompson Fault, which they identify as Upper Horsethief Creek Group, were



metamorphosed at a structural level some 4 km higher than that of the Columbia Mountains. It seems, however, to the author, to be too much of a coincidence for three sets of strata, originally contemporaneous, to have been displaced vertically by relative distances of 4 km and 7 km before being metamorphosed, only to be returned eventually to the same relative structural level. The geochemical evidence presented here appears to support this conclusion.

#### 4.5 Sample Collection and Analysis

Over 100 metasedimentary samples, weighing about 2 kg each, were collected from the vicinity of the Malton Gneiss Complex. To the west of the Complex, heavy vegetation and weathering of hillside outcrops meant that most of the 20+ samples collected from the Kaza Group were from road cuts (Highway 5 and Cariboo Lodge road). About a dozen samples were collected from the Robina Creek area on the Malton Range, where metasediments have been thrust over the Malton Gneiss Complex along a fault zone consisting of several metres of mylonite and muscovitic granulated quartzite. Further south, in the Monashee Mountains, around Mount Albreda, Mount Lempriere and the headwaters of a southern tributary to Clemina Creek, about 10 samples were collected from metasediments, probably of the Monashee Horsethief Creek Group, apparently infolded with the gneisses of the Malton Gneiss Complex (Morrison, 1979). South of the Complex, about 10 Monashee Horsethief Creek Group samples were collected from road cuts on Highway 5 and from around Paradise Lake. To the east of the Malton Gneiss Complex, approximately 50 samples were collected from the Miette Group, along Canoe River road, from Packsaddle, Bulldog and Ptarmigan Creeks and from the northern cirque on Mount Blackman. All samples were collected as objectively as possible, to provide a representative suite at each locality.

The samples were analysed for 11 major and up to 14 trace (Ce, La, Ba, Nb, Zr, Y, Sr, Rb, Zn, Cu, Ni, Co, Cr, Li) elements, on a PW 1212 X-ray spectrometer at Durham University, by Dr. J.G. Holland, using calibration techniques that optimised against the international standards (Flanagan 1973) and a specially cast set of glass standards (Brown *et al.*, 1970). These analyses are shown in Appendix B (tables 19–31).





#### 4.6 Geochemistry

The metasedimentary rocks have been subjected to metamorphism (possibly polyphase) up to amphibolite facies conditions and so it would be desirable to use those trace elements which are believed to be least mobile during metamorphism in order to reconstruct their pre-metamorphic characters. However, plots of Nb, P, Y and Zr showed no features of interest whereas plots of other trace elements and some major elements showed definite differences between the three stratigraphic groups (Kaza, Miette and Monashee Horsethief Creek) which could not easily be related to their metamorphic histories.

Inspection of tables 19–22 in Appendix B and figures 4.2–4.12 shows that the psammites and pelites from Robina Creek are geochemically similar to those from the Kaza Group. Hence it is possible that the Robina Creek metasediments remain as an outlier of the Kaza Group, following the thrusting of that group over the Malton Gneiss Complex.

In figures 4.2 and 4.3, the log of the ratio  $\text{SiO}_2/\text{Al}_2\text{O}_3$  is used as an index of sedimentary compositional maturity against the log of the ratio  $\text{Na}_2\text{O}/\text{K}_2\text{O}$ , measuring the composition of the feldspar or the feldspar/biotite ratio or the detrital illite content of the sediment, after Pettijohn *et al.* (1973). Using their sedimentary terminology to describe the bulk chemistry of these metasediments, it can be seen that the metasediments from each of the three stratigraphic groups can be distinguished. In figure 4.2, the Kaza Group pelites (including those from Robina Creek) form a clearly defined, compositionally compact and sedimentarily mature unit of low  $\text{SiO}_2/\text{Al}_2\text{O}_3$ . The Miette Group pelites cover a broader compositional range and appear to be derived largely from arkosic sediments, although the Canoe River road sub-group of semipelites appear to have a greywacke or lithic arenite character. The Monashee Horsethief Creek Group semipelites can be clearly distinguished, in figure 4.2, from both the Kaza Group pelites and the Miette Group pelites and semipelites. They appear to be derived from greywackes or lithic arenites.

Figure 4.3 shows the compositional ranges of the psammites from the three groups. These overlap in the lithic arenite field, but are still clearly distinguishable from each other. The Kaza Group psammites (including those from Robina Creek) appear to



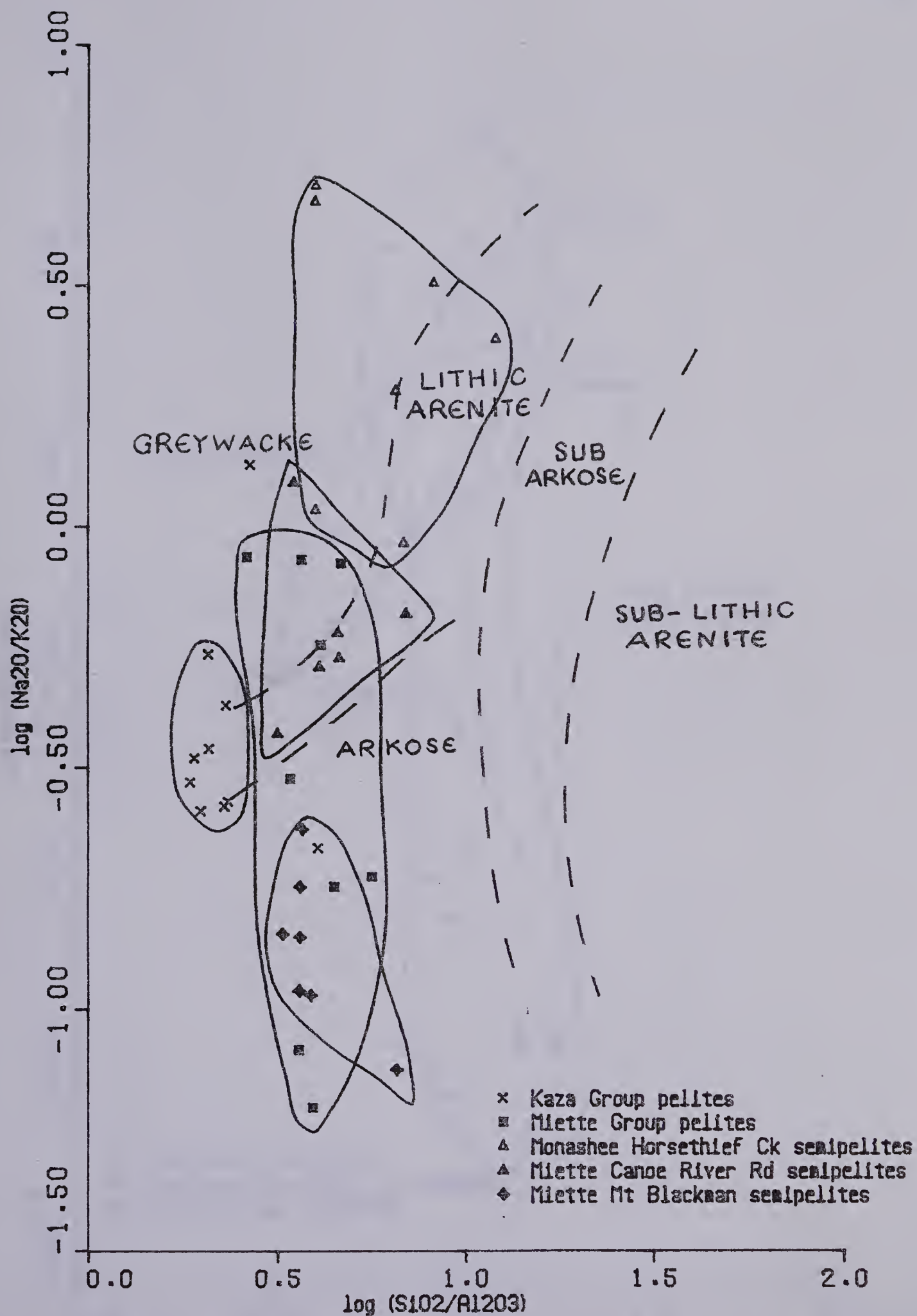


Figure 4.2 Classification (after Pettijohn et al., 1973) of the pelitic rocks from the Kaza, Miette and Monashee Horsethief Creek Groups in the Valemount area.



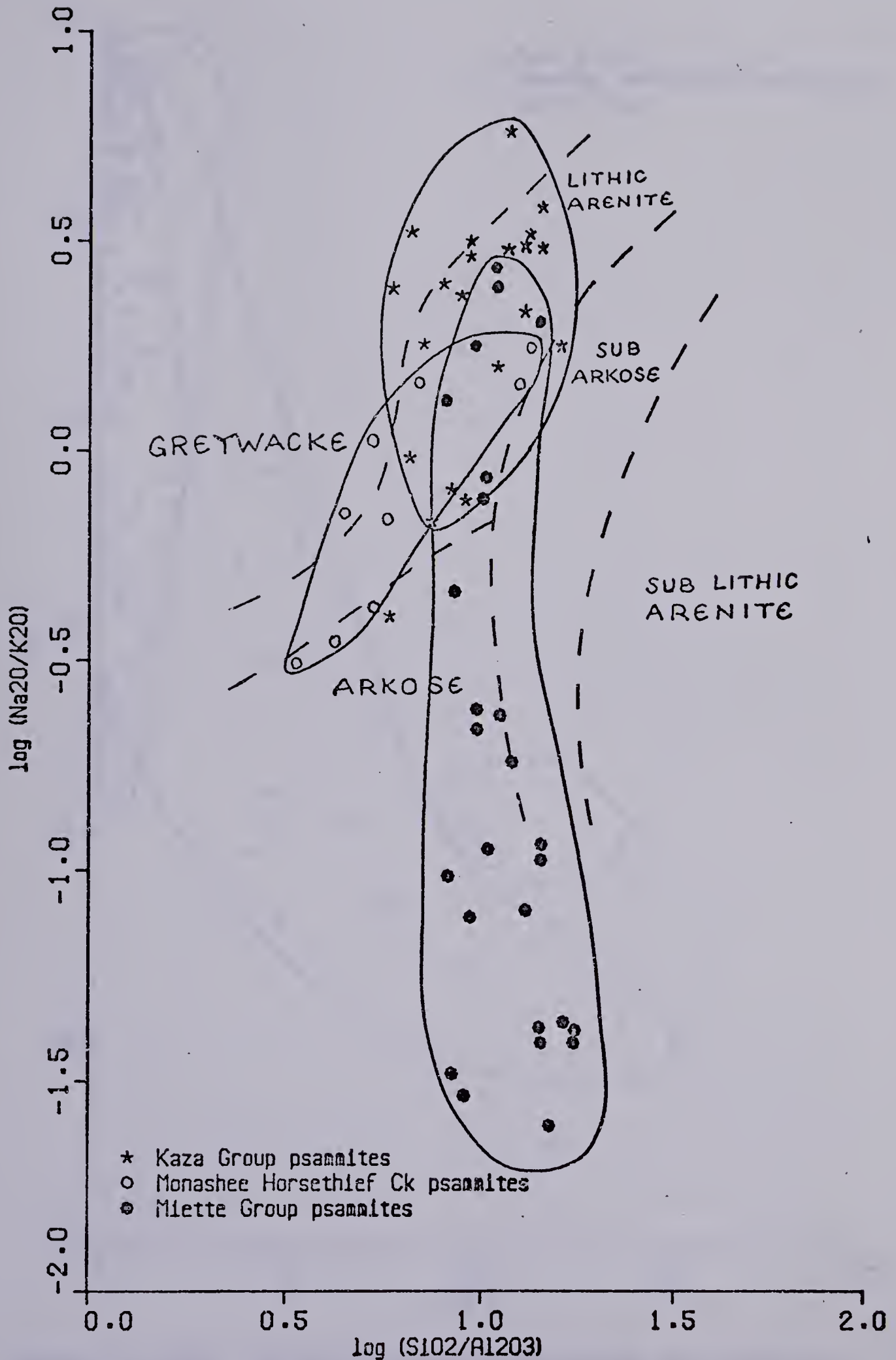


Figure 4.3 Classification (after Pettijohn et al., 1973) of the psammite rocks from the Kaza, Mlette and Monashee Horsethief Creek Groups in the Valenmount area.





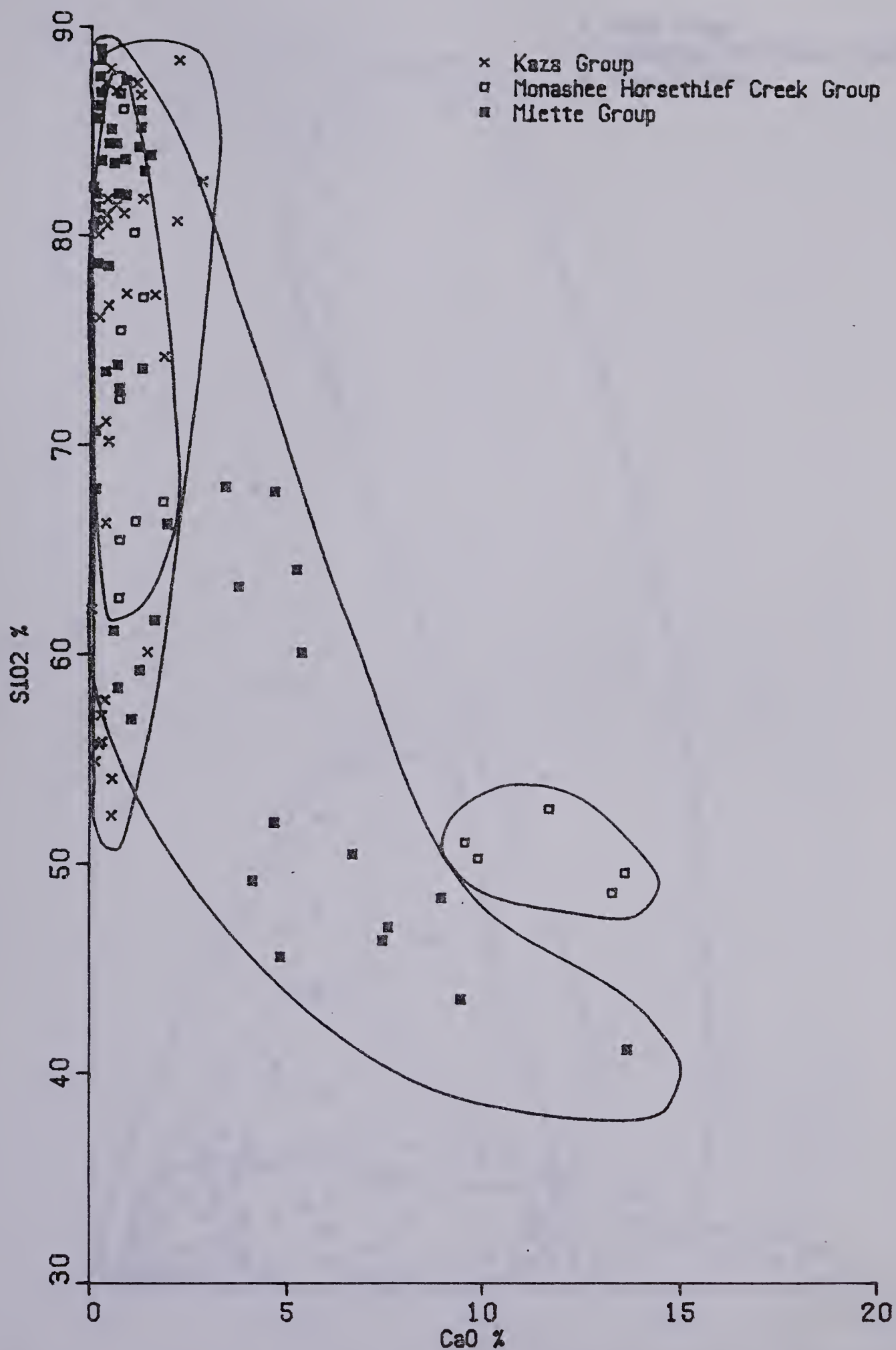


Figure 4.4 SiO<sub>2</sub> v CaO plot for metasediments from the Kaza, Mlette and Monashee Horsethief Creek Groups in the Valenmount area



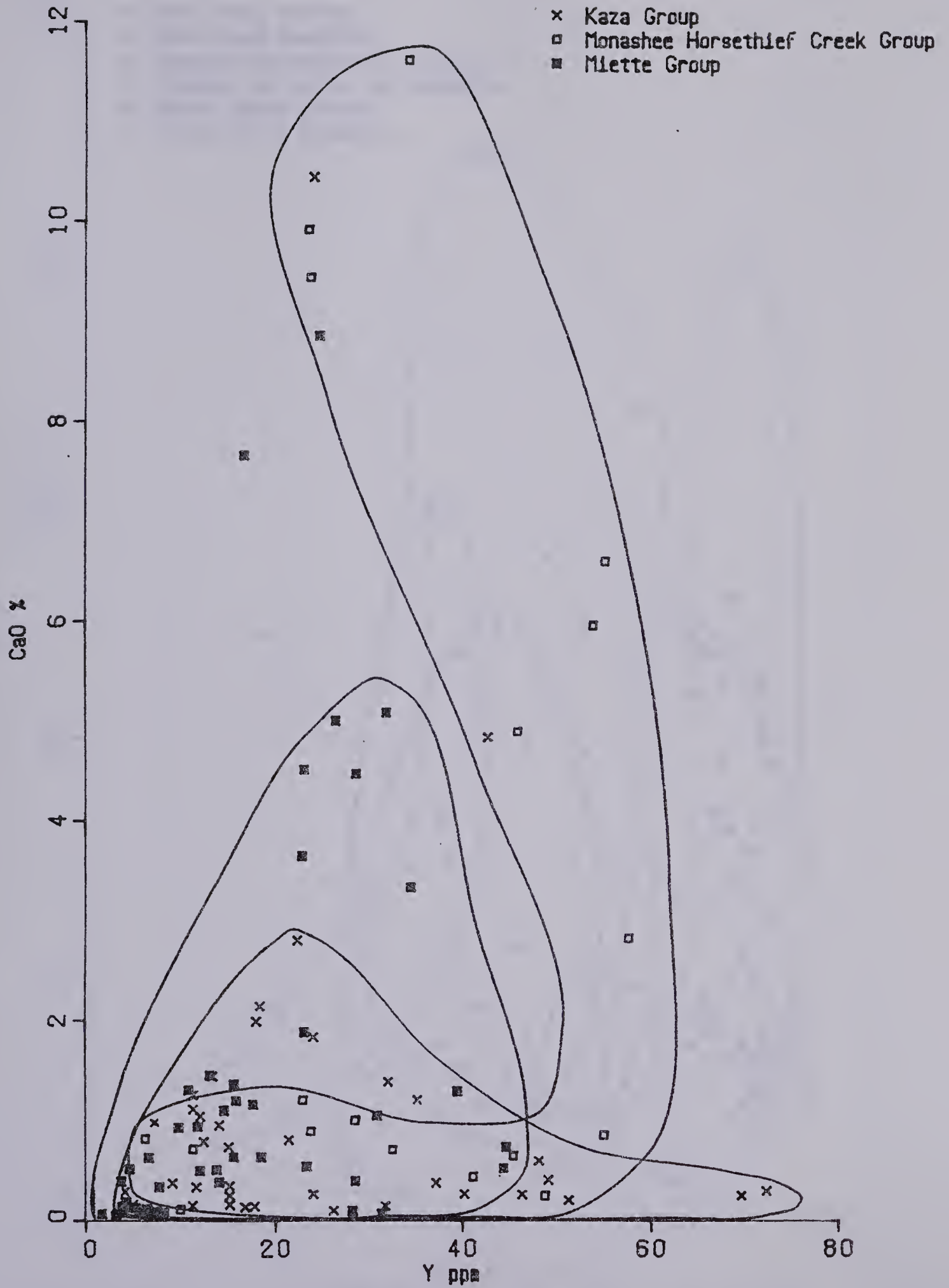


Figure 4.5 CaO v Y plot for metasediments from the Kaza, Milette and Monashee Horsethief Creek Groups in the Valemount area





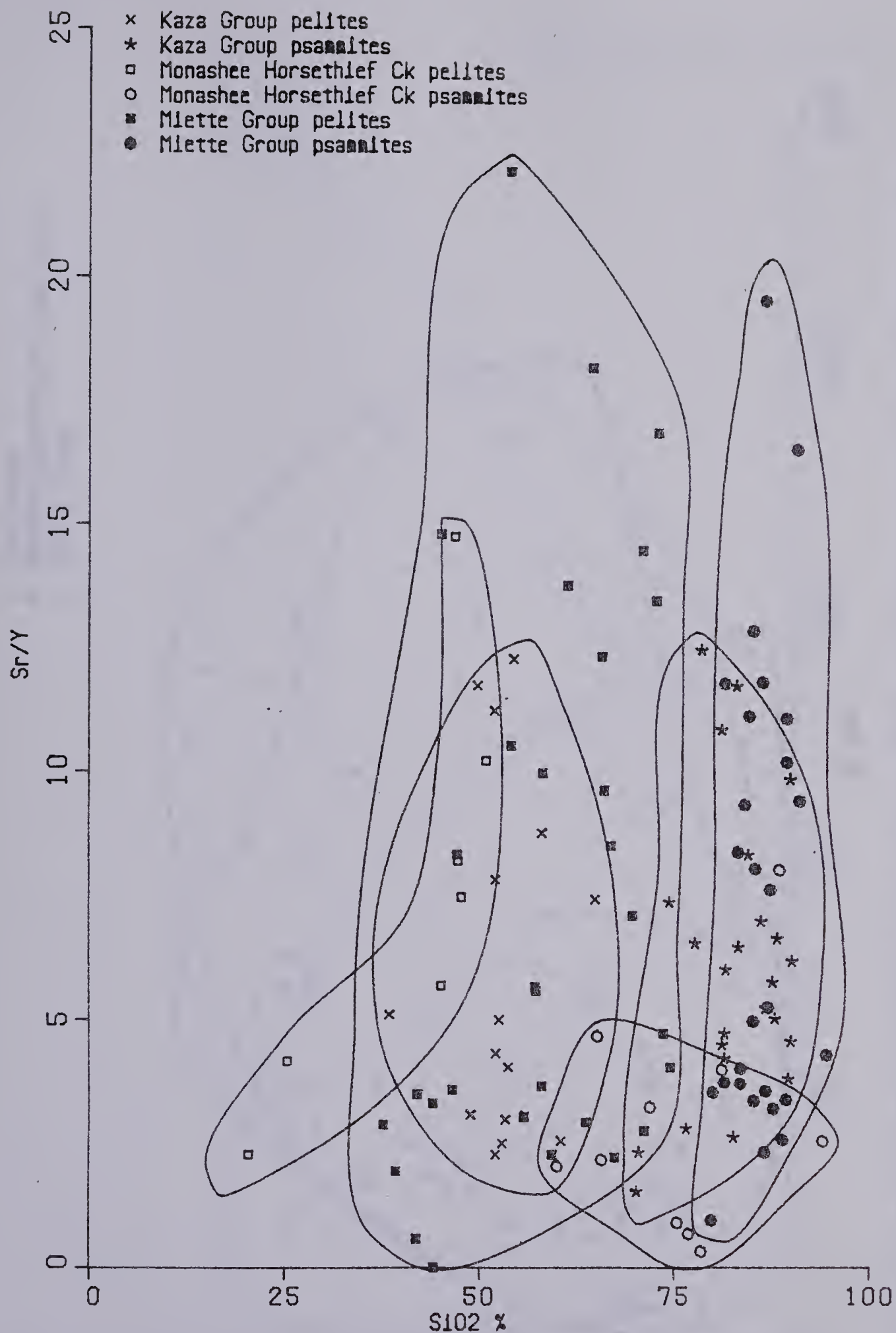


Figure 4.6 Sr/Y v S102 plot for pelites and psammites from the Kaza, Miette and Monashee Horsethief Creek Groups in the Valemount area



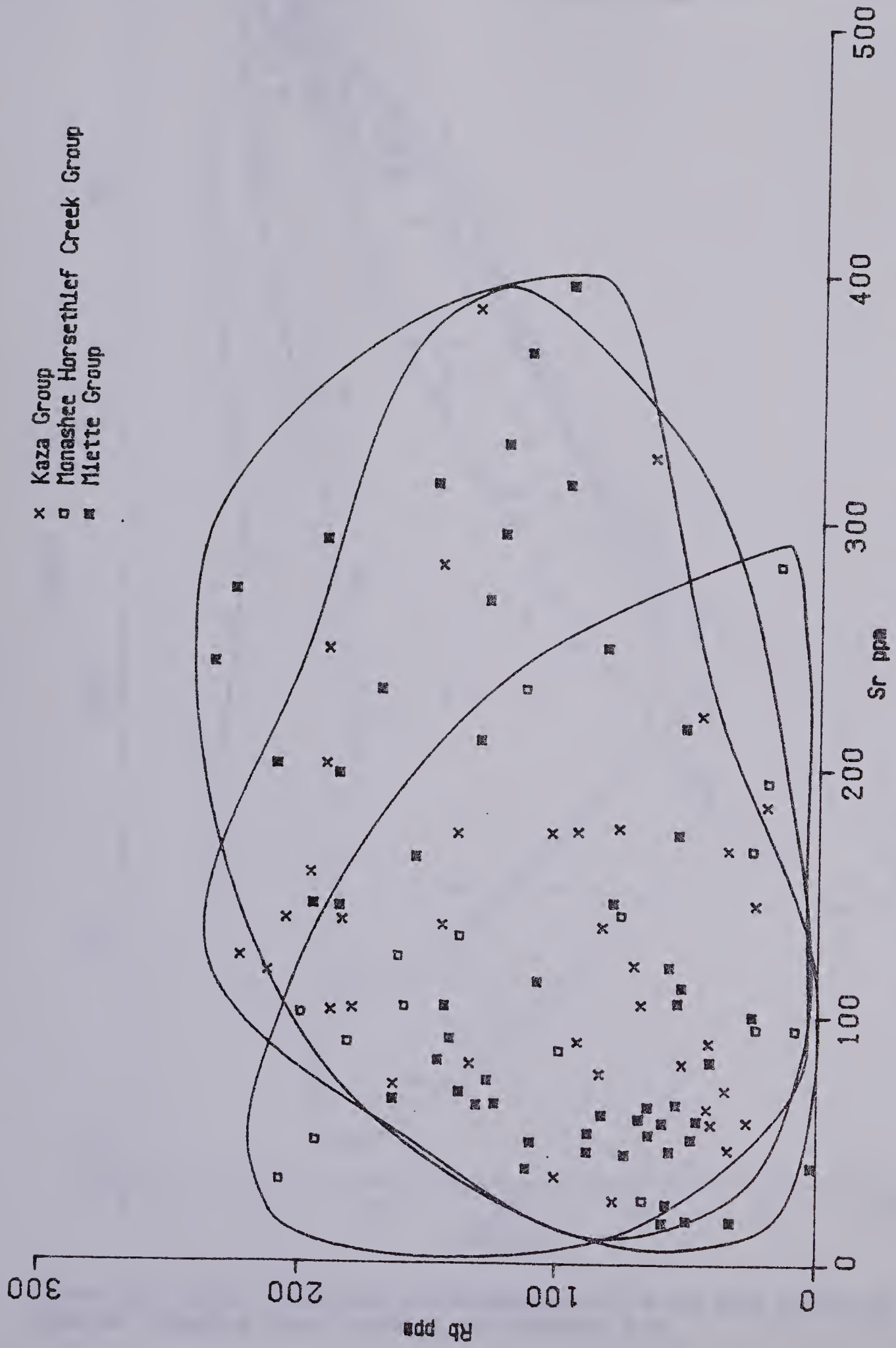


Figure 4.7 Rb v Sr plot for metasediments from the Kaza, Mlette and Monashee Horsethief Creek Groups in the Valcourt area



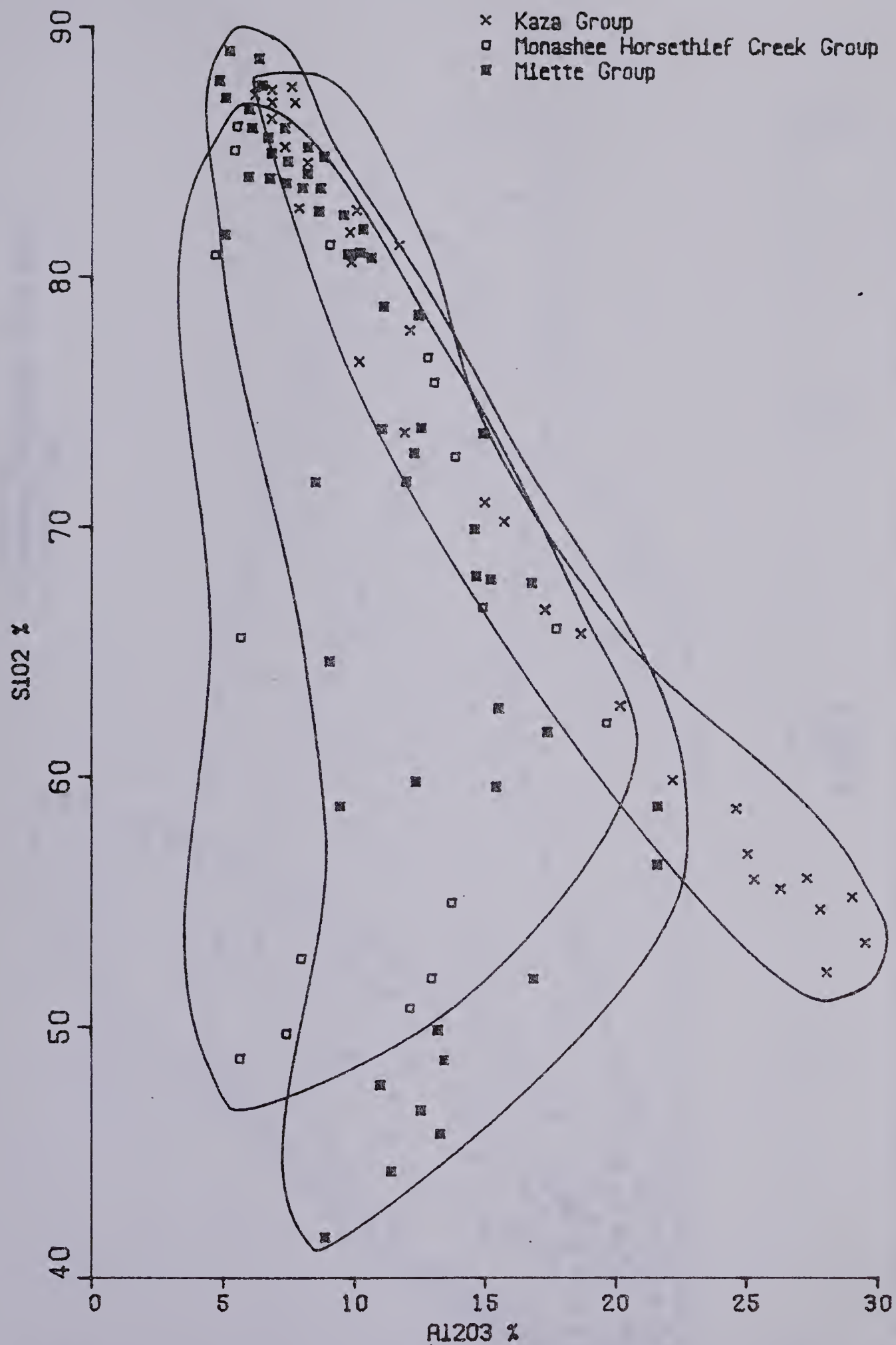


Figure 4.8  $\text{SiO}_2$  v  $\text{Al}_2\text{O}_3$  plot for metasediments from the Kaza, Miette and Monashee Horsethief Creek Groups in the Valemount area





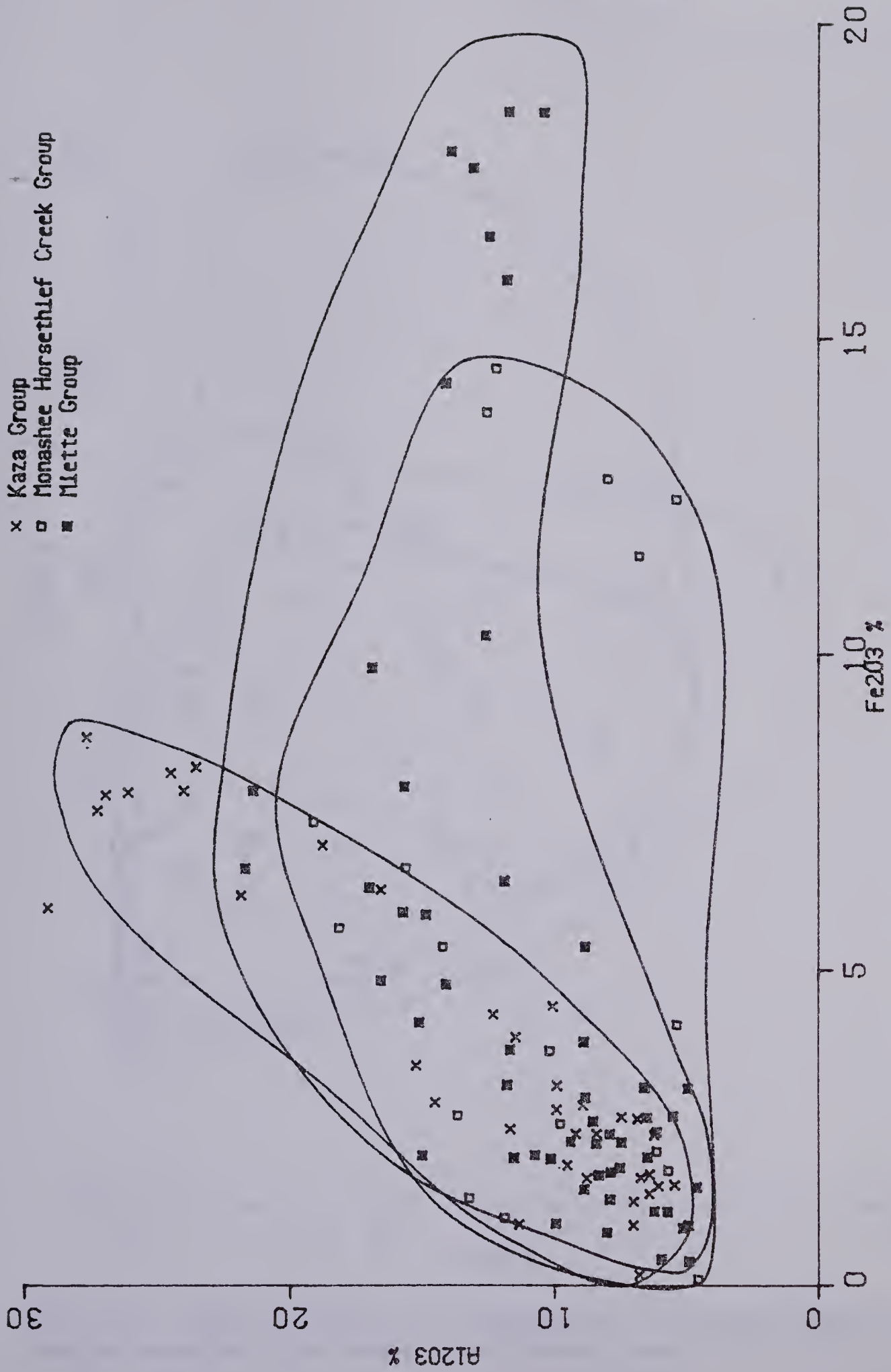


Figure 4.9  $\text{Al}_2\text{O}_3$  v  $\text{Fe}_2\text{O}_3$  plot for metasediments from the Kaza, Mletie and Monashee Horsethief Creek Groups in the Valemount area



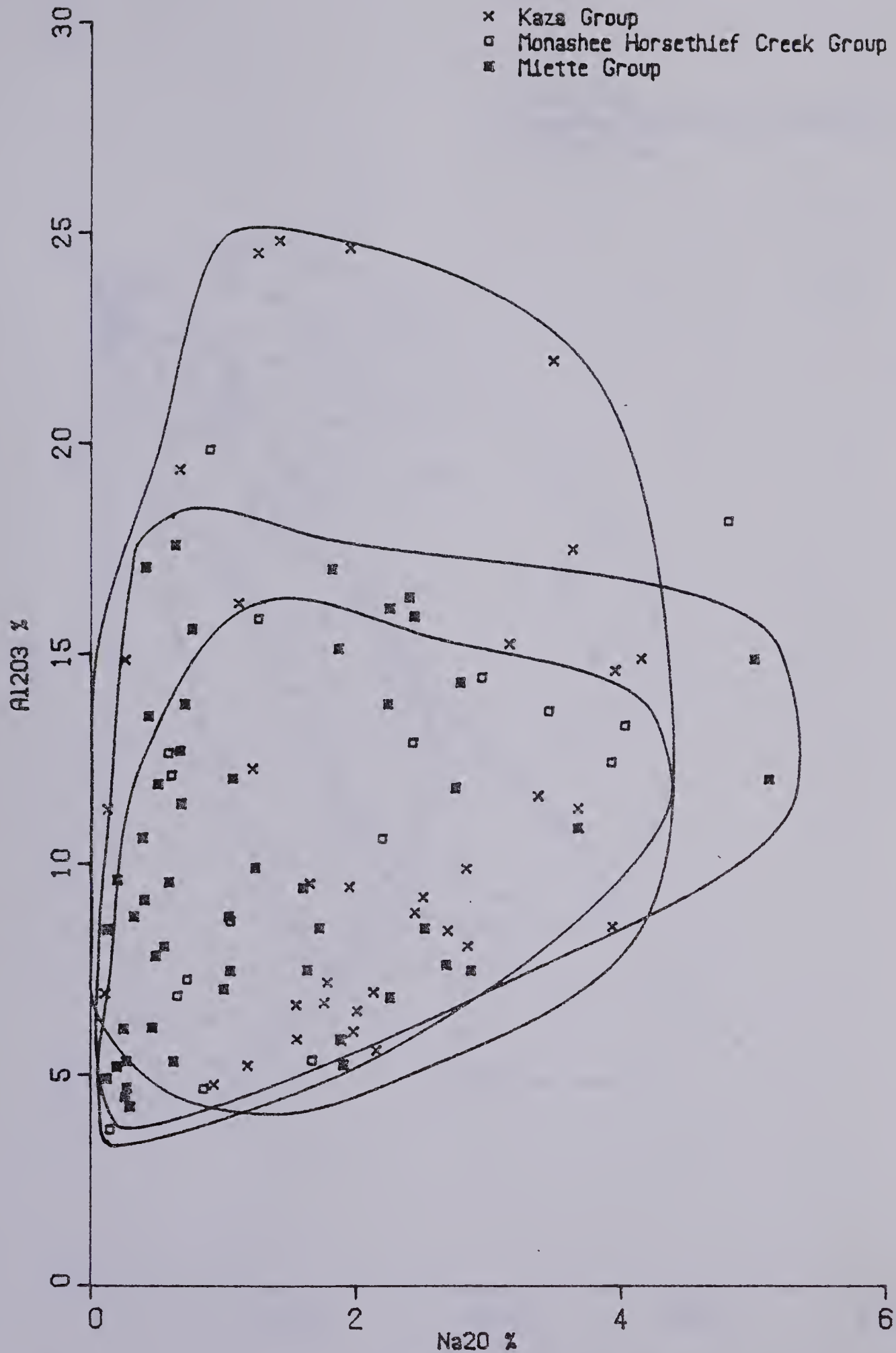


Figure 4.10  $\text{Al}_2\text{O}_3$  v  $\text{Na}_2\text{O}$  plot for metasediments from the Kaza, Miette and Monashee Horsethief Creek Groups in the Valcourt area





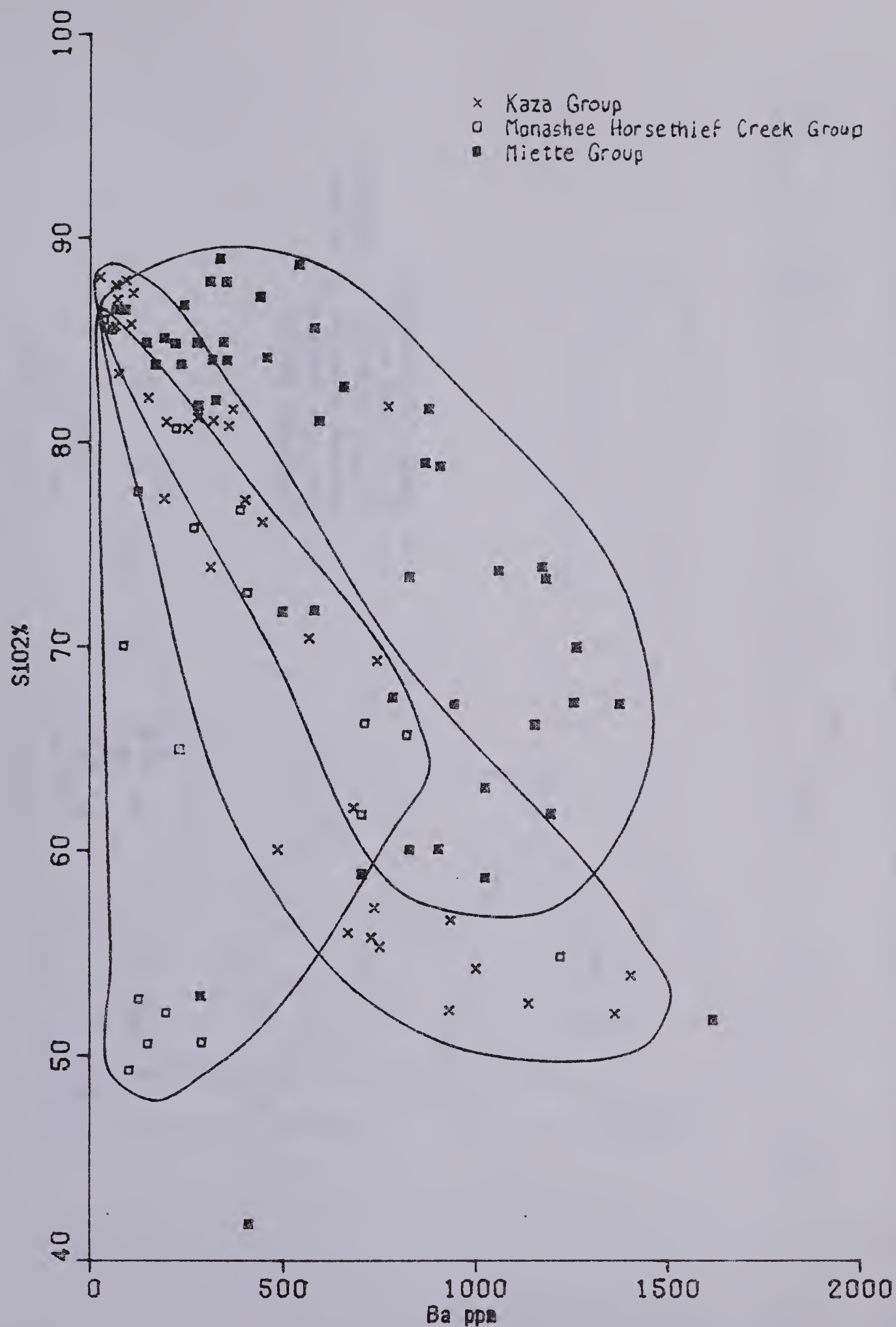


Figure 4.11  $\text{SiO}_2$  v Ba plot for metasediments from the Kaza, Miette and Monashee Horsethief Creek Groups in the Valemount area



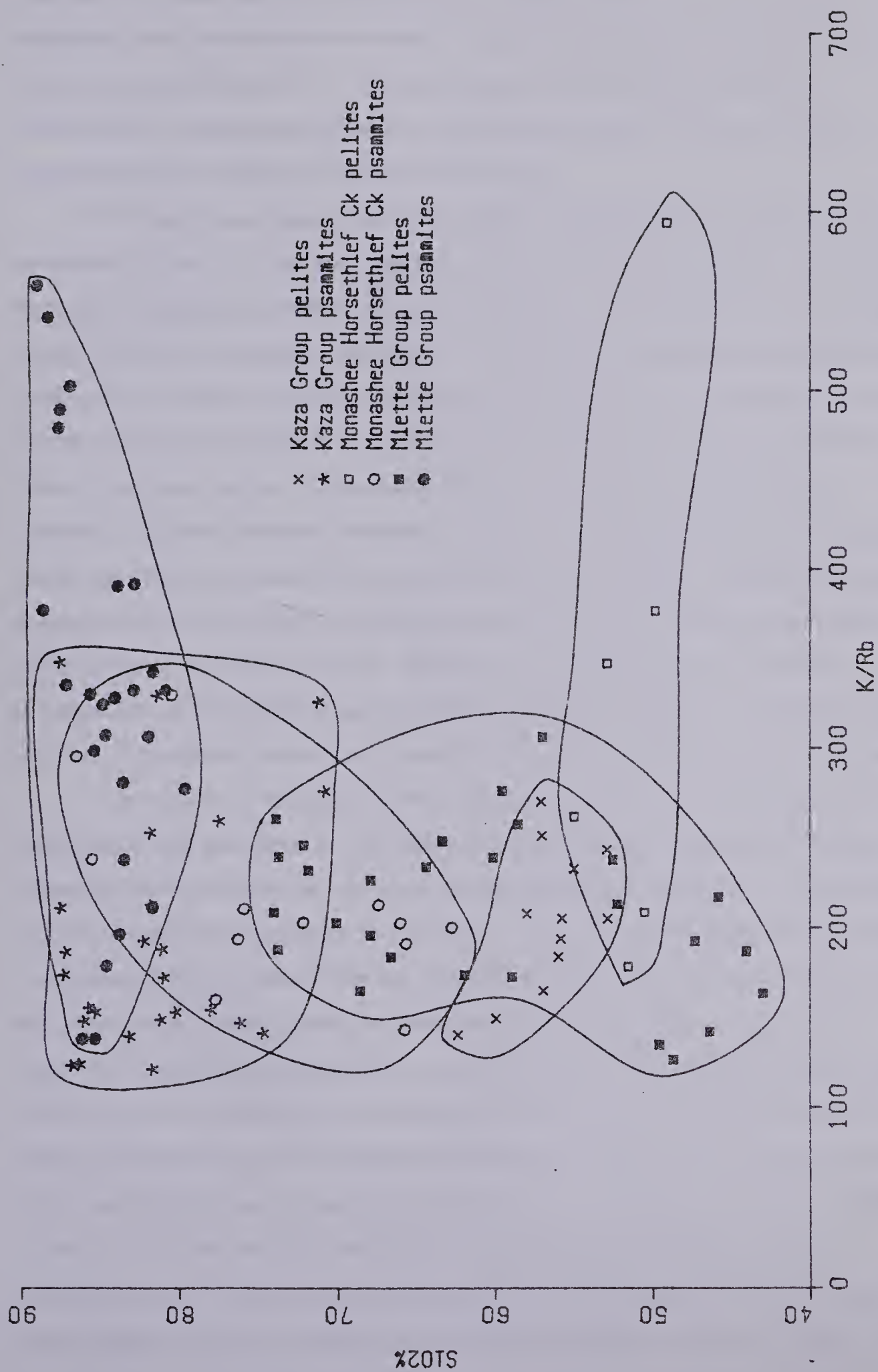


Figure 4.12 S102 vs K/Rb plot for psammilites and pelrites from the Kaza, Mlette and Monashee Horsethief Creek Groups in the Valenmount area



have been lithic arenites with  $\log \text{SiO}_2/\text{Al}_2\text{O}_3$  of approximately unity, whereas the psammites from the Monashee Horsethief Creek Group appear to have been lithic arenites with  $\log \text{SiO}_2/\text{Al}_2\text{O}_3 < 1$ . The psammites from the Miette Group have  $\log \text{SiO}_2/\text{Al}_2\text{O}_3$  of approximately unity, but tend to plot largely in the arkosic field, although they also overlap into the lithic arenite field.

The Kaza Group metasediments are further distinguished from those of the Monashee Horsethief Creek and Miette Groups by being poorer in calcium, reflecting their lower plagioclase contents (figures 4.4 and 4.5). Semipelites are rare in the Kaza Group, but are more common than pelites in the Miette and Monashee Horsethief Creek Groups. On the other hand, the Kaza Group metasediments are not especially poor in strontium (figures 4.6 and 4.7) suggesting that there may have been some strontium mobility into these rocks. This is confirmed by the strontium isotope evidence (chapter 5). Figure 4.6 shows that the Sr/Y ratios in the Miette Group reach higher values than in the Kaza or Monashee Horsethief Creek Groups, probably reflecting the higher proportion of Sr-accepting, Y-rejecting minerals such as plagioclase in the former group (Lambert and Holland, 1974). Balashov *et al.* (1964) have shown that Y is preferentially concentrated in marine shales but relatively depleted in fresh water shales, and part of the Miette Group could have been deposited in a fresh water environment.

The maturity of the original sediments of the Kaza Group, versus the relative immaturity of the sediments of the Miette and Monashee Horsethief Creek Groups is shown in figures 4.8 and 4.9. In figure 4.8, the pelites and psammites of the Kaza Group, including Robina Creek samples, lie on one line, with  $\text{Al}_2\text{O}_3$  decreasing as  $\text{SiO}_2$  increases. The pelites and semipelites of the Miette and Monashee Horsethief Creek Groups contain less  $\text{Al}_2\text{O}_3$  and the Miette pelites and semipelites are comparatively rich in  $\text{SiO}_2$ . In figure 4.9, the pelites and psammites of the Kaza Group (including Robina Creek samples) show a smooth progression from high  $\text{Fe}_2\text{O}_3$ , high  $\text{Al}_2\text{O}_3$  to low  $\text{Fe}_2\text{O}_3$  and low  $\text{Al}_2\text{O}_3$ . The pelites and semipelites of the Miette and Monashee Horsethief Creek Groups are richer in  $\text{Fe}_2\text{O}_3$ , the Miette Group containing up to 20%  $\text{Fe}_2\text{O}_3$ . By contrast, the  $\text{Al}_2\text{O}_3$  vs  $\text{Na}_2\text{O}$  plot of figure 4.10 does not differentiate between the three stratigraphic groups of metasediments, nor does the Kaza Group appear to be particularly mature in that plot, the metasediments from Mount Blackman appearing as the most mature sub-group of those





plotted. This anomalous plot can perhaps be explained by the relative mobility of sodium during metamorphism.

Figures 4.11 and 4.12 give some indication of the original mineralogy of the sediments, as well as showing clear distinctions between the three groups. Figure 4.11 shows a fairly clear distinction in Ba content between the three groups, the Monashee Horsethief Creek Group having lower Ba contents than the Kaza Group, which in turn has lower Ba contents than the Miette Group. These variations possibly reflect the potassium feldspar content of the original sediments. Figure 4.12 shows the variation in K/Rb ratios between the various groups. Similar ratios in the pelites and psammites of the Kaza Group may indicate a similar mineralogy in the shales and sandstones of this group, so far as the K and Rb are concerned. the most likely mineral is detrital feldspar. The Kaza Group appears to have formed as a mature sediment. The Monashee Horsethief Creek Group and the Miette Group, on the other hand, have widely differing K/Rb ratios for the pelitic and psammitic fractions, the Miette psammites and Monashee Horsethief Creek pelites having much higher K/Rb ratios than the other fractions. The higher K/Rb ratios of the Monashee Horsethief Creek pelites suggests there was a lower proportion of clay minerals in the sediments from which they were derived, a conclusion consistent with figure 4.2, where the Monashee Horsethief Creek pelites plotted in the greywacke field.

Thus the geochemistry of the Kaza, Miette and Monashee Horsethief Creek Groups appears to confirm the suggestion that each Group represents a separate lithological assemblage and that none of the Groups can be confidently correlated with any of the others. The Kaza Group appears to be derived from the most mature sediments and the Miette Group from the least mature.



## 5. GEOCHRONOLOGY

### 5.1 Introduction

No previous geochronological studies have been made of the Malton Gneiss Complex, except that already published by the author (Chamberlain *et al.*, 1979), but some K–Ar studies have been conducted on the metasediments around the Complex. Price and Mountjoy (1970) published a K–Ar age on post-kinematic biotite in the Selwyn Range, and Charlesworth *et al.* (1967) have published some K–Ar studies on detrital micas in the Jasper and Tete Jaune Cache regions to the northeast and northwest of the present study area. (See chapter 1). Various authors have published the results of geochronological studies on rock suites south of the Malton Gneiss Complex (Lowden *et al.*, 1963; Wanless *et al.*, 1967; Wanless and Reesor, 1975; Okulitch *et al.*, 1975; Wanless and Okulitch, 1976; Duncan, 1978.) (See section 5.4).

The present studies were undertaken in an attempt to obtain an overall view of the history of the area including, if possible, its relationship to other nearby regions. Petrological and structural studies of the gneisses and metasediments in the area have shown that they are both polymetamorphic and polydeformational, but the virtual absence of chloritization and biotitization, together with minimum late stage alteration of feldspar, rules out the possibility of any large scale hydrothermal alteration. Hence, the extent to which these metamorphic episodes can be dated, or alternatively, the extent to which the "metamorphic veil" of Berger and York (1981) can be pierced, by the rubidium–strontium whole rock isochron method, depends on the diffusion history of the rubidium and strontium in the rocks.

Laboratory studies of diffusion are difficult to extrapolate to low temperatures and/or true geological conditions, but Kesmarky (1977) has shown that both rubidium and <sup>87</sup>–strontium are mobile, at least to distances equivalent to granite grain size, at temperatures of 890°C, atmospheric pressures and anhydrous conditions. Other workers have estimated rates of diffusion of different types and have discussed the theory of diffusion and closure. (Wetherill *et al.*, 1955; Baadsgaard *et al.*, 1961; Hart *et al.*, 1968; Dodson, 1973; Giletti, 1974; Harrison and Clarke, 1979) The behaviour of rubidium and strontium is similar to that of argon. The rate of diffusion depends on





many variables, including temperature, pressure, lattice type, crystal grain boundaries, mineral assemblages, fluids present and the type of diffusion (volume or non-volume, self- or interdiffusion). The complex natural geologic situation is difficult to reproduce exactly, either mathematically or in the laboratory. Geological experience has shown, however, that rocks metamorphosed to the garnet zone of metamorphism tend not to be isotopically homogenized with respect to rubidium and strontium during metamorphism; whereas, those metamorphosed above the staurolite-kyanite grade tend to have their rubidium-strontium systematics partially or completely upset. For example, Lambert *et al.* (1982) have shown that the garnet zone Leven Schists of Scotland yield rubidium-strontium whole rock isochron ages that have not been reset by metamorphism, whereas, the nearby kyanite zone Monadhliath Schists yield rubidium-strontium whole rock metamorphic ages. Similarly, Ghosh (personal communication, 1982) has found that rubidium-strontium whole rock isochrons on Mesozoic metasediments, in the Kootenay area of British Columbia, yield sedimentary ages on formations below the garnet zone, but that there is a metamorphic "scatterchron" for the Lardeau Formation, the only example studied by him which lies above the staurolite-kyanite isograd. Hence, it seems that at about 500°C, large scale migration of rubidium and <sup>87</sup>strontium begins but may not be completed, in that the rock may not be completely rehomogenized with respect to the rubidium and strontium isotopes. The results of Harrison and Clarke's (1979) work on the cooling of the Quottoon pluton lead to a similar conclusion.

The gneisses of the Malton Gneiss Complex are of middle amphibolite facies, and the metasediments in the vicinity of the Complex range from garnet grade to kyanite grade, the majority being in the staurolite-kyanite zone. (Figure 3.1). Hence, they have been raised into the temperature range of 450°C to 550°C, where the diffusion coefficients change by several orders of magnitude over a narrow temperature range. Detailed inhomogeneities, especially in fluid concentrations, in the wide range of rock types present in the area appear to have resulted in an irregular pattern of diffusion paths and distances during regional metamorphism. These irregularities often appear to be independent of the lithology or the geochemistry of the rocks, so that it is not possible to distinguish groups of pelites, for example, or low-niobium gneisses, that



have rubidium–strontium systematics distinct from, say, semipelites, or high–niobium gneisses. The only pattern which emerges appears to be that the more refractory strontium–rich rocks, of low Rb : Sr ratio, tend to preserve the older ages; whereas, the potassium–rich, strontium–poor rocks, of high Rb : Sr ratio, tend to yield younger ages. On rubidium – strontium isochron diagrams with a large scatter of points, possible upper and lower limits to the true age of the rock have been calculated.

## 5.2 Analyses

Rubidium–strontium analyses were made on about 200 whole rock samples from all the major rock units. Uranium–lead analyses were made on zircons separated from about 10 of these rock samples. Rubidium and strontium concentrations were obtained by X.R.F. and cross checked by isotope dilution measurements (Pankhurst and O'Nions, 1973). Rubidium and strontium were separated from approximately 200 mg of sample using standard barium nitrate co–precipitation and/or ion exchange column methods. Uranium and lead were separated from approximately 20 mg of zircon using Krogh's (1973) method. Uranium, lead and strontium isotopic ratios were measured on a V.G Micromass 30 mass spectrometer. Rubidium was analysed on a laboratory built 30 inch vertical radius solid source mass spectrometer. Isochrons were calculated using the methods of Brooks *et al.*, (1972). Table 32 (appendix C) shows the good correlation obtained on duplicate strontium isotope ratio measurements in both inter– and intra–laboratory tests. The type of computer program used to compute the results appears to introduce more variation than the aliquotting of the sample, the chemical separation, the laboratory blank or the mass spectrometric analysis. Tables 33 and 34 show the results of regular checks on standards and blanks. (All  $^{87}\text{Sr}/^{86}\text{Sr}$  values are standardized and quoted at the  $2\sigma$  level of confidence.) Internationally recognized constants have been used throughout (Steiger and Jager, 1977)



## 5.3 Results and Discussion

### 5.3.1 Grey Gneiss

Rubidium–strontium data on about 20 Grey Gneiss whole rock samples (collected from every geographical region of the Malton Block) are shown in figure 5.1 and table 35 (appendix C). The considerable scatter of points seen in figure 5.1 is typical of a poly-metamorphic rock. Petrographic and geochemical studies have shown that there has been some exchange of alkalis in and out of these gneissic rocks, during at least two periods of metamorphism. The distribution of the points suggests that there has been exchange of rubidium and strontium in these rocks rather than total loss or gain. The best straight line through all the points, except for the three obviously aberrant ones, yields an age of  $3195 \pm 39$  Ma. and an initial  $^{87}\text{Sr}/^{86}\text{Sr}$  ratio of  $0.6990 \pm 5$ . This initial ratio is clearly impossible and appears to be the result of the exact distribution of the erroneous points, especially those near the origin. If the eight points showing the largest amount of scatter about this line are omitted from the calculation, an age of  $3093 \pm 46$  and an initial strontium  $^{87}\text{Sr}/^{86}\text{Sr}$  ratio of  $0.7001 \pm 6$  are obtained on a twelve point isochron (the twelve open symbols on figure 5.1). This age and initial ratio are probably close to the truth, but the errors quoted are the errors on this twelve point isochron rather than the true errors on the age and initial ratio of the Grey Gneiss. In any case, the initial ratio must be low which indicates direct or almost direct derivation from the Archean mantle, and the age, which must be close to 3 Ga, is interpreted as the igneous event forming the calc-alkaline tonalitic protolith of the Grey Gneiss. A strontium evolution diagram (figure 5.2) shows that the initial ratio is on or near the postulated mantle growth curve.

Figure 5.3 shows the uranium–lead evidence obtained on separated zircons. The appearance of zircons suggests that they have been reheated or re-annealed: only a few have retained any suggestion of the hyacinth colour and metamict texture typical of Archean zircons. Their appearance ranges from brown subhedral partially metamict crystals to transparent anhedral or subhedral clear, clean crystals; but there is no sharp division such as might suggest a mixed population. The six Grey Gneiss samples lie close to a chord intersecting concordia at c.2450 Ma and c.1250 Ma. The considerable scatter about this line, however, together with the physical appearance of the zircons and the





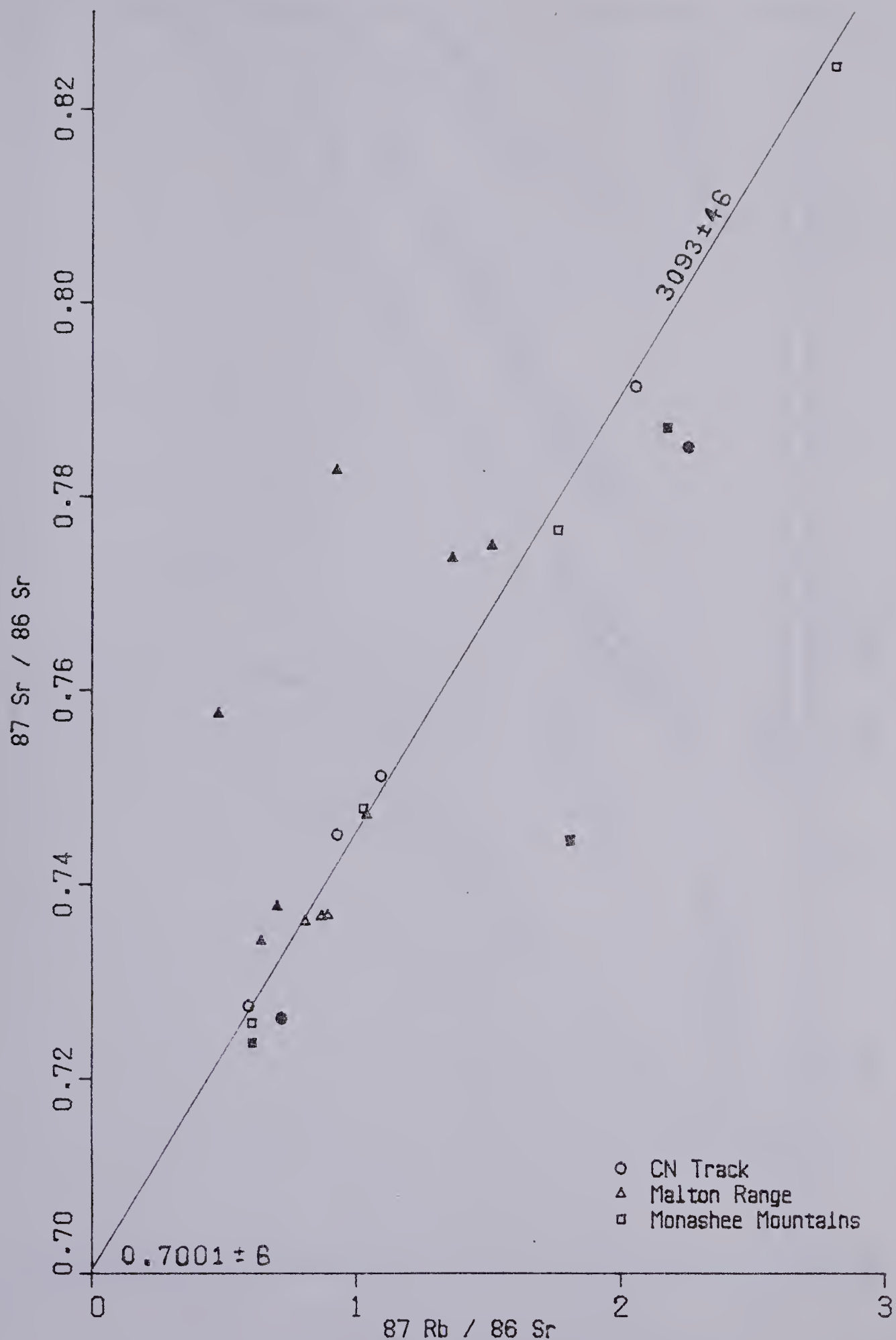


Figure 5.1 Rb-Sr isochron diagram for the Grey Gneiss of the Malton Gneiss Complex. Solid symbols represent data points not used in the isochron calculation (see text).



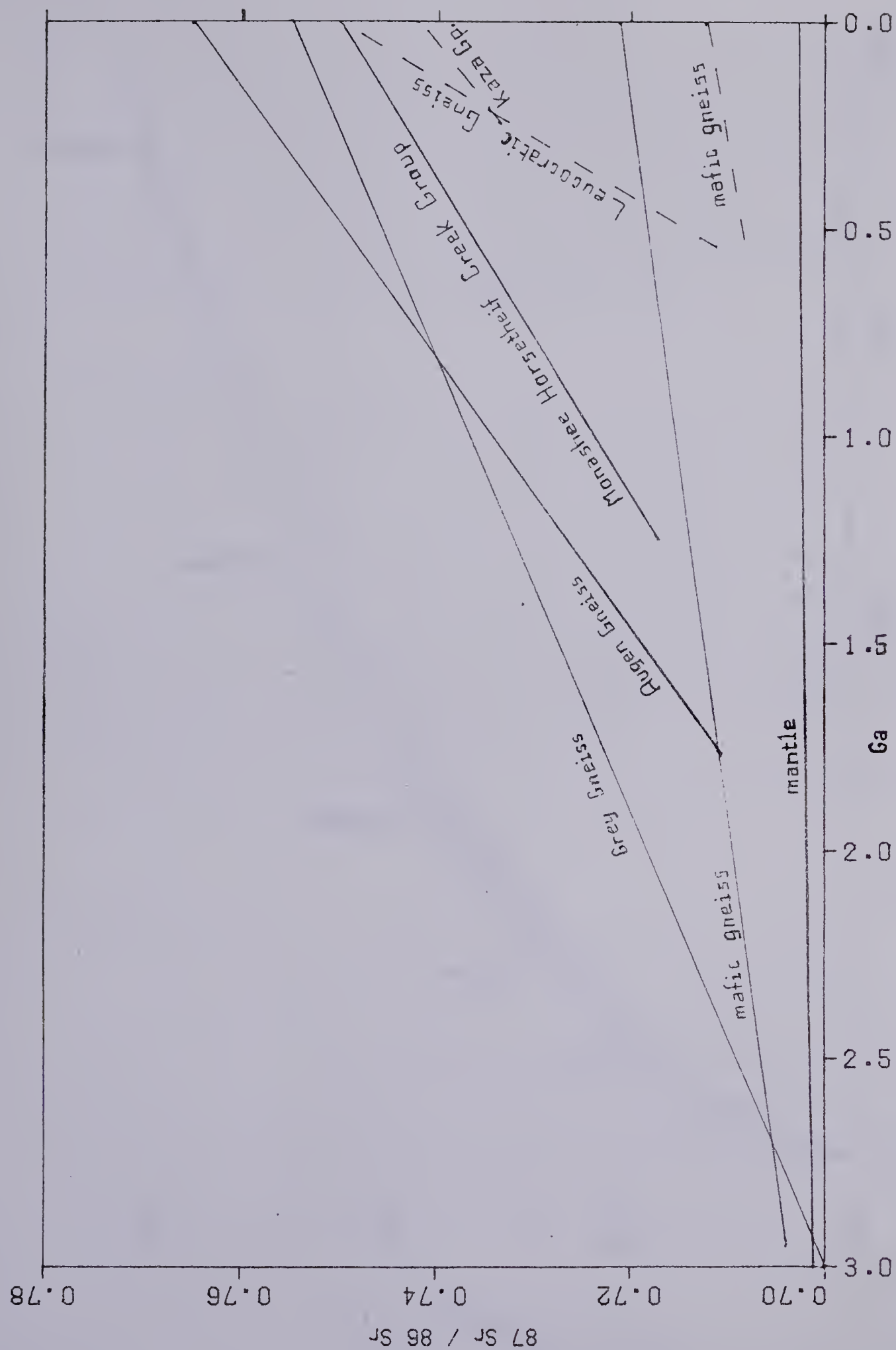


Figure 5.2 Strontium evolution diagram for rocks west of the Rocky Mountain Trench in the Valemount area





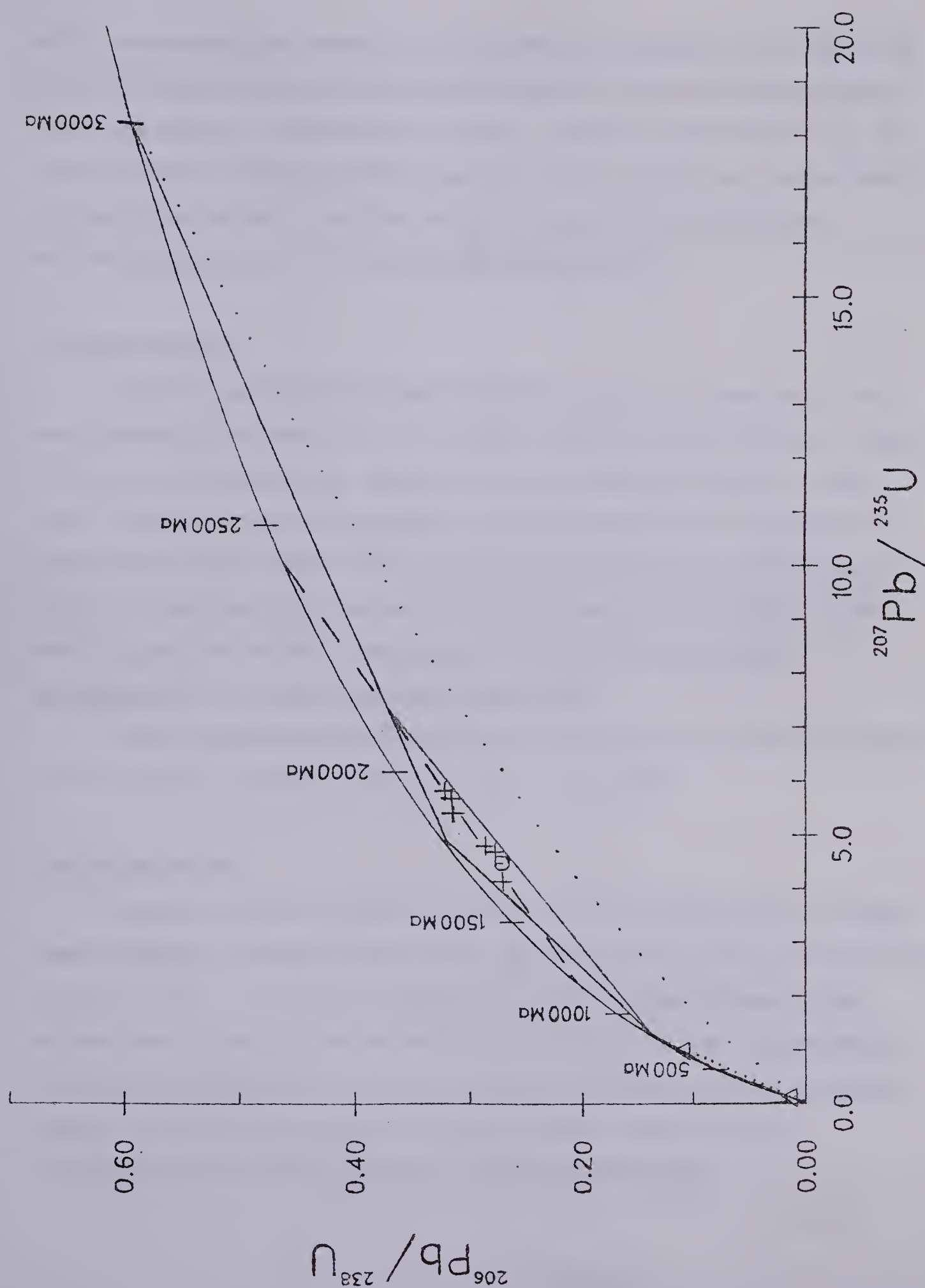


Figure 5.3 Concordia plot of zircons from the Grey Gneiss (+), the Leucocratic Gneiss (Δ) and the Mount Blackman Gneiss (○) of the Malton Gneiss Complex. Solid line represents multi-stage lead loss. Dashed line represents single stage lead loss. Dotted line represents diffusive lead loss.



lack of any corroborative evidence for a 2500 Ma event, suggests that this may not be an episodic lead loss line, and that the correct model for these zircons may be that of multi-stage lead loss. Alternatively, the rubidium – strontium data may be wrong. The calculated uranium–lead dates (table 46, appendix C) give 2120 Ma as a minimum age for the Grey Gneiss and this is consistent with intrusion at c.3000 Ma followed by multi-stage lead loss at c.1770 Ma, and c.550 Ma (figure 5.3).

### 5.3.2 Mafic Gneiss

Figure 5.4 and table 36 (appendix C) give the rubidium–strontium data for the mafic gneisses of the Malton Block. The rubidium–strontium isochron diagram of figure 5.4 shows considerable scatter indicative of a poly-metamorphic history for these rocks. The maximum age of the gneisses, as shown by the upper line, appears to be approximately  $2950 \pm 50$  Ma. This is interpreted as an igneous event, and the age is close to that obtained for the intrusion of the Grey Gneiss protolith ( $3093 \pm 46$  Ma), which suggests that the oldest mafic rocks in the complex were intruded at approximately the same time as the oldest felsic rocks.

The lower line shown on figure 5.4 yields an age similar to the minimum obtained on the Leucocratic Gneiss and is discussed under heading 5.3.4.

### 5.3.3 Augen Gneiss

Figure 5.5 and table 37 give the rubidium–strontium isotope data for the Augen Gneiss. It appears to have formed at  $1767 \pm 20$  Ma (Hudsonian), with a strontium 87/86 ratio of  $0.7105 \pm 2$ . The scatter of points in figure 5.5 provides evidence of later metamorphism, while the strontium evolution pattern (figure 5.2) and the geochemistry (chapter 3) are consistent with a protolith derived from the local mafic gneiss by partial melting. The Grey Gneiss and the mafic gneiss probably suffered their first metamorphism at this time as implied by the multi-stage lead model.





Figure 5.4 Rb-Sr isochron diagram for the mafic gneisses west of the Rocky Mountain Trench in the Malton Gneiss Complex. The diagram shows possible maximum and minimum ages for the mafic gneisses.





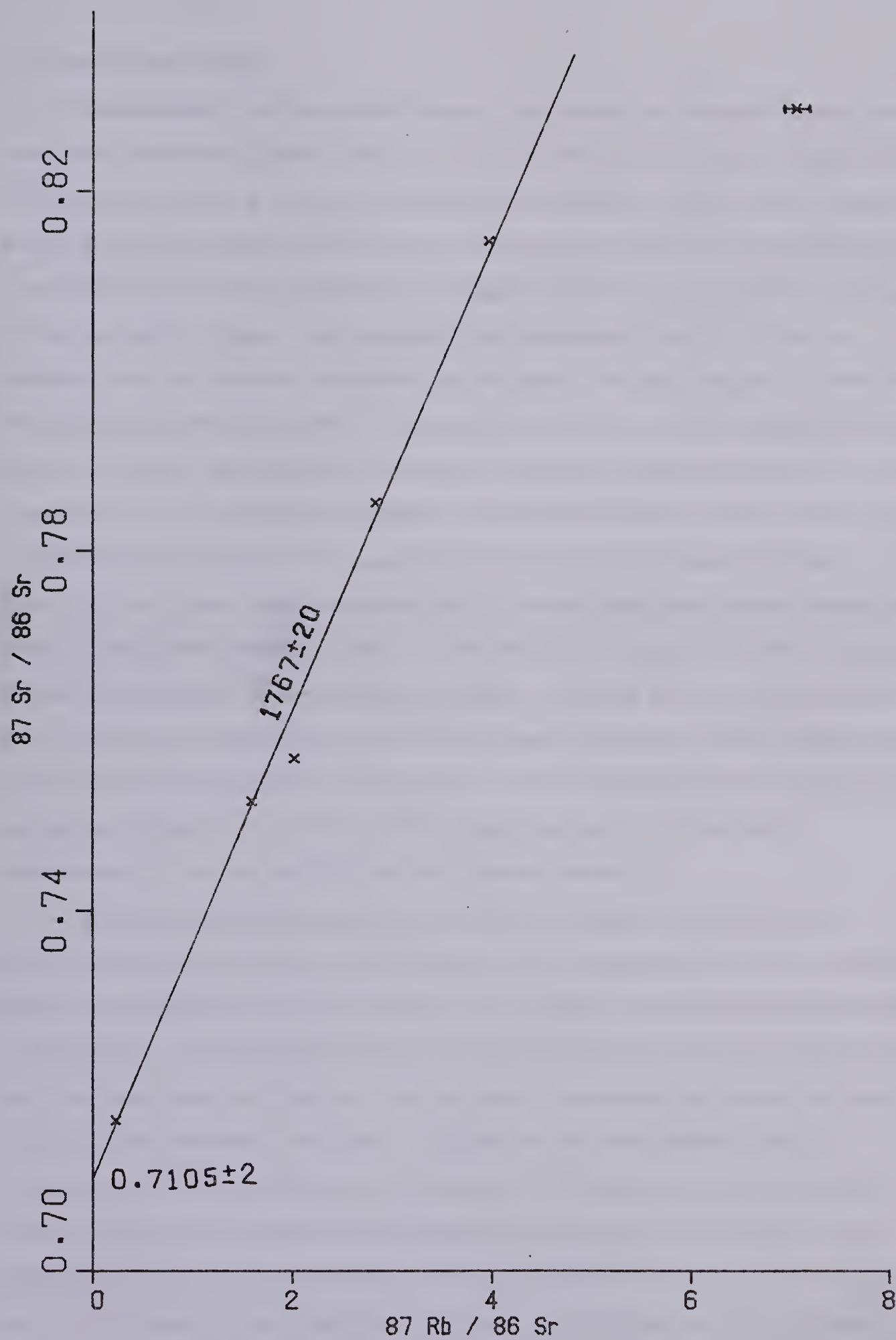


Figure 5.5 Rb-Sr isochron diagram for the Augen Gneiss of the Malton Gneiss Complex



### 5.3.4 Leucocratic Gneiss

Geochemically, the Leucocratic Gneiss is very similar to the Augen Gneiss, both being mildly peralkaline granitic rocks, but the strontium isotope evidence suggests that the Leucocratic Gneiss is not simply reheated and remobilised Augen Gneiss. Figures 5.6 and 5.2 show that the initial  $87/86$  ratio of the Leucocratic Gneiss was probably much lower than the  $87/86$  ratio reached by the Augen Gneiss at any probable time of intrusion for the Leucocratic Gneiss. The true age of the Leucocratic Gneiss is difficult to ascertain from the rubidium – strontium data because of the large amount of scatter on the isochron diagram (figure 5.6). There appears to be a lower limit of about 550 Ma, and this is close to the lower limit on the age of the mafic gneisses (figure 5.4). If this is a real event, it may represent an intrusion of leucocratic magma produced by the partial remobilization and mixing of the Augen Gneiss with another previously intruded leucocratic rock, since field evidence shows that some Leucocratic Gneiss predates the younger mafic dykes (plates 2.2 and 2.11), and the zircon evidence (see below) suggests an older minimum age for the Leucocratic Gneiss. The cause of any c.500 Ma melting of the Leucocratic and Augen gneisses could have been an intrusion of mafic magma, and, if so, the initial strontium  $87/86$  ratio ( $0.7082 \pm 1$ ) on the c.500 Ma mafic line (figure 5.4) is low enough to imply a fresh influx of mafic magma at this time rather than a remobilisation of the original 2950 Ma mafic gneiss (figure 5.2).

Uranium and lead isotopic analyses on zircons suggest the presence of a pre-550 Ma leucocratic rock, as stated above. Zircons separated from two Leucocratic Gneiss samples (5886 and 5901R) gave Pb 207/206 ages of 840 Ma and 820 Ma (table 46, appendix C). These ages tend to be minima, suggesting that the original leucocratic rock is at least as old as c.840 Ma. The positions of these samples on the concordia plot (figure 5.3) are consistent with a multi-stage lead model, with episodic lead loss occurring at c.1700 Ma, c.850 Ma, c.550 Ma and c.100 Ma (shown by the solid lines) and/or a diffusive lead model with lead being lost by diffusion from c.850 Ma to the present day (shown by the dotted line). The multi-stage model would indicate lead loss during the intrusion of the Augen Gneiss protolith at c.1700 Ma, during the intrusion of a leucocratic magma at c.850 Ma, during a possible partial remelting episode at c.550 Ma and during a Cretaceous reheating episode. The diffusion model would indicate the



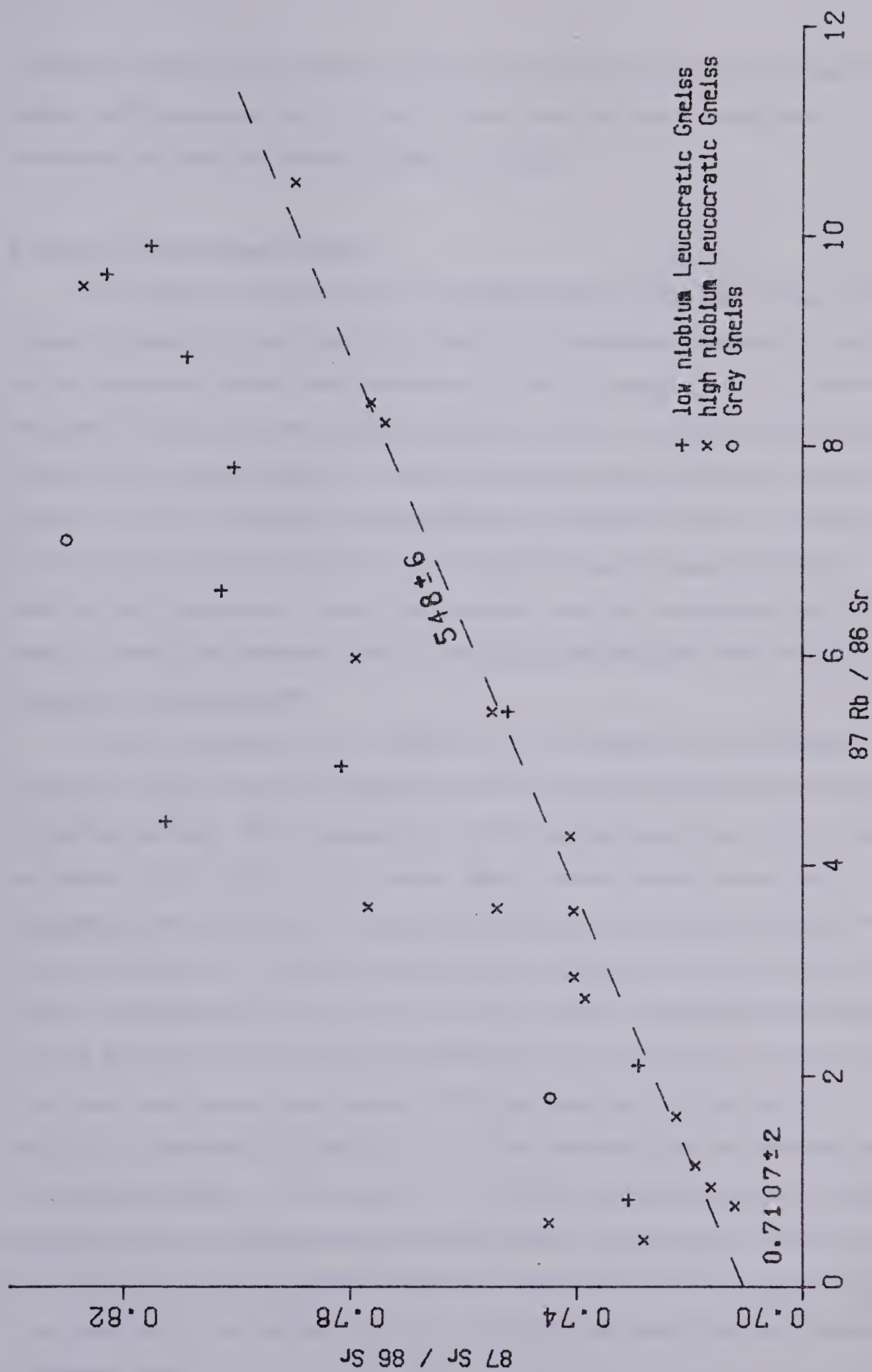


Figure 5.6 Rb-Sr Isochron diagram for the Leucocratic Gneiss of the Malton Gneiss Complex, showing a possible lower limit to the age of this gneiss.





formation of zircons at or before c.840 Ma, during the original intrusion of leucocratic magma, with the gradual loss of Pb by diffusion since that time. In practice a combination of these processes probably took place.

### 5.3.5 Kaza Group Metasediments

The rubidium–strontium data on the metasediments of the Kaza Group are shown in table 40 (appendix C) and figure 5.7. There is a considerable scattering of the points on the rubidium–strontium isochron diagram (figure 5.7), possibly due to variable initial strontium 87/86 ratios in the original sediments, as well as to differing degrees of diffusion during metamorphism. A 250 Ma reference isochron drawn on figure 5.7 gives a lower limit to the age of the metasediments and may represent an updating event. The scattering of the points on the isochron diagram may be caused by a lack of strontium homogenization in the original sediments, and the comparatively high 87/86 values of these points probably reflects the long crustal residence time of these Precambrian metasediments.

There is a sizeable body of evidence for a late Permian or early Triassic (Tahltanian) orogeny along the boundary between the Intermontane Belt and the Omineca Crystalline Belt (Dott, 1961; Douglas *et al.*, 1970; Campbell and Tipper, 1971; Paterson and Harakal, 1974; Okulitch, 1975; Struik, 1981). Easterly dipping subduction is suggested by the presence of 200–281 Ma batholiths in the Monashee Horsethief Creek Group (Lowden *et al.*, 1963) and a 254 Ma granitic gneiss east of Kelowna (Okulitch, 1975). In the Barkerville–Cariboo River area, Struik (1981) has described the Pundata thrust at the base of the allochthonous Antler Formation as post–early Permian; and in the Pinchi Lake area, Paterson and Harakal (1974) have described two periods of deformation, separated by a period of blue–schist metamorphism, all occurring during the Tahltanian Orogeny. K–Ar ages of 211–218 Ma are considered as cooling ages marking the end of the second period of deformation, and the peak of metamorphism in the Cache Creek Group is dated at 255 Ma. It is possible that the thrusting of the Kaza Group eastwards over the Malton Block on the North Thompson Fault may also have been a Tahltanian event.



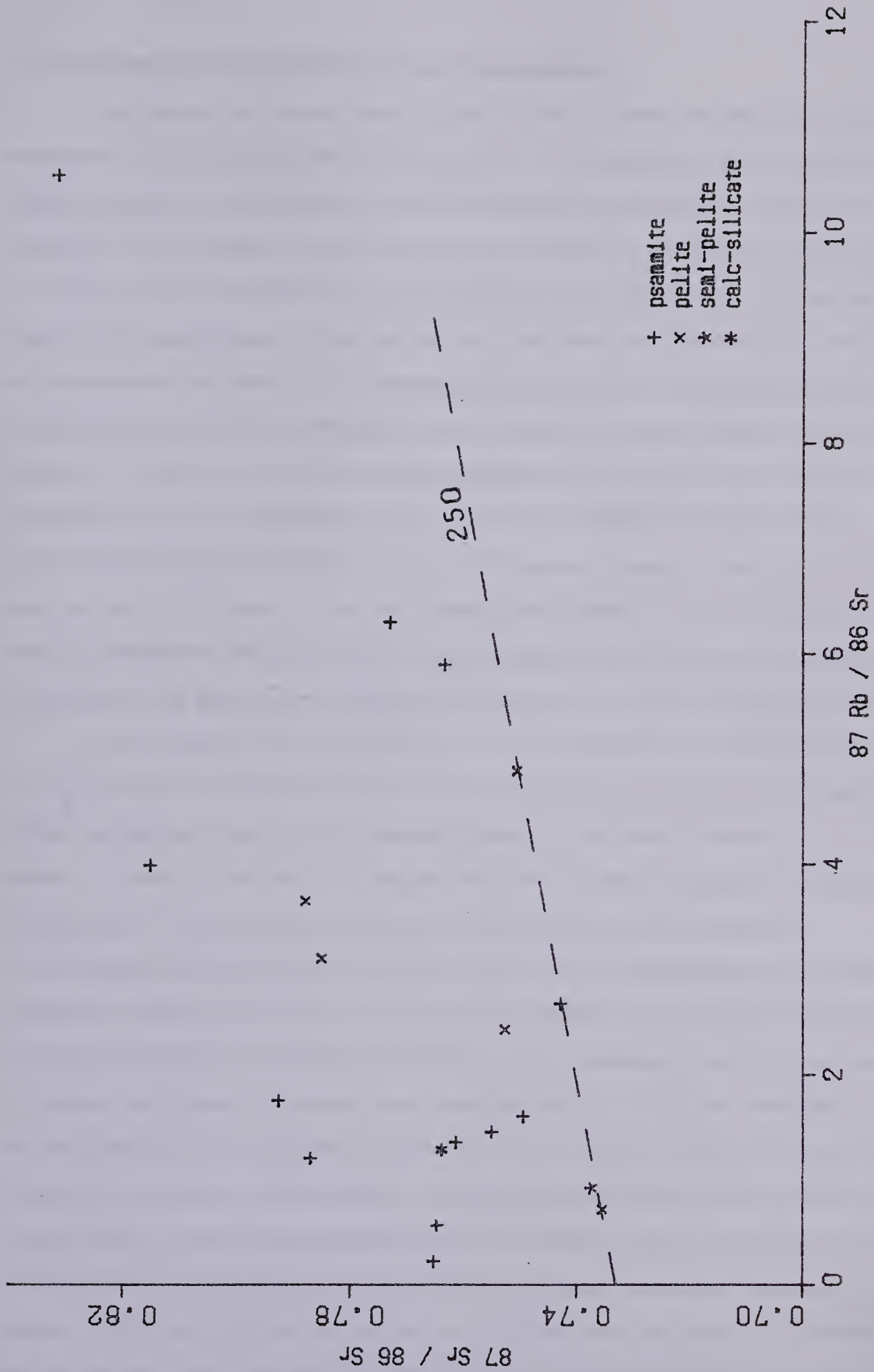


Figure 5.7 Rb-Sr isochron diagram for metasediments from the Kaza Group in the Valemount area. The wide scatter is probably due to the highly variable initial strontium ratios of the sediments as well as to variations in the degree of diffusion during metamorphism. The reference isochron of 250 Ma gives a possible lower limit to the age of the latest metamorphic event.



### 5.3.6 Monashee Horsethief Creek Group Metasediments

The rubidium–strontium isochron data for the Monashee Horsethief Creek Group are shown in figure 5.8 and table 39 (appendix C). The data base is poor, since of the available samples, only three meta–turbidite samples were suitable for analysis and plotting. The three points on the isochron approximate to a straight line yielding an age of  $1246 \pm 23$  Ma and an initial strontium 87/86 ratio of  $0.7170 \pm 2$ . This age may be a metamorphic, sedimentary or source rock age. The latter two are unlikely in the view of the polymetamorphic nature of the metasediments, as well as the high grade of the metamorphism attained in the Monashee Horsethief Creek Group ( $>600^\circ$  C and  $>6$  kb, Ghent *et al.*, 1980). The 1250 Ma age probably dates the peak of the Monashee Horsethief Creek Group metamorphism. Ghent *et al.* (1980) have shown that this metamorphism occurred towards the end of the second phase of folding (F2), a large scale isoclinal deformation on southerly dipping axial planes. This was also the time at which the Monashee Horsethief Creek Group sediments were thrust over (and in places infolded with) the gneisses of the Malton Block (Ghent *et al.*, 1977; Morrison, 1979).

The orientation of the Windfall Creek Thrust parallels that of the axial planes of the isoclinal folds in the Monashee Horsethief Creek Group, as well as that of some Middle Jurassic structures in the Shuswap Complex to the south (Okulitch *et al.*, 1975). Hence it is possible that the F2 folding and thrusting occurred during the Columbian Orogeny, but it is more likely to have been much earlier: Schutze (personal communication, 1980) has obtained Rb–Sr isochron ages in the Shuswap and Monashee Horsethief Creek Group similar to those found in the Malton Block, namely Valhalla Gneiss 850 Ma and Messiter Summit Gneiss 570 Ma. Zircon separates from the Grey Gneiss of the Malton Block give a concordia lower intercept age of c.1250 Ma. Morrison (1979) has reported post F2 leucosome penetration of the Monashee Horsethief Creek Group, equating it with at least one episode of leucosome (Leucocratic Gneiss) intrusion of the Malton Gneiss. Field evidence shows that the F2 thrusting is older than the thrusting on the North Thompson Fault (Morrison, 1979), and the latter is possibly Tahltanian. Thus, on balance, the evidence appears to suggest a c.1250 Ma major episode of deformation and metamorphism in the Monashee Horsethief Creek Group, during which it was infolded with the gneisses of the Malton Block.





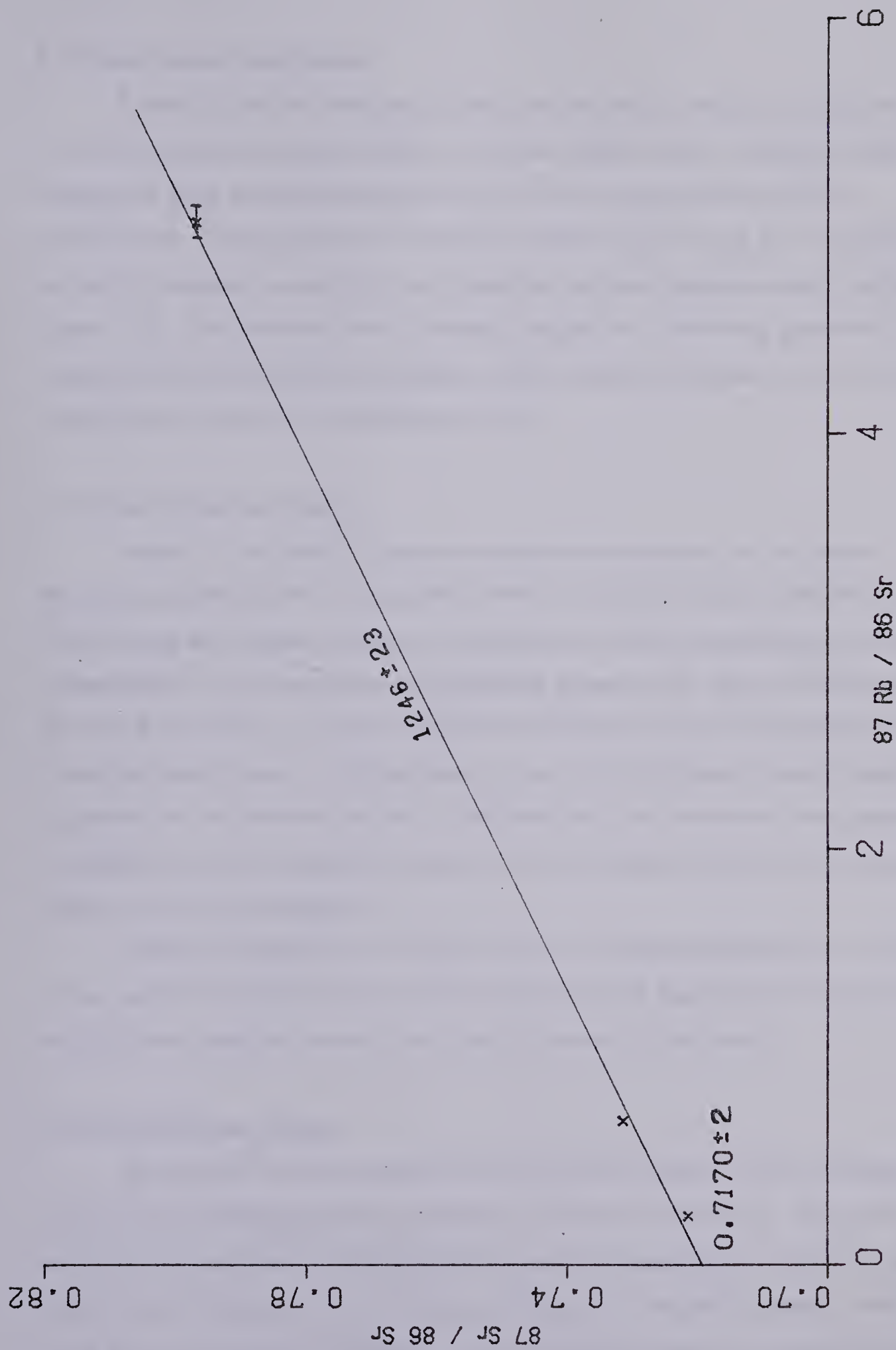


Figure 5.8 Rb-Sr Isochron diagram for metasediments from the Monashee Horsethief Creek Group in the Valenmount area.



### 5.3.7 Hugh Allan Creek Gneiss

Turning to the rock units east of the Rocky Mountain Trench, figure 5.9 and table 41 give the rubidium–strontium data for the felsic gneiss south of Hugh Allan Creek. The data base is small, but the three points do lie on a line within the limits of their measurement. The age is  $806 \pm 13$  Ma and the initial ratio  $0.7222 \pm 15$ . The samples are highly radiogenic, resulting in a very steep line on the strontium evolution diagram (figure 5.10). The strontium isotopic evidence appears to confirm the geochemical (chapter 3) and structural (Oke and Simony, 1981) evidence that these rocks are unrelated to any others exposed in the immediate vicinity.

### 5.3.8 Mount Blackman Gneiss

Figure 5.11 and table 42 give the rubidium–strontium data for the Mount Blackman paragneiss north of Hugh Allan Creek. The points are quite scattered on the isochron diagram, possibly because of incomplete strontium homogenization during metamorphism. The maximum age of the gneiss appears to be  $1899 \pm 33$  Ma and the minimum  $913 \pm 20$  Ma. However, the lead 207/206 age of zircons separated from the Mount Blackman Gneiss is 1950 Ma (table 42), and a 207/206 age is normally regarded as a minimum. Hence either the Rb–Sr 1899 Ma line is not a maximum, having been downdated by a later metamorphic event, or the zircons are inherited and are dating the source rock of this paragneiss.

These dates cannot be correlated with any of the ages determined on rock units to the west of the Rocky Mountain Trench, reinforcing the argument that these units have had a different geologic history from those to the west of the Trench.

### 5.3.9 Bulldog Creek Gneiss

The rubidium–strontium data on the Bulldog Creek Gneiss are not sufficiently clear to allow definite isochrons or definitive conclusions to be drawn. The scatter is interpreted as being due to variable diffusion during metamorphism. Figure 5.12 and table 44 give the data and the lines drawn on figure 5.12 represent possible upper and lower limits for the age of this gneiss. The geochemistry (chapter 3) suggests that the felsic and mafic gneisses in this area may be cogenetic, and it is possible that 1090 Ma



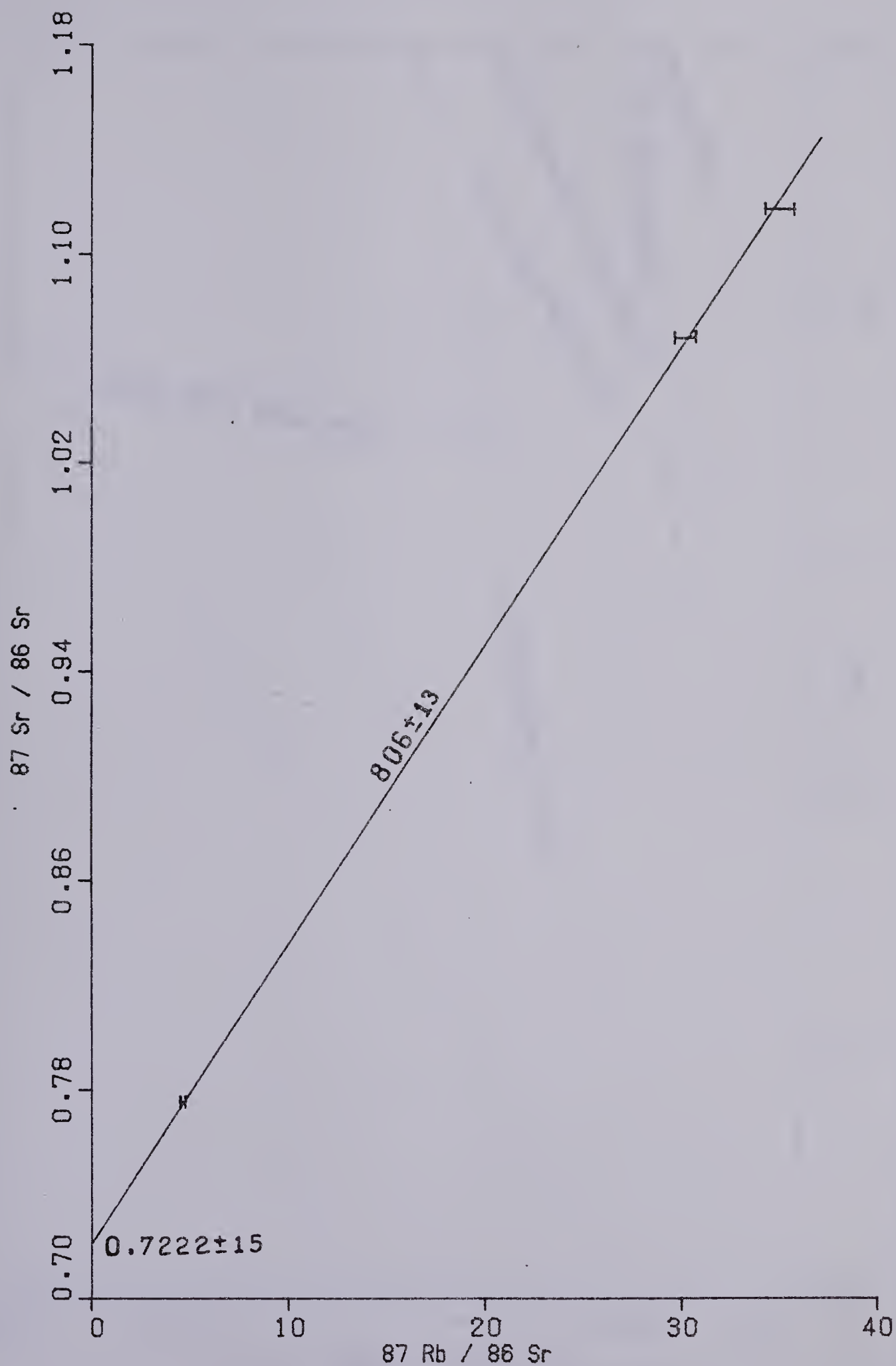


Figure 5.9 Rb-Sr isochron diagram for the Hugh Allan Creek Gneiss of the Malton Gneiss Complex





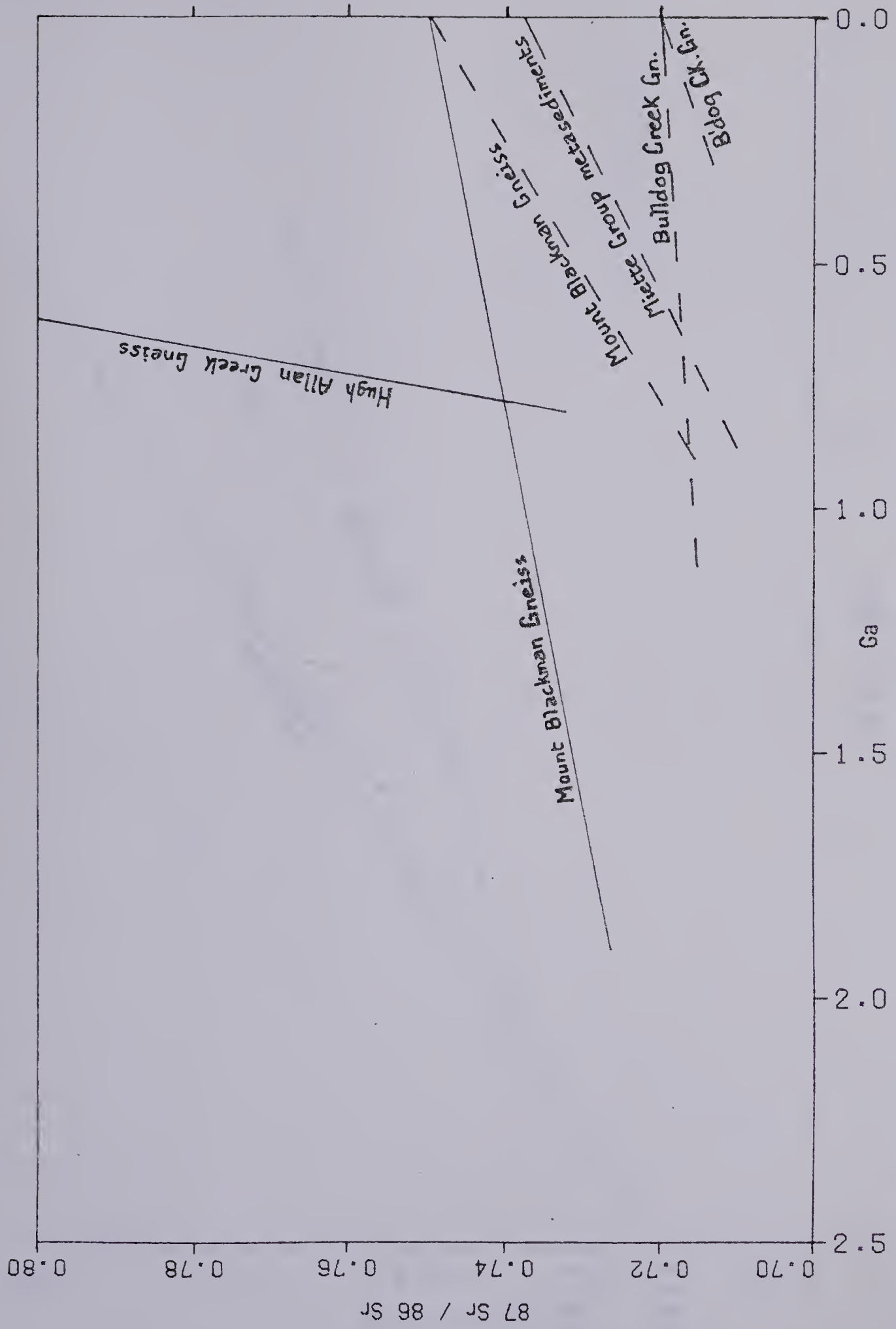


Figure 5.10 Strontium evolution diagram for rocks east of the Rocky Mountain Trench in the Valemount area



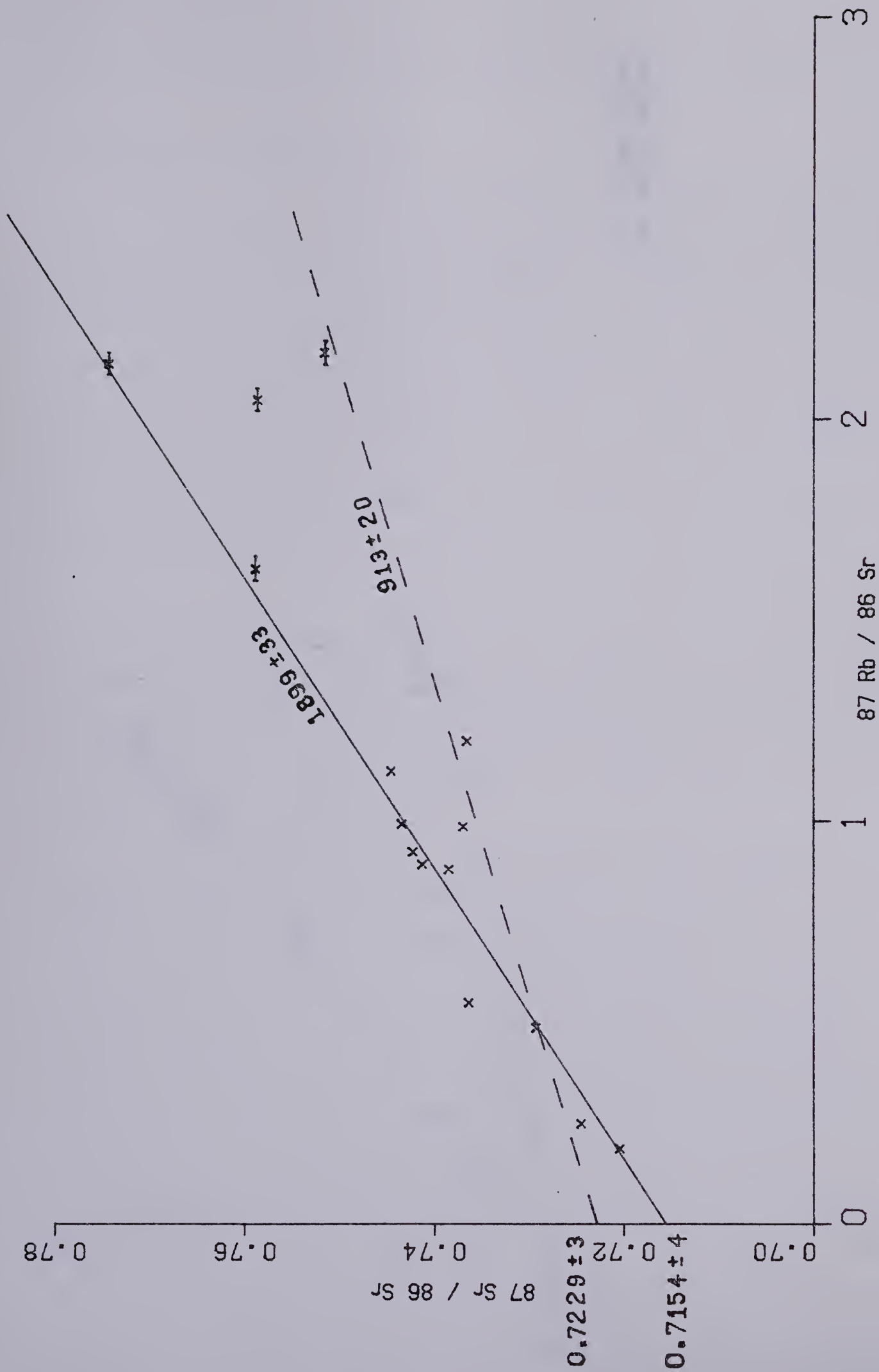


Figure 5.11 Rb-Sr Isochron diagram for the Mount Blackman Gneiss of the Malton Gneiss Complex. A possible first metamorphic event is shown by the solid line and a possible later event by the dashed line.



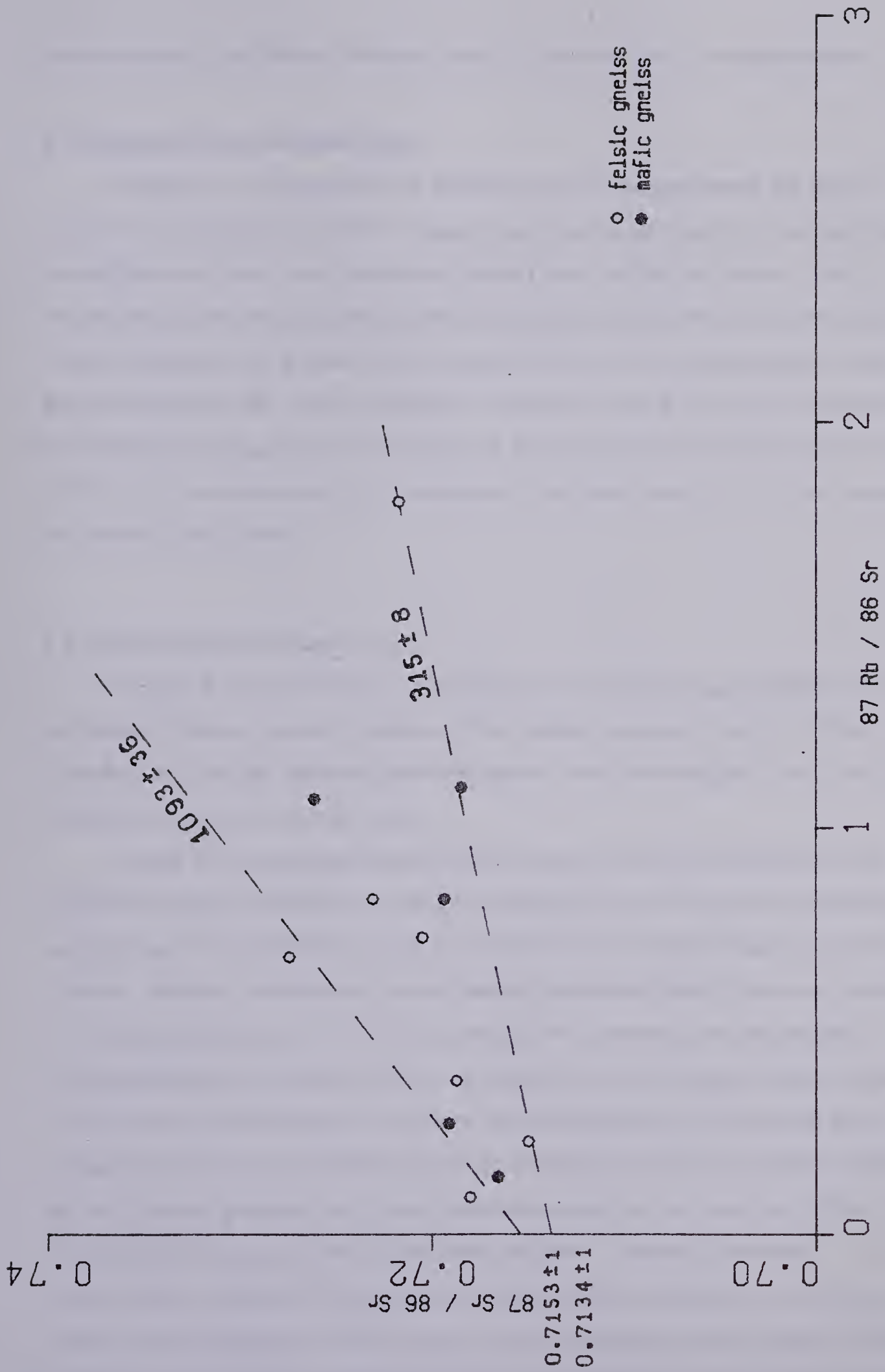


Figure 5.12 Rb-Sr Isochron diagram for the Bulldog Creek Gneiss of the Malton Gneiss Complex, showing possible upper and lower limits to the age of the gneiss.





approximates to their time of intrusion, and 315 Ma their time of metamorphism.

#### 5.3.10 Miette Group Metasediments

Rubidium – strontium data for the Miette Group metasediments are given in figure 5.13 and tables 43 and 45. These include the metasediments on the north face of Mount Blackman which were mapped as Miette Group by Oke and Simony (1981). Polymetamorphism and variable diffusion have again scattered the data points on the isochron diagrams, but a lower limit for each of the two main groups appears to be approximately 900 Ma. This is equivalent to the lower limit ( $913 \pm 20$ ) on the age of the Mount Blackman paragneiss. A sub group of three samples from the Miette give an age of  $315 \pm 40$ , which appears to be equivalent to the lower limit ( $315 \pm 8$ ) on the age of the Bulldog Creek Gneiss.

#### 5.4 Comparison with other areas

Figures 5.15 and 5.16 show a comparison between the ages obtained in this area and those of nearby regions. Because of the "collage" nature of much of British Columbia, only the age determinations obtained on rock units thought to be a part of the same plate or plates have been used.

Figure 5.15 shows age determinations west of the Rocky Mountain Trench. The Kaza Group age is included on this diagram although the rocks may have originated on a separate plate from the Malton Block, the c.250 Ma event possibly marking the time of collision. Similarly, the Shuswap and Monashee Horsethief Creek Group may have been on a separate plate prior to c.1250 Ma, although the preliminary imprecise age of 3000 Ma obtained by Duncan (1978) on gneisses from the Shuswap Complex agrees well with the c.3000 Ma ages of the Grey and Mafic Gneisses of the Malton Block. Duncan's (1978) imprecise 2000 Ma age and Wanless and Reesor's (1975) c.1950 Ma age on Shuswap gneisses (interpreted as intrusive ages) do not coincide with the  $1767 \pm 20$  Ma age of intrusion of the Augen Gneiss protolith. Schutze's (personal communication, 1980) 847 Ma age on the Valhalla Gneiss correlates well with the c.840 Ma age suggested for the intrusion of the Leucocratic Gneiss protolith. Schutze's (personal communication, 1980) 568 Ma age on the Messiter Summit Gneiss is close to



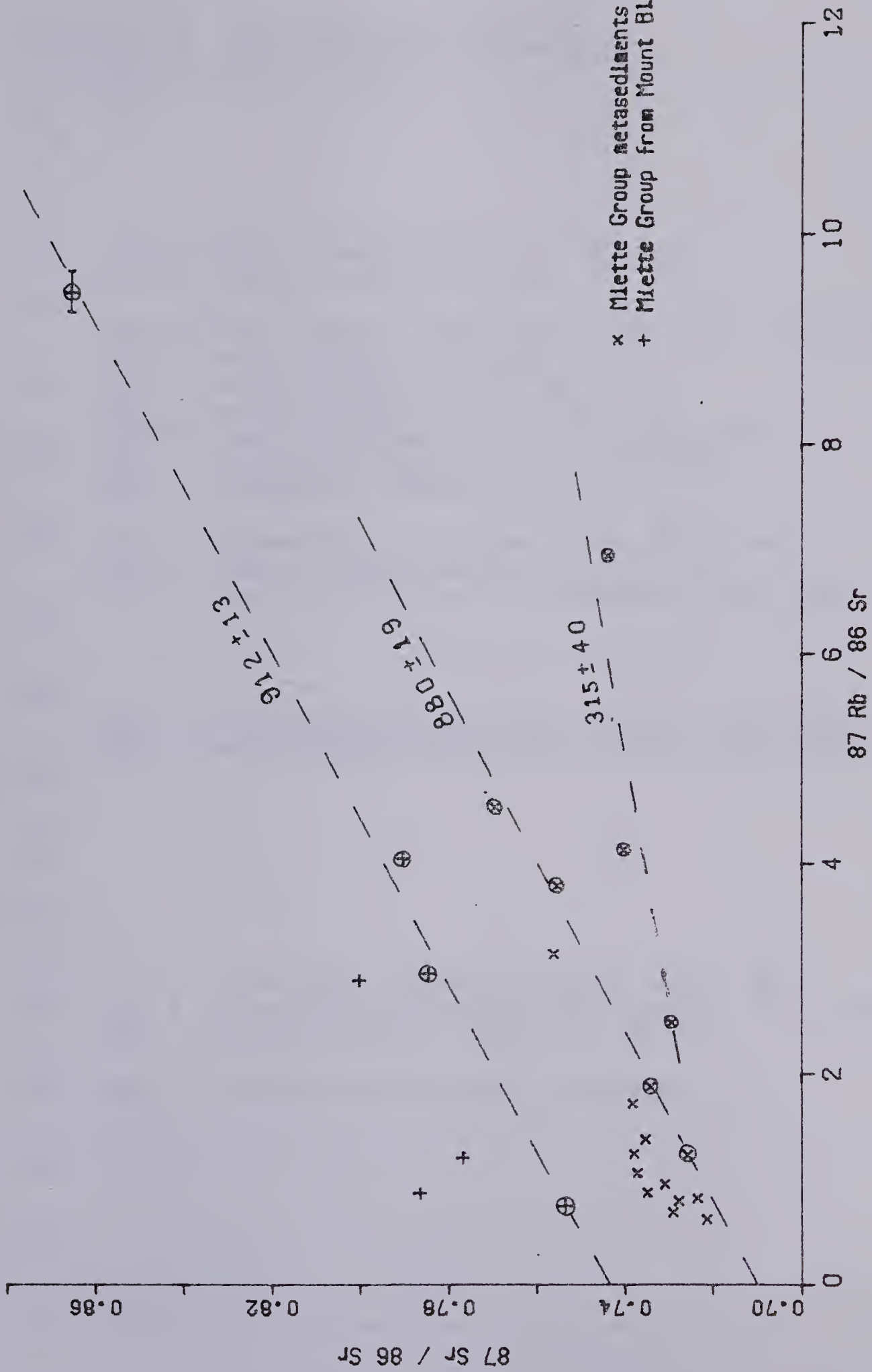
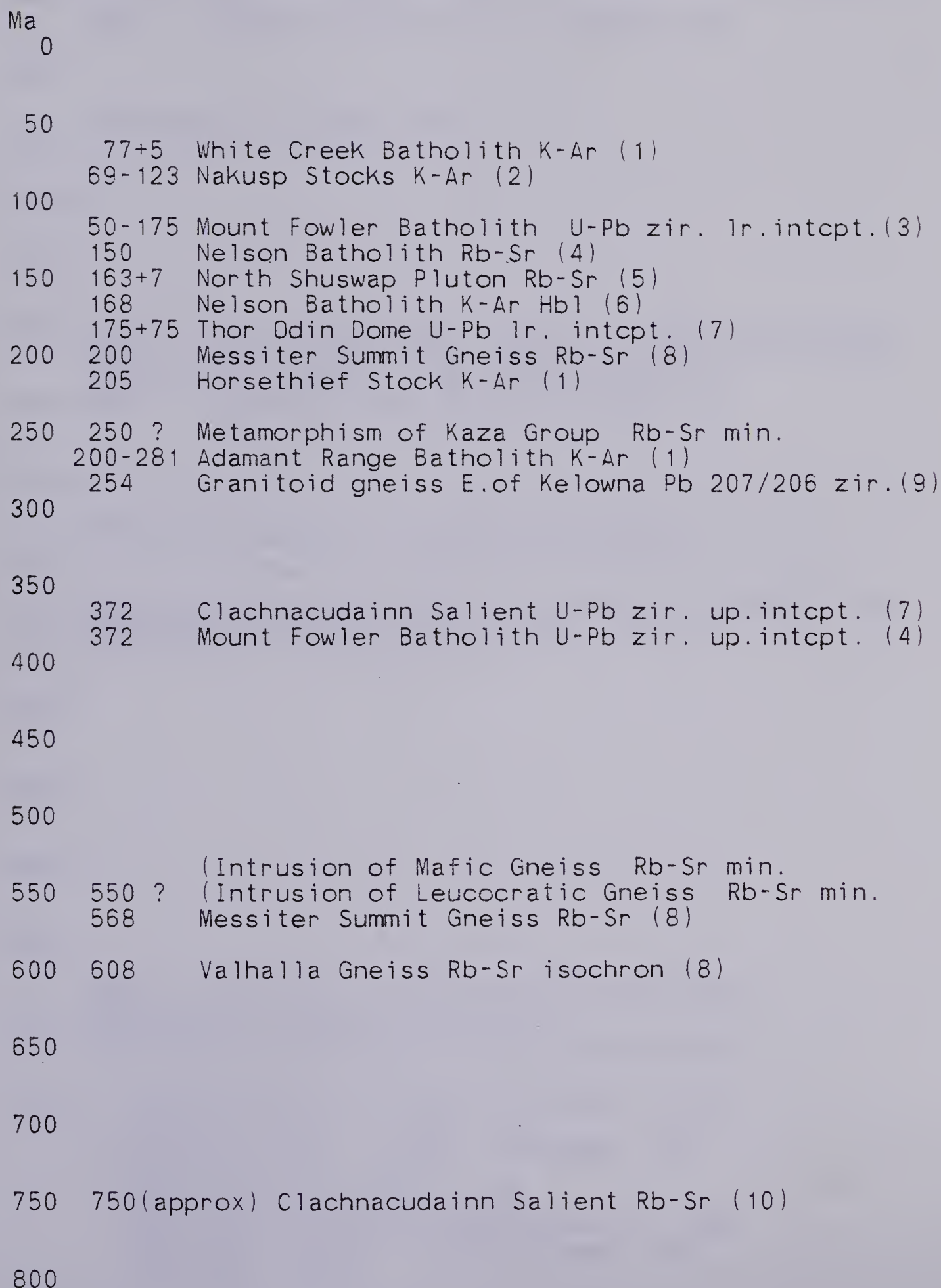


Figure 5.13 Rb-Sr Isochron diagram for metasediments from the Mlette Group in the Valemount area, showing possible ages of metamorphic events. Points used in the isochron calculations are circled.



Figure 5.14 Age determinations west of  
The Rocky Mountain Trench







850	840 ?	Intrusion of Leucocratic Gneiss Pb 207/206 zir.
	847	Valhalla Gneiss Rb-Sr isochron (8)
900		
950	930(approx)	Shuswap Rb-Sr (11)
\ /\ /\		
1000		
1200	1246+23	Met. of Monashee Horsethief Creek Group Rb-Sr
	1250	Metamorphism Grey Gneiss U-Pb zir. 1r. intcpt.
	1305+52	Hellroaring Creek Stock Rb-Sr (4)
1400	1320	Lower Purcell oldest K-Ar age (5)
1600		
1800	1767+20	Intrusion of Augen Gneiss Rb-Sr
	1960+35-45	Thor Odin Dome U-Pb zircons up.intcpt. (5)
2000	2000(approx)	Shuswap Rb-Sr (11)
2200		
2400		
2600		
2800		
	2950 ?	Intrusion of Mafic Gneiss Rb-Sr max.
3000	3000(approx)	Shuswap Rb-Sr (9)
	3000(approx)	Intrusion of Grey Gneiss Rb-Sr
Key:		
	1=Lowdon et al., 1963	2=Hyndman, 1968
	3=Okulitch et al., 1975	
	4=Duncan et al., 1979	5=Pigage, 1977
	6=Nguyen et al., 1968	
	7=Wanless and Ressor, 1975	
	8=Schutze (personal communication), 1980	
	9=Okulitch, 1975	10=Blenkinsop, 1972
	11=Duncan, 1978	

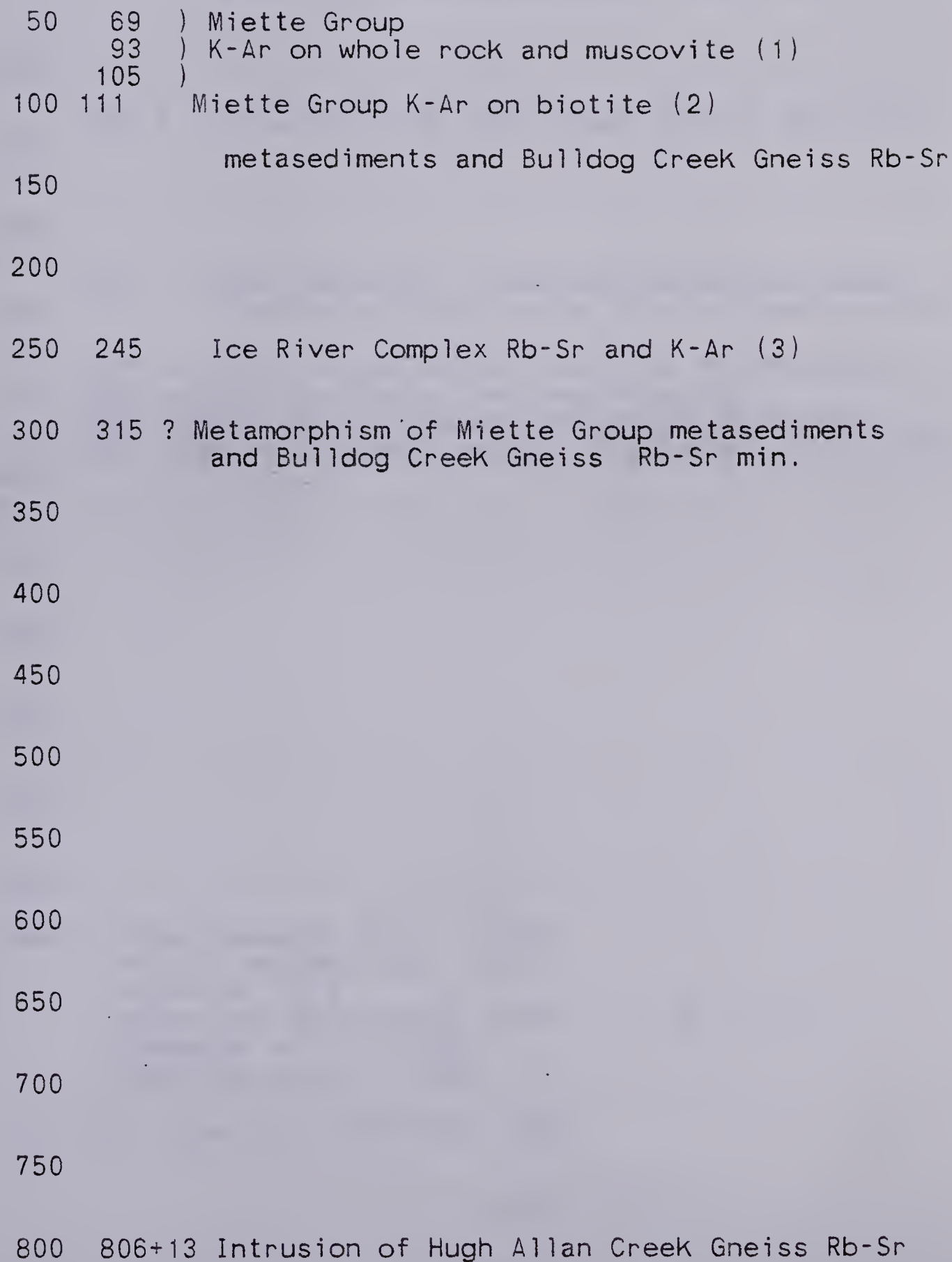
All Rb-Sr ages are whole rock ages.



Figure 5.15 Age determinations east of  
The Rocky Mountain Trench

Ma

0





850

900 900 ? Metamorphism of Mount Blackman Gneiss and  
Miette Group metasediments Rb-Sr min.

\\//\\//

1000

1100 ? Intrusion of Bulldog Creek Gneiss Rb-Sr max.  
1200

1400

1535 Rocky Mountains "unmetamorphosed equivalent of  
1600 Horsethief Creek Group" K-Ar minimum age (6)

1776 Miette Group source rock K-Ar minimum age (1)  
1800 1800(approx) Pre-Purcell metamorphism (5)

1900 ? Met. Mount Blackman paragneiss Rb-Sr max.

1950 Mount Blackman paragneiss source ? Pb 207/206 zir.  
2000

2200

2400

2600

2800

3000

Key: 1=Charlesworth et al., 1967  
2=Price and Mountjoy, 1970  
3=Currie, 1975  
4=Ryan and Blenkinsop, 1971 (  $=1.42 \times 10$  )  
5=Wheeler et al., 1972  
6=Wanless et al., 1967

All Rb-Sr ages are whole rock ages.





the  $528 \pm 29$  Ma and the  $548 \pm 6$  Ma minimum ages obtained on the Mafic and Leucocratic Gneisses of the Malton Block, interpreted as a time of metamorphism and partial melting. The c.250 Ma age of the Kaza Group is interpreted as a time of collision between the Malton Block and the Kaza Group, the latter being thrust over the former along the North Thompson Fault during the Tahlitanian Orogeny. Some corroboration is lent to this theory by the ages of the batholiths penetrating the Monashee Horsethief Creek group. These ages of 200 Ma to 281 Ma (Lowdon *et al.*, 1963), previously thought to be anomalous, could be explained by the presence of an eastward dipping subduction zone at this time. Jurassic ages have been observed in the Shuswap and in the Monashee Horsethief Creek Group but not in the Malton Block. The Cretaceous batholith and pluton ages are regarded as evidence of Cretaceous westward dipping subduction along the line of the Rocky Mountain Trench.

Figure 5.16 shows the evidence for this Cretaceous orogeny on the east side of the Rocky Mountain Trench. Previously dated events on the east of the trench are few in number and difficult to correlate with each other. The Pb 207/206 age of 1950 Ma obtained on zircons from the Mount Blackman paragneiss can be interpreted as a minimum age for the source rock of this gneiss, and the rubidium – strontium maximum age of c.1900 Ma, as their time of primary metamorphism. The latter compares with a pre – Purcell metamorphism of approximately 1800 Ma quoted by Wheeler *et al.* (1972). Charlesworth *et al.* (1967) obtained a 1776 Ma potassium – argon minimum age for the source rock of the Miette Group of metasediments, and the rubidium – strontium age of c.900 Ma may represent their time of primary metamorphism. The Bulldog Creek Gneiss may have been intruded at about 1100 Ma and the Hugh Allan Creek Gneiss at  $806 \pm 13$  Ma.



## 6. OXYGEN ISOTOPE STUDIES

### 6.1 Introduction

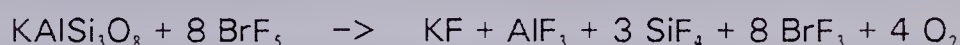
The problems towards which the oxygen isotope studies were directed were the relationships between the gneisses east and west of the Rocky Mountain Trench, the relationship between the gneisses and the surrounding schists, and the pre-metamorphic history of the gneisses.

Twenty four whole rock samples and one feldspar separate were analysed, the whole rock samples representing all the gneissic types from all the main geographical areas and two of the metasedimentary groups, the Miette and the Kaza.

### 6.2 Analytical Procedure

#### 6.2.1 Oxygen extraction

The bromine pentafluoride method of Clayton and Mayeda (1963) was used to extract the oxygen. Samples of approximately 20 mg of finely ground dried powder were weighed into thin foil boats, and then loaded into nickel extraction tubes in a nitrogen chamber. The tubes were then returned to the extraction line and were pretreated with  $\text{BrF}_5$  for about one hour to remove any oxygen compounds which had formed on their walls during loading. After pre-treatment, the tubes were evacuated and then a measured amount of  $\text{BrF}_5$  was condensed into each tube by immersion in liquid nitrogen. The amount of  $\text{BrF}_5$  used in each tube was approximately 1/400 mole, several times the stoichiometric requirement, to ensure complete reaction. The tubes were then closed and heated overnight at about  $600^\circ\text{C}$  using external electrical resistance furnaces, whilst the upper ends of the tubes were kept cool with circulating air. The oxygen is released by complete reduction of all the minerals present in the sample. The reaction equation for potassium feldspar, shown below, is typical:





The oxygen was extracted from each tube in turn, the next morning, after the furnaces had been removed and the tubes cooled to room temperature. A trap cooled by liquid nitrogen removed all possible volatile contaminants ( $\text{BrF}_5$ ,  $\text{BrF}_3$ ,  $\text{Br}_2$ ,  $\text{SiF}_4$  and  $\text{HF}$ ), and the oxygen pressure was measured before it was converted to carbon dioxide by passing it over red-hot carbon in the presence of a platinum catalyst. The carbon dioxide was condensed out with liquid nitrogen, the yield measured by manometer and the gas sealed in a glass tube for transport to the mass spectrometer.

### 6.2.2 Mass spectrometry

The oxygen isotopic ratio  $^{16}\text{O}/^{18}\text{O}$  of each sample was measured on a Micromass 602 D double collecting permanent magnet mass spectrometer, using KMCC calcite as a working reference. The two Faraday Cup collectors allow direct measurement of  $^{16}\text{O}/^{18}\text{O}$  by the True Ratio Measurement Bridge System, in which the minor counter ( $^{18}\text{O}$ ) is stopped as soon as the major counter ( $^{16}\text{O}$ ) reaches a count of  $10^6$ . This ratio (R) is, in theory, independent of the sample pressure, but in practice, it was found that best results were obtained when reference and sample pressures were set approximately equal, by adjustment of the inlet system. Because of the double inlet method, no fractionation correction is needed as the sample depletes. An average of six good measurements was taken, the enrichment calculated directly by:

$$\delta^{18}\text{O} = (\text{R.sample} - \text{R.reference})/\text{R.reference}$$

and the result corrected to SMOW (for the Reference used here) by the equation:

$$\delta^{18}\text{O.SMOW} = \delta^{18}\text{O.raw} + 18.37 + (\delta^{18}\text{O.raw} \times 18.37)/1000$$

## 6.3 Results

$\delta^{18}\text{O}$  values corrected to SMOW are given in the last column of table 6.1 and in figure 6.1. They show that the gneisses east of the Rocky Mountain Trench, in the Mount Blackman area, have  $\delta^{18}\text{O}$  values close to normal crustal values, the mafic rocks being between 7.33 ‰ and 8.21 ‰ and the felsic between 9.43 ‰ and 10.07 ‰.





Table 6.1 Oxygen isotopic measurements on whole rock and feldspar samples from the Malton Gneiss Complex

Sample	Lithology	Location	Lab. number	Oxygen yield		6 18 O	
				actual	theoretical	measured	SMOW
5805 (WR)	mafic gneiss	C.N. Track	1258-4161	14.11	14.43	-12.84	5.29
5819B (WR)	mafic gneiss	Malton Range	1258-4161	13.88	13.70	-13.05	5.08
5901M (WR)	mafic gneiss	Monashee Mts.	1258-4164	13.72	13.70	-13.35	4.78
5842C (WR)	Grey Gneiss	Malton Range	1220-4053	14.61	15.03	-10.41	7.77
5897C (WR)	Grey Gneiss	Monashee Mts.	1250-4140	13.64	15.17	-8.48	9.73
5903D (WR)	Grey Gneiss	C.N. Track	1220-4055	13.34	14.84	-12.42	5.72
5903D (fsp)	Grey Gneiss	C.N. Track	1272-4204			-12.64	5.50
5814 (WR)	Leucocratic Gneiss	C.N. Track	1220-4051	13.82	15.20	-11.63	6.53
5815 (WR)	Leucocratic Gneiss	C.N. Track	1250-4136	15.48	15.25	-11.03	7.13
5817 (WR)	Leucocratic Gneiss	C.N. Track	1250-4137	14.58	15.37	-11.19	6.97
5823 (WR)	Leucocratic Gneiss	Malton Range	1220-4052	14.08	15.29	-10.25	7.93
5840A (WR)	Leucocratic Gneiss	Monashee Mts.	1250-4138	14.61	15.20	-11.76	6.39
5845B (WR)	Leucocratic Gneiss	Malton Range	1220-4054	14.47	15.29	-11.96	6.19
5901B (WR)	Augen Gneiss	Monashee Mts.	1494-4832	13.57	14.68	-10.66	7.84
5901C (WR)	Augen Gneiss	Monashee Mts.	1220-4056	14.09	14.92	-11.11	7.06
5890M (WR)	mafic gneiss	Mt. Blackman	1258-4155	13.58	13.84	-10.90	7.33
6150H (WR)	mafic gneiss	Mt. Blackman	1494-4835	13.57	13.94	-10.30	8.21
6150Q (WR)	mafic gneiss	Mt. Blackman	1494-4830	13.39	13.89	-10.62	7.88
5890E (WR)	felsic gneiss	Mt. Blackman	1250-4139	14.59	15.22	-8.49	9.72
5890H (WR)	felsic gneiss	Mt. Blackman	1250-4141	14.77	15.10	-8.78	9.43
6150D (WR)	felsic gneiss	Mt. Blackman	1494-4834	13.56	14.89	-8.47	10.07
5834 (WR)	(low silica	Kaza Group	1258-4162	14.54	14.90	-7.84	10.39
5850 (WR)	(psammite	Miette Group	1258-4163	13.99	14.55	-7.38	10.85



# Introduction

The purpose of this study is to investigate the effects of various factors on the growth of a specific plant species. The study was conducted over a period of six months, during which time the plants were grown under different conditions. The results of the study are presented in the following sections.

The first section discusses the methodology used in the study, including the selection of the plant species, the experimental design, and the data collection process. The second section presents the results of the study, showing the growth of the plants under different conditions. The third section discusses the implications of the results and the conclusions drawn from the study.

The study was conducted in a controlled environment, where the plants were grown in pots. The pots were placed in a greenhouse, where the temperature and humidity were controlled. The plants were watered regularly, and the soil was kept moist. The results of the study show that the growth of the plants was significantly affected by the different conditions. The plants grown under the most favorable conditions showed the highest growth, while the plants grown under the least favorable conditions showed the lowest growth.

The results of the study have important implications for the cultivation of this plant species. The study shows that the growth of the plants can be improved by providing them with the most favorable conditions. This information can be used by farmers and growers to optimize the growth of their plants and increase their yields.

## Key to Figure 6.1

- 1=Taylor's (1968) divisions
- 2=Berridale Batholith I-type granitoids  
O'Neil and Chappell, 1977
- 3=Berridale Batholith S-type granitoids  
O'Neil and Chappell, 1977
- 4a=Ancient Gneiss Complex 3.6 Ga orthogneisses  
Taylor and Magaritz, 1975
- 4b=Ancient Gneiss Complex 3.6 Ga paragneisses  
Taylor and Magaritz, 1975
- 5=Barberton area, 3.6 Ga tonalite domes  
Taylor and Magaritz, 1975
- 6=Barberton area, Hood Granite  
Taylor and Magaritz, 1975
- 7=Barberton area, 2.6-2.8 Ga Younger Granites  
Taylor and Magaritz, 1975
- 8a=Footprint Gneiss upper amphibolite facies orthogneiss  
Longstaffe and Schwarcz, 1977
- 8b=Footprint Gneiss middle amphibolite facies orthogneiss  
Longstaffe and Schwarcz, 1977
- 9=Twilight Gneiss granulite facies paragneiss  
Longstaffe and Schwarcz, 1977
- 10=Claylake Gneiss granulite facies orthogneiss  
Longstaffe and Schwarcz, 1977
- 11=Cedarlake Gneiss amphibolite facies orthogneiss  
Longstaffe and Schwarcz, 1977
- 12=Pakwash Gneiss mid-upper amphibolite facies paragneiss  
Longstaffe and Schwarcz, 1977
- 13=Archean clastic metasediments  
Longstaffe and Schwarcz, 1977
- 14=Archean mafic metavolcanics  
Longstaffe and Schwarcz, 1977
- 15=Archean granitoids  
Longstaffe and Birk, 1981
- 16=Archean granitoids (altered)  
Longstaffe and Birk, 1981
- 17=Archean large mafic enclaves  
Longstaffe and Schwarcz, 1977
- 18=Malton Block Mafic Gneiss and amphibolite
- 19=Malton Block Grey Gneiss
- 20=Malton Block Leucocratic Gneiss
- 21=Malton Block Augen Gneiss
- 22=Mount Blackman amphibolite
- 23=Mount Blackman felsic gneiss
- 24a=Kaza Group metasediments
- 24b=Miette Group metasediments

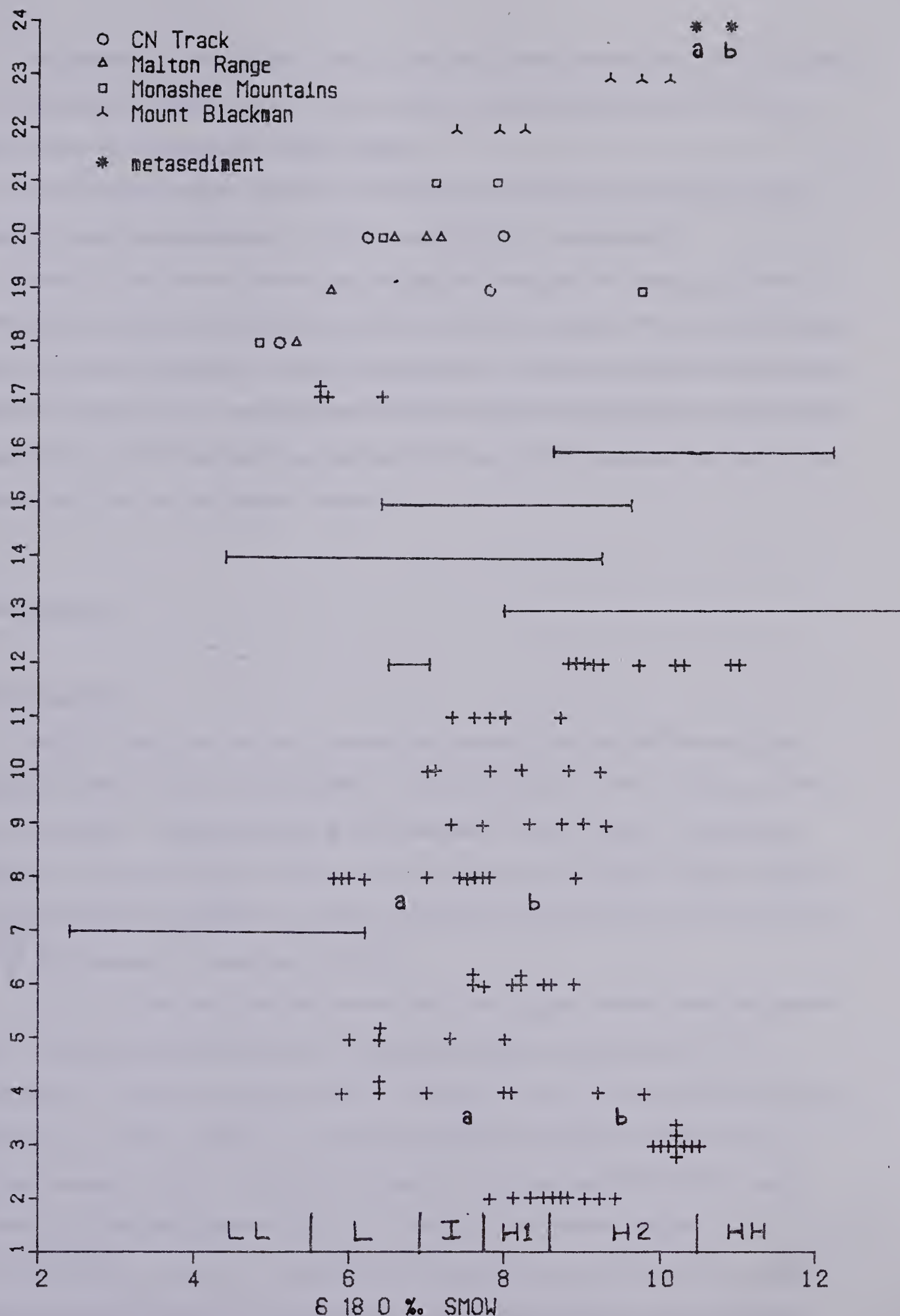


Figure 6.1 Oxygen isotopic compositions of whole rocks from the Malton Gneiss Complex compared with those from other Archean complexes and with those from the Berridale Batholith





The gneisses of the Malton Block, in contrast, have generally very low  $\delta^{18}\text{O}$  values, the mafic samples ranging from 4.78 ‰ to 5.29 ‰ and the felsic from 5.72 ‰ to 9.73 ‰ (with two anomalously higher values).

The metasedimentary samples from the Kaza and Miette Groups yield values typical of crustal metasediments, 10.39 ‰ and 10.88 ‰ respectively.

Table 6.1 also shows that the actual oxygen yields are not always equivalent to the theoretical yields, although they are within 10% in every case. The theoretical values quoted here were calculated from X.R.F. analyses and so may be subject to  $\pm 5\%$  errors. This probably accounts for most of the discrepancy between the actual and theoretical oxygen yields, and the true discrepancy may be close to the 2% quoted by Clayton and Mayeda (1963) for this extraction method.

## 6.4 Discussion

### 6.4.1 Introduction

Taylor (1968) was the first to divide the granitic rocks into different groups according to their whole rock  $\delta^{18}\text{O}$  SMOW values (see Fig. 6.1). His six groups were LL, L, I, H<sub>1</sub>, H<sub>2</sub> and HH. Granophyres were most abundant in the LL group, rhyolites and obsidians in the L group, minor intrusives in the I group and batholiths in the H groups. He suggested that the addition of pelitic components to the magma would account for the high  $\delta^{18}\text{O}$  values of the aluminous granites.

In 1977, O'Neil and Chappell showed that the oxygen isotopic ratios of granitic rocks of the Berridale Batholith in S.E. Australia correlated perfectly with their petrogenesis. Chappell and White (1974) had already classified the granites as being of sedimentary (S-type) or igneous (I-type) origin, using mineralogical, chemical and strontium isotopic criteria. As shown in figure 6.1, the average  $\delta^{18}\text{O}$  SMOW values obtained by O'Neil and Chappell (1977) on I- and S-type granites ranged from 7.9 ‰ to 9.4 ‰ and 9.99 ‰ to 10.5 ‰ respectively, the higher values in the S-type granites being interpreted as due to a concentration of the heavy isotope in clay minerals by fractionation during crustal weathering processes. As O'Neil and Chappell (1977) pointed out, however, the total range of  $\delta^{18}\text{O}$  values obtained on granitic rocks throughout the



world is much larger than that observed in the Silurian/Devonian Berridale Batholith.

Taylor and Magaritz (1975) showed that Archean granitic rocks tend to have lower  $\delta^{18}\text{O}$  values than Phanerozoic granitic rocks. Meta-igneous Archean granitic rocks of the Ancient Gneiss Complex gave  $\delta^{18}\text{O}$  SMOW values ranging from 5.9 ‰ to 8.1 ‰ whereas the metasedimentary rocks in the Complex gave values of 9.2 ‰ and 9.8 ‰. (All these values lie below the range of the Berridale Batholith S-type, as is shown in figure 6.1) Tonalite Domes from the Barberton area, of the same age as the Ancient Gneiss Complex and of presumed igneous origin, gave  $\delta^{18}\text{O}$  values in the same range as the meta-igneous rocks of the Ancient Gneiss Complex. The  $\delta\text{D}$  values of these two suites, however, differed markedly, those of the Tonalite Domes lying within the normal igneous range and those of the Ancient Gneiss Complex being less than  $-85$  ‰. Taylor and Magaritz (1975) suggest that the  $\text{H}_2\text{O}$  in these ancient gneisses is "juvenile", being derived from a mantle not yet heavily contaminated with subducted oceanic lithosphere. The slightly higher  $\delta^{18}\text{O}$  values of the Igneous Hood Granite can be attributed to their longer crustal residence time, whereas the very low  $\delta^{18}\text{O}$  values of the younger granites is almost certainly due to regional low temperature alteration effects, since the rocks are chloritized and the quartz-feldspar pairs out of equilibrium.

A remarkably similar pattern has been recorded in the Archean rocks of the Superior Province of the Canadian Shield by Longstaffe and Schwarcz (1977) and Longstaffe and Birk (1981). Whole rock  $\delta^{18}\text{O}$  SMOW values in the Footprint Gneiss range from 5.8 ‰ to 8.9 ‰ with a cluster at 7.4 ‰ to 7.8 ‰ (figure 6.1). Thus, much of the gneiss is isotopically too light for direct derivation from Archean clastic metasediments which range from 8 ‰ to 13 ‰ (Longstaffe and Schwarcz, 1977). The lower values (5.9 ‰ to 7.1 ‰) were obtained on gneiss samples exhibiting disequilibrium isotopic mineral fractionations and upper amphibolite facies metamorphism. Indeed, depletion in the heavy oxygen isotope appears to be quite common in higher grade metamorphic terranes (Shieh and Schwarcz, 1974; Fourcade and Javoy 1973). The "normal" gneiss in the 7.4 ‰ to 7.8 ‰ range may also have suffered heavy oxygen loss, but this is less likely, since the metamorphic grade is middle amphibolite facies and the minerals are approaching equilibrium. The Twilight Gneiss may also have suffered some loss of  $^{18}\text{O}$  as it has been metamorphosed to granulite facies and the  $\delta^{18}\text{O}$  values are



somewhat low for a paragneiss. However, they are remarkably similar to those of the Claylake Gneiss (an orthogneiss), also of granulite facies grade, and to those of the Cedar Lake Gneiss. Hence, Longstaffe (1979) suggested that the granulite facies rocks underwent isotopic exchange with the volumetrically more important amphibolite facies meta-igneous rocks such as the Cedar Lake Gneiss. The  $\delta^{18}\text{O}$  values (8.8 ‰ to 11.99 ‰) yielded by those Pakwash paragneisses subjected to relatively mild metamorphism lie in the range of Archean clastic metasediments, whereas the highly metamorphosed Pakwash paragneisses appear to have lost  $^{18}\text{O}$  during metamorphism, yielding  $\delta^{18}\text{O}$  values of 6.53 ‰ to 6.99 ‰.

Longstaffe (1979) and Longstaffe and Birk (1981) have described other Archean granitoid rocks from the Superior Province which have undergone post-crystallization  $^{18}\text{O}/^{16}\text{O}$  changes. The Burditt Lake greenschist facies metavolcanics appear to have gained  $^{18}\text{O}$  during low temperature alteration or weathering; and later to have lost  $^{18}\text{O}$  during intrusion of the Burditt Lake granodiorite by oxygen isotope exchange with low  $^{18}\text{O}/^{16}\text{O}$  magmatic fluids. The Jackson Lake Complex granodiorite has been depleted in  $^{18}\text{O}$  by exchange with low  $^{18}\text{O}/^{16}\text{O}$  fluids (probably meteoric water) migrating along a fault line. The Essox Lake porphyry and the Burditt Lake pluton have gained  $^{18}\text{O}$  during late stage deuteritic autometasomatism. This last, Longstaffe and Birk (1981) suggest, is more or less confined to high level intrusive stocks and plutons, being very rare in batholiths or gneissic rocks.

Longstaffe and Birk (1981) have also shown that in isotopically unaltered granitoid rocks,  $\delta^{18}\text{O}$  values tend to increase with  $\text{SiO}_2$  contents, because of the strong fractionation of  $^{18}\text{O}$  into quartz during crystallization.

Hence, in summary, the average  $\delta^{18}\text{O}$  values of isotopically unaltered Archean igneous, sedimentary and metamorphic rocks tend to be lower than those of geologically younger rocks of the same type. Bearing in mind this fact, the  $^{18}\text{O}/^{16}\text{O}$  ratios in granitoid gneisses of all ages closely resemble those of their protoliths and hence may be useful as petrogenetic indicators, providing the gneisses have not suffered large scale  $^{18}\text{O}$  depletion or enrichment since their formation. Such oxygen isotopic alteration may be caused by:

1.  $^{18}\text{O}$  depletion or enrichment by open system oxygen isotope exchange with a lower







(e.g. basalt) or higher (e.g. clastic sedimentary rock)  $\delta^{18}\text{O}$  reservoir, during upper amphibolite to granulite facies metamorphism, or during an episode of partial melting (Longstaffe, 1979, suggests that temperatures of 650°C to 700°C are necessary).

2.  $^{18}\text{O}$  depletion or enrichment by isotopic exchange with fluids migrating from a geologically younger intrusion of different isotopic composition.
3.  $^{18}\text{O}$  depletion by low temperature hydrothermal alteration and oxygen isotopic exchange with meteoric water (including water migrating along a fault zone).
4.  $^{18}\text{O}$  depletion by hydrothermal alteration during the original intrusion of the igneous protolith, as described by Magaritz and Taylor (1976). Taylor (1976, 1977) has shown, however, that only a small proportion of the intrusive rock is isotopically disturbed during this process. Nonetheless, the amount of alteration may vary with the country rock in question.
5.  $^{18}\text{O}$  enrichment by low temperature alteration and weathering processes.
6.  $^{18}\text{O}$  enrichment by deuteric or autometasomatic action (but Longstaffe and Birk (1981) have suggested that this is rare in gneissic terranes).

Finally, positive correlation of  $\delta^{18}\text{O} \text{ ‰}$  with  $\text{SiO}_2\%$  in a suite of rocks suggests a lack of secondary oxygen isotopic enrichment.

These guidelines have been used to interpret the oxygen isotope data obtained on the rocks of the Malton Gneiss Complex.

#### 6.4.2 Archean mafic gneiss

$\delta^{18}\text{O}$  values of 4.7 ‰ to 5.2 ‰ have been measured on the Archean mafic gneiss, lying to the west of the Rocky Mountain Trench, (figure 6.1 and table 6.1). These values are lower than those generally accepted for the Archean mantle (5.7 ‰), which suggests that these rocks may have suffered some oxygen isotopic exchange with meteoric water. Figure 6.2 shows a positive correlation between  $\delta^{18}\text{O}$  and  $\text{SiO}_2$ , suggesting that there has been no large scale oxygen isotopic alteration, and there are no signs of extensive post-metamorphic hydrothermal alteration or weathering. The metamorphic grade is not above middle amphibolite facies and there is no large reservoir of low  $\delta^{18}\text{O}$  rocks in the vicinity with which they could have exchanged oxygen isotopes.



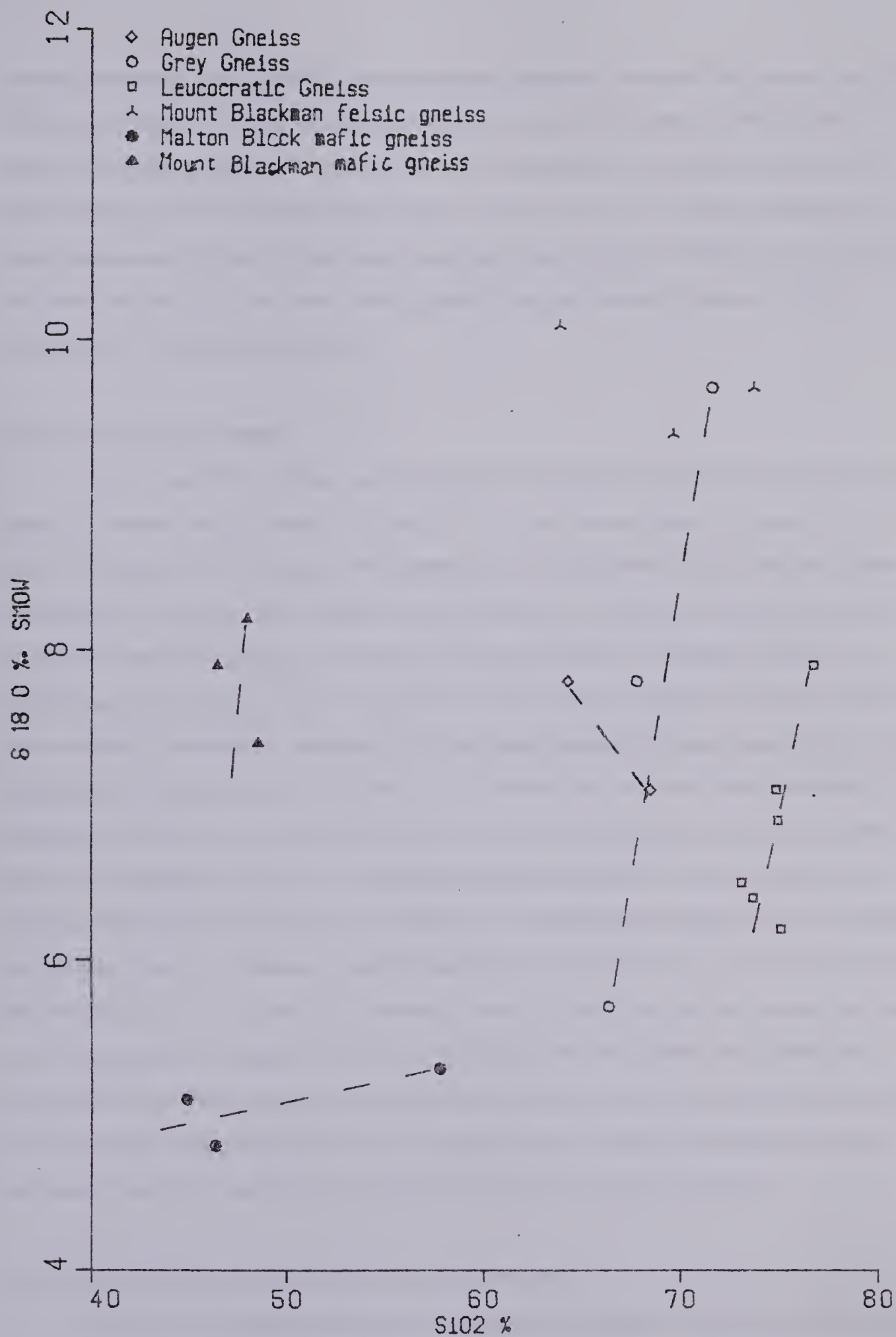


Figure 6.2 Oxygen isotopic composition versus silica content for certain gneisses from the Malton Gneiss Complex



Isotopic exchange could possibly have occurred between them and the igneous protoliths of the Leucocratic or Augen Gneisses during intrusion of the latter, but this seems unlikely since the present  $\delta^{18}\text{O}$  values of the mafic gneiss are well below those of the felsic gneisses. Thus, it seems reasonable to assume that the  $^{18}\text{O}$  values measured on these gneisses are close to those existing at the time of their formation, and, since they fall within the range for Archean metavolcanics (Longstaffe and Schwarcz 1977), confirm their meta-igneous nature.

#### 6.4.3 Archean Grey Gneiss

The Archean Grey Gneiss, outcropping to the west of the Rocky Mountain Trench, gave  $\delta^{18}\text{O}$  values ranging from 5.7 ‰ to 9.7 ‰. The lowest values lie about 0.2 ‰ below the range for the Archean orthogneisses of the Ancient Gneiss Complex (Taylor and Magaritz 1975), and the highest value lies about 0.1 ‰ above the range given by Longstaffe and Birk (1981) for Archean granitoid batholiths and gneisses (figure 6.1). The  $\delta^{18}\text{O}$  values display positive correlation with  $\text{SiO}_2$  content (figure 6.2), the gneisses show no sign of extensive weathering or hydrothermal alteration and metamorphic grade is not above middle amphibolite facies. It is possible that magmatic fluids emanating from the igneous precursors of the Augen and/or Leucocratic Gneisses could have enriched some of the samples in  $^{18}\text{O}$ , but the sample with the lowest  $\delta^{18}\text{O}$  value lies below the range of the Augen and Leucocratic Gneisses. This sample also appears to be in oxygen isotopic equilibrium, a feldspar separate having a  $\delta^{18}\text{O}$  value (5.5 ‰) very close to that of the whole rock (5.7 ‰), and so is unlikely to have suffered isotopic exchange with low  $^{18}\text{O}/^{16}\text{O}$  hydrothermal meteoric waters. The sample with the highest  $\delta^{18}\text{O}$  value may possibly have suffered some low temperature  $^{18}\text{O}$  enrichment during weathering, but the samples generally appear not to have suffered oxygen isotopic exchange since their formation, their  $\delta^{18}\text{O}$  values thus confirming their meta-igneous character.

#### 6.4.4 Post-Archean Leucocratic and Augen Gneisses

The post-Archean Leucocratic Gneiss, which also occurs only to the west of the Trench, yielded  $\delta^{18}\text{O}$  values ranging from 6.2 ‰ to 7.9 ‰ (figure 6.1) and shows a positive correlation with  $\text{SiO}_2$  (figure 6.2). This gneiss is not highly weathered nor





hydrothermally altered. Its metamorphic grade is not above middle amphibolite facies and there are no nearby younger igneous intrusions which could have contaminated it. Hence, since its  $\delta^{18}\text{O}$  values appear to lie within the range for post-Archean meta-igneous granitoids, they confirm its orthogneissic character.

The post-Archean Augen Gneiss, found only to the west of the Rocky Mountain Trench, gave  $\delta^{18}\text{O}$  values of 7.1 ‰ and 7.8 ‰ (figure 6.1 and table 6.1), which fall within the range expected for a post-Archean orthogneiss. The negative correlation between the  $\delta^{18}\text{O}$  ‰ and  $\text{SiO}_2\%$  values (figure 6.2) suggests that there has been some post crystallization oxygen isotope exchange.

#### 6.4.5 Gneisses East of the Rocky Mountain Trench

The mafic and felsic gneisses from the Mount Blackman area, to the east of the Rocky Mountain Trench, show little correlation between their  $\text{SiO}_2\%$  and  $\delta^{18}\text{O}$  ‰ values (figure 6.2). Hence they may have suffered oxygen isotopic alteration and their  $\delta^{18}\text{O}$  values may not be reliable indicators of their petrogenesis. However, these  $\delta^{18}\text{O}$  values are much higher than those obtained on the mafic and felsic gneisses lying to the west of the Trench (figure 6.1), and temperatures have probably not been high enough to allow oxygen isotopic exchange with the nearby voluminous high  $\delta^{18}\text{O}$  metasediments of the Miette Group. The  $\delta^{18}\text{O}$  values on the felsic gneisses span the boundary of O'Neil and Chappell's (1977) I-type and S-type granites. This is not surprising since thin section studies show their paragneissic nature and geochemical studies show their extreme immaturity and chemical similarity to granite. The  $\delta^{18}\text{O}$  values on the mafic gneisses tend to confirm their post-Archean meta-igneous character and to demonstrate their distinctiveness from the mafic gneiss lying to the west of the Rocky Mountain Trench.

Thus the  $\delta^{18}\text{O}$  measurements on the whole rock and mineral separates from the Malton Gneiss Complex tend to confirm the meta-igneous character of all the gneisses to the west of the Rocky Mountain Trench, namely, the Archean Mafic and Grey Gneisses and the post-Archean Leucocratic and Augen Gneisses. They also tend to confirm the meta-igneous character of the post-Archean mafic Mount Blackman Gneisses as well as the metasedimentary character of the felsic post-Archean Mount Blackman Gneisses. Finally, they confirm the distinction between the gneisses east and west of the Trench;



and generally disprove any genetic relationship between the metasediments and the gneisses of the Malton Gneiss Complex.

### 6.5 Strontium Isotopic Evidence

A plot of initial strontium 87/86 ratios versus  $\delta^{18}\text{O}$  values is given in figure 6.3. It shows that for the gneisses in general, the  $\delta^{18}\text{O}$  values increase with the initial strontium 87/86 ratios, although the Archean mafic gneiss has lower  $\delta^{18}\text{O}$  values than the Grey Gneiss. However, the initial 87/86 values of the mafic gneisses are not well defined, and its  $\delta^{18}\text{O}$  values may have been lowered by later alteration as discussed under heading 6.4.2. One Grey Gneiss sample has an exceptionally high  $\delta^{18}\text{O}$  value, possibly due to low temperature  $^{18}\text{O}$  enrichment during weathering. Both  $\delta^{18}\text{O}$  values and initial strontium 87/86 ratios are measures of crustal residence time. Hence, it is not surprising to find a positive correlation between the two. As might be expected, the Mount Blackman paragneiss has higher  $\delta^{18}\text{O}$  and 87/86 I.R. values than the orthogneisses to the west of the Rocky Mountain Trench. Both the Miette and the Kaza metasediments appear to have higher  $\delta^{18}\text{O}$  and 87/86 I.R. values than any of the gneisses, thus reflecting their time of crustal residence and weathering as sediments.



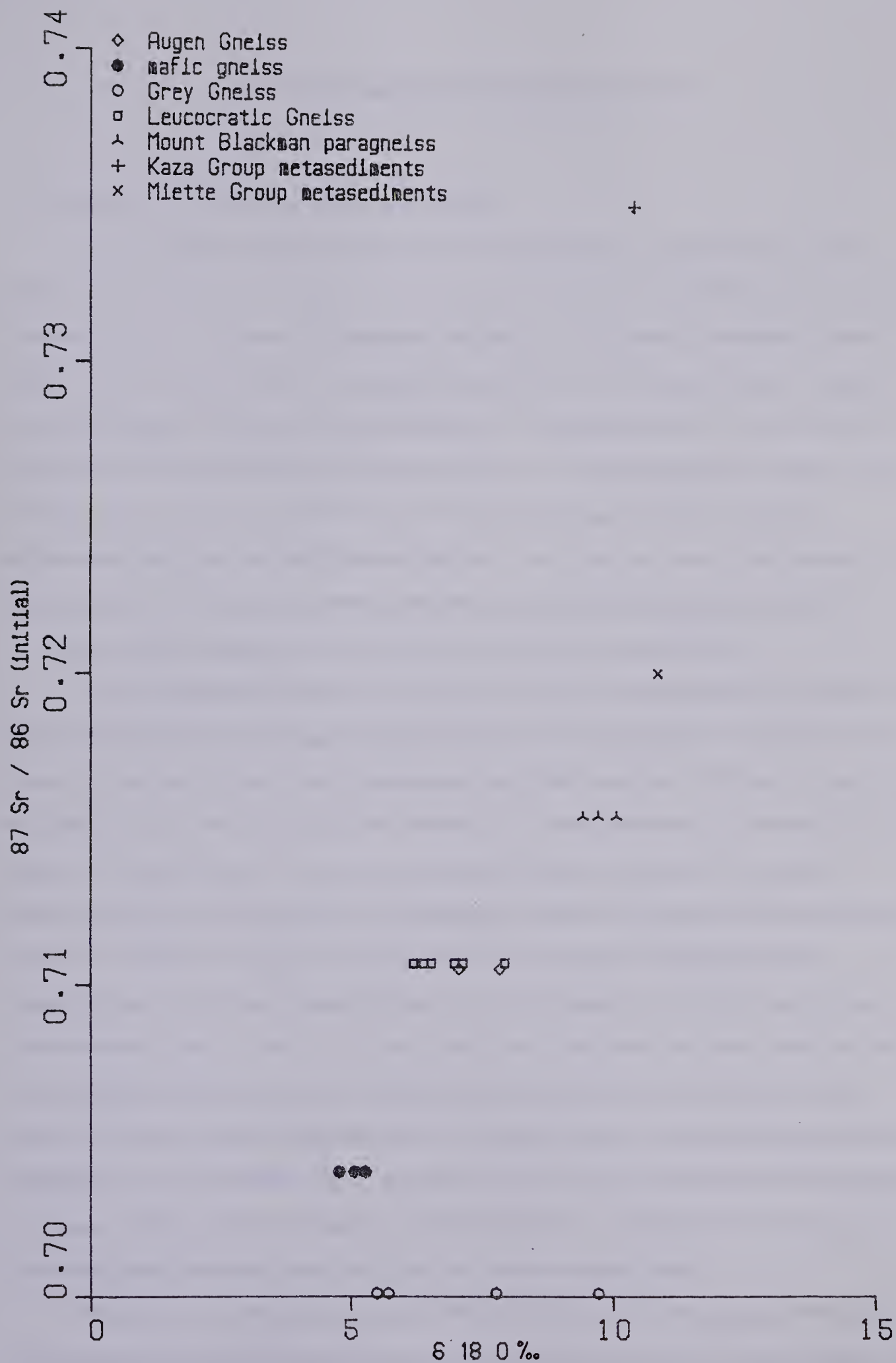


Figure 6.3  $^{18}\text{O}/^{16}\text{O}$  v  $^{87}\text{Sr}/^{86}\text{Sr}$  initial ratio plot for the rocks of the Malton Gneiss Complex





## 7. CONCLUSIONS AND SPECULATION

### 7.1 The nature of the Rocky Mountain Trench

No correlation was found between the formations on opposite sides of the Rocky Mountain Trench. The gneisses west of the Trench in the Malton Block consist of a bimodal suite of Archean orthogneisses intruded by a Hudsonian peralkaline granite gneiss, with further intrusions of peralkaline granitic as well as alkali basaltic magmas during the Upper Proterozoic and the Cambrian. The gneisses east of the Trench are comprised of three apparently unrelated outcrops. The Mount Blackman Gneiss is the earliest and consists of probable early Proterozoic immature granitic sediments, metamorphosed at about 1900 Ma and 900 Ma. The other two are orthogneisses. The Bulldog Creek Gneiss was apparently intruded as a granodiorite, perhaps at about 1100 Ma, and the Hugh Allan Creek Gneiss as a granite at about 800 Ma.

The metasediments west of the Trench consist of the Monashee Horsethief Creek Group in the south and the Kaza Group in the north. The Monashee Horsethief Creek Group formed as fairly immature greywackes and lithic arenites. The Kaza Group formed as feldspar poor mature argillites and arenites. The metasediments to the east of the Trench, the Miette Group, formed as extremely immature, feldspar rich arkoses. Metamorphism of the Kaza Group metasediments west of the Trench may have occurred during the Tahltanian Orogeny and consisted of low pressure sillimanite grade metamorphism. The major metamorphism of the Monashee Horsethief Creek Group metasediments, also to the west of the Trench, occurred during or soon after the second of three major folding episodes, probably at about 1250 Ma. It consisted of high pressure sillimanite grade metamorphism and migmatization. The major metamorphism of the Miette Group metasediments to the east of the Trench occurred during the second of two major folding episodes, possibly at about 900 Ma. It consisted of low pressure sillimanite grade metamorphism which did not include migmatization.

This lack of correlation across the Rocky Mountain Trench suggests that major thrusting across it has not been the most recent event in this area. Indeed, Clague (1974) states that the Trench cuts across the Laramide fold and thrust structures between latitudes 47°N and 59°N. In the Valemount area, the most recent movement on the



Trench appears to be normal faulting (Oke and Simony, 1981), which may also be the explanation for the outcrops of Miette Group Metasediment and Bulldog Creek Gneiss in the Trench in the Bulldog Creek area (frontispiece). Cretaceous westward dipping subduction may have occurred along the line of the Trench, as is suggested by the Cretaceous potassium – argon ages of the formations to the east and of the plutons and stocks to the west of the Trench. Thus the Rocky Mountain Trench appears to mark the edge of the Precambrian North American Craton as well as being a suture line marking the closing of Cretaceous westward dipping subduction, along which later transcurrent and normal faulting has occurred.

## 7.2 Geological History of the Area

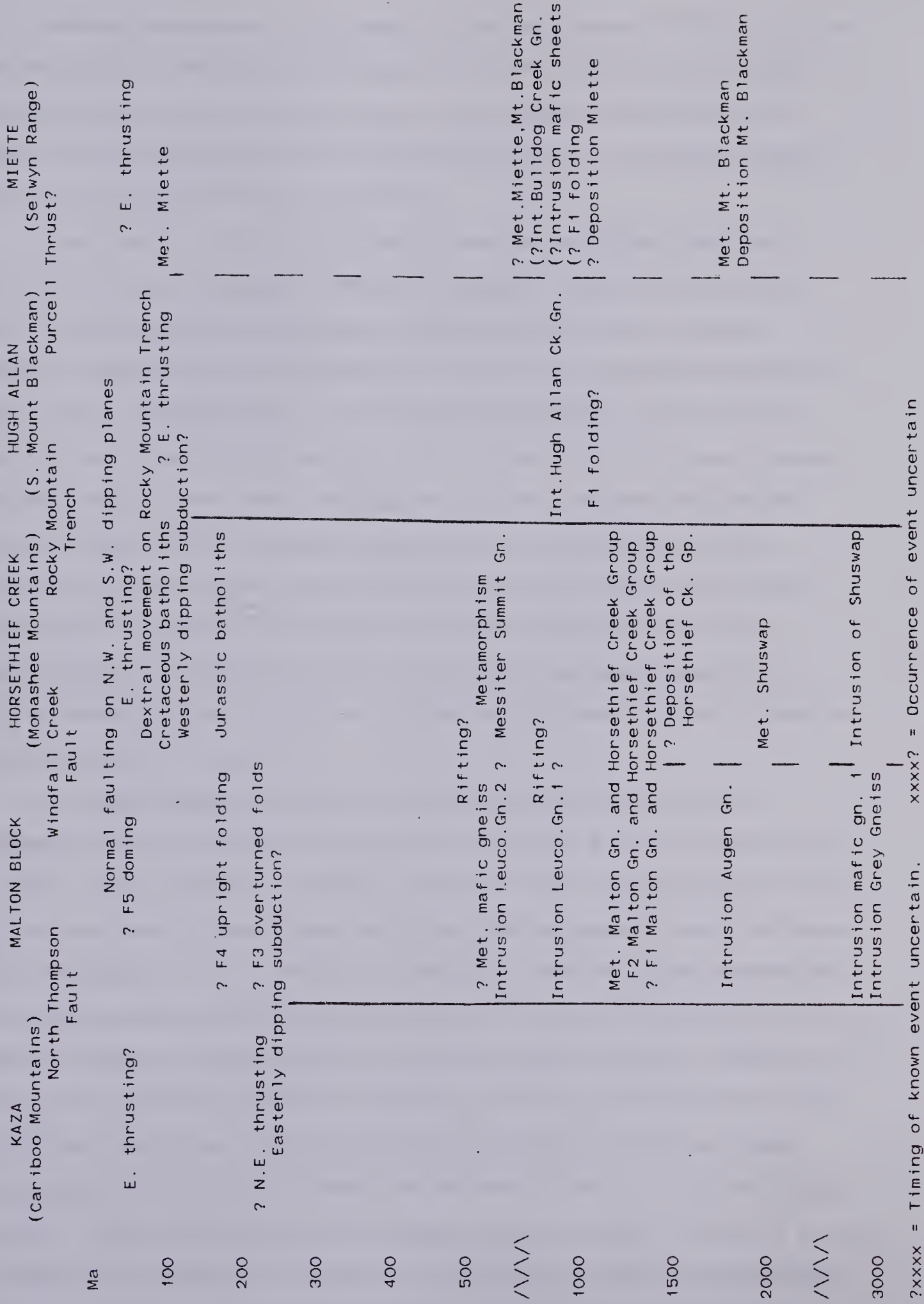
A suggested history of the area of the Malton Gneiss Complex is shown in figure 7.1. This tabulation suggests that the area may be composed of at least three, and possibly five interlocking lithospheric plates, microplates, or parts of plates. The edges of these plates are marked by thick black lines in figure 7.1.

The oldest rocks in the Complex underlie those parts of the Malton Range and the Monashee Mountains which compose the Malton block. Here a bimodal suite of Archean orthogneisses appears to have originated 3.0 Ga ago by the separate intrusions of mantle derived calc-alkaline tonalitic and alkali basaltic magmas or alkali gabbroic cumulates. These formations were intruded at about 1.8 Ga by a mildly peralkaline granitic magma, probably formed by partial melting of the pre-existing mafic rock, and now forming a lineated augen gneiss. Meanwhile, the protoliths of the Monashee Horsethief Creek Group metasediments were being deposited as mature sandstones and mudstones, and at some time, or times earlier than 1.25 Ga were twice isoclinally folded together with the gneisses of the Malton Block. The second folding episode was accompanied by thrusting on planes dipping to the south and was closely followed by high grade metamorphism to sillimanite grade probably at about 1.25 Ga (East Kootenay Orogeny of McMechan and Price, 1982).

Fresh influxes of leucocratic mildly peralkaline granitic magma and alkaline basaltic magma probably occurred at about 840 Ma and 550 Ma. The former possibly marks a rifting episode, perhaps that of the separation of this microplate from its parent plate. If



Figure 7.1 Tabulation of the geological history of the Malton Gneiss Complex area







so, it is contemporaneous with rifting dated by Kistler and Peterman (1978) in California. A second period of rifting in California (dated by the same authors) is approximately contemporaneous with the c.550 Ma intrusion of leucocratic peralkaline and mafic magmas in the Malton Block and the c.570 Ma metamorphism of the Messiter Summit Gneiss in the Monashee Horsethief Creek Block.

A third period of folding on this Malton–Monashee Horsethief Creek plate produced folds overturned to the northeast and plunging to the southeast (Morrison, 1979). These could have formed during a Tahltanian period of easterly dipping subduction, which ended with the collision of the Kaza Group metasediments against the western side of the Malton Block. This is the approximate time at which the Stikine Block may have arrived at its Mesozoic position, 1300 km south of its present position (Monger and Irving, 1980). Hence, this may mark the time of collision between the Stikine and Malton blocks. Wrangellia is believed to have collided with Stikinia in mid–Jurassic to early Cretaceous times (Irving *et al.*, 1981). Hence, if Stikinia were already joined to the Malton and Monashee Horsethief Creek Blocks, the Jurassic metamorphism and deformation detected in the latter may have been caused by the arrival of Wrangellia. The  $F_4$  folding on northwest trending axes in the Malton Block may also be a response to this event.

Northward movement of these now accreted terranes probably did not commence until the late Cretaceous or early Tertiary (Monger and Irving, 1980; Irving *et al.*, 1981). It may have been preceded by Cretaceous westerly dipping subduction along the line of the Rocky Mountain Trench, as the North Atlantic began to open. Riddihough (1982) has suggested 50–150 mm/yr of northeasterly relative movement between the North American and Farallon plates during the period 100 Ma to 60 Ma (figure 7.2). The Cadomin Formation has been recognized as evidence of early Cretaceous orogeny in the western Rocky Mountains (Schultheis and Mountjoy, 1978). Price and Mountjoy (1970) demonstrated that premetamorphic deformation and thrusting in the Selwyn Range probably began in early Cretaceous times and had ended by about 111 Ma, which is the potassium – argon age of biotite porphyroblasts, growing at random orientations, across the foliation and schistosity of the Miette Group. Royce *et al.* (1975) have established a similar timing for deformation on the Idaho–Wyoming Thrust Belt. The Cache Creek



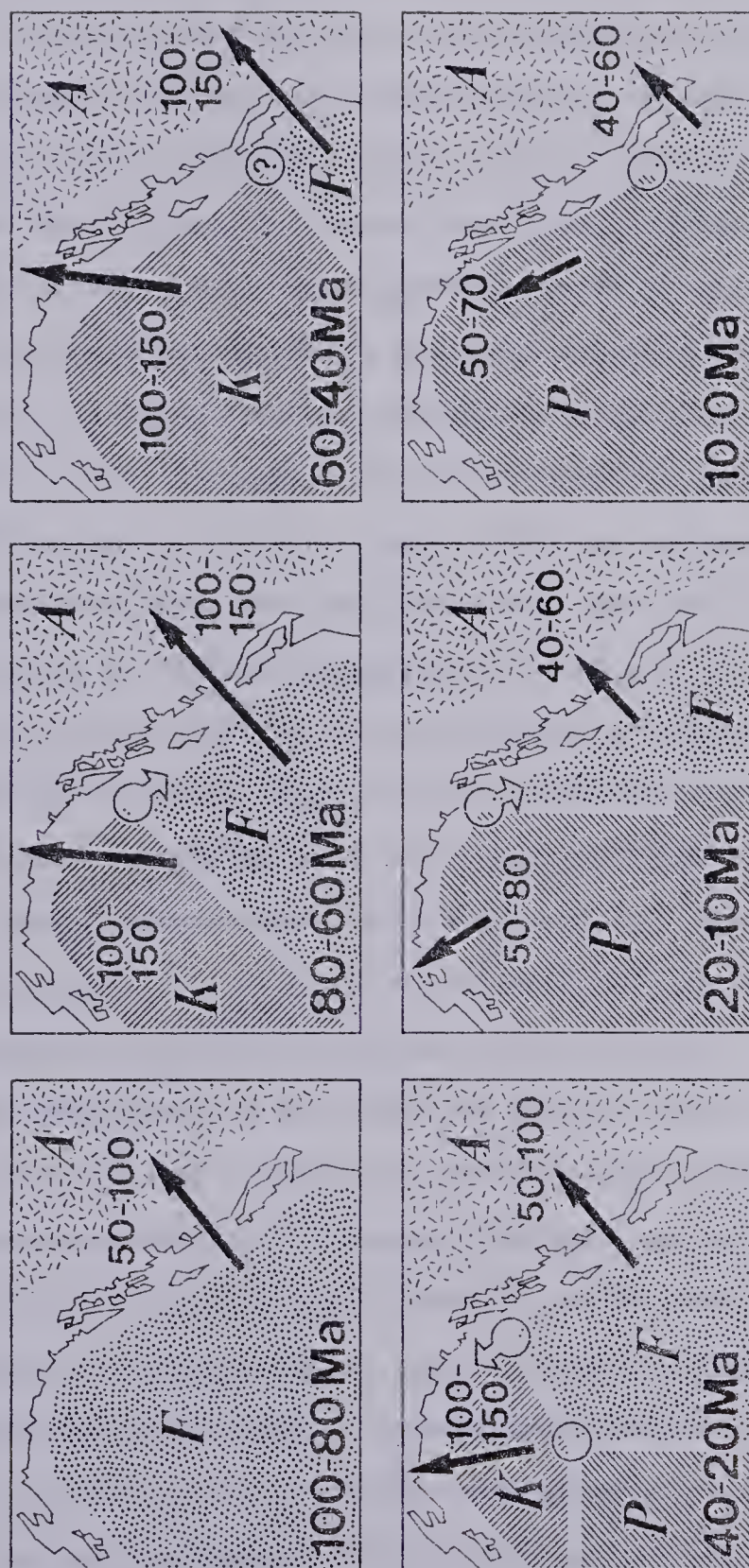


Figure 4 Plate interactions off western Canada during the last 100 Ma, from a consensus of plate reconstructions (principal sources and

Plates are as in Figure 2). Arrows and numbers represent movement relative to America plate in mm/yr or km/Ma. Open circles are triple

junction positions with movement where known.

Figure 7.2 Relative movements of the North American, Farallon and Kula plates during the last 100 Ma. (Ridd, 1982).





Group and overlying deposits were thrust westwards onto the Stikine terrane at about this same time (Monger and Irving, 1980) and it may also have been the time at which the Hugh Allan Creek Gneiss was also thrust eastwards onto the North American Craton (figure 7.1). When the North American Craton reached the subduction zone, subduction would have ceased, and may have jumped westward, resulting in the mid-Cretaceous to early Tertiary plutons of the Coast Plutonic Complex (Monger and Price, 1979).

Subduction of the ridge between the Farallon and Kula plates at about 60 Ma would have resulted in dextral transcurrent movement along faults roughly parallel to the Kula-North American plate boundary, during the period c.60 Ma to c.40 Ma (Riddihough, 1982). This is consistent with the geological evidence for the timing (late Cretaceous or early Tertiary) of the northward motion of the Cordilleran exotic terranes (Monger and Irving, 1980; Irving *et al.*, 1981). Atwater (1970) has suggested that the Kula-Farallon-North American triple junction may have been in southern California at this time, and the rate of movement suggested by Riddihough (1982) would allow for at least 2000 km of relative northward movement between the Kula and North American plates between 60 Ma and 40 Ma. Much of this movement may have taken place on the Rocky Mountain Trench. Templeman-Kluit (1977) reported evidence for approximately 400 km of dextral transcurrent movement on the northern Rocky Mountain Trench, in the late Cretaceous or early Tertiary. Clague (1974) has shown that the southern Rocky Mountain Trench movements postdate Laramide structures, and Tipper (1981), using upper Pliensbachian ammonites, has shown that the greatest relative dextral transcurrent movement in the Canadian Cordillera occurred between the craton and Quesnellia.

The relative directions of movement changed again at about 40 Ma (figure 7.2), as the Kula Plate itself was subducted northwards, and the main process occurring along the western edge of the North American plate reverted to northeasterly subduction of the Farallon Plate (Riddihough, 1982). This subduction persisted until about 10 Ma, and was probably responsible for the late Tertiary northeasterly directed thrusts in the Rocky Mountains and over the Metamorphic Core Complexes (Coney, 1980). It is also possible that Stelck and Hedinger's (1975) Lower Cambrian archaeocyathid bearing rocks were thrust eastward at this time. At about 10 Ma subduction of the Pacific-Farallon ridge initiated dextral transcurrent movement north of the ridge, whilst subduction of the Juan





de Fuca remnant of the Farallon plate continues south of the ridge boundary.



## 8. REFERENCES CITED

- Aitken, J.D. 1969. Documentation of the sub-Cambrian unconformity, Rocky Mountain Main Ranges, Alberta. *Can. J. Earth Sci.* 6, 193-200.
- Armstrong, R.L. 1968. Mantled gneiss domes in the Albion Range, southern Idaho. *Geol. Soc. Am. Bull.* 79, 1295-1314.
- Armstrong, R.L. 1972. Low-angle (denudation) faults, hinterland of the Sevier orogenic belt, eastern Nevada and western Utah. *Geol. Soc. Am. Bull.* 83, 1729-1754.
- Armstrong, R.L., Taubeneck, R.W. and Hales, P.E. 1977. Rb-Sr and K-Ar geochronology of Mesozoic granitic rocks and their isotopic composition, Oregon, Washington and Idaho. *Geol. Soc. Am. Bull.* 88, 397-411.
- Atwater, T. 1970. Implications of plate tectonics for the Cenozoic tectonic evolution of western North America. *Geol. Soc. Am. Bull.* 81, 3513-3536.
- Baadsgaard, H., Lipson J. and Folinsbee, R.E. 1961. The leakage of radiogenic argon from sanidine. *Geochim. Cosmochim. Acta* 25, 147-157.
- Balashov, Y.A., Ronov, A.B., Migdisov, A.A. and Turanskaya, N.V. 1964. The effect of climate and facies environment on the fractionation of the rare earths during sedimentation. *Geochem. Int.* 1964, 951-969.
- Banks, N.G. 1980. Geology of a zone of metamorphic core complexes in southeastern Arizona. *Geol. Soc. Am. Mem.* 153, 177-216.
- Barker, F. 1979. Trondhjemite: definition, environment and hypotheses of origin. *In*: Barker, F. (ed.): *Trondhjemites, dacites and related rocks*. Elsevier, 2-12.
- Berger, G.W. and York, D. 1981.  $^{40}\text{Ar}/^{39}\text{Ar}$  dating of the Thanet gabbro, Ontario: looking through the Grenvillian metamorphic veil and implications for paleomagnetism. *Can. J. Earth Sci.* 18, 266-273.
- Berry, M.J. and Forsyth, D.A. 1975. Structure of the Canadian Cordillera. *Can. J. Earth Sci.* 8, 788-801.
- Bickle, M.J. and Nisbet, E. 1972. The oceanic affinities of some Alpine mafic rocks based on their Ti-Zr-Y contents. *J. geol. Soc. London* 128, 267-271.
- Blenkinsop, J. 1972. Computer assisted mass spectrometry and its application to Rb/Sr geochronology. Unpublished Ph.D. thesis, University of British Columbia, Vancouver.
- Bloxham, T.W. and Lewis, A.D. 1972. Ti, Zr and Cr in some British pillow lavas and their petrogenetic affinities. *Nature Phys. Sci.* 237, 134-136.
- Bouger Gravity Anomaly Map of Canada (1 inch to 40 miles). 1967. Observations Branch, Department of Energy Mines and Resources, Ottawa.
- Brooks, C., Hart, S.R. and Wendt, I. 1972. Realistic use of two-error regression treatments as applied to rubidium-strontium data. *Rev. Geophys. Space Phys.* 10, 551-577.



- Brown, G.M., Emeleus, C.H., Holland, J.G. and Phillips, R. 1970. Mineralogical, chemical and petrological features of Apollo 11 rocks and their relationship to igneous processes. *Proc. Apollo 11 Lunar Sci. Conf., Geochim. Cosmochim. Acta Suppl.* 1, Vol. 1, 195-219. Pergamon Press.
- Brown, R.L. and Murphy, D.C. 1982. Kinematic interpretation of mylonitic rocks in part of the Columbia River fault zone, Shuswap terrane, British Columbia. *Can. J. Earth Sci.* 19, 456-465.
- Brown, R.L., Tippet, C.R. and Lane, L.S. 1978. Stratigraphy, facies changes and correlations in the northern Selkirk Mountains, southern Canadian Cordillera. *Can. J. Earth Sci.* 15, 1129-1140.
- Campbell, R.B. 1967. McBride map area. *In: Report of Activities, Geol. Surv. Canada, Paper 67-1, Pt. A*, 53-55.
- Campbell, R.B. 1968. Canoe River, British Columbia (934). *Geol. Surv. Canada, map 15-1967*.
- Campbell, R.B. 1970. Structural and metamorphic transitions from infrastructure to superstructure, Cariboo Mountains, British Columbia. *In: Structure of the Southern Canadian Cordillera*. Wheeler, J.O. (ed.), *Geol. Assoc. Canada Special Paper No. 6*, 67-72.
- Campbell, R.B. 1972. Geological map of part of the south eastern Canadian Cordillera. *In: Wheeler, J.O., Campbell, R.B., Reeson, J.E. and Mountjoy, E.W. (eds.): Structural style of the Southern Canadian Cordillera. Field Excursion XO1-AO1, XXIV Int. Geol. Cong. Montreal 1972*.
- Campbell, R.B. and Charlesworth, H.A.K. 1970. Geology of the region between Prince George and Jasper. *In: Edmonton Geol. Soc. Guidebook 1970*, 84-93.
- Campbell, R.B. and Tipper, H.W. 1971. Bonaparte Lake map area, British Columbia. *Geol. Surv. Canada, Mem.* 363, 80-81.
- Campbell, R.B., Mountjoy, E.W. and Young, F.G. 1973. Geology of McBride map area, British Columbia. *Geol. Surv. Canada, Paper 72-35*. 104 pp.
- Caner, B. 1970. Electrical conductivity structure in Western Canada and petrological interpretation. *J. Geomagn. Geoelec.* 22, 113-129.
- Cann, J.A. 1970. Rubidium, strontium, yttrium, zirconium and niobium in some ocean floor basaltic rocks. *Earth Planet. Sci. Lett.* 10, 7-11.
- Chamberlain, V.E., Lambert, R.St J. and Holland, J.G. 1978. Preliminary subdivisions of the Malton Gneiss Complex, British Columbia. *Current Research, Geol. Surv. Canada, Paper 78-1A*, 491-492.
- Chamberlain, V.E., Lambert, R.St J. and Holland, J.G. 1980a. Petrology and geochemistry of the Archean rocks of the Malton Gneiss Complex, British Columbia. *Precambrian Res.* 11, 1-9.
- Chamberlain, V.E., Lambert, R.St J. and Holland, J.G. 1980b. The Malton Gneiss: Archean gneisses in British Columbia. *Precambrian Res.* 11, 297-306.
- Chamberlain, V.E., Lambert, R.St J., Baadsgaard, H. and Gale, N.H. 1979. Geochronology of the Malton Gneiss Complex of British Columbia. *Current Research, Geol. Surv. Canada, Paper 79-1B*, 45-50.





- Chandra, N.N. and Cumming, G.L. 1972. Seismic refraction studies in western Canada. *Can. J. Earth Sci.* 9, 1099–1109.
- Chappell, B.W. and White, A.J.R. 1974. Two contrasting granite types. *Pacific Geology* 8, 173–174.
- Charlesworth, H.A.K., Weiner, J.L., Akehurst, A.J., Bielenstein, H.U., Evans, C.R., Griffiths, R.E., Remington, D.B., Stauffer, M.R. and Steiner, J. 1967. Precambrian Geology of the Jasper Region, Alberta. *Res. Council Alta. Bull.* 23. 74 pp.
- Clague, J.J. 1974. The St. Eugene Formation and the development of the southern Rocky Mountain Trench. *Can. J. Earth Sci.* 11, 916–938.
- Clayton, R.N. and Mayeda, T.K. 1963. The use of bromine pentafluoride in the extraction of oxygen from oxides and silicates for isotopic analysis. *Geochim. Cosmochim. Acta* 27, 43–52.
- Coles, R.L., Haines, G.V. and Hannaford, W. 1976. Large scale magnetic anomalies over western Canada and the Arctic: a discussion. *Can. J. Earth Sci.* 13, 790–802.
- Coney, P.J. 1974. Structural analysis of the Snake Range decollement, east-central Nevada. *Geol. Soc. Am. Bull.* 85, 973–978.
- Coney, P.J. 1980. Cordilleran metamorphic core complexes: An overview. *Geol. Soc. Am. Mem.* 153, 7–31.
- Coney, P.J., Jones, D.L. and Monger, J.W.H. 1980. Cordilleran suspect terranes. *Nature* 288, 329–333.
- Cosgrove, M.E. 1972. The geochemistry of the potassium-rich Permian volcanic rocks of Devonshire, England. *Contrib. Mineral. Petrol.* 36, 155–170.
- Craw, D. 1978. Metamorphism, structure and stratigraphy in the Southern Park Ranges, British Columbia. *Can. J. Earth Sci.* 15, 86–98.
- Currie, K.L. 1975. The Geology and Petrology of the Ice River Alkaline Complex. *B.C. Geol. Surv. Canada Bull.* 245. 68 pp.
- Daly, R.A. 1925. The geology of Ascension Island. *Proc. Am. Acad. Arts Sci.* 60, 1–80.
- Davis, G.A., Monger, J.W.H. and Burchfiel, B.C., 1978. Mesozoic construction of the Cordilleran "collage", central British Columbia to central California. *In: Mesozoic Paleogeography of the Western United States*. D.G. Howell and K.A. McDougall (eds.), *Soc. Econ. Paleontol. and Mineral. Pacific Coast Paleogeography Symp.* 2, 1–32.
- Davis, G.A., Anderson, J.L., Frost, C.G. and Shackelford, T.J. 1980. Mylonitization and detachment faulting in the Whipple-Buckskin-Rawhide Mountains terrane, southeastern California and western Arizona. *Geol. Soc. Am. Mem.* 153, 79–129.
- Davis, G.H. 1980. Structural characteristics of metamorphic core complexes, southern Arizona. *Geol. Soc. Am. Mem.* 153, 35–77.
- Dickin, A.P. 1981. Isotope geochemistry of Tertiary igneous rocks from the Isle of Skye, N.W. Scotland. *J. Petrol.* 22, 155–189.
- Dickinson, W.R. 1976. Sedimentary basins developed during the evolution of Mesozoic-Cenozoic arc trench systems in western North America. *Can. J. Earth Sci.* 13, 1268–1287.



- Dodson, M.H. 1973. Closure temperature in cooling geochronological and petrological systems. *Contrib. Mineral. Petrol.* 40, 259–274.
- Dott, R.H., 1961, Permo–Triassic diastrophism in the Western Cordillera System. *Am. J. Sci.* 259, 561–582.
- Douglas, R.J.W., Gabrielse, H, Wheeler, J.O., Stott, D.F. and Belyea, H.R., 1970, Geology of Western Canada. /n: *Geology and Economic Minerals of Canada*. Geol. Surv. Canada, Econ. Geol. Rep. 1, 365–488.
- Dragert, H. and Clark, G.K.C. 1977. A detailed investigation of the Canadian Cordillera geomagnetic transition anomaly. *J. Geophys.* 42, 373–390.
- Drury, S.A. 1983. The petrogenesis and setting of Archaean metavolcanics from Karnataka State, South India. *Geochim. Cosmochim. Acta* 47, 317–329.
- Duncan, I.D. 1978. Rb/Sr whole rock evidence for three Pre–Cambrian events in the Shuswap Complex, S.E. B.C. /n: *Abstracts with Programs*, Geol. Assoc. Can. Annual Meeting, Toronto, Ont. 392–393.
- Duncan, I.J., Parrish, R.R. and Armstrong, R.L., 1979, Rb/Sr geochronology of the post tectonic intrusive events in the Ominica Crystalline Belt, Southeastern British Columbia. Cordilleran Section of the Geological Association of Canada, Program with Abstracts, Vancouver, 1979, 15.
- Eisbacher, G.H. 1977. Mesozoic–Tertiary basin models for the Canadian Cordillera and their geological constraints. *Can. J. Earth Sci.* 14, 2414–2421.
- Ellis, R.M. and Chandra, B., 1981. Seismicity in the Mica Reservoir (McNaughton Lake) area; 1973–1978. *Can. J. Earth Sci.* 18, 1708–1716.
- Ewart, A. and Taylor, S.R. 1969. Trace element geochemistry of the rhyolitic volcanic rocks, central North Island, New Zealand: phenocryst data. *Contrib. Mineral. Petrol.* 22, p. 127–146.
- Field, D. and Elliot, R.B. 1974. The chemistry of gabbro/amphibolite transitions in South Norway. *Contrib. Mineral. Petrol.* 47, 63–76.
- Flanagan, F.J. 1973. 1972 values for international geochemical reference samples. *Geochim. Cosmochim. Acta* 37, 1189–1200.
- Fourcade, S. and Javoy, M. 1973. Rapports  $^{18}\text{O}/^{16}\text{O}$  dans les roches du vieux socle catazonal d'In Onzzal (Sahara Algerien). *Contrib. Mineral. Petrol.* 42, 235–244.
- Fritz, W.H. 1975. Broad correlations of some Lower and Middle Cambrian strata in the North American Cordillera. *Geol. Surv. Canada, Paper* 75–1A, 533–540.
- Fulton, R.J. and Walcott, R.I. 1975. Lithospheric flexure as shown by the deformation of glacial lake shorelines in southern British Columbia. /n: *Krumbein Volume*, E.H.T. Whitter (ed.), *Geol. Soc. Am. Mem.* 142, 163–173.
- Fyles, J.T. and Eastwood, G.E.P. 1962. Geology of the Ferguson area, Lardeau District, British Columbia. *British Columbia Dept. Mines, Bull.* 45. 92 pp.
- Ghent, E.D., Simony, P.S. and Knitter, C.C. 1980. Geometry and pressure–temperature significance of the kyanite–sillimanite isograd in the Mica Creek area, British Columbia. *Contrib. Mineral. Petrol.* 74, 67–73.
- Ghent, E.D., Simony, P.S., Mitchell, W., Perry, J., Robbins, D. and Wagner, J. 1977. Structure and metamorphism in southeast Canoe River area, British Columbia. /n: *Report of Activities*, *Geol. Surv. Canada, Paper* 77–10, 13–17.





- Giletti, B.J. 1974. Diffusion related to geochronology. *In: Geochemical Transport and Kinetics*, A.W. Hofman, B.J. Giletti, H.S. Yoder and R.A. Yund (eds.), Carnegie Inst. Washington Publ. 634, 61–76.
- Giovanella, C.A. 1967. Structural relationships of the metamorphic rocks along the Rocky Mountain Trench at Canoe River. *In: Report of Activities, Part A*, Geol. Surv. Canada, Paper 67–1A, 60–61.
- Goodwin, A.M. and Smith, I.E.M. 1980. Chemical discontinuities in Archean metavolcanic terrains and the development of Archean crust. *Precambrian Res.* 10, 301–311.
- Gough, D.I., Bingham, D.K., Ingham, M.R. and Alabi, A.O. 1982. Conductive structures in southwestern Canada: A regional magnetometer array study. *Can. J. Earth Sci.* 19, 1680–1690.
- Griffiths, J.R. 1977. Mesozoic–Early Cretaceous volcanism, plutonism and mineralization in southern British Columbia. A plate tectonics synthesis. *Can. J. Earth Sci.* 14, 1611–1624.
- Haines, G.V., Hannaford, W. and Riddihough, R.P. 1971. Magnetic anomalies over British Columbia and the adjacent Pacific Ocean. *Can. J. Earth Sci.* 8, 387–391.
- Hallberg, J.A. and Williams, D.A.C. 1972. Archaean mafic and ultramafic rock associations in the eastern Goldfields region, Western Australia. *Earth Planet. Sci. Lett.* 15, 191–200.
- Harrison, T.M. and Clarke, G.K.C. 1979. A model of the thermal effects of igneous intrusion and uplift as applied to the Quottoon pluton, British Columbia. *Can. J. Earth Sci.* 16, 411–420.
- Hart, S.R., Davis, G.L., Steiger, R.H. and Tilton, G.R. 1968. A comparison of the isotopic mineral age variations and petrologic changes induced by contact metamorphism. *In: Radiometric Dating for Geologists*, E.I. Hamilton and R.M. Farquhar (eds.), Interscience Publishers, pp 73–110.
- Helwig, J. 1974. Eugeosynclinal basement and a collage concept of orogenic belts. *Soc. Econ. Paleontol. Mineral. Spec. Pub.* 19, 359–376.
- Hendrickson, A.E. and White, P.O. 1964. Promax: a quick method for rotation to oblique simple structure. *Brit. J. Statist. Psychol.* 17, 65–70.
- Hyndman, D.W. 1968. Petrology and structure of Nakusp map area. *B.C. Geol. Surv. Canada Bull.* 161. 95 pp.
- Irvine, T.N. and Baragar, W.R.A. 1971. A guide to the chemical classification of the common volcanic rocks. *Can. J. Earth Sci.* 8, 523–548.
- Irving, E., Monger, J.W.H. and Yole, R.W. 1981. New Paleomagnetic evidence for displaced terranes in British Columbia. *In: The Continental Crust and its Mineral Deposits*. D. Strangway (ed.), Geol. Assoc. Canada Spec. Paper 20, 441–455.
- Jones, D.L., Silberling, N.J. and Hillhouse, J. 1977. Wrangellia – A displaced terrane in northwestern North America. *Can. J. Earth Sci.* 14, 2565–2577.
- Judge, A. 1977. Terrestrial heat flow and the thermal structure of the eastern Canadian Cordillera. *Geol. Assoc. Canada Prog. with Abst.* 2, 28.
- Kesmarky, S. 1977. Rates of migration of alkali and strontium ions in a heated quartz monzonite. Unpublished M.Sc. thesis, University of Alberta, Edmonton.





- Kistler, R.W. and Peterman, Z.E. 1973. Variations in Sr, Rb, K, Na and initial  $\text{Sr}^{87}/\text{Sr}^{86}$  in Mesozoic granitic rocks and intruded wall rocks in central California. *Geol. Soc. Am. Bull.* 84, 3489–3511.
- Kistler, R.W. and Peterman, Z.E. 1978. Reconstruction of crustal blocks of California on the basis of initial strontium isotopic compositions of Mesozoic granitic rocks. *U.S. Geol. Surv. Prof. Paper* 1071. 17pp.
- Krogh, T.E. 1973. A low contamination method for hydrothermal decomposition of zircon and extraction of U and Pb for isotopic age determinations. *Geochim. Cosmochim. Acta* 37, 485–494.
- Lambert, R.St J. and Holland, J.G. 1974. Yttrium geochemistry applied to petrogenesis utilizing calcium–yttrium relationships in minerals and rocks. *Geochim. Cosmochim. Acta* 33, 1393–1414.
- Lambert, R.St J., Holland, J.G. and Owen, P.F. 1974. Chemical petrology of a suite of calc-alkaline lavas from Mount Ararat, Turkey. *J. Geol.* 82, 419–438.
- Lambert, R.St J., Holland, J.G. and Winchester, J.A. 1982. A geochemical comparison of the Dalradian Leven Schists and the Grampian Division Monadhliath Schists of Scotland. *J. geol. Soc. London* 139, 71–84.
- Longstaffe, F.J. 1979. The oxygen isotope geochemistry of Archean granitoids. *In*: Barker, F. (ed.): *Trondhjemites, dacites and related rocks*. Elsevier, 363–399.
- Longstaffe, F.J. and Birk, D. 1981. Oxygen isotope evidence for the origin of discrete granitoid plutons from the Archean western Wabigoon Belt, northwestern Ontario. *Precambrian Res.* 14, 21–30.
- Longstaffe, F.J. and Schwarcz, H.P. 1977.  $^{18}\text{O}/^{16}\text{O}$  of Archean clastic metasedimentary rocks: a petrogenetic indicator for Archean gneisses? *Geochim. Cosmochim. Acta* 41, 1303–1312.
- Lowdon, J.A., Stockwell, C.H., Tipper, H.W. and Wanless, R.K. 1963. Age determinations and geological studies. *Geol. Surv. Canada, Paper* 62–17. 140 pp.
- Magaritz, M. and Taylor, H.P., Jr. 1976.  $^{18}\text{O}/^{16}\text{O}$  and D/H studies along a 500 km traverse across the Coast Range batholith and its country rocks, central British Columbia. *Can. J. Earth Sci.* 13, 1514–1536.
- McMechan, M.E. and Price, R.A. 1982. Superimposed low-grade metamorphism in the Mount Fisher area, southeast British Columbia—implications for the East Kootenay Orogeny. *Can. J. Earth Sci.* 19, 476–489.
- Mereu, R.F., Majumdar, S.C. and White, R.E. 1977. The structure of the crust and upper mantle under the highest ranges of the Canadian Rockies from a seismic refraction survey. *Can. J. Earth Sci.* 14, 196–208.
- Misch, P. 1960. Regional structural reconnaissance in central-northeast Nevada and some adjacent areas: Observations and interpretations. *Intermountain Ass. Petroleum Geol. Guidebook*. 11th Annual Field Conf. 17–42.
- Monger, J.W.H. 1977. Upper Paleozoic rocks of the western Canadian Cordillera and their bearing on Cordilleran evolution. *Can. J. Earth Sci.* 14, 1832–1859.
- Monger, J.W.H. and Irving, E. 1980. Northward displacement of north-central British Columbia. *Nature* 285, 289–294.



- Monger, J.W.H. and Price, R.A. 1979. Geodynamic evolution of the Canadian Cordillera – progress and problems. *Can. J. Earth Sci.* 16, 770–791.
- Monger, J.W.H., Price, R.A. and Tempelman-Kluit, D.J. 1982. Tectonic accretion and the origin of the two major metamorphic and plutonic welts in the Canadian Cordillera. *Geology* 10, 70–75.
- Monger, J.W.H., Souther, J.G. and Gabrielse, H. 1972. Evolution of the Canadian Cordillera: a plate-tectonic model. *Am. J. Sci.* 272, 577–602.
- Morrison, 1979. Structure and Petrology of the southern portion of the Malton Gneiss, British Columbia. *Current Research*, *Geol. Surv. Canada*, Paper 79–1B, 407–410.
- Muller, J.E. 1977. Evolution of the Pacific Margin, Vancouver Island, and adjacent regions. *Can. J. Earth Sci.* 14, 2062–2085.
- Nguyen, K.K., Sinclair, A.J and Libby, W.G. 1968. Age of the northern part of the Nelson Batholith. *Can. J. Earth Sci.* 5, 955–957.
- Noble, D.C. and Haffty, J. 1969. Minor-element and revised major-element contents of some European pantellerites and comendites. *J. Petrol.* 10, 502–509.
- Nockolds, S.R. 1954. Average chemical compositions of some igneous rocks. *Bull. Geol. Soc. Amer.* 65, 1007–1032.
- O'Connor, J.T. 1965. A classification for quartz-rich igneous rocks based on feldspar ratios. *U.S. Geol. Surv. Prof. Paper* 525–B, 79–84.
- Oke, C. and Simony, P.S. 1981. Basement gneisses of the western Rocky Mountains, Hugh Allan Creek area, British Columbia. *Current Research*, *Geol. Surv. Canada*, Paper 81–1A, 181–184.
- Okulitch, A.V. 1975. Stratigraphy and structure of the western margin of the Shuswap Metamorphic Complex, Vernon (82L) and Seymour Arm (82M) map-areas, British Columbia. *Geol. Surv. Canada*, Paper 75–1A, 27–28.
- Okulitch, A.V., Wanless, R.K. and Loveridge, W.D. 1975. Devonian plutonism in south-central British Columbia. *Can. J. Earth Sci.* 12, 1760–1769.
- O'Neil, J.R. and Chappell, B.W. 1977. Oxygen and hydrogen isotope relations in the Berridale batholith. *J. geol. Soc. London* 133, 559–571.
- Pankhurst, R.J. and O'Nions, R.K. 1973. Determination of Rb/Sr and  $^{87}\text{Sr}/^{86}\text{Sr}$  ratios of some standard rocks and evaluation of X-ray fluorescence. *Chem. Geol.* 12, 127–136.
- Paterson, I.A. and Harakal, J.E. 1974. Potassium-argon dating of blueschists from Pinchi Lake, central British Columbia. *Can. J. Earth Sci.* 11, 1007–1011.
- Pearce, J.A. and Cann, J.R. 1973. Tectonic setting of basic volcanic rocks determined using trace element analysis. *Earth Planet. Sci. Lett.* 19, 290–300.
- Pell, J. and Simony, P. 1981. Stratigraphy, structure and metamorphism in the southern Cariboo Mountains, British Columbia. *Current Research*, *Geol. Surv. Canada*, Paper 81–1A, 227–230.
- Pettijohn, F.J., Potter, P.E. and Siever, P. 1973. *Sand and sandstone*. Springer-Verlag; New York, Heidelberg, Berlin.





- Pigage, L.C. 1977. Rb-Sr dates for granodiorite intrusions on the northeast margin of the Shuswap Metamorphic Complex, Cariboo Mountains, British Columbia. *Can. J. Earth Sci.* 14, 1690-1695.
- Pinsent, H.R. 1971. Precambrian geology along the Fraser River between Mount Robson and Tete Jaune Cache, British Columbia. Unpublished M.Sc. thesis. University of Alberta, Edmonton.
- Poulton, T.P. and Simony, P.S. 1980. Stratigraphy, sedimentology and regional correlation of the Horsethief Creek Group (Hadrynian), Late Precambrian in the northern Purcell and Selkirk Mountains, British Columbia. *Can. J. Earth Sci.* 17, 1708-1724.
- Price, R.A. 1967. Operation Bow-Athabasca, Alberta and British Columbia. *In: Report of Activities, Geol. Surv. Canada, Paper 67-1, Pt. A*, 106-112.
- Price, R.A. 1981. The Cordilleran foreland thrust and fold belt in the Southern Canadian Rocky Mountains. *In: Thrust and Nappe Tectonics*. N.J. Price and K. MacClay (eds.), *Geol. Soc. Lond. Spec. Publ.* 9, 427-448.
- Price, R.A. and Mountjoy, E.W. 1966. Operation Bow-Athabasca, Alberta and British Columbia. *In: Report of Activities, Geol. Surv. Canada, Paper 66-1*, 116-121.
- Price, R.A. and Mountjoy, E.W. 1970. Geologic structure of the Canadian Rocky Mountains between Bow and Athabasca Rivers - a progress report. *Geol. Assoc. Canada Spec. Paper* 6, 7-25.
- Read, P.B. and Brown, R.L. 1981. Columbia River fault zone: southeastern margin of the Shuswap and Monashee Complexes, southern British Columbia. *Can. J. Earth Sci.* 18, 1127-1145.
- Rehrig, W.A. and Reynolds, S.J. 1980. Geologic and geochronologic reconnaissance of a northwest-trending zone of metamorphic core complexes in southern and western Arizona. *Geol. Soc. Am. Mem.* 153, 131-157.
- Reynolds, S.J. and Rehrig, W.A. 1980. Mid-Tertiary plutonism and mylonitization, South Mountains, central Arizona. *Geol. Soc. Am. Mem.* 153, 159-176.
- Riddihough, R.P. 1982. One hundred million years of plate tectonics in Western Canada. *Geoscience Canada* 9, 28-34.
- Roberts, R.J. and Crittenden, M.D. 1973. Orogenic mechanisms, Sevier orogenic belt, Nevada and Utah. *In: Gravity and Tectonics*. K.A. DeJong and R. Scholten (eds.), John Wiley and Sons, New York. pp 409-428.
- Rogers, G.C. 1981. McNaughton Lake seismicity - more evidence for an Anahim hot spot? *Can. J. Earth Sci.* 18, 826-828.
- Rogers, G.C., Ellis, R.M. and Hasegawa, H.S. 1980. The McNaughton Lake earthquake of May 14, 1978. *Bull. Seismol. Soc. Am.* 70, 1771-1786.
- Royce, F., Warner, M.A. and Reese, D.L. 1975. Thrust belt structural geometry and related stratigraphic problems, Wyoming-Idaho-Northern Utah. *Rocky Mtn. Assoc. Geol.* 1975 Symp. 41-54.
- Ryan, B.D. and Blenkinsop, J. 1971. Geology and geochronology of the Hellroaring Creek Stock, British Columbia. *Can. J. Earth Sci.* 8, 85-95.
- Schulthesis, N.H. and Mountjoy, E.W. 1978. Cadomin Conglomerate of western Alberta - a result of early Cretaceous uplift of the Main Ranges. *Bull. Can. Petrol. Geol.* 26, 297-342.





- Schweickert, R.A. 1976. Early Mesozoic rifting and fragmentation of the Cordilleran orogen in western U.S.A. *Nature* 260, 586–591.
- Shaw, D.M. 1972. The origin of the Apsley Gneiss, Ontario. *Can. J. Earth Sci.* 9, 18–35.
- Shieh, Y.N. and Schwarcz, H.P. 1974. Oxygen isotope studies of granite and migmatite, Grenville Province of Ontario, Canada. *Geochim. Cosmochim. Acta* 38, 21–45.
- Simony, P.S. and Wind, G. 1970. Structure of the Dogtooth Range and adjacent portions of the Rocky Mountain trench. *Geol. Assoc. Canada Special Paper* 6, 41–51.
- Simony, P.S., Ghent, E.D., Craw, D., Mitchell, W. and Robbins, D.B. 1980. Structural and metamorphic evolution of northeast flank of Shuswap Complex, Southern Canoe River area, British Columbia. *Geol. Soc. Am. Mem.* 153, 445–461. *Canada Spec. Paper* 6, 7–39.
- Slind, O.L. and Perkins, G.D. 1966. Lower Palaeozoic and Proterozoic sediments of the Rocky Mountains between Jasper, Alberta and Pine River, British Columbia. *Bull. Can. Petrol. Geol.* 14, 442–468.
- Spence, G.D., Clowes, R.M. and Ellis, R.M. 1977. Depth limits on the Moho discontinuity in the southern Rocky Mountain Trench, Canada. *Bull. Seismol. Soc. Am.* 67, 543–546.
- Steiger, R.H. and Jager, E. 1977. Subcommittee on geochronology: convention on the use of decay constants in geo- and cosmochemistry. *Earth Planet. Sci. Lett.* 36, 359–362.
- Stelck, C.R. and Hedinger, A.S. 1975. Archaeocyathids and the Lower Cambrian Continental Shelf of the Canadian Cordillera. *Can. J. Earth Sci.* 12, 2014–2020.
- Struick, L.C. 1981. A re-examination of the type area of the Devonian–Mississippian Cariboo Orogeny, central British Columbia. *Can. J. Earth Sci.* 18, 1767–1775.
- Sutherland Brown, A. 1957. Geology of the Antler Creek area, British Columbia. *British Columbia Dept. Mines, Bull.* 38. 105 pp.
- Sutherland Brown, A. 1963. Geology of the Cariboo River area, British Columbia. *British Columbia Dept. Mines, Bull.* 47. 60 pp.
- Taylor, G.C., Campbell, R.B. and Norford, B.S. 1972. Silurian igneous rocks in the western Rocky Mountains, north-eastern British Columbia. *In: Report of Activities, April to October 1971. Geol. Surv. Can. Paper* 72–1, 228–229.
- Taylor, H.P., Jr. 1968. The oxygen isotope geochemistry of igneous rocks. *Contrib. Mineral. Petrol.* 19, 1–71.
- Taylor, H.P., Jr. 1976. Water–rock interactions and the origin of H<sub>2</sub>O in granitic batholiths (abstract). *William Smith Lecture, Geol. Soc. Newsletter* 5, 14–15.
- Taylor, H.P., Jr. 1977. Water/rock interactions and the origin of H<sub>2</sub>O in granitic batholiths. *J. geol. Soc. London* 133, 509–558.
- Taylor, H.P., Jr. and Magaritz, M. 1975. Oxygen and hydrogen isotope studies of 2.6–3.5 b.y. old granites from the Barberton Mountain Land, Swaziland and the Rhodesian craton, South Africa (abstract). 1975 Ann. Meetings, *Geol. Soc. Am. Abstr. Prog.* 7, 1293.
- Templeman-Kluit, D.J. 1977. Stratigraphic and structural relations between Selwyn Basin, Pelly–Cassiar Platform, and Yukon Crystalline Terrane in the Pelly Mountains, Yukon. *Geol. Surv. Canada, Paper* 77–1A, 223–227.



- Thompson, R.N. 1969. Tertiary granites and associated rocks of the Marsco area, Isle of Skye. *J. geol. Soc. London* 124, 349–385.
- Tipper, H.W. 1981. Offset of an Upper Pleinsbachian geographical zonation in the North American Cordillera by transcurrent movement. *Can. J. Earth Sci.* 18, 1788–1792.
- Tipper, H.W., Woodsworth, G.J. and Gabrielse, H. 1981. Tectonic Assemblage Map of the Canadian Cordillera and adjacent parts of the United States of America. *Geol. Surv. Canada, Map* 1505A.
- Todd, V.R. 1973. Tectonic mobilization of Precambrian gneiss during metamorphism and thrusting, Grouse Creek Mountains, north-western Utah. *Geol. Soc. Am. Abstr. Prog.* 5, 116.
- Todd, V.R. 1980. Structure and petrology of a Tertiary gneiss complex in northwestern Utah. *Geol. Soc. Am. Mem.* 153, 349–384.
- Wanless, R.K. and Okulitch, A.V. 1976. Geochronologic studies of the Shuswap Metamorphic Complex, British Columbia, *Can. J. Earth Sci.* 12, 326–332.
- Wanless, R.K. and Reesor, J.E. 1975. Precambrian zircon age of orthogneiss in the Shuswap Metamorphic Complex, Southern B.C. *Geol. Assoc. Canada Prog. with Abst.* 1, 47.
- Wanless, R.K., Stevens, R.D., Lachance, G.R. and Edmonds, C.M. 1967. Age determinations and geological studies, K–Ar isotopic ages. Report 7, *Geol. Surv. Canada, Paper* 66–17, 76.
- Weaver, B.L., Tarney, J. and Windley, B. 1981. Geochemistry and petrogenesis of the Fiskenaesset anorthosite complex, southern west Greenland: nature of the parent magma. *Geochim. Cosmochim. Acta* 45, 711–725.
- Wetherill, G.W., Aldrich, L.T. and Davis, G.L. 1955.  $A^{40}/K^{40}$  ratios of feldspars and micas from the same rock. *Geochim. Cosmochim. Acta* 8, 171–172.
- Wheeler, J.O. and Gabrielse, H. 1972. The Canadian structural province. In: *Variations in Tectonic Styles in Canada*. R.A. Price and R.J.W. Douglas (eds.), *Geol. Assoc. Canada. Spec. Paper* 11, 1–81.
- Wheeler, J.O., Campbell, R.B., Reesor, J.E. and Mountjoy, E.W. 1972. Structural style of the Southern Canadian Cordillera; Field Excursion XO1–AO1, XXIV Int. Geol. Cong. Montreal 1972.
- Wickens, A.J. 1977. The upper mantle of southern British Columbia. *Can. J. Earth Sci.* 14, 1100–1115.
- Wickens, A.J. and Pec, K. 1968. A crust–mantle profile from Mould Bay Canada to Tucson, Arizona. *Bull. Seismol. Soc. Am.* 58, 1821–1831.
- Winchester, J.A. and Floyd, P. 1976. Geochemical magma–type discrimination: application to altered and metamorphosed basic igneous rocks. *Earth Planet. Sci. Lett.* 28, 459–469.
- Winchester, J.A., Lambert, R.St J. and Holland, J.G. 1981. Geochemistry of the western part of the Moinian assemblage. *Scot. J. Geol.* 17, 281–294.
- Wood, D.A. 1978. Major and trace element variations in the Tertiary lavas of eastern Iceland and their significance with respect to the Iceland Geochemical Anomaly. *J. Petrol.* 19, 393–436.



- Yoder, H.S. 1973. Contemporaneous basaltic and rhyolitic magmas. *Am. Mineral.* 58, 153-171.
- Young, F.G. 1979. The lowermost Palaeozoic McNaughton Formation and equivalent Cariboo Group of Eastern British Columbia: piedmont and tidal complex. *Geol. Surv. Can. Bull.* 288. 60 pp.





## 9. APPENDICES



## 9.1 Appendix A (X.R.F. Analyses of Gneissic Rocks)



Table 1: X.R.F. Analyses on Mafic Gneiss from the C.N. Track

Sample:	AC8	AC9	AC10	AC14	AC15	5502	5803	5804	5805	5806	5807	5808
SiO <sub>2</sub>	50.7	54.7	48.7	50.9	43.0	50.6	47.6	53.9	57.8	48.6	54.2	49.5
Al <sub>2</sub> O <sub>3</sub>	14.7	14.0	13.5	14.4	13.2	13.7	14.8	13.7	14.3	14.4	13.5	14.6
Fe <sub>2</sub> O <sub>3</sub>	9.7	10.9	14.7	11.6	14.8	11.7	13.4	10.8	8.8	13.5	11.0	11.1
MgO	8.9	5.5	5.1	6.6	8.3	8.2	8.8	7.0	5.7	8.0	6.9	9.6
CaO	7.6	7.7	8.1	8.8	9.7	9.9	9.1	8.1	6.8	9.6	8.4	9.9
Na <sub>2</sub> O	3.3	4.3	2.9	3.3	2.4	3.5	2.7	2.6	3.5	3.2	2.8	2.7
K <sub>2</sub> O	4.00	1.11	3.07	2.28	3.91	1.00	1.75	2.27	1.68	0.99	1.43	1.34
TiO <sub>2</sub>	0.87	1.25	2.55	1.34	2.54	1.09	1.16	1.11	0.93	1.21	1.12	0.89
MnO	0.18	0.20	0.24	0.23	0.26	0.19	0.24	0.17	0.14	0.25	0.22	0.18
S	0.00	0.00	0.00	0.00	0.00	0.00	0.00	0.00	0.00	0.00	0.00	0.00
P <sub>2</sub> O <sub>5</sub>	0.09	0.44	1.22	0.50	1.77	0.25	0.38	0.14	0.32	0.36	0.32	0.22
Ce												
La												
Ba	1077	393	1526	995	1933	260	571	718	567	358	753	340
Nb	39	61	60	60	60	20	16	37	29	16	24	17
Zr	163	230	286	172	177		108	121	191	179	128	100
Y	28	40	34	33	21	19	24	36	38	25	32	26
Sr	316	556	452	382	493	476	438	406	412	393	297	296
Rb	92	20	82	34	52	13	46	75	60	22	54	36
Zn	154	112	129	109	110	139	208	211	127	206	352	150
Cu	6	7	78	5	7	6	18	32	41	26	12	8
Ni	147	54	26	65	73	113	92	70	41	72	76	183
Co						80	80	110	70	100	80	100
Cr						-	150	240	290	130	230	530
V						-	240	220	180	270	230	210
Li						4	13	9	10	8	5	6
Y/Nb	0.72	0.66	0.57	0.55	0.35	0.95	1.50	0.97	1.31	1.56	1.33	1.53





Table 1 continued ...

Sample:	5809	5812	5902A	5902B	5902D	5902E	5903E	5903F	5903G	Mean (n=21)	s.d.
SiO <sub>2</sub>	51.0	54.5	47.31	51.10	49.36	49.71	48.45	55.07	58.20	51.19	3.69
Al <sub>2</sub> O <sub>3</sub>	14.8	13.5	12.04	14.31	14.63	14.76	14.17	12.88	12.92	13.94	0.76
Fe <sub>2</sub> O <sub>3</sub>	12.2	11.4	14.57	12.99	12.87	12.43	14.99	13.56	11.69	12.32	1.70
MgO	5.0	6.5	10.92	5.33	6.99	7.15	6.49	3.31	2.70	6.81	1.99
CaO	7.5	7.6	10.46	7.99	7.80	8.95	9.50	6.54	5.95	8.38	1.21
Na <sub>2</sub> O	3.3	3.3	1.96	2.89	3.10	2.72	2.68	2.47	2.84	2.97	0.50
K <sub>2</sub> O	2.59	1.51	1.62	2.63	2.96	1.88	1.58	3.13	3.14	2.18	0.92
TiO <sub>2</sub>	2.06	1.09	0.75	1.86	1.49	1.62	1.59	2.06	1.73	1.44	0.53
MnO	0.15	0.18	0.19	0.20	0.22	0.19	0.21	0.18	0.17	0.20	0.03
S	0.00	0.00	0.04	0.04	0.03	0.03	0.02	0.10	0.03	0.01	0.03
P <sub>2</sub> O <sub>5</sub>	1.42	0.50	0.13	0.66	0.55	0.57	0.30	0.70	0.64	0.55	0.43
Ce											
La											
Ba	1078	739	300	1114	870	896	591	1609	1278	856	459
Nb	83	34	15	32	31	36	18	29	48	36	19
Zr	601	37	45	235	166	174	152	333	311	196	117
Y	55	34	16	31	33	32	35	35	49	59	33
Sr	381	412	251	407	281	465	268	341	323	383	82
Rb	105	55	61	58	134	45	41	75	72	59	29
Zn	277	206	142	115	233	104	138	124	90	163	66
Cu	18	13	3	8	36	23	92	53	27	25	24
Ni	20	63	63	40	67	55	65	27	25	68	40
Co	70	100	-	-	-	-	-	-	-	88	15
Cr	110	170	206	62	61	60	104	27	18	159	131
V	140	220	-	-	-	-	-	-	-	214	39
Li	12	12	-	-	-	-	-	-	-	9	3
Y/Nb	0.66	1.00	1.07	0.97	1.06	0.89	1.94	1.69	1.23		



Table 2: X.R.F. Analyses on Grey Gneiss from the C.N. Track

Sample:	5498	5810	5811	5903A	5903B	5903D	5903H	5903I	5903J	Mean (n=9)	s.d.
SiO <sub>2</sub>	63.8	78.5	67.1	67.62	71.50	66.36	68.51	65.27	69.18	68.65	4.30
Al <sub>2</sub> O <sub>3</sub>	13.7	14.2	14.1	13.76	13.98	15.40	15.66	15.54	14.79	14.57	0.79
Fe <sub>2</sub> O <sub>3</sub>	7.1	3.0	6.1	5.69	2.92	5.01	3.83	5.45	3.85	4.77	1.50
MgO	2.9	9.6	1.8	1.36	0.79	1.08	0.65	1.06	0.60	1.20	0.75
CaO	5.1	2.0	2.9	2.82	1.89	2.65	1.79	3.30	2.44	2.77	1.00
Na <sub>2</sub> O	3.5	3.3	3.4	3.32	3.77	3.76	3.81	4.12	4.48	3.72	0.39
K <sub>2</sub> O	3.02	4.96	3.64	4.44	4.66	4.83	4.98	4.25	4.02	4.31	0.66
TiO <sub>2</sub>	0.64	0.41	0.91	0.68	0.30	0.67	0.55	0.68	0.44	0.58	0.16
MnO	0.11	0.05	0.10	0.09	0.05	0.05	0.06	0.08	0.05	0.07	0.02
S	0.00	0.00	0.01	0.03	0.03	0.04	0.04	0.04	0.03	0.02	0.02
P <sub>2</sub> O <sub>5</sub>	0.18	0.06	0.19	0.20	0.10	0.17	0.11	0.21	0.12	0.15	0.05
Ce											
La											
Ba	958	184	1448	1305	832	2659	2564	2196	1207	1484	833
Nb	15	13	23	25	20	18	23	20	18	19	4
Zr	199	343	258	271	167	282	444	282	325	286	81
Y	31	19	47	48	29	33	37	45	35	36	9
Sr	398	367	317	279	197	364	297	353	341	324	60
Rb	90	137	142	118	160	89	90	90	82	111	29
Zn	91	39	111	83	40	32	25	31	24	53	33
Cu	7	10	23	15	3	9	6	3	11	11	6
Ni	30	5	9	24	20	18	11	17	11	16	8
Co	71	110	40	-	-	-	-	-	-	-	-
Cr	-	20	160	12	17	12	12	10	16	32	52
V	-	20	80	-	-	-	-	-	-	50	42
Li	4	6	11	-	-	-	-	-	-	7	4
Y/Nb	2.07	1.46	2.04	1.92	1.45	1.83	1.61	2.25	1.94		
D.F.	+1.5	+1.0	+1.2	+1.9	+2.8	+3.4	+3.4	+4.1	+4.1		



Table 3: X.R.F. Analyses on Leucocratic Gneiss (high niobium) from the C.N. Track

Sample	AC16	5499	5500	5501	5814	5817	5904	Mean (n=7)	s.d.
SiO <sub>2</sub>	66.2	64.9	61.4	72.4	73.2	74.9	63.78	68.11	5.30
Al <sub>2</sub> O <sub>3</sub>	16.0	16.8	18.3	14.7	13.7	13.4	17.08	15.71	1.80
Fe <sub>2</sub> O <sub>3</sub>	4.1	4.5	4.7	2.1	3.0	1.9	4.89	3.60	1.30
MgO	1.2	0.8	1.1	0.4	0.1	0.7	0.84	0.73	0.38
CaO	1.8	1.6	1.9	1.1	0.6	0.4	2.34	1.39	0.71
Na <sub>2</sub> O	4.7	4.8	5.2	4.0	4.3	4.7	5.00	4.67	0.41
K <sub>2</sub> O	5.12	5.66	5.97	4.99	4.67	3.87	4.73	5.00	0.69
TiO <sub>2</sub>	0.70	0.59	0.91	0.24	0.32	0.17	0.84	0.54	0.30
MnO	0.06	0.17	0.13	0.03	0.08	0.03	0.15	0.09	0.06
S	0.00	0.00	0.00	0.00	0.00	0.00	0.05	0.01	0.02
P <sub>2</sub> O <sub>5</sub>	0.23	0.12	0.31	0.04	0.00	0.00	0.31	0.14	0.14
Ce									
La									
Ba	1245	1929	2858	632	130	266	1852	1273	1001
Nb	78	62	22	97	92	89	44	69	28
Zr	486	286	37	239	96	352	62	223	167
Y	28	31	12	48	29	35	18	29	12
Sr	243	192	230	156	39	86	186	162	75
Rb	166	85	67	176	74	96	79	106	45
Zn	48	82	73	25	61	32	70	56	22
Cu	38	8	5	12	6	10	11	13	11
Ni	7	4	3	11	4	5	bdl	5	3
Co	-	70	71	50	90	30	-	62	23
Cr	-	-	-	-	20	210	10	80	113
V	-	-	-	-	bdl	10	-	-	-
Li	1	6	5	5	4	4	-	5	1
Y/Nb	0.36	0.50	0.55	0.49	0.32	0.39	0.41	-	-
D.F.	+4.7	+5.5	+6.8	+3.3	+3.1	+2.6	+5.8	-	-





Table 4: X.R.F. Analyses on Leucocratic Gneiss (low niobium) from the C.N. Track

Sample: AG11	5803X	5813	5815	5816	5902C	5903C	5903D2	5903(1)	Mean (n=9)	s.d.
SiO <sub>2</sub>	67.6	75.5	74.73	71.5	63.45	72.16	73.52	72.74	70.21	5.17
Al <sub>2</sub> O <sub>3</sub>	14.5	12.8	12.62	13.7	13.96	13.94	13.12	13.35	13.58	0.61
Fe <sub>2</sub> O <sub>3</sub>	5.3	2.1	2.60	3.9	9.74	2.70	2.48	2.91	4.60	3.13
MgO	0.1	0.1	0.21	0.3	0.84	0.50	0.38	0.56	0.58	0.65
CaO	1.9	0.6	0.34	1.2	2.95	1.93	1.75	1.50	2.04	1.74
Na <sub>2</sub> O	4.5	3.9	4.39	4.6	2.82	3.21	3.32	3.10	3.72	0.66
K <sub>2</sub> O	5.50	4.89	4.84	4.42	4.55	5.04	4.87	5.35	4.63	0.97
TiO <sub>2</sub>	0.33	0.12	0.17	0.33	1.10	0.35	0.24	0.34	0.45	0.37
MnO	0.10	0.03	0.05	0.07	0.12	0.05	0.05	0.05	0.08	0.05
S	0.00	0.00	0.02	0.00	0.03	0.03	0.03	0.03	0.02	0.02
P <sub>2</sub> O <sub>5</sub>	0.04	0.00	0.03	0.05	0.43	0.09	0.05	0.07	0.13	0.17
Ce										
La	400	51	68	346	2969	1570	1106	1362	1054	952
Ba	125	79	54	54	56	17	13	14	51	34
Nb	1063	229	477	871	579	260	170	191	470	316
Zr	103	97	46	41	64	17	11	17	50	34
Sr	68	12	38	108	174	284	207	218	173	136
Rb	136	284	108	92	189	142	152	174	148	66
Zn	77	83	90	123	206	34	27	22	87	58
Cu	6	5	10	19	11	bdl	9	14	12	10
Ni	7	9	18	7	13	11	14	12	11	4
Co	-	20	-	30	-	-	-	-	15	7
Cr	-	-	11	-	bdl	13	19	18	15	4
V	-	Bdl=10	-	10	-	-	-	-	4	0
Li	1	4	1	4	-	-	-	-	-	-
Y/Nb	00.82	1.23	0.85	0.76	1.14	1.00	0.85	1.21	-	-
D.F.	+5.3	+2.5	+2.9	+3.6	+1.4	+2.4	+2.3	+1.9	-	-



Table 5: X.R.F. Analyses on Mafic Gneiss from the Malton Range

Sample:	5819A	5819B	5824	5825	5826	5892C	5892F	5894C	5894H	Mean (n=9)	s.d.
SiO <sub>2</sub>	45.94	44.8	50.4	43.6	50.9	48.48	46.64	50.35	49.33	47.82	2.67
Al <sub>2</sub> O <sub>3</sub>	13.09	15.4	14.2	14.4	13.9	13.65	13.89	14.83	14.84	14.17	0.72
Fe <sub>2</sub> O <sub>3</sub>	14.45	14.2	11.5	17.1	11.9	13.82	12.60	12.15	12.24	13.33	1.77
MgO	10.50	11.1	7.2	7.2	8.0	7.56	9.35	7.89	7.73	8.50	1.46
CaO	11.06	8.2	8.1	7.9	8.8	10.40	11.49	8.02	9.00	9.22	1.40
Na <sub>2</sub> O	2.23	2.2	3.1	2.3	3.0	2.79	2.40	3.17	3.60	2.75	0.50
K <sub>2</sub> O	0.71	2.67	1.83	3.88	2.13	1.22	1.44	1.89	1.51	1.92	0.92
TiO <sub>2</sub>	1.58	1.16	1.76	2.48	1.04	1.66	1.76	1.19	1.21	1.54	0.45
MnO	0.24	0.20	0.24	0.27	0.20	0.21	0.21	0.15	0.17	0.21	0.04
S	0.02	0.00	0.00	0.00	0.00	0.02	0.02	0.02	0.03	0.01	0.01
P <sub>2</sub> O <sub>5</sub>	0.28	0.22	0.65	0.95	0.30	0.20	0.21	0.32	0.36	0.39	0.25
Ce											
La											
Ba	178	500	610	896	515	110	124	593	423	439	262
Nb	58	14	31	22	14	59	38	27	24	32	17
Zr	286	92	170	146	107	115	127	104	103	139	60
Y	54	22	34	36	28	29	26	27	32	32	9
Sr	279	251	307	212	309	230	307	334	324	284	43
Rb	15	84	68	239	104	45	53	58	40	78	65
Zn	119	160	153	365	160	118	109	91	61	148	88
Cu	14	9	31	21	65	bd1	3	12	36	21	20
Ni	107	206	55	75	111	40	116	128	61	100	50
Co	-	105	-	118	-	-	-	-	-	-	-
Cr	183	-	-	-	-	54	281	80	89	137	94
V	-	-	-	-	-	-	-	-	-	-	-
Li	1	15	-	24	-	-	-	-	-	-	-
Y/Nb	0.93	0.14	1.10	1.64	2.00	0.49	0.68	1.00	1.33		



Table 6: X.R.F. Analyses on Grey Gneiss from the Malton Range

Sample:	5842B	5842C	5843A	5843B	5843C	5844A	5844D	5893C1	5893C2	5894D	Mn. n=10	s.d.
SiO <sub>2</sub>	70.3	67.8	66.05	66.7	65.61	76.7	75.0	71.97	71.98	73.41	70.55	3.90
Al <sub>2</sub> O <sub>3</sub>	14.6	14.7	14.54	14.9	14.86	14.1	14.4	13.84	13.29	14.56	14.38	0.50
Fe <sub>2</sub> O <sub>3</sub>	3.3	5.1	5.12	4.8	4.95	1.3	1.1	3.23	3.50	1.11	3.35	1.67
MgO	1.5	2.1	2.20	2.3	2.52	0.5	0.4	0.90	0.77	0.20	1.34	0.89
CaO	3.0	3.1	3.95	3.4	3.62	0.5	1.1	2.21	2.75	1.87	2.55	1.12
Na <sub>2</sub> O	3.7	3.1	2.95	3.0	3.07	4.8	4.9	2.74	2.99	4.94	3.62	0.90
K <sub>2</sub> O	3.02	3.11	4.24	4.11	4.42	1.93	2.88	4.44	4.14	3.75	3.60	0.83
TiO <sub>2</sub>	0.46	0.72	0.63	0.63	0.63	0.14	0.13	0.45	0.38	0.10	0.43	0.23
MnO	0.05	0.07	0.07	0.06	0.07	0.01	0.05	0.05	0.06	0.02	0.05	0.02
S	0.00	0.00	0.03	0.00	0.03	0.00	0.00	0.02	0.03	0.03	0.01	0.02
P <sub>2</sub> O <sub>5</sub>	0.10	0.17	0.21	0.19	0.23	0.00	0.01	0.14	0.12	0.02	0.12	0.09
Ce												
La												
Ba	788	744	1004	1178	1088	617	698	833	741	760	845	183
Nb	12	20	22	23	23	11	16	13	10	2	15	7
Zr	114	246	184	185	160	111	88	249	247	102	169	64
Y	18	37	51	60	43	30	40	26	26	15	35	14
Sr	467	407	521	576	466	283	294	261	261	316	385	117
Rb	116	163	162	196	155	76	105	126	107	60	127	42
Zn	52	93	60	74	67	15	28	38	35	7	47	27
Cu	14	4	20	9	3	11	4	20	18	2	11	7
Ni	14	16	21	15	bdl	10	4	14	26	12	13	8
Co	-	-	-	72	-	46	-	-	-	-	-	-
Cr	-	-	21	-	125	-	-	8	283	15	90	118
V	-	-	-	-	-	-	-	-	-	-	-	-
Li	-	-	-	34	-	11	-	-	-	-	-	-
Y/Nb	1.50	1.85	2.32	2.61	1.86	2.73	2.50	2.00	2.60	7.50		
D.F.	+1.8	+0.4	+1.5	+1.1	+1.5	+1.8	+3.3	+1.0	+1.6	+4.7		





Table 7: X.R.F. Analyses on Leucocratic Gneiss (high niobium) from the Malton Range

Sample:	5820	5821	5823	5844B	5886	5894A	Mean (n=6)	s.d.
SiO <sub>2</sub>	74.6	74.9	74.1	73.9	74.20	73.85	74.26	0.41
Al <sub>2</sub> O <sub>3</sub>	13.5	13.3	13.8	13.5	12.87	13.88	13.48	0.37
Fe <sub>2</sub> O <sub>3</sub>	2.1	2.1	2.3	3.4	2.61	1.87	2.40	0.55
MgO	0.2	0.2	0.2	1.1	0.11	0.12	0.32	0.38
CaO	0.4	0.4	0.4	1.6	0.56	1.23	0.77	0.52
Na <sub>2</sub> O	4.8	4.4	4.8	3.3	4.61	5.70	4.60	0.77
K <sub>2</sub> O	4.24	4.52	4.33	2.68	4.77	3.10	3.94	0.84
TiO <sub>2</sub>	0.19	0.15	0.15	0.35	0.17	0.15	0.19	0.08
MnO	0.02	0.04	0.04	0.05	0.05	0.04	0.04	0.01
S	0.00	0.00	0.00	0.00	0.04	0.03	0.01	0.02
P <sub>2</sub> O <sub>5</sub>	0.00	0.00	0.00	0.02	0.02	0.04	0.01	0.02
Ce								
La								
Ba	152	148	251	545	386	251	289	153
Nb	152	141	150	23	142	173	130	54
Zr	561	490	665	236	672	541	528	160
Y	72	60	63	15	63	63	56	20
Sr	41	31	43	290	50	125	97	101
Rb	99	88	84	170	69	46	93	42
Zn	15	25	17	65	9	17	25	20
Cu	7	3	7	6	4	13	7	4
Ni	5	2	10	23	16	9	11	8
Co	45	-	50	60	-	-	52	8
Cr	-	-	-	-	6	3	4	4
V	-	-	-	-	-	-	-	-
Li	3	-	2	20	-	-	-	-
Y/Nb	0.47	0.43	0.42	0.65	0.44	0.36		
D.F.	+3.4	+2.9	+3.5	-0.1	+3.5	+4.9		



Table 8: X.R.F. Analyses on Leucocratic Gneiss (low niobium) from the Malton Range

Sample:	5845A	5845B	5845C	5387	5892A	5892B	5892D	5892E1
SiO <sub>2</sub>	75.31	75.1	78.0	65.23	77.73	75.73	75.66	75.68
Al <sub>2</sub> O <sub>3</sub>	12.50	12.9	12.7	14.77	12.82	12.71	12.91	12.52
Fe <sub>2</sub> O <sub>3</sub>	2.74	2.5	1.9	6.82	0.99	1.68	1.91	1.74
MgO	0.06	0.1	0.1	2.72	0.13	0.02	0.05	0.13
CaO	0.86	0.6	0.7	2.52	1.77	0.71	0.58	0.95
Na <sub>2</sub> O	3.13	3.2	3.7	2.58	5.66	3.93	3.57	4.46
K <sub>2</sub> O	5.05	5.30	4.83	4.36	0.75	5.08	5.15	4.32
TiO <sub>2</sub>	0.22	0.16	0.74	0.09	0.08	0.09	0.12	0.09
MnO	0.05	0.05	0.03	0.11	0.02	0.02	0.03	0.03
S	0.03	0.00	0.00	0.03	0.02	0.03	0.02	0.03
P <sub>2</sub> O <sub>5</sub>	0.05	0.01	0.00	0.12	0.02	0.01	0.02	0.02
Ce								
La								
Ba	299	345	293	539	29	35	116	87
Nb	65	65	63	29	129	157	144	129
Zr	441	522	496	167	308	232	257	219
Y	87	90	93	40	158	155	138	118
Sr	57	51	54	154	162	36	43	92
Rb	146	187	161	299	20	242	198	158
Zn	91	107	15	108	6	71	52	35
Cu	19	16	11	7	6	9	4	15
Ni	7	6	15	19	15	12	18	21
Co	-	45	46	-	-	-	-	-
Cr	10	-	-	81	13	16	18	bd!
V	-	-	-	-	-	-	-	-
Li	-	4	2	-	-	-	-	-
Y/Nb	1.33	1.38	1.48	1.38	1.22	0.99	0.96	0.91
D.F.	+1.6	+1.6	+1.7	-0.6	+3.3	+2.9	+2.2	+3.2



Table 8 continued..

Sample:	5892E2	5893A	5893B	5894B	5894E	5894G	Mean (n=14)	s.d.
SiO <sub>2</sub>	76.36	73.37	72.85	75.18	61.36	74.83	73.74	4.7
Al <sub>2</sub> O <sub>3</sub>	12.95	14.51	12.95	12.42	13.87	13.04	13.11	2.3
Fe <sub>2</sub> O <sub>3</sub>	1.53	2.24	3.33	2.61	9.21	2.20	2.96	2.3
MgO	0.14	0.81	0.73	0.00	2.55	0.10	0.54	0.92
CaO	1.71	0.96	1.87	0.72	4.14	0.82	1.35	1.00
Na <sub>2</sub> O	5.44	2.64	3.40	3.62	4.61	3.63	3.83	0.93
K <sub>2</sub> O	1.53	5.08	4.18	5.21	2.73	5.08	4.19	1.50
TiO <sub>2</sub>	0.09	0.26	0.46	0.15	0.96	0.20	0.27	0.27
MnO	0.22	0.03	0.04	0.05	0.12	0.03	0.06	0.06
S	0.03	0.03	0.02	0.02	0.03	0.02	0.02	0.01
P <sub>2</sub> O <sub>5</sub>	0.00	0.08	0.15	0.02	0.42	0.03	0.07	0.11
Ce								
La								
Ba	64	991	1086	27	274	396	327	340
Nb	131	10	19	97	102	53	85	48
Zr	247	115	244	331	240	282	293	119
Y	143	13	18	118	101	62	95	48
Sr	181	167	347	12	160	90	115	88
Rb	62	169	105	240	138	103	159	74
Zn	17	21	34	106	71	20	54	38
Cu	10	8	13	9	9	20	11	5
Ni	17	17	1	16	36	4	15	9
Co	-	-	-	-	-	-	46	0.7
Cr	12	19	21	7	27	10	20	21
V	-	-	-	-	-	-	-	-
Li	-	-	-	-	-	-	-	-
Y/Nb	1.09	1.30	0.68	1.22	0.99	1.17		
D.F.	+3.5	+0.6	+1.6	+2.3	+2.6	+2.4		





Table 9: X.R.F. Analyses on Mafic Gneiss from the Monashee Mountains

Sample:	5901L	5901M	6152M	6152Q	6152S	6152T	6152Z	6412E	Mean (n=8)	s.d.
SiO <sub>2</sub>	48.17	46.51	46.72	51.95	48.24	48.74	55.48	43.37	48.65	3.67
Al <sub>2</sub> O <sub>3</sub>	15.05	14.76	14.73	14.14	13.81	14.04	14.23	13.70	14.31	0.49
Fe <sub>2</sub> O <sub>3</sub>	13.46	14.72	12.73	15.64	17.32	16.98	12.34	15.21	14.93	1.88
MgO	5.20	6.74	7.48	3.88	3.59	3.46	2.83	8.97	5.27	2.23
CaO	8.40	7.00	10.13	6.44	8.36	8.01	6.03	10.04	8.05	1.53
Na <sub>2</sub> O	3.76	2.92	2.66	2.70	2.72	3.00	3.59	2.48	2.98	0.46
K <sub>2</sub> O	2.67	2.96	3.63	3.19	3.20	3.18	3.54	3.98	3.29	0.41
TiO <sub>2</sub>	2.57	2.30	1.84	1.94	2.48	2.36	1.77	2.25	2.19	0.30
MnO	0.20	0.22	0.25	0.24	0.33	0.31	0.16	0.25	0.25	0.06
S	0.03	0.10	0.01	0.15	0.10	0.09	0.35	0.01	0.11	0.11
P <sub>2</sub> O <sub>5</sub>	0.49	0.78	0.00	0.00	0.00	0.00	0.00	0.90	0.27	0.39
Ce			64	114	98	102	114	77	95(n=6)	20
La			34	61	52	54	62	32	49(n=6)	13
Ba	426	714	1927	153	990	965	1233	827	904	535
Nb	68	39	41	58	81	81	44	29	55	20
Zr	150	221	110	453	324	334	425	180	275	128
Y	42	40	20	62	53	55	54	31	45	14
Sr	328	484	680	93	295	279	562	276	375	188
Rb	73	120	73	87	133	122	108	120	105	24
Zn	119	131	139	192	168	159	95	140	143	30
Cu	10	34	4	54	21	20	71	2	27	25
Ni	42	53	64	2	7	3	3	45	27	26
Co										
Cr	59	21	94	10	23	18	10	60	37	31
V										
Li										
Y/Nb	0.62	1.03	0.49	1.07	0.65	0.68	1.23	1.07		



Table 10: X.R.F. Analyses on Grey Gneiss from the Monashee Mountains

Sample:	5891A	5897Cl	5897E	5898A	5899A	5899C	5899D	5899E	5899F	5901G
SiO <sub>2</sub>	73.55	71.62	71.76	62.09	59.38	61.85	67.89	73.39	65.21	60.89
Al <sub>2</sub> O <sub>3</sub>	13.42	14.10	10.56	15.21	15.79	16.20	14.43	14.05	13.11	14.89
Fe <sub>2</sub> O <sub>3</sub>	2.15	2.58	4.59	7.02	8.23	6.48	4.85	2.22	5.80	7.31
MgO	0.81	0.88	3.40	2.88	3.69	3.76	1.67	0.19	1.93	2.95
CaO	1.56	2.14	3.47	3.92	3.35	3.17	2.54	1.05	5.44	5.52
Na <sub>2</sub> O	2.96	5.03	0.69	3.04	3.88	5.40	3.79	3.65	3.46	4.11
K <sub>2</sub> O	5.09	3.19	5.00	4.24	4.23	2.06	3.93	5.10	3.92	3.24
TiO <sub>2</sub>	0.34	0.31	0.38	1.03	0.94	0.74	0.59	0.24	0.74	0.70
MnO	0.03	0.05	0.17	0.08	0.16	0.07	0.08	0.04	0.15	0.13
S	0.03	0.03	0.03	0.03	0.03	0.03	0.03	0.03	0.03	0.03
P <sub>2</sub> O <sub>5</sub>	0.07	0.08	0.05	0.48	0.25	0.24	0.20	0.05	0.21	0.24
Ce										
La										
Ba	1661	737	684	1364	1257	1249	936	1046	1264	649
Nb	14	15	10	18	13	13	17	23	17	13
Zr	278	142	143	295	163	187	223	186	280	132
Y	28	25	16	37	31	26	38	98	29	35
Sr	249	149	96	396	222	283	331	234	242	471
Rb	140	57	172	177	154	62	106	159	100	111
Zn	14	49	19	90	143	54	67	24	80	130
Cu	9	6	2	52	25	7	10	8	6	9
Ni	16	8	35	21	25	19	21	18	26	19
Co										
Cr	33	6	81	41	48	49	21	5	11	21
V										
Li										
Y/Nb	2.00	1.67	1.60	2.06	2.38	2.00	2.24	4.26	1.71	2.69
D.F.	+1.4	+3.9	-3.8	+1.2	+1.5	+2.4	+2.0	+2.8	+3.2	+3.2



Table 10 continued...

Sample:	5901H	6152P	6153G	6414A	Mean (n=14)	s.d.
SiO <sub>2</sub>	60.78	70.54	77.77	61.71	67.03	6.03
Al <sub>2</sub> O <sub>3</sub>	14.79	14.26	11.96	14.51	14.09	1.50
Fe <sub>2</sub> O <sub>3</sub>	7.33	3.56	1.25	8.09	5.10	2.4
MgO	2.95	1.09	0.48	2.00	2.05	1.2
CaO	5.12	1.38	1.68	3.39	3.12	1.5
Na <sub>2</sub> O	4.71	3.36	2.82	2.70	3.54	1.2
K <sub>2</sub> O	3.28	5.38	3.91	6.19	4.20	1.1
TiO <sub>2</sub>	0.66	0.50	0.13	1.36	9.61	0.3
MnO	0.12	0.06	0.03	0.17	0.09	0.06
S	0.03	0.01	0.00	0.01	0.03	0.01
P <sub>2</sub> O <sub>5</sub>	0.23	0	0	0.49	0.19	0.16
Ce		105	55	122	94	35
La		57	34	60	50	14
Ba	585	847	754	2774	1129	571
Nb	15	18	13	29	16	5
Zr	96	208	90	207	188	66
Y	30	51	26	64	38	21
Sr	394	90	128	160	246	118
Rb	89	235	108	162	129	53
Zn	126	148	14	96	75	49
Cu	8	4	3	7	11	13
Ni	24	5	1	9	18	9
Co						
Cr	50	13	9	5	28	23
V						
Li						
Y/Nb	2.00	2.83	2.00	2.20		
D.F.	+3.9	+2.0	+0.4	+2.1		





Table 11: X.F.R. Analyses on Leucocratic Gneiss (high niobium) from the Monashee Mountains

Sample:	5897A	5898G	5900A	5900B	5900C	5901A	5901I	5901J	5901P	5901Q	5901R
SiO <sub>2</sub>	58.32	69.91	75.78	65.77	73.69	72.72	75.09	74.30	64.06	68.39	68.49
Al <sub>2</sub> O <sub>3</sub>	15.99	14.19	12.16	14.91	12.65	13.82	11.58	12.54	14.92	13.99	14.17
Fe <sub>2</sub> O <sub>3</sub>	10.60	4.18	2.59	5.90	3.54	3.08	4.17	3.17	8.57	5.44	5.74
MgO	1.44	0.62	0.02	0.59	0.18	0.35	0.00	0.12	0.24	0.04	0.01
CaO	3.16	2.64	0.12	2.75	0.50	0.40	0.48	0.71	2.35	2.44	1.88
Na <sub>2</sub> O	4.02	4.44	4.37	5.15	4.38	4.53	3.37	4.46	4.38	4.84	4.73
K <sub>2</sub> O	4.15	3.37	4.68	4.04	4.57	4.75	4.90	4.32	4.18	4.08	4.21
TiO <sub>2</sub>	1.50	0.41	0.22	0.56	0.33	0.22	0.25	0.23	0.79	0.48	0.49
MnO	0.21	0.08	0.04	0.16	0.06	0.05	0.12	0.07	0.32	0.19	0.17
S	0.03	0.07	0.02	0.03	0.03	0.05	0.03	0.04	0.04	0.03	0.03
P <sub>2</sub> O <sub>5</sub>	0.57	0.10	0.01	0.13	0.07	0.02	0.02	0.04	0.15	0.09	0.08
Ce											
La											
Ba	2646	912	62	751	174	91	46	266	438	808	793
Nb	119	37	137	83	299	163	218	141	148	160	151
Zr	1013	304	366	376	413	748	1233	697	775	293	265
Y	79	23	71	43	109	83	95	82	71	72	67
Sr	181	193	23	231	47	35	55	42	179	186	182
Rb	83	73	76	105	111	113	76	59	67	33	42
Zn	159	230	20	68	129	29	122	96	168	181	200
Cu	12	87	7	19	9	8	8	4	10	9	8
Ni	15	9	30	13	10	14	20	13	10	12	14
Co											
Cr	2	20	bd1	2	4	7	18	11	3	bd1	10
V											
Li											
Y/Nb	0.66	0.62	0.52	0.52	0.36	0.51	0.44	0.58	0.48	0.45	0.44
D. f.	+3.2	+3.6	+2.7	+5.4	+2.8	+3.2	+1.2	+2.9	+4.0	+4.9	+4.4



Table 11 continued..

Sample:	5901S	5901T	5901U	5901V	6152B	6152C	6152E	6152K	6152U	6412A	6412B
SiO <sub>2</sub>	71.38	63.74	60.73	66.48	71.27	64.60	74.60	76.44	71.91	75.45	65.44
Al <sub>2</sub> O <sub>3</sub>	12.90	15.84	13.48	14.08	14.68	15.41	13.60	12.81	15.10	11.88	17.75
Fe <sub>2</sub> O <sub>3</sub>	3.76	6.82	8.51	7.95	3.51	7.27	2.48	1.67	3.98	4.03	3.36
MgO	0.80	0.62	3.31	0.08	0.04	0.27	0.06	0.16	0.22	0.54	0.77
CaO	1.59	2.32	4.90	1.97	0.91	2.23	0.32	0.37	1.10	0.47	1.20
Na <sub>2</sub> O	4.46	4.93	3.93	4.00	4.44	5.44	4.06	3.27	4.19	3.47	5.99
K <sub>2</sub> O	4.62	4.29	3.37	4.41	4.90	4.23	4.77	5.17	3.27	4.12	5.15
TiO <sub>2</sub>	0.32	0.90	1.16	0.67	0.37	0.66	0.23	0.18	0.37	0.21	0.16
MnO	0.19	0.20	0.15	0.24	0.10	0.26	0.05	0.03	0.10	0.12	0.16
S	0.03	0.03	0.03	0.04	0.01	0.01	0.00	0.01	0.01	0.00	0.01
P <sub>2</sub> O <sub>5</sub>	0.05	0.31	0.42	0.09	0	0	0	0	0	0.01	0.06
Ce					500	254	263	127	328	350	125
La					279	143	138	75	180	205	68
Ba	195	910	606	543	175	361	64	183	112	63	843
Nb	156	92	105	133	103	73	137	77	140	311	96
Zr	411	271	438	335	293	184	826	266	862	1385	363
Y	77	55	64	66	49	46	71	40	74	143	39
Sr	59	214	321	148	100	86	25	35	39	54	80
Rb	98	69	119	84	40	68	101	121	113	33	59
Zn	59	86	98	146	94	114	42	15	161	129	43
Cu	6	11	19	18	2	5	1	2	7	<2	7
Ni	43	7	21	17	1	2	2	2	2	3	2
Co											
Cr	37	bdl	42	5	<2	4	3	8	11	<2	3
V											
Li											
Y/Nb	0.49	0.60	0.61	0.50	0.48	0.63	0.52	0.52	0.53	0.46	0.41
D.F.	+3.3	+5.0	+5.0	+2.0	+3.2	+3.9	+5.7	+2.6	+1.5	+2.3	



Table 11 continued..

Sample:	6412C	6412D	6412F	6412G	6413A	Mean (n=27)	s.d.
SiO <sub>2</sub>	63.37	64.04	61.86	65.37	71.90	68.70	5.21
Al <sub>2</sub> O <sub>3</sub>	17.05	17.18	16.36	17.83	16.55	14.57	1.81
Fe <sub>2</sub> O <sub>3</sub>	5.33	4.60	7.43	3.44	1.86	4.93	2.28
MgO	0.90	0.92	2.09	0.67	0.81	0.59	0.73
CaO	2.11	2.33	3.72	1.45	0.33	1.66	1.20
Na <sub>2</sub> O	5.23	5.23	5.76	6.00	5.56	4.62	0.75
K <sub>2</sub> O	5.38	5.10	2.06	4.86	2.91	4.29	0.76
TiO <sub>2</sub>	0.60	0.58	0.80	0.41	0.18	0.50	0.32
MnO	0.24	0.14	0.28	0.15	0.03	0.15	0.08
S	0.01	0.05	0.01	0.04	0.00	0.03	0.02
P <sub>2</sub> O <sub>5</sub>	0.18	0.20	0.19	0.06	0.01	0.11	0.14
Ce	92	121	221	254	142	231	120
La	41	64	135	166	76	130	70
Ba	743	2610	253	928	89	580	669
Nb	52	76	157	104	135	134	63
Zr	88	295	852	354	459	524	330
Y	21	31	106	39	81	67	28
Sr	89	241	217	90	15	117	85
Rb	71	85	27	36	123	77	30
Zn	72	53	410	37	30	110	84
Cu	5	17	10	6	<2	11	16
Ni	<2	<2	8	<2	6	11	10
Co							
Cr	5	3	19	<2	3	8	11
V							
Li							
Y/Nb	0.40	0.41	0.68	0.38	0.60		
D.f.	+6.2	+6.3	+4.6	+7.1	+3.8		





Table 12:X.R.F. Analyses on Leucocratic Gneiss (low niobium) from the Monashee Mountains

Sample:	5897B	5897D	5898B	5898D	5898E	5898F	5898H	5899B	5901D	5901E	5901F
SiO <sub>2</sub>	67.18	75.52	72.34	65.44	65.26	78.19	70.98	64.53	73.59	75.46	75.78
Al <sub>2</sub> O <sub>3</sub>	13.33	13.95	14.30	14.06	13.51	11.72	14.30	15.87	13.57	12.89	13.48
Fe <sub>2</sub> O <sub>3</sub>	9.64	2.94	2.50	6.60	6.73	2.72	3.18	5.97	2.67	1.45	1.77
MgO	3.82	0.39	0.42	2.26	2.92	0.03	0.74	1.21	0.32	0.21	0.46
CaO	0.02	1.25	1.98	3.19	3.57	0.27	2.32	2.92	0.83	0.41	0.47
Na <sub>2</sub> O	0.37	3.40	5.29	2.89	2.87	6.91	4.36	5.21	6.01	5.07	2.46
K <sub>2</sub> O	4.62	5.03	2.71	4.48	4.01	0.08	3.69	3.26	2.69	4.27	5.27
TiO <sub>2</sub>	0.80	0.34	0.32	0.76	0.78	0.08	0.27	0.74	0.24	0.16	0.22
MnO	0.05	0.05	0.04	0.09	0.11	0.01	0.05	0.06	0.04	0.02	0.02
S	0.05	0.03	0.03	0.03	0.03	0.02	0.04	0.06	0.03	0.02	0.03
P <sub>2</sub> O <sub>5</sub>	0.10	0.10	0.08	0.21	0.21	0.01	0.07	0.16	0.03	0.04	0.05
Ce											
La											
Ba	485	663	837	850	976	5	696	1268	706	74	577
Nb	36	59	9	29	53	339	10	27	73	63	12
Zr	522	329	179	326	211	1420	130	920	245	168	143
Y	37	56	7	39	59	228	8	33	61	55	12
Sr	16	109	312	229	355	36	530	434	130	34	102
Rb	192	182	46	203	125	5	70	97	41	115	173
Zn	95	73	24	118	116	1	720	32	24	7	21
Cu	28	5	28	5	15	bdl	75	81	6	bdl	2
Ni	25	28	9	24	24	21	10	10	16	9	15
Co											
Cr	56	11	10	65	35	7	19	5	29	21	16
V											
Li											
Y/Nb	1.03	0.95	0.78	1.34	1.11	0.67	0.80	1.22	0.84	0.87	1.00
D.F.	-7.4	+2.3	+4.3	+0.8	+0.04	+0.04	+3.1	+4.8	+4.5	+3.9	+0.2



Table 12 continued ..

Sample:	6152F	6153B	6413B	6413C	6413E	6413F	6413H	6414B	6414C	Mean (n=20)	s.d.
SiO <sub>2</sub>	74.27	76.95	73.68	62.41	71.72	74.12	66.82	61.45	62.83	70.08	5.08
Al <sub>2</sub> O <sub>3</sub>	13.63	12.63	13.32	16.03	14.15	13.40	14.50	15.41	15.75	13.99	1.11
Fe <sub>2</sub> O <sub>3</sub>	2.92	1.84	2.60	7.57	3.54	2.69	6.09	7.49	7.65	4.43	2.49
MgO	0.01	0.17	1.05	2.24	0.78	0.75	2.31	1.81	1.09	1.15	1.07
CaO	0.54	0.38	0.58	2.59	2.23	0.56	2.55	3.31	1.78	1.59	1.18
Na <sub>2</sub> O	3.74	4.70	3.69	4.16	4.22	3.95	4.92	3.85	4.28	4.12	1.39
K <sub>2</sub> O	4.78	3.27	4.90	4.49	3.17	4.43	2.23	5.33	4.81	3.88	1.28
TiO <sub>2</sub>	0.23	0.15	0.31	0.61	0.33	0.23	0.72	1.21	1.13	0.48	0.33
MnO	0.07	0.03	0.04	0.14	0.07	0.07	0.09	0.19	0.17	0.07	0.05
S	0.01	0.02	0.00	0.04	0.01	0.00	0.04	0.00	0.01	0.03	0.02
P <sub>2</sub> O <sub>5</sub>	0.00	0.00	0.03	0.09	0.06	0.01	0.20	0.52	0.49	0.12	0.15
Ce	279	104	166	141	148	183	106	173	197	166	53
La	144	50	84	77	75	104	47	100	117	89	31
Ba	39	54	271	566	1219	589	541	2112	1221	687	513
Nb	107	126	96	87	294	150	40	67	103	89	87
Zr	656	346	585	676	1093	570	240	442	626	491	343
Y	88	123	140	82	219	107	38	55	86	77	62
Sr	20	15	41	109	197	101	186	192	85	162	146
Rb	76	87	102	110	88	82	64	197	248	115	64
Zn	136	17	37	161	46	88	71	123	143	103	154
Cu	10	5	4	28	39	5	38	9	6	20	23
Ni	1	3	12	22	18	9	10	4	13	14	8
Co											
Cr	2	8	3	58	5	3	34	3	4	20	20
V											
Li											
Y/Nb	0.82	0.98	1.5	0.94	0.74	0.71	0.95	0.82	0.83		
D.f.	+2.2	+2.4	+1.5	+2.6	+2.6	+1.7	+2.0	+3.7	+3.6		



Table 13: X.R.F. Analyses on Augen Gneiss from the Monashee Mountains

Sample:	5901B	5901C	5901N	6152D	6153F	6154A	6154B	6154C	Mean (n=8)	s.d.
SiO <sub>2</sub>	64.30	68.37	75.63	68.36	73.43	70.38	73.30	69.16	70.36	3.62
Al <sub>2</sub> O <sub>3</sub>	13.52	14.46	12.59	15.50	13.71	14.84	13.73	15.27	14.20	0.99
Fe <sub>2</sub> O <sub>3</sub>	7.51	4.91	2.88	4.81	3.26	3.89	3.52	4.19	4.37	1.45
MgO	1.83	0.81	0.19	0.08	0.33	0.69	1.09	0.66	0.71	0.56
CaO	3.60	2.23	1.51	1.05	0.55	1.14	0.41	1.68	1.52	1.03
Na <sub>2</sub> O	3.15	3.49	5.93	5.23	3.89	3.04	1.88	2.55	3.65	1.35
K <sub>2</sub> O	4.32	4.78	0.90	4.62	4.63	5.54	5.72	6.07	4.57	1.61
TiO <sub>2</sub>	1.17	0.65	0.23	0.46	0.33	0.57	0.46	0.52	0.55	0.28
MnO	0.11	0.07	0.08	0.19	0.06	0.05	0.04	0.06	0.08	0.05
S	0.05	0.03	0.03	0.00	0.01	0.01	0.01	0.00	0.08	0.16
P <sub>2</sub> O <sub>5</sub>	0.44	0.20	0.02	0.00	0.00	0.00	0.00	0.00	0.08	0.16
Ce				395	260	223	259	172	262(n=5)	83
La				227	133	115	137	90	140(n=5)	52
Ba	1191	1270	204	67	88	1143	773	973	714	516
Nb	41	60	95	133	100	22	16	21	61	44
Zr	515	622	205	441	528	300	268	330	401	147
Y	72	67	33	56	85	85	57	72	66	17
Sr	186	196	247	64	24	160	83	209	146	79
Rb	146	123	23	78	111	178	225	246	141	74
Zn	117	73	31	68	35	31	34	60	56	30
Cu	16	2	18	4	4	0	2	23	9	9
Ni	26	26	10	2	4	4	2	3	10	10
Co										
Cr	18	20	7	42	9	11	7	14	11	6
V										
Li										
Y/Nb	1.76	1.12	0.35	0.42	0.85	3.86	3.56	3.43		
D.f.	+1.7	+2.6	+3.4	+5.2	+2.1	+1.8	-1.1	+1.9		





Table 14: X.R.F. Analyses on Mafic Gneiss from Bulldog Creek Area

Sample:	AC49	AC51	5495	5831E	5833	5884B	6407A	Mean (n=7)	s.d.
SiO <sub>2</sub>	41.5	45.1	48.0	51.1	50.2	52.07	57.02	49.28	5.0
Al <sub>2</sub> O <sub>3</sub>	15.6	12.8	18.5	11.3	15.0	13.47	15.32	14.57	2.3
Fe <sub>2</sub> O <sub>3</sub>	17.2	17.1	10.2	16.2	11.0	15.02	10.46	13.88	3.2
MgO	8.9	8.1	8.2	5.6	6.1	4.60	4.65	6.59	1.8
CaO	6.6	9.8	7.9	6.7	9.5	6.35	4.86	7.39	0.8
Na <sub>2</sub> O	2.2	2.0	2.7	0.3	3.7	2.29	2.82	2.29	1.0
K <sub>2</sub> O	5.33	2.02	3.21	4.61	1.42	3.18	3.63	3.34	1.4
TiO <sub>2</sub>	2.20	2.19	0.96	2.67	2.43	2.33	1.25	2.00	0.6
MnO	0.17	0.23	0.16	0.21	0.17	0.19	0.16	0.18	0.03
S	0.00	0.02	0.00	0.25	0.01	0.46	0.02	0.11	0.2
P <sub>2</sub> O <sub>5</sub>	0.39	0.70	0.23	0.01	0.58	0.04	0.33	0.47	0.3
Ce							55		
La							15		
Ba	870	592	624	1095	368	1078	1363	856	348
Nb	17	22	19	31	87	30	11	31	26
Zr	212	191	221	324	261	286	173	238	54
Y	39	42	34	57	31	51	30	41	10
Sr	356	216	703	442	722	259	463	452	199
Rb	149	61	81	190	41	82	111	102	52
Zn	182	174	120	154	105	115	81	133	38
Cu	31	37	8	116	109	100	46	64	43
Ni	70	64	54	13	13	48	5	38	27
Co			90	118	106			105(n=3)	14
Cr			220			20	6	82(n=3)	120
V			180						
Li			25	34	10			23(n=3)	12
Y/Nb	2.29	1.91	1.79	1.84	0.36	1.70	2.73		



Table 15: X.R.F. Analyses on Felsic Gneiss from Bulldog Creek Area

Sample:	5831A	5831B	5831C	5831D	5832	5884A	5884C	6408A	6408B	Mean (n=8)	s.d.
SiO <sub>2</sub>	62.3	72.6	62.8	63.7	61.3	65.06	62.30	62.60	71.01	63.88	3.09
Al <sub>2</sub> O <sub>3</sub>	16.1	15.1	15.8	14.8	16.7	15.59	15.07	15.23	15.38	15.58	0.61
Fe <sub>2</sub> O <sub>3</sub>	7.5	1.9	7.5	6.7	7.1	7.20	7.03	7.03	1.90	6.50	1.88
MgO	2.6	0.4	2.9	3.0	2.8	3.45	3.41	3.43	1.07	2.83	0.78
CaO	2.8	2.6	2.8	3.5	4.1	3.50	4.10	4.51	1.95	3.41	0.85
Na <sub>2</sub> O	4.8	6.6	4.2	5.0	0.44	3.54	3.48	3.57	3.65	1.42	6.6
K <sub>2</sub> O	2.68	0.59	2.96	2.1	1.91	3.45	3.28	2.94	4.81	3.02	0.90
TiO <sub>2</sub>	0.90	0.13	0.89	0.83	0.78	0.88	0.86	0.86	0.34	0.79	0.19
MnO	0.10	0.03	0.10	0.10	0.10	0.09	0.10	0.10	0.03	0.08	0.04
S	0.00	0.00	0.00	0.00	0.02	0.28	0.00	0.00	0.07	0.13	0.00
P <sub>2</sub> O <sub>5</sub>	0.19	0.00	0.17	0.18	0.18	0.05	0.03	0.28	0.08	0.14	0.08
Ce								64	61	62.5 (n=2)	2
La								35	25	30 (n=2)	7
Ba	860	198	1219	979	680	1082	1193	1211	3228	1307	799
Nb	55	362	44	18	12	20	17	12	3	23	18
Zr	331	1565	315	226	307	304	277	209	193	270	53
Y	37	140	35	30	23	28	25	26	1	26	11
Sr	352	467	387	448	843	464	502	566	383	493	158
Rb	102	17	127	116	79	76	77	85	104	96	19
Zn	84	23	82	82	75	63	57	60	32	67	18
Cu	22	28	8	2	35	111	39	12	11	30	35
Ni	27	10	23	23	24	26	17	14	2	20	8
Co	82										
Cr						39	32	34	9	29 (n=4)	13
V											
Li	21										
Y/Nb	0.67	0.39	0.80	1.67	1.92	1.40	1.47	2.17	0.33		174
D.F.	+2.4	+5.6	+1.2	+3.1	-4.5	+1.0	+0.8	+2.8			



Table 16: X.R.F. Analyses on Mafic Gneiss from Mount Blackman

Sample:	5890A	5890D	5890J	5890M	5895C	5895F	5895G	5895M	5895N	5896C
SiO <sub>2</sub>	48.17	47.80	46.53	48.60	50.48	55.91	45.84	49.71	46.01	45.90
Al <sub>2</sub> O <sub>3</sub>	13.09	13.73	12.73	13.23	14.86	16.72	11.54	13.11	11.06	14.10
Fe <sub>2</sub> O <sub>3</sub>	14.41	14.27	16.09	14.25	16.45	9.09	18.79	17.12	18.76	15.36
MgO	8.74	8.97	7.11	8.73	7.40	5.49	7.43	5.79	7.17	9.38
CaO	11.06	10.19	7.78	10.56	3.46	4.42	9.94	7.15	11.04	10.46
Na <sub>2</sub> O	2.21	2.44	1.36	2.28	0.31	2.41	1.05	3.41	1.13	1.89
K <sub>2</sub> O	0.66	0.91	3.51	0.69	3.97	4.42	1.76	0.75	1.19	1.12
TiO <sub>2</sub>	1.29	1.33	3.22	1.31	2.56	1.04	2.92	2.40	2.97	1.41
MnO	0.21	0.21	0.24	0.20	0.17	0.12	0.23	0.19	0.25	0.18
S	0.03	0.02	0.18	0.03	0.07	0.03	0.07	0.01	0.06	0.02
P <sub>2</sub> O <sub>5</sub>	0.13	0.13	1.25	0.12	0.28	0.36	0.43	0.34	0.36	0.16
Ce										
La										
Ba	67	148	1124	151	1476	629	257	131	155	207
Nb	11	8	39	10	20	33	26	13	26	8
Zr	98	96	275	95	170	102	335	217	306	105
Y	29	29	50	25	41	32	62	58	59	30
Sr	204	250	172	253	21	266	223	220	225	206
Rb	12	36	136	19	361	21	59	20	35	57
Zn	98	90	132	93	172	142	139	178	140	104
Cu	106	139	29	91	252	9	387	173	403	186
Ni	124	107	58	117	51	30	79	83	84	161
Co										
Cr	240	236	18	226	83	118	118	81	115	192
V										
Li										
Y/Nb	2.64	3.63	1.28	2.50	2.05	0.97	2.38	4.46	2.27	3.75





Table 16 continued...

Sample:	6150H	6150Q	6150T	Mean	s.d.
SiO <sub>2</sub>	48.08	46.50	48.23	4829	2.72
Al <sub>2</sub> O <sub>3</sub>	13.76	17.14	13.19	13.71	1.74
Fe <sub>2</sub> O <sub>3</sub>	12.94	13.32	14.20	15.00	2.59
MgO	10.74	10.17	9.06	8.17	1.59
CaO	10.24	6.37	11.26	8.76	2.66
Na <sub>2</sub> O	2.41	2.03	2.74	1.97	0.82
K <sub>2</sub> O	1.17	3.85	0.66	1.90	1.46
TiO <sub>2</sub>	1.34	1.18	1.38	1.87	0.80
MnO	0.19	0.18	0.20	0.20	0.03
S	0	0.01	0	0.04	0.05
P <sub>2</sub> O <sub>5</sub>	0	0	0	0.27	0.33
Ce	14	31	17	21 (n=3)	9
La	15	14	12	14 (n=3)	1.5
Ba	218	621	40	402	445
Nb	7	23	7	18	11
Zr	75	107	82	159	93
Y	21	25	28	35	18
Sr	296	229	170	210	67
Rb	28	180	9	98	119
Zn	107	192	90	129	35
Cu	231	4	84	161	30
Ni	201	64	106	97	47
Co					
Cr	361	37	255	160	100
V					
Li	3	1.09	4		
Y/Nb					



Table 17: X.R.F. Analyses on Felsic Gneiss from Mount Blackman

Sample:	5890B	5890C	5890E1	5890E2	5890F	5890H	5890I	5890K	5890N	5890P
SiO <sub>2</sub>	72.91	72.55	73.69	73.03	70.40	69.79	70.40	71.92	73.10	71.91
Al <sub>2</sub> O <sub>3</sub>	14.25	14.44	13.72	14.18	14.92	14.42	15.46	14.46	14.21	12.96
Fe <sub>2</sub> O <sub>3</sub>	1.84	1.96	1.79	1.89	2.74	3.37	2.71	2.64	2.21	3.79
MgO	0.61	0.41	0.45	0.40	0.82	1.50	0.85	0.99	0.89	1.41
CaO	1.05	1.26	1.14	1.12	1.69	2.88	2.11	2.23	1.71	2.12
Na <sub>2</sub> O	4.64	4.28	3.95	4.05	4.61	4.35	5.05	4.58	3.98	4.05
K <sub>2</sub> O	4.38	4.74	4.91	5.00	4.30	3.07	2.85	2.66	3.47	2.99
TiO <sub>2</sub>	0.22	0.25	0.25	0.27	0.37	0.43	0.39	0.37	0.32	0.32
MnO	0.03	0.03	0.02	0.02	0.04	0.05	0.05	0.04	0.03	0.05
S	0.03	0.03	0.03	0.03	0.03	0.03	0.03	0.03	0.03	0.04
P <sub>2</sub> O <sub>5</sub>	0.04	0.05	0.06	0.02	0.09	0.10	0.11	0.09	0.06	0.17
Ce										
La										
Ba	1057	773	957	992	1108	1126	1317	1047	751	690
Nb	8	10	13	8	11	0	10	12	11	18
Zr	143	143	208	179	203	195	124	255	173	169
Y	7	7	6	8	10	9	7	4	9	14
Sr	287	232	229	240	371	403	274	238	366	327
Rb	102	171	162	151	112	77	71	86	85	93
Zn	16	40	47	31	42	37	33	50	14	50
Cu	14	7	bdl	9	12	17	15	12	bdl	15
Ni	12	8	6	27	17	43	9	29	9	13
Co										
Cr	21	23	11	bdl	24	21	8	20	22	41
Li										
Y/Nb	0.88	0.70	0.46	1.00	0.91		0.70	0.33	0.82	0.78
D.F.	+3.7	+3.7	+3.0	+3.3	+3.9	+2.8	+4.0	+2.9	+2.1	+1.4



Table 17 continued..

Sample:	5890Q	5890R	5890T	5895A	5895D	5895H	5895J	5895K	5895L	5895P
SiO <sub>2</sub>	71.90	71.79	71.29	71.57	72.96	72.29	69.15	73.20	73.46	68.12
Al <sub>2</sub> O <sub>3</sub>	14.11	15.03	14.69	14.25	13.87	14.95	14.56	14.10	13.81	15.13
Fe <sub>2</sub> O <sub>3</sub>	2.23	1.91	2.90	2.29	1.97	2.43	1.80	2.12	3.49	3.28
MgO	0.63	0.57	0.99	1.04	0.84	0.61	1.03	0.56	0.70	1.31
CaO	1.75	1.43	1.64	2.18	1.28	0.43	4.08	1.18	1.01	2.65
Na <sub>2</sub> O	4.21	4.26	4.03	4.56	5.13	5.78	5.06	3.88	3.23	4.23
K <sub>2</sub> O	4.61	4.62	3.84	3.56	3.45	3.04	2.93	4.93	5.27	4.47
TiO <sub>2</sub>	0.32	0.27	0.44	0.31	0.35	0.32	0.26	0.23	0.27	0.41
MnO	0.03	0.02	0.03	0.04	0.03	0.03	0.06	0.02	0.02	0.05
S	0.12	0.04	0.03	0.03	0.02	0.03	0.03	0.03	0.03	0.03
P <sub>2</sub> O <sub>5</sub>	0.08	0.06	0.10	0.16	0.09	0.12	0.10	0.07	0.09	0.12
Ce										
La										
Ba	19800	902	1367	1192	1058	880	533	1057	1058	952
Nb	13	6	15	7	15	11	9	7	10	17
Zr	166	109	183	183	193	156	177	156	164	217
Y	8	11	3	26	11	14	12	6	8	18
Sr	370	410	281	417	289	216	256	233	116	182
Rb	136	143	108	89	75	74	94	164	171	149
Zn	29	30	32	33	16	44	27	41	42	18
Cu	19	11	34	8	9	5	26	2	5	10
Ni	10	12	17	bdl	6	15	2	bdl	24	18
Co										
Cr	25	17	17	bdl	46	13	15	11	349	18
V										
Li										
Y/Nb	+3.6	+3.7	+2.4	+3.4	+3.7	+4.2	+5.2	+3.6	+4.8	+2.1





Table 17 continued ...

Sample:	5895Q	5895R	5896B	6150A	6150B	6150C	6150D	6150E	6150F	6150G
SiO <sub>2</sub>	69.68	73.22	69.41	68.16	72.68	62.75	63.82	74.70	76.09	67.63
Al <sub>2</sub> O <sub>3</sub>	14.21	13.92	15.04	15.63	14.66	17.23	16.99	13.58	13.78	15.65
Fe <sub>2</sub> O <sub>3</sub>	3.28	1.47	3.10	4.24	2.14	5.64	5.29	1.55	0.48	4.24
MgO	1.75	0.41	0.83	2.24	0.73	3.37	3.52	0.91	0.16	2.62
CaO	2.38	1.65	2.35	2.40	1.34	2.93	2.60	3.38	0.65	2.55
Na <sub>2</sub> O	4.87	3.91	4.89	5.10	4.14	2.71	3.93	3.77	2.77	3.95
K <sub>2</sub> O	3.07	5.01	3.71	1.73	4.04	4.77	3.25	1.97	6.01	2.84
TiO <sub>2</sub>	0.52	0.19	0.44	0.56	0.32	0.71	0.70	0.16	0.06	0.57
MnO	0.05	0.03	0.04	0.04	0.03	0.07	0.07	0.04	0.01	0.06
S	0.03	0.14	0.03	0.00	0.01	0.01	0.01	0.01	0.00	0.01
P <sub>2</sub> O <sub>5</sub>	0.17	0.06	0.16	0.00	0.00	0.00	0.00	0.00	0.00	0.00
Ce				140	203	90	78	12	52	101
La				83	125	49	44	12	34	59
Ba	1036	965	1089	1392	1068	1344	1272	596	1436	1049
Nb	12	8	14	11	4	13	10	4	3	11
Zr	244	139	193	177	153	180	193	68	84	151
Y	17	9	11	18	11	31	20	6	6	18
Sr	261	172	350	374	298	350	347	333	236	288
Rb	101	162	131	79	132	203	161	53	132	127
Zn	50	20	53	67	40	77	71	9	4	57
Cu	15	24	14	3	4	1	3	3	6	1
Ni	5	8	15	16	3	25	22	4	3	16
Co										
Cr	85	6	7	30	7	51	46	17	10	34
V										
Li										
Y/Nb	1.42	1.13	0.79						2	164
D.F.	+3.1	+3.5	+4.5	+2.3	+2.7	+0.3	+0.8	+1.8	+1.8	+1.0



Table 17 continued ...

Sample:	6150I	6150J	6150MI	6150M2	6150M3	6150N	6150P	6150R	6150S	Mean (n=39)	s.d.
SiO <sub>2</sub>	72.41	70.48	73.19	72.88	73.15	69.37	68.70	74.50	72.17	71.39	2.70
Al <sub>2</sub> O <sub>3</sub>	15.62	16.84	14.80	15.02	14.44	15.83	15.85	14.15	15.70	14.76	0.90
Fe <sub>2</sub> O <sub>3</sub>	1.58	1.08	1.86	1.97	2.06	3.74	4.18	1.38	1.87	2.53	1.10
MgO	0.77	0.76	0.83	0.81	0.85	2	1.59	0.40	0.73	1.06	0.75
CaO	0.90	2.63	0.89	0.86	0.87	1.94	1.41	1.19	2.04	1.82	0.82
Na <sub>2</sub> O	3.74	6.77	3.60	3.49	3.31	3.58	2.43	3.67	4.82	4.21	0.82
K <sub>2</sub> O	4.79	1.28	4.64	4.76	5.09	3.17	5.50	4.54	2.40	3.89	1.24
TiO <sub>2</sub>	0.23	0.11	0.24	0.25	0.29	0.39	0.35	0.20	0.32	0.33	0.15
MnO	0.02	0.02	0.03	0.03	0.03	0.05	0.04	0.02	0.02	0.06	0.08
S	0.01	0.00	0.01	0.01	0.01	0.01	0.01	0.00	0.01	0.04	0.07
P <sub>2</sub> O <sub>5</sub>	0.00	0.00	0.00	0.00	0.00	0.00	0.00	0.00	0.00	0.05	0.07
Ce	59	582	71	98	79	75	114	102	159	96(n=15)	46
La	37	270	41	59	46	42	61	54	84	55(n=15)	26
Ba	1044	385	1262	1185	1278	766	1109	1072	566	993(n=39)	294
Nb	7	1	8	7	7	17	22	4	5	10	6.5
Zr	127	391	180	197	174	194	587	141	111	180	86
Y	5	336	10	17	17	18	46	8	10	12(n=39)	8
Sr	198	330	197	210	196	170	136	205	333	273	78
Rb	165	36	152	149	159	143	195	149	102	123	43
Zn	27	10	28	28	28	60	61	25	19	36	18
Cu	1	2	0	2	2	1	1	2	17	9	8
Ni	1	8	3	3	4	7	6	3	3	11	9
Co											
Cr	11	4	14	13	17	20	16	11	8	28	54
V											
Li											
Y/Nb	0.71	336	2	2.43	2.43	1.06	2.09	2.00	2.00		
D.F.	+2.5	+6.6	+1.9	+1.8	+1.6	+0.6	+0.4	+3.9	+3.4		



Table 18: X.R.F. Analyses on Felsic Gneiss  
from Mount Blackman South of  
Hugh Allan Creek

Sample:	6151C	6151G	6151H	Mean (n=3)	s.d.
SiO <sub>2</sub>	75.42	76.14	65.63	72.40	5.87
Al <sub>2</sub> O <sub>3</sub>	13.44	13.39	15.06	13.96	0.95
Fe <sub>2</sub> O <sub>3</sub>	1.77	1.62	7.75	3.71	3.50
MgO	0.09	0.06	0.05	0.07	0.02
CaO	0.59	0.33	2.12	1.01	0.97
Na <sub>2</sub> O	3.93	3.75	3.07	3.58	0.45
K <sub>2</sub> O	4.74	4.71	6.02	5.16	0.75
TiO <sub>2</sub>	0.12	0.10	0.61	0.28	0.29
MnO	0.03	0.02	0.17	0.07	0.08
S	0.01	0.00	0.01	0.01	0.01
P <sub>2</sub> O <sub>5</sub>	0	0	0	0	0
Ce	137	58	800	332	408
La	63	27	456	182	238
Ba	25	30	142	66	66
Nb	133	118	74	108	30
Zr	244	215	1613	691	799
Y	122	111	64	99	31
Sr	12	14	47	24	20
Rb	155	157	83	132	42
Zn	56	57	127	80	41
Cu	4	3	10	6	4
Ni	3	3	1	2	1
Co					
Cr	9	12	<2	7	6
V					
Li					
Y/Nb	0.92	0.94	0.86		
D.F.	+2.0	+2.1	+3.0		





## 9.2 Appendix B (X.R.F. Analyses of Metasedimentary Rocks)



Table 19: X.R.F. Analyses on psammites from the Kaza Group

Sample:	5835A	5835B	5835C	5836B	5837	5838A	5839A	5839B	5840B	5841
SiO <sub>2</sub>	81.2	74.4	83.3	77.5	81.4	80.7	81.9	87.5	85.3	81.3
Al <sub>2</sub> O <sub>3</sub>	9.2	12.0	7.6	12.2	8.9	10.1	9.9	6.4	7.8	10.3
Fe <sub>2</sub> O <sub>3</sub>	2.4	3.9	2.5	2.4	3.1	2.9	1.9	1.6	2.5	3.1
MgO	1.3	1.9	1.1	1.5	1.3	1.2	1.1	0.7	0.9	1.3
CaO	2.1	1.8	2.8	1.4	0.7	0.1	1.2	0.9	0.3	0.1
Na <sub>2</sub> O	2.6	3.6	2.1	3.5	2.8	1.9	2.6	2.1	1.7	1.6
K <sub>2</sub> O	0.89	1.60	0.34	1.15	1.28	2.52	1.10	0.53	1.25	1.91
TiO <sub>2</sub>	0.31	0.47	0.26	0.32	0.30	0.22	0.29	0.19	0.26	0.40
MnO	0.06	0.05	0.10	0.03	0.05	0.03	0.03	0.02	0.02	0.04
S	0.00	0.00	0.00	0.00	0.00	0.35	0.00	0.19	0.00	0.00
P <sub>2</sub> O <sub>5</sub>	0.04	0.37	0.00	0.09	0.02	0.04	0.04	0.06	0.04	0.05
Ce										
La	200	301	68	189	252	354	155	71	181	254
Ba	8	7	18	6	8	6	17	7	6	11
Nb	251	255	253	155	185	116	351	246	278	277
Zr	18	24	22	13	15	17	35	14	15	18
Y	80	174	184	163	91	80	223	138	105	82
Sr	49	94	20	37	88	133	47	24	70	83
Rb	34	67	32	34	50	33	25	19	27	25
Zn	4	5	3	2	16	22	2	13	11	14
Cu	20	31	23	14	17	28	7	13	16	21
Ni	35	-	-	75	-	46	-	25	29	38
Co										
Cr										
Li	21			36		12		8	23	26
D.F.	- 3.2	-1.2	-4.1	- 1.6	-3.8	-4.4	-3.4	-5.3	-5.8	-5.5



Table 19 continued ...

Sample:	5853A	5853B	5854	5857A	5857B	Mean (n=15)	s.d.
SiO <sub>2</sub>	81.1	81.8	77.3	88.4	76.3	81.3	3.9
Al <sub>2</sub> O <sub>3</sub>	9.2	9.6	10.5	5.6	12.7	9.5	2.0
Fe <sub>2</sub> O <sub>3</sub>	2.8	1.8	4.4	1.5	4.1	2.7	0.9
MgO	1.2	0.8	2.2	0.7	2.1	1.3	0.5
CaO	0.1	0.1	0.8	2.1	0.2	1.0	0.9
Na <sub>2</sub> O	3.9	2.5	2.8	0.9	1.2	2.4	0.9
K <sub>2</sub> O	1.44	3.08	1.56	0.52	2.92	1.47	0.83
TiO <sub>2</sub>	0.31	0.27	0.44	0.19	0.50	0.32	0.09
MnO	0.03	0.03	0.07	0.11	0.03	0.04	0.03
S	0.00	0.00	0.00	0.00	0.00	0.04	0.10
P <sub>2</sub> O <sub>5</sub>	0.02	0.02	0.03	0.10	0.03	0.06	0.09
Ce							
La							
Ba	318	761	401	34	450	266	183
Nb	6	10	11	12	7	9	4
Zr	203	186	319	306	311	246	66
Y	11	15	21	18	24	19	6
Sr	120	175	136	85	168	127	48
Rb	71	102	86	46	166	60	49
Zn	48	29	84	24	84	32	29
Cu	6	11	19	1	9	9	7
Ni	21	9	39	12	26	22	13
Co	36	-	51	-	50	43(n=9)	15
Cr							
Li	16	-	31	-	50		
D.F.	-2.1	-2.7	-3.9	-6.5	-5.5		





Table 20: X.R.F. Analyses on pelites from the Kaza Group semi-pelite

Sample:	5818A	5834	5836A	5838B	5855A	Mean(n=5)	s.d.	5856
SiO <sub>2</sub>	56.2	60.2	57.0	62.5	66.7	60.5	4.3	53.2
Al <sub>2</sub> O <sub>3</sub>	24.8	22.3	24.9	19.7	16.6	21.7	3.5	17.9
Fe <sub>2</sub> O <sub>3</sub>	8.0	6.2	8.3	6.9	6.3	7.1	1.0	11.7
MgO	3.2	2.6	2.9	3.5	2.8	3.0	0.4	3.5
CaO	0.5	1.4	0.2	0.0	0.2	0.5	0.6	4.0
Na <sub>2</sub> O	1.9	3.5	1.2	0.6	1.1	1.7	1.1	3.6
K <sub>2</sub> O	4.47	2.63	4.52	5.92	5.02	4.52	1.21	4.01
TiO <sub>2</sub>	0.86	0.74	0.68	0.75	0.88	0.78	0.08	1.52
MnO	0.07	0.07	0.08	0.08	0.04	0.07	0.02	0.13
S	0.01	0.13	0.14	0.02	0.43	0.15	0.17	0.00
P <sub>2</sub> O <sub>5</sub>	0.14	0.19	0.20	0.07	0.12	0.14	0.05	0.46
Ce								
La	709	374	917	669	698	673	194	1368
Ba	21	19	12	16	14	14	7	26
Nb	182	266	73	260	230	202	80	412
Zr	42	32	40	26	15	31	11	33
Y	207	281	118	62	113	156	87	384
Sr	197	144	229	353	213	227	77	137
Rb	109	116	158	91	90	113	28	183
Zn	63	37	76	17	23	43	25	8
Cu	54	50	65	49	23	48	15	7
Ni		90	94		64	83(n=3)	16	94
Co								
Cr								
Li		36	46		62	48(n=3)	13	56
D.F.	-1.59	-1.6	-2.7	-1.8	-3.9			+1.71



Table 21: X.R.F. Analyses on psammites from Robina Creek Area.

Sample:	6409A	6411A	6411C	6411D	6411I	Mean (n=5)	s.d.
SiO <sub>2</sub>	87.45	86.11	86.84	85.88	87.54	86.76	0.76
Al <sub>2</sub> O <sub>3</sub>	6.80	6.69	6.84	7.31	6.71	6.87	0.25
Fe <sub>2</sub> O <sub>3</sub>	1.43	2.36	1.60	1.67	1.48	1.71	0.38
MgO	0.97	1.10	1.02	1.07	0.94	1.02	0.07
CaO	0.34	1.00	1.06	1.14	0.84	0.88	0.32
Na <sub>2</sub> O	2.14	1.92	1.86	2.00	1.55	1.89	0.22
K <sub>2</sub> O	0.71	0.62	0.59	0.70	0.74	0.67	0.06
TiO <sub>2</sub>	0.21	0.26	0.19	0.21	0.22	0.22	0.03
MnO	0.03	0.04	0.06	0.07	0.04	0.05	0.01
S	0.00	0.00	0.00	0.00	0.00	0.00	0.00
P <sub>2</sub> O <sub>5</sub>	0.02	0.07	0.06	0.07	0.04	0.05	0.02
Ce	60	38	54	54	44	50	9
La	20	11	12	14	8	12	6
Ba	104	79	69	87	107	73	40
Nb	5	5	4	4	6	5	1
Zr	144	132	120	115	155	133	17
Y	9	12	11	11	12	9	4
Sr	60	69	56	57	47	58	8
Rb	29	34	39	38	35	29	12
Zn	18	25	15	16	19	19	4
Cu	7	5	6	6	5	5	2
Ni	10	4	4	8	6	5	3
Cr	21	24	18	19	24	17	8
Li							



Table 22: X.R.F. Analyses on pelites from Robina Creek Area

Sample:	6400B	6400C	6409B	6411E	6411G	6411H	Mean (n=6)	s.d.
SiO <sub>2</sub>	57.84	55.94	55.38	55.89	52.49	54.83	55.40	1.75
Al <sub>2</sub> O <sub>3</sub>	24.67	26.65	29.07	27.55	27.96	27.71	27.18	1.65
Fe <sub>2</sub> O <sub>3</sub>	7.93	7.77	6.05	7.79	8.55	7.23	7.55	0.85
MgO	2.95	2.68	2.37	2.53	3.50	2.46	2.75	0.42
CaO	0.32	0.30	0.09	0.17	0.40	0.47	0.29	0.14
Na <sub>2</sub> O	1.22	1.55	1.68	2.01	1.48	1.37	1.55	0.27
K <sub>2</sub> O	4.55	4.50	5.04	3.65	5.03	5.33	4.68	0.60
TiO <sub>2</sub>	0.84	0.89	0.62	0.78	0.97	0.96	0.84	0.13
MnO	0.10	0.08	0.06	0.09	0.09	0.08	0.08	0.01
S	0.03	0.02	0.04	0.00	0.05	0.00	0.02	0.02
P <sub>2</sub> O <sub>5</sub>	0.18	0.13	0.09	0.13	0.17	0.12	0.14	0.03
Ce	76	72	99	90	98	100	89	12
La	39	37	52	37	35	41	40	6
Ba	732	723	1406	651	913	957	897	276
Nb	18	20	12	17	20	23	18	4
Zr	168	177	98	130	188	250	169	52
Y	46	37	32	51	48	48	44	7
Sr	137	159	250	133	143	101	154	51
Rb	184	200	195	146	203	188	186	21
Zn	90	94	59	145	108	121	103	29
Cu	36	25	20	10	42	21	26	12
Ni	22	23	14	36	21	41	26	10
Co								
Cr	99	113	101	113	125	119	112	10
Li								





Table 23: X.R.F. Analyses on psammites and pelite from Mount Albreda

psammites					Mean			s.d.	pelite 6153E
Sample: 5901k	6152G	6152I	6152W	6152Y	(n=4)				
SiO <sub>2</sub>	75.13	76.67	72.62	75.84	67.36	73.12	4.22	49.31	
Al <sub>2</sub> O <sub>3</sub>	11.56	13.42	13.93	12.96	14.86	13.79	0.81	15.04	
Fe <sub>2</sub> O <sub>3</sub>	2.76	1.47	3.11	1.39	5.63	2.90	1.99	14.15	
MgO	0.74	0.49	1.17	0.26	1.52	0.86	0.59	7.12	
CaO	0.82	0.25	0.74	0.88	2.85	1.18	1.15	8.28	
Na <sub>2</sub> O	4.22	2.45	4.11	3.91	2.85	3.33	0.81	2.84	
K <sub>2</sub> O	4.39	5.14	4.03	4.99	4.15	4.58	0.57	2.43	
TiO <sub>2</sub>	0.13	0.17	0.39	0.19	0.81	0.39	0.30	1.40	
MnO	0.03	0.03	0.04	0.03	0.08	0.05	0.02	0.19	
S	0.03	0.01	0.01	0.01	0.06	0.02	0.03	0.11	
P <sub>2</sub> O <sub>5</sub>	0.21	0.00	0.00	0.00	0.00	0.00	0.00	0	
Ce		108	131	110	120	117	11	33	
La		61	76	61	59	64	8	21	
Ba	118	397	411	279	952	510	300	587	
Nb	105	46	11	50	27	34	18	7	
Zr	264	121	172	139	289	180	76	118	
Y	70	49	32	55	58	49	12	23	
Sr	37	36	105	48	125	79	43	311	
Rb	38	212	162	193	159	181	25	88	
Zn	20	10	49	17	127	51	54	154	
Cu	7	10	8	4	69	23	31	106	
Ni	20	2	5	3	5	4	2	131	
Co									
Cr	14	9	22	15	16	16	5	80	
Li	0.67							3.29	
D.F.	+2.0	-0.12	+1.60	+2.10	+0.97				



Table 24: X.R.F. Analyses on psammities from Mt. Lempriere and Highway 5, south of Lempriere

Sample:	Mt. Lempriere			Highway 5			Mean		
	6405A	6405C	6405D	5888A	5888C	(n=2)	s.d.	s.d.	
SiO <sub>2</sub>	77.26	62.38	66.77	80.64	66.19	73.42	10.22		
Al <sub>2</sub> O <sub>3</sub>	11.27	20.12	16.43	9.33	18.73	14.03	6.65		
Fe <sub>2</sub> O <sub>3</sub>	3.96	7.53	6.87	2.51	5.37	3.94	2.02		
MgO	1.95	3.49	3.56	1.36	1.71	1.54	0.25		
CaO	1.16	0.49	0.99	0.87	9.88	2.00	6.37		
Na <sub>2</sub> O	2.18	0.81	1.20	3.77	2.33	3.05	1.02		
K <sub>2</sub> O	1.51	4.55	3.50	1.05	4.83	2.94	2.67		
TiO <sub>2</sub>	0.48	0.98	0.91	0.36	0.76	0.56	0.28		
MnO	0.06	0.09	0.11	0.03	0.06	0.05	0.02		
S	0.18	0.11	0.12	0.03	0.06	0.05	0.02		
P <sub>2</sub> O <sub>5</sub>	0.00	0.06	0.16	0.05	0.10	0.08	0.04		
Ce	48	76	56						
La	16	34	21						
Ba	118	704	505	207	811	509	427		
Mo									
Nb	9	19	16	13	20	17	5		
Zr	214	205	221	311	258	285	37		
Y	23	42	29	24	46	35	16		
Sr	139	91	136	97	107	102	7		
Rb	78	184	141	26	206	116	117		
Zn	56	95	92	30	95	63	46		
Cu	41	10	15	0	37	19	26		
Ni	18	45	36	17	18	18	1		
Co									
Cr	44	106	96	31	63	47	23		
Li									
D.F.	-9.5	=4.6	-5.1	-2.1	-4.8				



Table 25: X.R.F. Analyses on semi-pelites from Clemina Creek & Highway 5 South of Lempriere

Sample:	Clemena Creek			s.d.
	6153D	6153H	Mean(n=2)	
SiO <sub>2</sub>	49.93	48.89	49.41	0.74
Al <sub>2</sub> O <sub>3</sub>	7.51	5.99	6.75	1.07
Fe <sub>2</sub> O <sub>3</sub>	12.03	12.86	12.45	0.59
MgO	14.33	17.31	15.82	2.11
CaO	13.63	13.30	13.47	0.23
Na <sub>2</sub> O	1.56	1.13	1.35	0.30
K <sub>2</sub> O	0.81	0.36	0.59	0.32
TiO <sub>2</sub>	0.69	0.71	0.70	0.01
MnO	0.23	0.26	0.25	0.02
S	0.09	0.03	0.06	0.04
P <sub>2</sub> O <sub>5</sub>	0.00	0.00	0.00	0.00
Ce	21	16	14	11
La	18	15	17	2
Ba	288	80	184	147
Nb	3	4	4	1
Zr	52	39	46	9
Y	19	17	18	1
Sr	283	97	190	132
Rb	14	5	10	6
Zn	143	224	97	106
Cu	117	61	89	40
Ni	124	266	195	100
Co				
Cr	158	756	457	423
Li				
D.F.	-7.7	-11.7		

Highway 5			Mean(n=2)	s.d.
5888B	5888D			
50.68	51.72	51.20	0.74	
12.77	12.97	12.87	0.14	
14.40	13.65	14.03	0.53	
7.97	7.94	7.96	0.02	
9.88	9.48	9.68	0.28	
2.33	2.37	2.35	0.03	
0.48	0.50	0.49	0.01	
1.10	1.04	1.07	0.04	
0.21	0.19	0.20	0.01	
0.06	0.02	0.04	0.03	
0.13	0.12	0.13	0.01	
154	131	143	16	
4	1	3	2	
78	74	76	3	
23	23	23	0	
189	169	179	14	
19	23	21	3	
94	102	48	65	
111	5	56	78	
74	41	58	23	
183	187	185	3	
-3.5	-3.6			





Table 26: X.R.F. Analyses on Psammites and Semi-pelites from Paradise Lake

Sample:	Psammites		Semi-pelites		Mean(n=2)	s.d.
	5891E1	5891E2	5891B	5891D		
SiO <sub>2</sub>	86.11	86.72	65.88	53.06	59.47	9.07
Al <sub>2</sub> O <sub>3</sub>	6.50	6.00	5.54	7.84	6.69	1.63
Fe <sub>2</sub> O <sub>3</sub>	2.18	2.11	4.24	12.73	8.49	6.00
MgO	1.01	1.11	6.18	12.36	9.27	4.37
CaO	0.78	0.76	16.39	11.68	14.04	3.33
Na <sub>2</sub> O	1.93	1.65	0.72	0.63	0.68	0.06
K <sub>2</sub> O	1.09	1.28	0.30	0.72	0.51	0.30
TiO <sub>2</sub>	0.30	0.24	0.36	0.78	0.57	0.30
MnO	0.02	0.03	0.30	0.03	0.17	0.19
S	0.03	0.02	0.03	0.03	0.03	0.00
P <sub>2</sub> O <sub>5</sub>	0.04	0.07	0.05	0.14	0.10	0.06
Ce						
La						
Ba	70	54	87	191	139	74
Nb	14	7	35	36	36	0.7
Zr	212	146	213	119	166	66
Y	7	12	28	34	31	4
Sr	100	97	510	84	297	301
Rb	38	36	18	17	18	1
Zn	29	26	69	124	97	39
Cu	10	9	0	7	4	5
Ni	28	26	25	96	61	50
Co						
Cr	53	24	35	670	353	449
Li						
D.F.			-0.58	-9.2		



Table 27: X.R.F. Analyses on psammites from the Miette Group

Sample:	AC3	AC5	AC6	AC7	Mean (n=4)	s.d.
SiO <sub>2</sub>	83.8	84.9	84.0	84.6	84.33	0.44
Al <sub>2</sub> O <sub>3</sub>	8.4	8.3	9.2	7.7	8.40	0.53
Fe <sub>2</sub> O <sub>3</sub>	1.8	1.4	1.5	1.9	1.65	0.21
MgO	0.9	0.7	0.7	0.9	0.80	0.10
CaO	0.9	0.5	0.3	1.1	0.70	0.32
Na <sub>2</sub> O	2.7	2.8	2.5	2.2	2.55	0.23
K <sub>2</sub> O	1.22	1.04	1.60	1.17	1.26	0.21
TiO <sub>2</sub>	0.24	0.12	0.17	0.28	0.20	0.06
MnO	0.03	0.02	0.02	0.05	0.03	0.01
S	0.00	0.00	0.00	0.00	0.00	0.00
P <sub>2</sub> O <sub>5</sub>	0.06	0.10	0.08	0.07	0.08	0.01
Ce						
La						
Ba	170	188	313	348	255	77
Nb	6	7	8	8	7	1
Zr	151	97	122	174	136	29
Y	10	5	8	15	10	4
Sr	112	98	103	176	122	31
Rb	53	27	57	55	48	12
Zn	29	15	20	28	23	6
Cu	7	11	10	1	7	4
Ni	14	14	22	12	16	4
Co						
Cr						
Li						



Table 27 continued..

Pack Saddle Creek								
Sample:	AC23	AC24	AC25	AC26	AC43	6410	Mean (n=9)	s.d.
SiO <sub>2</sub>	85.4	83.7	82.2	84.8	83.8	79.09	83.00	2.44
Al <sub>2</sub> O <sub>3</sub>	8.6	8.3	5.5	6.9	8.3	11.97	8.64	2.16
Fe <sub>2</sub> O <sub>3</sub>	0.9	1.87	3.19	3.08	2.42	2.26	2.21	0.64
MgO	2.2	1.4	1.0	3.4	0.9	1.16	1.28	0.91
CaO	0.07	1.3	0.6	0.4	0.4	0.95	0.41	0.44
Na <sub>2</sub> O	2.32	2.30	2.20	1.25	2.31	2.97	3.03	1.28
K <sub>2</sub> O	0.14	0.21	0.08	0.08	0.36	0.27	0.18	0.11
TiO <sub>2</sub>	0.01	0.02	0.10	0.02	0.04	0.03	0.06	0.04
MnO	0.04	0.02	0.01	0.01	0.03	0.04	0.02	0.01
S	0.04	0.02	0.01	0.01	0.03	0.04	0.02	0.01
Ce						58		
La						21		
Ba	281	337	313	223	453	876	527	252
Nb	5	6	4	2	7	7	6	2
Zr	104	123	87	82	271	191	136	66
Y	8	11	7	4	14	12	17	28
Sr	19	56	26	21	113	43	52	28
Rb	59	49	61	34	109	91	75	28
Zn	3	10	14	12	32	14	10	9
Cu	4	6	8	6	3	12	6	3
Ni	9	9	17	12	21	7	12	4
Co								
Cr						27		
Li								









Table 28 continued ...

Sample:	Sheared Igneous Rocks				Sheared Igneous Rocks	
	5828A	5829B	5829C	5846B	5848	Mean (n=5)
						s.d.
SiO <sub>2</sub>	72.0	73.5	74.1	73.8	74.0	73.85
Al <sub>2</sub> O <sub>3</sub>	9.3	12.4	12.6	15.4	11.5	12.98
Fe <sub>2</sub> O <sub>3</sub>	3.0	3.9	3.3	2.0	2.0	2.80
MgO	2.2	1.9	2.1	0.8	0.8	1.40
CaO	7.7	0.6	0.4	1.3	0.6	2.12
Na <sub>2</sub> O	1.7	2.8	5.1	5.0	3.7	4.15
K <sub>2</sub> O	2.42	4.20	1.82	1.42	2.98	2.61
TiO <sub>2</sub>	0.42	0.60	0.55	0.23	0.40	0.45
MnO	0.12	0.05	0.03	0.02	0.02	0.03
S	0.93	0.00	0.00	0.00	0.18	0.05
P <sub>2</sub> O <sub>5</sub>	0.12	0.12	0.10	0.03	0.05	0.08
Ce						0.04
La						
Ba	587	843	1177	1178	1084	1071
Nb	18	25	43	15	20	26
Zr	199	292	305	192	231	255
Y	17	19	29	16	16	20
Sr	246	91	122	215	271	175
Rb	83	145	58	57	131	98
Zn	32	69	36	27	16	37
Cu	13	13	1	12	8	9
Ni	27	24	18	11	10	16
Co	44	.53		54	60	53 (n=4)
Cr						6
Li	14	14		6	15	12
D.F.	+0.23	-1.4	+0.41	+2.3	+0.8	-3.1
						42
						446
						5
						142
						25
						372
						114
						172
						25
						152
						94



Table 29: X.R.F. Analyses on pelites and psammites from Bulldog Creek Area

Sample:	Pelites				Psammites						
	AC46	AG50	5830A	5830B	6407B	Mean (n=5)	s.d.	AC47	AG48	Mean (n=2)	s.d.
SiO <sub>2</sub>	68.2	70.4	66.4	68.2	57.09	66.06	4.66	82.1	89.0	85.60	3.0
Al <sub>2</sub> O <sub>3</sub>	17.3	15.8	16.2	14.7	22.21	17.24	2.62	10.3	6.1	8.20	2.0
Fe <sub>2</sub> O <sub>3</sub>	5.0	4.2	5.8	4.7	6.55	5.25	0.83	1.9	0.4	1.15	0.75
MgO	1.2	3.2	2.3	2.3	2.04	2.39	0.69	0.9	0.2	0.55	0.35
CaO	0.0	0.1	1.9	3.4	0.99	0.76	0.78	0.5	0.0	0.25	0.25
Na <sub>2</sub> O	0.4	0.8	2.3	2.7	5.13	2.27	1.67	0.5	0.6	0.55	0.05
K <sub>2</sub> O	6.79	4.59	4.19	3.25	4.44	4.71	1.30	3.51	3.69	3.60	0.09
TiO <sub>2</sub>	1.03	0.68	0.67	0.58	0.89	0.77	0.17	0.32	0.05	0.19	0.14
MnO	0.02	0.05	0.07	0.08	0.07	0.06	0.02	0.06	0.01	0.04	0.03
S	0.00	0.00	0.00	0.00	0.00	0.00	0.00	0.00	0.00	0.00	0.00
P <sub>2</sub> O <sub>5</sub>	0.06	0.12	0.12	0.11	0.20	0.12	0.04	0.01	0.00	0.01	0.01
Ce					104						
La					63						
Ba	1387	1263	1158	1247	2105	1432	344	891	514	703	189
Nb	38	19	12	17	12	20	10	19	1	10	9
Zr	606	311	266	201	312	339	139	244	86	165	79
Y	31	28	23	34	31	29	4	12	5	9	4
Sr	68	195	286	292	326	233	93	98	47	73	26
Rb	297	188	190	119	120	183	65	143	82	113	31
Zn	54	76	65	53	74	64	10	31	1	16	15
Cu	5	7	11	11	41	7	4	5	6	6	1
Ni	43	28	22	15	22	26	9	15	6	11	5
Co	-	-	78	-	-	-	-	-	-	-	-
Cr	-	-	24	-	41	-	-	-	-	-	-
Li	-	-	-	-	-	-	-	-	-	-	-
D.F.	-2.4	-5.1	-0.99	-0.07	+3.7			-7.0	-5.7		





Table 30: X.R.F. Analyses on metasediments from Mount Blackman

Sample:	Pelites				Psammites					
	5889A	5889I	5889Q	5889S	Mean (n=4)	s.d.	5889B	5889C	5889D	5889E
SiO <sub>2</sub>	75.08	77.84	69.40	70.54	73.22	3.94	86.23	80.68	87.70	89.03
Al <sub>2</sub> O <sub>3</sub>	14.02	12.03	14.37	14.35	13.69	1.12	6.28	9.78	6.00	5.01
Fe <sub>2</sub> O <sub>3</sub>	1.37	2.86	4.52	3.26	3.00	1.30	2.47	2.44	1.23	0.99
MgO	0.70	1.25	1.84	1.37	1.29	0.47	0.71	1.08	0.16	0.37
CaO	3.01	0.00	2.79	1.14	1.74	1.43	1.25	0.00	0.00	0.00
Na <sub>2</sub> O	4.97	0.20	1.54	4.15	2.72	2.22	1.76	0.27	0.21	0.20
K <sub>2</sub> O	0.68	5.37	4.90	4.42	3.84	2.14	0.87	5.38	4.44	4.50
TiO <sub>2</sub>	0.09	0.39	0.44	0.50	0.36	0.18	0.29	0.28	0.09	0.07
MnO	0.02	0.01	0.05	0.05	0.03	0.02	0.05	0.01	0.01	0.01
S	0.03	0.03	0.03	0.02	0.03	0.01	0.02	0.03	0.03	0.02
P <sub>2</sub> O <sub>5</sub>	0.04	0.03	0.13	0.19	0.10	0.08	0.07	0.06	0.01	0.01
Ce										
La										
Ba	11	690	1109	1580	848	666	79	580	354	342
Nb	7	12	9	18	12	5	10	10	5	5
Zr	52	396	201	292	235	146	217	227	78	99
Y	4	24	21	45	24	17	16	6	4	4
Sr	219	49	175	277	180	97	54	70	44	66
Rb	34	176	194	128	133	72	48	138	76	67
Zn	21	4	66	20	28	27	17	1	3	1
Cu	21	5	10	7	11	7	16	10	14	11
Ni	16	27	37	58	35	18	22	36	0	13
Co										
Cr	26	42	18	15	25	12	51	46	38	40
Li										
D.F.	+2.8	-4.9	-0.9	+2.3						



Table 30 continued ....

Sample:	5889G	5889H	5889J	5889K2	5889L	5889M	5889N	5889T	Mean (n=12)	s.d.
SiO <sub>2</sub>	86.86	83.88	88.34	82.36	85.60	87.47	85.09	81.45	85.39	2.64
Al <sub>2</sub> O <sub>3</sub>	6.14	5.68	5.34	10.34	6.60	4.87	7.77	9.14	6.91	1.81
Fe <sub>2</sub> O <sub>3</sub>	1.18	2.70	1.13	1.03	2.71	1.65	2.18	2.69	1.87	0.70
MgO	0.37	1.69	0.28	0.46	0.74	0.95	0.99	0.92	0.72	0.42
CaO	0.00	1.46	0.00	0.00	1.18	0.77	0.43	0.00	0.42	0.56
Na <sub>2</sub> O	0.23	0.10	0.22	0.17	1.78	0.17	0.97	0.14	0.52	0.60
K <sub>2</sub> O	5.10	4.23	4.57	5.45	0.95	3.88	2.12	5.28	3.90	1.59
TiO <sub>2</sub>	0.07	0.14	0.06	0.11	0.30	0.14	0.19	0.28	0.17	0.09
MnO	0.01	0.04	0.01	0.01	0.05	0.02	0.06	0.01	0.02	0.02
S	0.02	0.03	0.03	0.02	0.03	0.02	0.02	0.02	0.02	0.01
P <sub>2</sub> O <sub>5</sub>	0.02	0.06	0.03	0.03	0.07	0.05	0.17	0.06	0.05	0.04
Ce										
La										
Ba	440	231	321	300	69	232	141	479	297	151
Nb	7	7	7	4	10	6	9	9	7	2
Zr	120	176	111	182	237	180	199	260	174	57
Y	2	14	6	10	18	22	14	17	11	6
Sr	58	48	62	40	60	57	51	64	56	9
Rb	85	108	70	116	58	67	58	129	85	29
Zn	6	9	1	2	27	1	20	3	8	13
Cu	17	bdl	4	2	11	8	13	17	10	6
Ni	16	34	19	1	27	19	51	39	23	15
Co										
Cr	45	34	28	34	53	30	36	561	83	144



Table 31: X.R.F. Analyses on semi-pelites and pelites from Mount Blackman

Sample:	Semi-pelites					Mean (n=6)	s.d.	Pelite 58951
	5890G	5890S	5890U	5895U	5895V	6150L		
SiO <sub>2</sub>	47.68	46.56	49.50	41.89	44.03	45.97	2.69	71.91
Al <sub>2</sub> O <sub>3</sub>	12.44	13.07	13.88	10.80	12.01	14.09	1.23	12.50
Fe <sub>2</sub> O <sub>3</sub>	15.97	16.59	17.60	18.84	18.79	17.69	1.15	6.43
MgO	6.84	6.87	6.30	7.60	8.74	11.36	1.87	2.20
CaO	7.80	7.45	4.15	13.78	9.56	4.78	3.50	0.54
Na <sub>2</sub> O	0.86	0.52	0.39	0.37	0.61	0.55	0.18	0.91
K <sub>2</sub> O	3.60	3.74	3.60	3.54	3.33	3.83	0.17	4.78
TiO <sub>2</sub>	3.12	3.39	3.70	2.67	2.41	2.57	0.51	0.63
MnO	0.27	0.25	0.22	0.27	0.20	0.15	0.05	0.05
S	0.12	0.19	0.05	0.10	0.05	0.04	0.05	0.02
P <sub>2</sub> O <sub>5</sub>	1.30	1.37	0.62	0.13	0.27	0.00	0.60	0.02
Ce						54		
La						25		
Ba	1217	965	857	387	343	228	400	497
Nb	56	52	39	13	11	11	21	16
Zr	262	270	336	175	182	167	68	161
Y	49	58	80	50	45	57	13	24
Sr	167	199	269	145	83	24	86	65
Rb	158	212	228	184	150	147	65	171
Zn	133	140	235	98	129	156	46	84
Cu	14	30	14	36	396	189	154	14
Ni	26	26	32	76	69	69	24	48
Co								
Cr	54	24	56	77	61	113	29	77
Li								
D.F.	-3.9	-4.5	-6.9	-1.8	-5.4	-10.5		-4.7





### 9.3 Appendix C (Isotope Data)



Table 32: Replicate Analyses

Each 87/86 value was obtained by a complete repetition of the chemical separation and mass spectrometric measurement. All isotopic measurements were made on a V.G. Micromass 30 mass spectrometer, using a 0.1N H<sub>3</sub>PO<sub>4</sub> loading method onto a single Ta filament. Oxford samples are standardized to an Eimer and Amend value of 0.70800. Edmonton samples are standardized to a N.B.S. SRM987 value of 0.71014.

Sample	Date	Place	Type of m/s Program	87/86 ± $\sigma$ measured	87/86 ± 2 $\sigma$ standardized
*5815	Nov. 1976 Oct. 1981	Oxford Edmonton	1 base line "	0.79528 ± 4 0.79502 ± 8	0.79518 ± 7 0.79491 ± 15
5842C	Jan. 1977 Jan. 1978	Oxford Edmonton	" "	0.74745 ± 5 0.74744 ± 5	0.74735 ± 11 0.74738 ± 10
*5845B	Nov. 1976 Oct. 1981	Oxford Edmonton	" "	0.82184 ± 7 0.82167 ± 4	0.82174 ± 14 0.82156 ± 8
JC 6	Mar. 1979 May, 1979	Edmonton Edmonton	" (modified) " (modified)	0.70447 ± 3 0.70449 ± 3	
JC 9	Oct. 1978 Oct. 1978 May, 1979	Edmonton " "	" " " (modified)	0.70447 ± 3 0.70446 ± 3 0.70437 ± 3	
JC 14	Oct. 1978 Oct. 1978 May 1979	Edmonton " "	" " " (modified)	0.70460 ± 1 0.70457 ± 2 0.70446 ± 4	
JC 23	Nov. 1978 Dec. 1978	Edmonton "	" "	0.70401 ± 7 0.70401 ± 4	
*JC 59	Jan. 1980 Jan. 1980	" "	" (modified) " (modified)	0.71339 ± 8 0.71300 ± 5	

\*Samples containing < 50 ppm strontium.



Table 33: Strontium Standard Isotopic Measurements

Standard	Date	Type of m/s program	filament type	$87/86 \pm \sigma$ measured
SRM987	May 1978	Bake out and source cleaned	Single Ta	0.71021 $\pm$ 2
"	16 May 1978	1 base line	"	0.71020 $\pm$ 3
"	2 June 1978	"	"	0.71019 $\pm$ 3
"	6 Sept. 1978	"	"	0.71019 $\pm$ 5
"	13 Sept. 1978	"	"	0.71017 $\pm$ 2
"	30 " "	"	"	0.71020 $\pm$ 4
"	8 Nov. 1978	"	"	0.71006 $\pm$ 5
"	8 " "	3 base line	"	0.71019 $\pm$ 6
"	12 Jan. 1979	1 base line	"	0.71016 $\pm$ 3
"	23 March 1979	3 base line	"	0.71023 $\pm$ 4
"	5 June " "	"	"	0.71050 $\pm$ 4
"	5 June " "	1 base line (modified)	"	0.71041 $\pm$ 4
"	5 June " "	"	"	
"	5 June " "	slit changed	"	0.71047 $\pm$ 5
"	6 June " "	1 base line	"	0.71008 $\pm$ 6
"	6 June " "	3 base line	"	
"	6 June " "	source cleaned	"	0.71040 $\pm$ 2
"	Nov. " "	"	"	0.71022 $\pm$ 1
"	4 Jan. 1980	1 base line (modified)	"	0.71031 $\pm$ 3
"	4 " " "	3 base line (modified)	"	0.71027 $\pm$ 3
"	4 " " "	"	"	0.71032 $\pm$ 3
"	4 " " "	"	"	0.71029 $\pm$ 4
"	5 " " "	"	"	0.71043 $\pm$ 4
"	21 July 1981	3 base line - paired	double Re	0.71036 $\pm$ 16
"	27 " " "	"	"	0.71025 $\pm$ 3
"	24 Aug. " " "	"	"	0.71027 $\pm$ 3
"	26 Aug. " " "	"	"	
"	10 Sept. " " "	"	"	
"	" " " "	Bake out	"	0.71020 $\pm$ 3
"	16 Oct. " " "	3 base line - paired	"	0.71020 $\pm$ 4
"	22 Oct. " " "	"	"	0.71028 $\pm$ 3
"	28 Oct. " " "	"	"	





Table 34: Measurement of Laboratory Blank

Date	Laboratory	nanogm $^{88}\text{Sr}$
1978	Geol 268	13.4
1978	"	12.6
1979	Chem E 462	2.5
1979	"	7.2
1980	"	5.4
1980	"	4.4
1981	Chem W466	8.7
1981	"	6.3



Table 35: Rb-Sr Data on Grey Gneiss

Sample	loc	$^{87}\text{Rb}/^{86}\text{Sr} \pm 2\%$	$^{87}\text{Sr}/^{86}\text{Sr} \pm 2\sigma_{\bar{x}}$
5498	CN	$0.586 \pm 12$	$0.72750 \pm 10$
5810	CN	$0.929 \pm 19$	$0.74547 \pm 7$
5811	CN	$1.11 \pm 2$	$0.75158 \pm 14$
*5842B	MR	$0.644 \pm 13$	$0.73434 \pm 16$
5842C	MR	$1.04 \pm 2$	$0.74728 \pm 5$
5843A	MR	$0.806 \pm 16$	$0.73643 \pm 5$
5843B	MR	$0.882 \pm 18$	$0.73652 \pm 4$
5843C	MR	$0.862 \pm 17$	$0.73676 \pm 7$
*5844A	MR	$0.696 \pm 14$	$0.73799 \pm 5$
5844B	MR	$1.52 \pm 3$	$0.77491 \pm 8$
*5844D	MR	$0.930 \pm 19$	$0.78285 \pm 2$
*5893C	MR	$1.38 \pm 3$	$0.77397 \pm 10$
*5894D	MR	$0.493 \pm 15$	$0.75787 \pm 2$
*5897C	MM	$1.04 \pm 2$	$0.74771 \pm 12$
*5899A	MM	$1.80 \pm 4$	$0.74484 \pm 6$
5899E	MM	$1.77 \pm 4$	$0.77647 \pm 12$
*5901G	MM	$0.611 \pm 12$	$0.72369 \pm 4$
5901H	MM	$0.585 \pm 12$	$0.72542 \pm 10$
5903B	CN	$2.08 \pm 4$	$0.79164 \pm 6$
*5903D	CN	$2.29 \pm 5$	$0.78503 \pm 5$
*5903I	CN	$0.722 \pm 14$	$0.72629 \pm 14$
*6153G	MM	$2.20 \pm 4$	$0.78699 \pm 6$
6154C	MM	$3.08 \pm 6$	$0.82675 \pm 8$

\* not included in isochron calculation



Table 36: Rb-Sr Data on Mafic Gneiss West of RMT

Sample	loc	$^{87}\text{Rb}/^{86}\text{Sr} \pm 2\%$	$^{87}\text{Sr}/^{86}\text{Sr} \pm 2\sigma \bar{x}$
5502	CN	$0.0839 \pm 17$	$0.70793 \pm 9$
5803	CN	$0.281 \pm 6$	$0.71029 \pm 8$
*5804	CN	$0.446 \pm 9$	$0.71216 \pm 10$
*5805	CN	$0.362 \pm 7$	$0.71229 \pm 8$
5806	CN	$0.153 \pm 3$	$0.70932 \pm 15$
*5807	CN	$0.452 \pm 9$	$0.71335 \pm 9$
*5808	CN	$0.327 \pm 7$	$0.71362 \pm 10$
*5809	CN	$0.680 \pm 14$	$0.71444 \pm 13$
5812	CN	$0.339 \pm 7$	$0.71075 \pm 6$
*5819B	MR	$0.840 \pm 17$	$0.71156 \pm 8$
*5824	MR	$0.573 \pm 11$	$0.71332 \pm 10$
5901L	MM	$0.577 \pm 12$	$0.71235 \pm 17$
5901M	MM	$0.642 \pm 13$	$0.73241 \pm 7$
*6152M	MM	$0.278 \pm 6$	$0.71423 \pm 7$
6152S	MM	$1.17 \pm 2$	$0.71707 \pm 3$
*6152Z	MM	$0.497 \pm 10$	$0.71460 \pm 12$
AC12	CN	$0.650 \pm 13$	$0.73176 \pm 9$
*AC13	CN	$1.50 \pm 3$	$0.72515 \pm 5$
*AC14	CN	$0.237 \pm 5$	$0.71131 \pm 8$

\* not included in isochron calculation





Table 37: Rb-Sr data on Augen Gneiss

Sample	loc	$^{87}\text{Rb}/^{86}\text{Sr} \pm 2\%$	$^{87}\text{Sr}/^{86}\text{Sr} \pm 2\sigma \bar{x}$
5901B	MM	$2.04 \pm 4$	$0.75779 \pm 8$
5901C	MM	$1.63 \pm 3$	$0.75194 \pm 12$
5901N	MM	$0.241 \pm 5$	$0.71667 \pm 11$
61521	MM	$4.02 \pm 8$	$0.81489 \pm 8$
6154A	MM	$2.84 \pm 6$	$0.78620 \pm 4$
*6154B	MM	$7.09 \pm 14$	$0.83009 \pm 14$

\* not included in isochron calculation



Table 38: Rb-Sr data on Leucocratic Gneiss

Sample	loc.	lith.	$^{87}\text{Rb}/^{86}\text{Sr} \pm 2\%$	$^{87}\text{Sr}/^{86}\text{Sr} \pm 2\sigma_x$
5499	CN	HiNb	$1.13 \pm 2$	$0.71891 \pm 10$
5500	CN	HiNb	$0.782 \pm 16$	$0.71168 \pm 15$
5501	CN	HiNb	$2.93 \pm 6$	$0.74072 \pm 6$
*5814	CN	HiNb	$4.96 \pm 10$	$0.74791 \pm 16$
5816	CN	LoNb	$2.10 \pm 4$	$0.72912 \pm 14$
5817	CN	HiNb	$2.77 \pm 6$	$0.73933 \pm 7$
5820	MR	HiNb	$5.93 \pm 12$	$0.77878 \pm 16$
5821	MR	HiNb	$8.21 \pm 16$	$0.77395 \pm 11$
5822	MR	HiNb	$1.61 \pm 3$	$0.72328 \pm 7$
5823	MR	HiNb	$5.46 \pm 11$	$0.75498 \pm 7$
5840A	MM	HiNb	$9.52 \pm 19$	$0.82737 \pm 7$
*5845A	MR	LoNb	$6.68 \pm 13$	$0.80395 \pm 3$
5845B	MR	LoNb	$9.58 \pm 19$	$0.82413 \pm 16$
5845C	MR	LoNb	$7.78 \pm 16$	$0.80161 \pm 8$
*5886	MR	HiNb	$3.58 \pm 7$	$0.75575 \pm 10$
*5892E	MR	LoNb	$4.95 \pm 10$	$0.78196 \pm 8$
5901A	MM	HiNb	$8.40 \pm 17$	$0.77573 \pm 18$
*5901D	MM	LoNb	$0.816 \pm 16$	$0.73128 \pm 24$
*5901E	MM	LoNb	$8.82 \pm 18$	$0.81019 \pm 14$
*5901F	MM	LoNb	$4.43 \pm 9$	$0.81280 \pm 12$
*5901I	MM	HiNb	$3.60 \pm 7$	$0.77678 \pm 8$
5901J	MM	HiNb	$3.58 \pm 7$	$0.74109 \pm 4$
*5901Q	MM	HiNb	$0.458 \pm 9$	$0.72841 \pm 8$
5901S	MM	HiNb	$4.30 \pm 9$	$0.74140 \pm 8$
5901U	MM	HiNb	$0.960 \pm 19$	$0.71648 \pm 26$
6152E	MM	LoNb	$9.92 \pm 20$	$0.81596 \pm 18$
AC1J	CN	LoNb	$5.44 \pm 11$	$0.75310 \pm 6$

\* not included in isochron calculation



Table 39: Rb-Sr Data on metasediments from the Horsethief Creek Group

Sample	$^{87}\text{Rb}/^{86}\text{Sr} \pm 2\%$	$^{87}\text{Sr}/^{86}\text{Sr} \pm 2\sigma \bar{x}$
5888A	0.694 $\pm$ 14	0.73129 $\pm$ 12
5888B	0.261 $\pm$ 5	0.72123 $\pm$ 12
5888C	5.02 $\pm$ 10	0.79702 $\pm$ 11
* 5891E	0.934 $\pm$ 19	0.78031 $\pm$ 13

Table 40: Rb-Sr Data on metasediments from the Kaza Group

5818A	2.47 $\pm$ 5	0.75306 $\pm$ 16
5834	1.33 $\pm$ 3	0.76385 $\pm$ 8
5835C	0.283 $\pm$ 6	0.76482 $\pm$ 14
5836B	0.590 $\pm$ 12	0.76575 $\pm$ 9
5853B	1.51 $\pm$ 3	0.75463 $\pm$ 8
5854	1.64 $\pm$ 3	0.74965 $\pm$ 42
5855A	4.89 $\pm$ 10	0.75080 $\pm$ 5
5856	0.925 $\pm$ 18	0.73726 $\pm$ 4
5857A	1.40 $\pm$ 3	0.76137 $\pm$ 2
5857B	6.35 $\pm$ 13	0.77335 $\pm$ 26
5901K	2.67 $\pm$ 5	0.74225 $\pm$ 6
6152I	4.02 $\pm$ 8	0.81489 $\pm$ 8
6152W	10.5 $\pm$ 2	0.83269 $\pm$ 8
6153E	0.733 $\pm$ 15	0.73501 $\pm$ 11
6400B	3.15 $\pm$ 6	0.78489 $\pm$ 11
6411A	1.28 $\pm$ 3	0.78655 $\pm$ 17
6411C	1.81 $\pm$ 4	0.79193 $\pm$ 6
6411G	3.70 $\pm$ 7	0.78820 $\pm$ 4

\* not included in isochron calculation





Table 41: Rb-Sr Data on Hugh Allan Creek Gneiss

Sample	$^{87}\text{Rb}/^{86}\text{Sr} \pm 2\%$	$^{87}\text{Sr}/^{86}\text{Sr} \pm 2\sigma \bar{x}$
6151C	$34.7 \pm 7$	$1.11936 \pm 10$
6151G	$30.0 \pm 6$	$1.07032 \pm 20$
6151H	$4.59 \pm 9$	$0.77514 \pm 6$

Table 42: Rb-Sr Data Mount Blackman Gneiss

Sample	Lith.	$^{87}\text{Rb}/^{86}\text{Sr} \pm 2\%$	$^{87}\text{Sr}/^{86}\text{Sr} \pm 2\sigma \bar{x}$
5890E	felsic	$1.63 \pm 3$	$0.75896 \pm 4$
5890H	felsic	$0.495 \pm 10$	$0.72900 \pm 10$
5890k	felsic	$0.937 \pm 19$	$0.74219 \pm 19$
* 5890M	mafic	$0.194 \pm 4$	$0.72042 \pm 8$
5890R	felsic	$0.905 \pm 18$	$0.74115 \pm 24$
* 5895A	felsic	$0.553 \pm 11$	$0.73616 \pm 3$
5895H	felsic	$0.888 \pm 18$	$0.73836 \pm 5$
5895P	felsic	$2.13 \pm 4$	$0.77428 \pm 6$
5895Q	felsic	$1.00 \pm 2$	$0.74339 \pm 10$
* 5896B	felsic	$0.970 \pm 19$	$0.73704 \pm 8$
6150D	felsic	$1.20 \pm 2$	$0.73682 \pm 12$
6150G	felsic	$1.14 \pm 2$	$0.74478 \pm 5$
* 6150H	mafic	$0.245 \pm 5$	$0.72461 \pm 6$
6150I	felsic	$2.16 \pm 4$	$0.75180 \pm 3$
* 6150Q	felsic	$2.04 \pm 4$	$0.75879 \pm 7$

\* not included in isochron calculation



Table 43: Rb-Sr Data on metasediments from the north cwm on Mount Blackman

Sample:	$^{87}\text{Rb}/^{86}\text{Sr} \pm 2\%$	$^{87}\text{Sr}/^{86}\text{Sr} \pm 2 \sigma \bar{x}$
5889A	$4.05 \pm 8$	$0.79030 \pm 8$
* 5889B	$0.867 \pm 20$	$0.78644 \pm 6$
5889I	$9.43 \pm 19$	$0.86559 \pm 12$
5889k	$0.747 \pm 15$	$0.75246 \pm 8$
5889N	$2.96 \pm 6$	$0.78461 \pm 4$
* 5889Q	$2.89 \pm 6$	$0.80022 \pm 6$
* 5889S	$1.20 \pm 2$	$0.77672 \pm 4$

Table 44: Rb-Sr Data on Gneisses from Bulldog Creek

5495	$0.298 \pm 6$	$0.71906 \pm 2$
* 5831A	$0.750 \pm 15$	$0.72051 \pm 4$
5831B	$0.0942 \pm 19$	$0.71796 \pm 12$
* 5831C	$0.849 \pm 17$	$0.72321 \pm 8$
5831D	$1.83 \pm 4$	$0.72173 \pm 7$
5831E	$1.11 \pm 2$	$0.71832 \pm 5$
5832	$0.219 \pm 4$	$0.71446 \pm 13$
* 5833	$0.147 \pm 3$	$0.71652 \pm 43$
* 5884B	$0.819 \pm 16$	$0.71920 \pm 6$
* 6408A	$0.389 \pm 8$	$0.71894 \pm 5$
* 6408B	$0.703 \pm 14$	$0.72736 \pm 6$
* AC49	$1.08 \pm 2$	$0.72622 \pm 9$

\* not included in isochron calculation



Table 45: Rb-Sr Data on metasediments from the  
Miette Group

Sample	$^{87}\text{Rb}/^{86}\text{Sr} \pm 2\%$	$^{87}\text{Sr}/^{86}\text{Sr} \pm 2\sigma \bar{x}$
* 5828A	0.874 $\pm$ 17	0.73479 $\pm$ 8
5828B	6.94 $\pm$ 14	0.74386 $\pm$ 14
5829B	4.13 $\pm$ 8	0.74019 $\pm$ 14
5829C	1.23 $\pm$ 3	0.72572 $\pm$ 6
* 5830A	1.72 $\pm$ 3	0.73819 $\pm$ 14
* 5830B	1.06 $\pm$ 2	0.73706 $\pm$ 14
5846A	2.49 $\pm$ 5	0.72934 $\pm$ 10
* 5846B	0.687 $\pm$ 14	0.72893 $\pm$ 11
5847	1.88 $\pm$ 4	0.73418 $\pm$ 5
* 5849	0.794 $\pm$ 16	0.72761 $\pm$ 10
* 5850	0.820 $\pm$ 16	0.72346 $\pm$ 16
* 5851	1.24 $\pm$ 2	0.73789 $\pm$ 5
* 5852	1.38 $\pm$ 3	0.73528 $\pm$ 3
* 6407A	0.620 $\pm$ 12	0.72128 $\pm$ 6
* 6407B	0.953 $\pm$ 19	0.73082 $\pm$ 10
AC47	3.79 $\pm$ 8	0.75523 $\pm$ 12
AC48	4.54 $\pm$ 9	0.76949 $\pm$ 6
* AC50	3.14 $\pm$ 6	0.75607 $\pm$ 8

\* not included in isochron calculation





Table 46: Uranium lead data on separated zircons

Sample	lith.	loc.	Measured ratios			U-Pb dates in M.a.		
			206/204	207/204	208/204	206/238	207/235	207/206
5498	Grey Gn.	CN	15500	2042	1500	1762	1928	2110
5810	"	CN	45400	5730	4994	1749	1887	2040
5811	"	CN	19150	2352	2009	1616	1785	1990
5842E	"	MR	17668	2217	17297	1761	1885	2030
5886	Hi Nb	MR	1586	136	38230	77	107.9	840
5895H	Felsic Gn.	MB	4454	547	5977	1544	1726	1950
5901R	Hi Nb	MM	4863	351	10933	654.7	694.3	820
5903B	Grey Gn.	CN	1884	244	4706	1575	1764	2000
5903D	"	CN	33380	4406	2931	1791	1948	2120
5903I	"	CN	16300	1824	1772	1542	1662	1820
o			1%	0.1%	0.1%			









54°00'

121°00'

120°00'

119°00'

118°00'

117°00'

116°00'

54°00'

# GEOLOGICAL MAP OF THE SOUTHEASTERN CANADIAN CORDILLERA

(after Campbell-1972, Okulitch et al-1975, Oke & Simony-1981, Read & Brown-1981, Tipper et al-1981, and Brown & Murphy-1982)

- Upper Cretaceous to Upper Tertiary volcanics (Kamloops)
- Upper Triassic to Lower Jurassic volcanics (Rossland, Nicola, Takla)
- Upper Triassic to Lower Jurassic sediments (Slocan, Sicamous)
- Mississippian to Triassic (Cache Creek)
- Devonian to Triassic (Milford, Kaslo, Fennell, Slide Mountain)
- Cambrian to Mississippian (Lardeau, Broadview, Eagle Bay)
- Cambrian to Devonian
- Proterozoic to Cambrian (Gog, McNaughton, Mahto, Hamill, Badshot, Mural)

- Cariboo Group
- Kaza Group
- Miette Group
- Horsethief Creek Gp. & Monashee Horsethief Creek Gp.
- Purcell Group
- Monashee Complex, North Shuswap Terrane & other undifferentiated metamorphics
- Granitoid gneiss

## Felsic intrusions

- Cretaceous and Tertiary
- Triassic and Jurassic
- Paleozoic

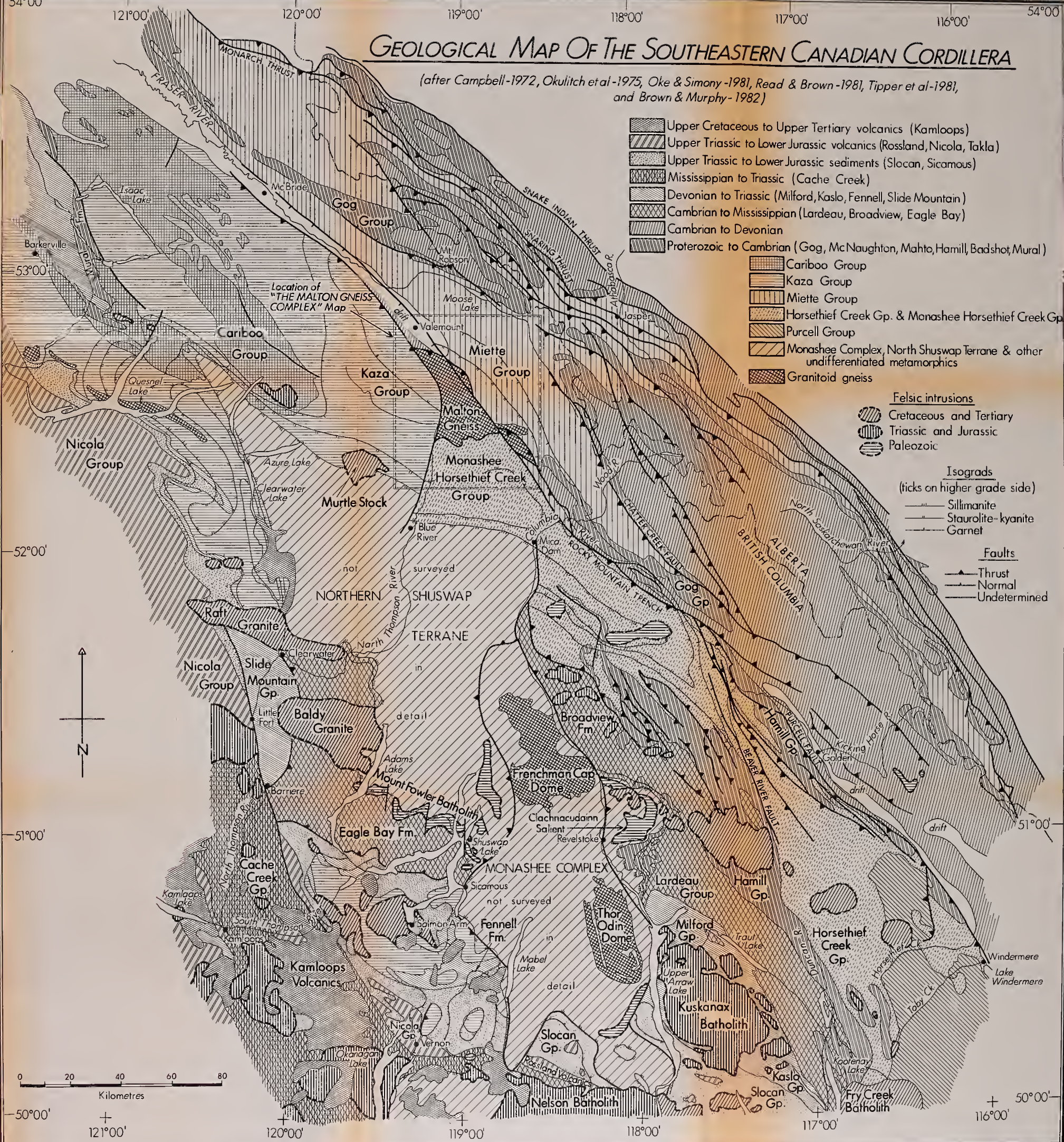
## Isograds

(ticks on higher grade side)

- Sillimanite
- Staurolite-kyanite
- Garnet

## Faults

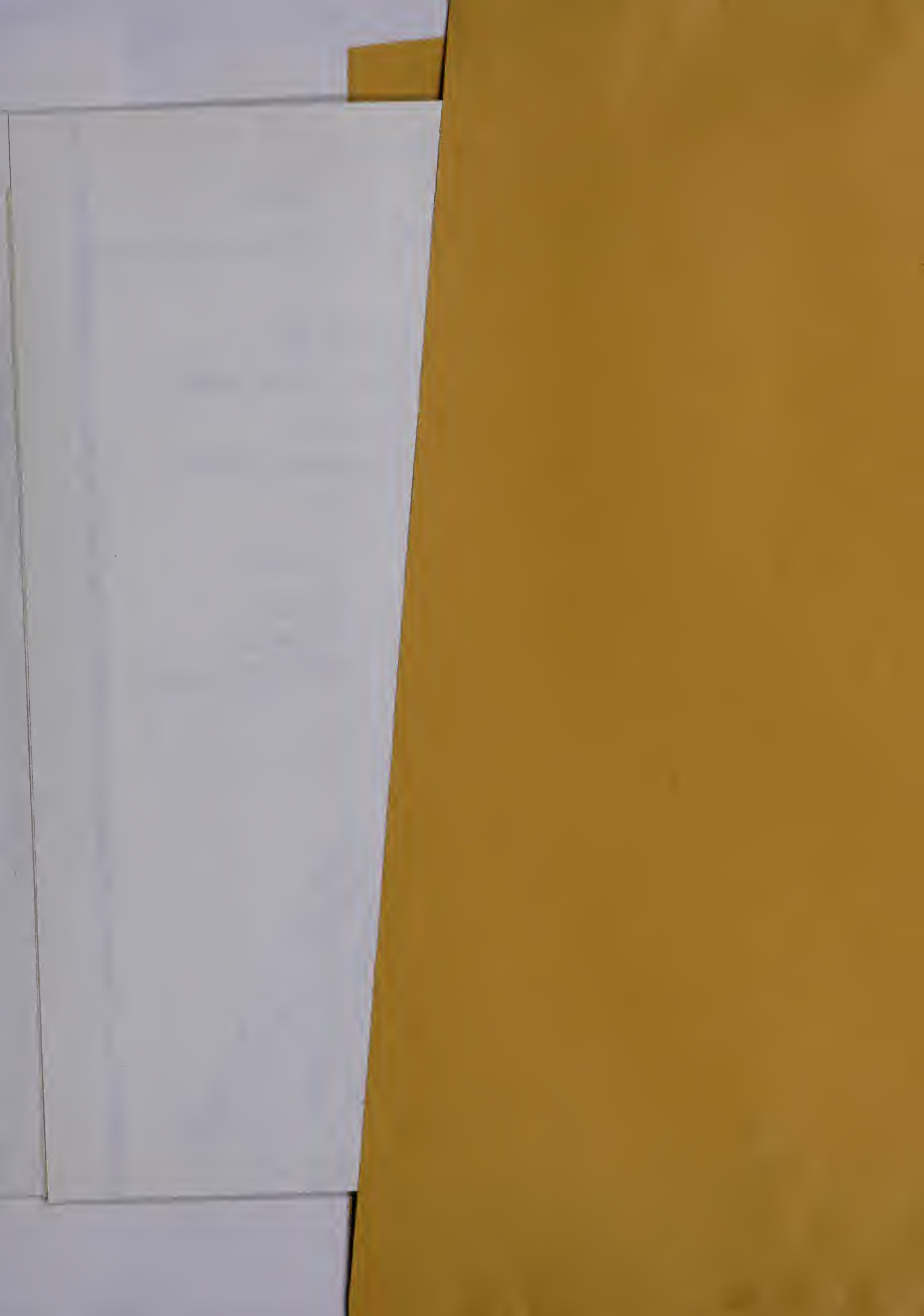
- Thrust
- Normal
- Undetermined













**B30375**